Design, Use and Interpretation of an Instrumented Dilatometer Test

Ontwerp, gebruik en interpretatie van een geïnstrumenteerde dilatometertest

Hao Shen

Promotoren: prof. dr. ir. W. Haegeman, prof. dr. ir. H. Peiffer
Proefschrift ingediend tot het behalen van de graad van
Doctor in de ingenieurswetenschappen: bouwkunde

UNIVERSITEIT
GENT

Vakgroep Civiele Techniek
Voorzitter: prof. dr. ir. P. Troch
Faculteit Ingenieurswetenschappen en Architectuur
Academiejaar 2017 - 2018

ISBN 978-94-6355-062-8
NUR 956
Wettelijk depot: D/2017/10.500/97

Members of the examination committee

Chair

Prof. Hendrik Van Landeghem	Ghent University, Belgium

Reading Committee

Prof. Adam Bezuijen	Ghent University, Belgium
Ir. Diego Marchetti	Studio Prof. Marchetti, Italy
Ir. Flor De Cock	Geo.be bvba, Belgium
Prof. Wim Cornelis	Ghent University, Belgium
Prof. Wouter De Corte	Ghent University, Belgium

Supervisors

Prof. Wim Haegeman	Ghent University, Belgium
Prof. Herman Peiffer	Ghent University, Belgium

″Only the ideas that we actually live are of any value.″
Hermann Hesse

“知之愈明，則行之愈篤；行之愈篤，則知之益明。”
朱熹

Acknowledgments

Foremost, I would like to express my gratitude to my supervisor Prof. Wim Haegeman and Prof. Herman Peiffer for the valuable advice, encouragement, and support during my time at UGent. I believe what I managed to learn from Wim and Herman will serve and enlighten me well in my future career.

Without the financial support from the program of China Scholarships Council (No.201306320157), my study in Belgium would not be possible. The work presented in this thesis is funded by Ghent University and Geosound.be. Dr. Benny Malengier from Geosound.be is acknowledged for his prompt and useful help and it has been pleasant to witness his gift for unravelling the confusing matter of the results.

In no particular order, I am indebted to Jeroen, Phil and Annick from Geosonda bvba for their professional help in the site operation as well as for the tough work on several days of very hot weather; Wim Verlinde from the Belgian Institute for Welding Technology for his valuable suggestion and great cooperation on welding the metal 3D printed parts; Wouter from the Belgian geotechnical department for his help on in situ testing set-ups and kindly allow me using the equipment in his department.

Being far away from home has never been easy, I deeply thank my mom for her support and dedication. Fortunately, I have huan-huan for her unwavering support, appreciation, and understanding, though she has been superior to me as she got her doctorate a bit sooner. The little home we have in Gent has provided more than a happy and joyful life, and the travels we made around Europe have given a lot of once-in-a-lifetime experience and many pleasant memories. I have also made quite some great friends in Ghent, as we cooked, hang out, and travelled together, which makes my life much more complete.

Last but not least, I would like to thank my friends and colleagues in Laboratory of Geotechnics, UGent. Prof. Adam Bezuijen has been brilliant in giving valuable advice and kind help in many aspects. Filip and Jan have been supportive in setting up my experimental devices, in particular, special thanks to

Filip for his patience with training me the “art of welding” as well as many other technical skills. Hilde and Linda have always been helpful in easing the difficulties in my life and work in Gent. Finally, I would like to thank my fellows (Ehsan, Michela, Kristine, Chenghui, Pham, Tiago, Hamzeh, Quan, Dongzhu, Peng, Alessandro, Tao, Penglu) in the lab, it has been a great pleasure to have you not only as my colleagues but also as great friends. The pleasant moments during the lunch talk will never be forgotten wherever I will be.

Contents

Glossary of symbols **xi**

Summary **xv**

Samenvatting **xix**

1 Introduction **1**
1.1 Outline of this thesis 3

2 The flat dilatometer test (DMT) **5**
2.1 Apparatus and operative aspects 5
2.1.1 The DMT equipment components 5
2.1.2 Test procedure 10
2.2 Interpretation of the test results 16
2.2.1 The DMT Indices 16
2.2.2 Soil unit weight 18
2.2.3 Soil stiffness 19
2.2.4 Stress history 23
2.2.5 Undrained strength C_u 26
2.2.6 K_0 in clays 27
2.2.7 Friction angle and K_0 in sands 28
2.2.8 Coefficient of consolidation 31
2.3 Modified dilatometer test 33
2.3.1 Review of the modified dilatometers 34
2.3.2 Data analysis 38
2.4 The dilatometer penetration stage 44
2.4.1 Review of the numerical and analytical analysis 44
2.4.2 The wedge cavity expansion effects 46
2.4.3 The thrust measurements 49

2.5 DMT-CPT relationships 52
2.5.1 The CPT parameters 53
2.5.2 DMT – CPT Relationships 54
2.6 Discussion and conclusion 56

3 The instrumented dilatometer: a laboratory prototype 59
3.1 Introduction 59
3.2 Prototype development 61
3.2.1 Design 61
3.2.2 3D printing of the instrumented dilatometer 65
3.2.3 LabVIEW program for the control & data acquisition (DAQ) system 68
3.3 Calibrations 69
3.3.1 Calibration of the instrument recording system 71
3.3.2 Simulation of the iDMT tests in the air 74
3.4 Calibration Chamber Testing 79
3.4.1 Soil material and equipment 79
3.4.2 Results and comparison 79
3.5 Conclusion 83

4 The iDMT apparatus and test procedure 85
4.1 Introduction 85
4.2 General principles of the iDMT 86
4.3 Apparatus Components 87
4.3.1 Instrumented dilatometer 88
4.3.2 Electro-pneumatic pressure control system 94
4.3.3 Cables and gas pressure source 96
4.4 A pseudo displacement-controlled algorithm 97
4.4.1 Algorithm description 97
4.4.2 Calculation of the piston velocity 98
4.5 Calibration 100
4.6 Test procedure 105
4.7 Conclusion 108

5 Testing and interpretation of the iDMT 111
5.1 Introduction 111
5.2 The DMT contact pressure p_0 113
5.3 The iDMT contact pressure p_c 115

5.3.1 Review of the pressure-displacement curves in the iDMT 115
5.3.2 An analytical approach to estimate p_c . . . 117
5.3.3 An example . . . 120
5.3.4 Typical applications in different soils . . . 124
5.4 The piston expansion . . . 135
5.4.1 Problem formulation . . . 135
5.4.2 Benchmark calculation . . . 138
5.4.3 Piston expansion calculation . . . 140
5.5 The iDMT indices . . . 141
5.6 Zwijnaarde test site . . . 142
5.6.1 Comparison of the iDMT and DMT pressure profiles . . . 143
5.6.2 Comparison of the indices K_D, E_D, I_D . . . 144
5.6.3 Comparison of common soil parameters . . . 147
5.7 Limelette test site . . . 149
5.7.1 Comparison of the iDMT and DMT pressure profiles . . . 150
5.7.2 Comparison of the index parameters K_D, E_D, I_D . . . 151
5.7.3 Comparison of common soil parameters . . . 153
5.8 Kruibeke test site . . . 155
5.8.1 Comparison of the iDMT and DMT pressure profiles . . . 156
5.8.2 Comparison of the index parameters K_D, E_D, I_D . . . 157
5.8.3 Comparison of common soil parameters . . . 157
5.9 Discussion on the pore-water pressure measurements . . . 159
5.10 Conclusion . . . 163

6 Conclusion and future work **167**
6.1 Conclusion of the present work . . . 167
6.2 Recommendations for further work . . . 170

Appendices **175**

A LabVIEW program **175**

B MATLAB codes for p_c estimation **179**

C Abaqus Input Codes on the piston expansion analysis **183**

Reference **189**

Glossary of frequently used symbols

A_c	projected area of the cone
A_d	projected area of the dilatometer blade
B_q	pore-water pressure parameter ratio
C_u	undrained shear strength
D	the piston/membrane diameter
E_D	dilatometer modulus
F_r	normalized friction ratio, in %
F_q	parasitic bearing force on the dilatometer neck and the friction reducer
F_b	side shear force on blade
I_C	The CPT soil behaviour type index
I_D	DMT material index
K_A	Rankine active stress coefficient
K_0	in situ coefficient of lateral earth pressure
K_D	horizontal stress index
K_P	Rankine passive stress coefficient
M_{CPT}	the CPT determined vertical drained constrained modulus
M_{DMT}	the DMT determined vertical drained constrained modulus
OCR	overconsolidation ratio
P	the measured pressure

P_D	thrust force during the DMT sounding
Q_{t1}	normalized cone penetration resistance
$R = G/S_u$	rigidity index of the soil
W	buoyant weight of DMT rods and blade

b	blade thickness
c_h	horizontal coefficient of consolidation
i	the normalization exponent
k_h	coefficient of permeability
p_0	the DMT contact pressure
p_1	the DMT pressure at 1.1 mm
p_c	the iDMT contact pressure
$p_{0.56}$	the iDMT pressure at 0.56 mm
$p_{0.85}$	the iDMT pressure at 0.85 mm
$p_{\text{lift-off}}$	the pressure at the instant membrane/piston starts moving
p_y	the pressure at the onset of yield
q	the applied stress
q_c	cone penetration resistance
q_d	dilatometer blade penetration resistance
q_t	corrected cone resistance
s	the piston/membrane displacement at centre
u	pore-water pressure
u_0	initial steady state pore-water pressure
$\bar{u}$	excess pore-water pressure
u_2	the pore-water pressure measured just behind the cone
$u_{\text{lift-off}}$	the pore-water pressure at the instant of the piston starts moving
s_u	undrained shear strength

w	blade width
$\phi^{'}$	effective friction angle
σ_{v0}	pre-insertion in situ vertical total stress
σ_{h0}	pre-insertion in situ horizontal total stress
σ'_{v0}	pre-insertion in situ vertical effective stress
σ'_{h0}	pre-insertion in situ horizontal effective stress
γ	shear strain
SBT	soil behavior type
SPT	the standard penetration test
CPT	the cone penetration test
CPTu	the piezocone penetration test
DMT	the flat dilatometer test
iDMT	the instrumented dilatometer test
PMT	the pressuremeter test
SBPMT	the self-boring pressuremeter test
OC	overconsolidated
LOC	lightly overconsolidated
HOC	heavily overconsolidated

Summary

There is a growing need for in situ testing in day to day geotechnical projects, especially for soils that cannot be easily sampled in the undisturbed state and for increasing the cost effectiveness of the soil investigation. The flat dilatometer test (DMT) is one of the major in situ tests adopted in many parts of the world, as it is a simple, reliable, and robust tool to obtain common soil parameters in situ. With the rapid advance in both the manufacturing means, such as the (metal) 3D printing, and the instrumentation means, such as the mini sensors and the LabVIEW system, it is of great interest to further discover the potential of the DMT by obtaining more measurements of the soil response. This thesis presents a review of the DMT and the modified DMT followed by the design, use, and interpretation of an instrumented dilatometer test (iDMT) to cope with the problems recognized in the review.

First, this thesis explores the existing literature on the DMT and the modified DMT in many aspects. The review of the DMT underpins further development and interpretation of the iDMT, and, more importantly, reveals the stress relief phenomenon during the blade installation stage. During the initial phase of the membrane expansion, this stress relief, in turn, results in a reloading process and therefore may influence the determination of the contact pressure p_0. Since the p_0 pressure is crucial in the DMT indices and consequently plays a pivotal role in the interpretation for soil parameters, it is of great interest to mitigate the influence of the unload-reload effects. Furthermore, the data analysis out of the literature of the modified DMT sheds light on the non-linear nature of the pressure-displacement measurements regardless of whether a membrane expansion or a piston expansion and thus recognizes the need for measuring full pressure-displacement curve in a larger displacement range for non-linear soil behaviours. The review of the modified DMT with regard to the devices and the instrumentations opens the way for the design and development of the new iDMT. In addition, the relationship between the DMT and the cone penetration test (CPT) is reviewed and discussed, which paves the way

for the comparison in the in situ testing campaign.

The design and development of the iDMT were iterative processes through prototyping. A laboratory prototype was first built for the proof-of-concept purpose. Details of the development with a 3D printing technique and calibrations in the lab are given and followed by the discussion on a preliminary calibration chamber test with both the iDMT blade and the DMT blade wished-in-place in a dry Mol sand for a comparison. With the experience gained in this pilot study, the iDMT and its test procedure are standardized for in situ testing. The latest iDMT is featured by the use of a 60-mm diameter rigid piston with a displacement up to 2.5 mm and pore-water pressure measurements at the piston center. The fabrication of the iDMT uses a hybrid manufacturing method which combines the metal 3D printed parts in 420 stainless steel infiltrated with bronze and the machined parts in 420 stainless steel by means of tungsten inert gas (TIG) welding with $CuSi_3$ as filler, which proves sufficiently robust for the geotechnical testing applications and may inspire future development of other geotechnical testing devices. Moreover, with the help of automatic control and continuous measurements, a pseudo displacement-controlled algorithm programmed in the state machine architecture in LabVIEW is developed for an iDMT test procedure allowing comparable conditions with the DMT. This may allow the use of the well-established DMT correlations with common soil parameters in the iDMT interpretation.

A testing campaign using the iDMT, the DMT, and the CPT is conducted at three sites in Belgium. Based on the observed pressure-displacement curves of the iDMT results and the presented review on the stress relief phenomenon, an analytical approach is proposed to estimate the iDMT contact pressure p_c. This approach programmed in MATLAB consists of determining the transitional "yield" point on the corrected loading curve and then estimating the iDMT contact pressure p_c using the post-yield phase of the curve via a proposed exponential-linear regression model. Note that an adapted Casagrande method is proposed for locating the "yield" point in case that a smooth loading curve is measured, rather than having an angular discontinuity. To investigate the rigid piston expansion process, a finite element method (FEM) analysis is carried out. Despite the simplification of the boundaries and the approximation of numerical results, the results indicate that the pressure p_1 required for a 1.1 mm central movement of the 60-mm diameter membrane can lead to approximate 0.56 mm and 0.85 mm displacement of a rigid piston with a diameter of 40 mm and 60 mm, respectively. Note that an alternative elliptical bound-

ary is used in the FEM analysis to prevent the broken elements (displacement jump). Then, the iDMT indices can be calculated based on the p_c pressure and the $p_{0.56}$ pressure at 0.56 mm/the $p_{0.85}$ pressure at 0.85 mm. The iDMT indices allow the potential derivation of common soil parameters via the well-established DMT relationships. Good agreement is achieved not only between the DMT indices, the CPT-predicted DMT indices, and the iDMT indices but also among the iDMT-derived, the-DMT derived, and the CPT-derived common soil parameters such as the coefficient of earth pressure at rest K_0, the overconsolidation ratio OCR, the undrained shear strength C_u, the effective friction angle $\phi^{'}$, and the DMT determined vertical drained constrained modulus M_{DMT}.

It is worth mentioning that the presented work in this thesis is the first stage of the use of iDMT in soil investigation. There is inevitably a trade-off between sticking to the original DMT test procedure or establishing a completely new iDMT test procedure. The adopted path, for now, is in the middle, which allows comparable conditions between the DMT and the iDMT. Albeit in this way the potential use of iDMT advantages such as the pore-water pressure measurements has not yet been fully taken. The iDMT is at least fully operational with the classic DMT relationships to derive common soil parameters for day to day geotechnical applications, and the problems, such as the influence of unload-reload effects on p_0, identified in the literature review has been successfully addressed.

Samenvatting

In situ testen hebben een groeiend aandeel in de dagelijkse geotechnische projecten, met name voor gronden die niet gemakkelijk kunnen worden bemonsterd. Ze zorgen tevens voor het verhogen van de kosteneffectiviteit van het bodemonderzoek. De dilatometer test (DMT) is in vele delen van de wereld aanvaard als een standaard in situ test, want het is een eenvoudig, betrouwbaar en robuust hulpmiddel om de gebruikelijke grondparameters in situ te bepalen. Met de snelle vooruitgang in zowel de fabricagemiddelen, zoals het (metaal) 3D printen, en in de instrumentatie, zoals mini sensoren en het LabVIEW communicatiesysteem, is het van mogelijk om het potentieel van de DMT verder te exploreren door meer studie en meetdata.

In dit proefschrift wordt een overzicht gegeven van de werking van de klassieke DMT en de reeds bestaande aangebrachte verbeteringen voor deze test waarna het ontwerp, het gebruik en de interpretatie van de meetparameters van een zelf ontworpen geïnstrumenteerde dilatometer test (iDMT) worden beschreven, hierbij tegemoetkomend aan geformuleerde tekortkomingen in de literatuurstudie van eerder ontworpen DMT's.

In eerste instantie wordt in dit proefschrift de bestaande literatuur inzake de DMT en de gewijzigde DMT breed verkend. Deze studie vormt dan de basis voor de verdere ontwikkeling van de iDMT en interpretatie van de meetresultaten, en, belangrijker nog, onthult het fenomeen van de spanningsrelaxatie tijdens de installatie van het dilatometerblad. Deze spanningsverlaging is op zijn beurt de oorzaak van een herbelastingsfase in de grond tijdens de membraanexpansie en zal derhalve de bepaling van de contactdruk p_0 beïnvloeden. Aangezien de p_0 druk belangrijk is voor de berekening van de DMT-indices en derhalve een cruciale rol speelt in de afleiding van de grondparameters, is het van groot belang om de invloed van de ontlastings-herbelastings-effecten op de grond goed in te schatten en te minimaliseren. Bovendien toont de data-analyse van meetresultaten uit de literatuur met een gemodificeerde DMT de niet-lineaire aard van de drukverplaatsingsmetingen ongeacht of een mem-

braan of een piston werd gebruikt. Dit noodzaakt het opmeten van de volledige drukverplaatsingscurve in een groter verplaatsingsbereik ter studie van het niet-lineair grondgedrag. Tot slot opent de literatuurstudie van de gewijzigde DMT met betrekking tot de gebruikte apparaten en instrumentatie de weg voor het ontwerp en de ontwikkeling van de nieuwe iDMT. Daarnaast wordt in de literatuurstudie de relatie tussen de DMT en de CPT resultaten onderzocht en besproken, waardoor een vergelijking van de eigen in situ testresultaten mogelijk wordt. Het ontwerp en de ontwikkeling van de iDMT is een iteratief proces via prototyping. Eerst wordt een laboratoriumprototype gebouwd voor de proof of concept. Hierbij worden de details van het ontwerp en de constructie met een 3D metaalprinttechniek besproken alsook de kalibraties in het laboratorium weergegeven. Vervolgens komt de bespreking van een eerste vergelijkende laboratoriumtest met zowel het iDMT-blad als het DMT-blad geïnstalleerd in een testput gevuld met droog Zand van Mol. Met de ervaring die in dit pilootonderzoek is opgedaan, worden de iDMT en de testprocedure gestandaardiseerd voor in situ metingen. Uiteindelijk wordt de iDMT ontworpen met een stijve zuiger met een diameter van 60 mm, met een verplaatsing tot 2,5 mm en poriënwaterdrukmetingen in het zuigercentrum. De constructie van de iDMT maakt gebruik van een hybride fabricage methode die de metalen 3D geprinte onderdelen in 420 roestvrij staal geïnfiltreerd met brons combineert met klassiek bewerkte delen in 420 roestvrij staal door middel van wolfraam inertgas (TIG) lassen met $CuSi_3$ als vulmiddel. Dit levert een voldoende robuust meettoestel voor de initieel voorziene geotechnische metingen en kan inspirerend werken voor de toekomstige ontwikkeling van andere geotechnische testapparatuur. Bovendien wordt op basis van een geautomatiseerd controlesysteem en continue metingen, een pseudo verplaatsingsgecontroleerd algoritme geprogrammeerd in de LabVIEW architectuur voor een iDMT test procedure vergelijkbaar met de DMT procedure. Dit kan het gebruik van de bestaande correlaties tussen DMT-indices en grondparameters in de iDMT-interpretatie mogelijk maken.

Een testcampagne met iDMT, DMT en CPT wordt uitgevoerd op drie locaties in België. Vertrekkend van de opgemeten drukverplaatsingscurves met de iDMT en het in de literatuurstudie toegelichte fenomeen van spanningsrelaxatie, wordt een analytische aanpak voorgesteld om de iDMT contactdruk p_c in te schatten. Deze aanpak, geprogrammeerd in MATLAB, bestaat uit het bepalen van het "vloei"-punt op de gecorrigeerde belastingscurve en vervolgens het schatten van de iDMT contactdruk p_c met behulp van de vloeifase

op de curve via een vooropgesteld exponentieel lineair regressiemodel. Een aangepaste Casagrande methode wordt voorgesteld om het "vloei" punt te lokaliseren indien een gladde belastingscurve wordt gemeten. Een gladde belastingscurve is alomtegenwoordig in in situ testresultaten, aangezien een hoekige discontinuiteit van de belastingscurve quasi uitsluitend wordt gemeten in zandgronden. Om de elastische belasting van de grond door de piston nader te bestuderen, is een FEM-analyse uitgevoerd. Hieruit blijkt dat de druk p1 die nodig is voor een 1,1 mm centrale verplaatsing van het membraan (met een diameter van 60 mm) in de klassieke DMT resulteert in ongeveer 0,56 mm en 0,85 mm verplaatsing van een stijve zuigerpiston met een diameter van respectievelijk 40 mm en 60 mm. In deze FEM-analyse wordt een alternatieve elliptische overgang gebruikt om breuk in de grond te voorkomen (verplaatsingssprong). Uiteindelijk kunnen de iDMT-indices worden berekend op basis van de p_c druk en de $p_{0,56}$ druk bij 0,56 mm verplaatsing of de $p_{0,85}$ druk bij 0,85 mm verplaatsing. Deze iDMT-indices maken het op hun beurt mogelijk de gebruikelijke grondparameters te bepalen via de gevestigde DMT- correlaties. Een goede overeenkomst wordt niet alleen bereikt tussen de DMT-indices, de uit CPT voorspelde DMT-indices en de iDMT-indices, maar ook tussen uit de iDMT, de DMT en de CPT afgeleide grondparameters zoals K_0, OCR, C_u, $\phi^{'}$ en M_{DMT}.

Het gepresenteerde werk in dit proefschrift is de eerste fase van het gebruik van de iDMT in grondonderzoek. Er is onvermijdelijk een afweging te maken tussen volledig vasthouden aan de oorspronkelijke DMT-interpretatie of het opzetten van een volledig nieuw kader voor de interpretatie van de iDMT resultaten. Het bewandelde pad is momenteel een compromis, waardoor vergelijking van resultaten mogelijk blijft. Hoewel het volledige gebruik van de iDMT met al zijn voordelen zoals de poriewaterdrukmetingen nog niet ten volle is benut, is de iDMT tenminste volledig operationeel, voorlopig nog gebruik makend van de klassieke DMT correlaties ter bepaling van de gebruikelijke grondparameters. Bijkomend zijn een aantal problemen zoals de invloed van ontlastings-herbelastings-effecten op p_0 geïdentificeerd en succesvol aangepakt.

Chapter 1

Introduction

Soils are inherently complicated and notoriously variable because of their geological origins, which generally involve the combination of the action of the climate and the irregular deposition over millions of years. Therefore, soils often have undesirable properties from the engineering perspective of a proposed structure. Compared to the drawn-out process of soil formation, the present form of soil investigation for engineering purposes only dates from centuries ago. According to Mayniel (1808) and Clayton et al. (1982), Bullet is one of the first to realize the importance of soil investigation for the foundations of earth-supporting structures in 1691. Trial holes were normally used to evaluate different layers of soils beneath a structure, while in case trial holes could not be made, "beating" the soil with a rafter was used alternatively by checking the sound and the penetration.

Modern soil investigation tools generally consist of geophysical methods, reconstituted/undisturbed sampling, and in situ testing. Geophysical methods such as the surface wave methods provide a spatial three-dimensional or two-dimensional picture in large areas while evaluation of mechanical behaviors of the soils still heavily rely on the methods of reconstituted/undisturbed sampling and in situ testing. Mitchell et al. (1978) foresaw the increasing need of in situ testing and pointed out the following reasons for using in situ testing over sampling:

1. To determine properties of soils, such as continental shelf and seafloor sediments and sands, that cannot be easily sampled in the undisturbed state;

2. To avoid some of the difficulties of laboratory testing, such as sample disturbance and the proper simulation of in situ stresses, temperature

and chemical and biological environments;

3. To test a volume of soil larger than that can conveniently be tested in the laboratory;

4. To increase the cost-effectiveness of an exploration and testing programme.

Note that the disturbance in sampling is de facto inevitable, so in reality samples disturbed to minor degrees are designated as undisturbed samples. The advantage of sampling is to allow laboratory testing of the soils with well-defined boundaries for the elemental soil properties. With the exception of the self-boring pressuremeter tests (SBPMT), this is impossible with in situ tests which have too complex boundary value problems to assess the stress-strain relations of the soils. Nevertheless, these difficulties do not remove the need of in situ testing for the sake of several aspects: (a) they can be done relatively quickly as compared with laboratory tests, (b) results are available immediately, (c) large numbers of data are obtained, and (d) vertical and lateral variability can be assessed over the site (Mayne et al. 2009).

A good number of in situ devices have been invented over the past century while only a few gained acceptance as routine testing tools worldwide, such as the standard penetration test (SPT), the cone penetration test (CPT), and the flat dilatometer test (DMT) (Robertson 2012). Specifically, the SPT involves a sample tube being driven into the ground by blows from a slide hammer; the CPT and the DMT both require a hydraulic penetration system to push the cone and the flat blade into the ground at a controlled rate, respectively.

Despite that the SPT's reliance on counting the number of hammer blows to drive a sample tube into the ground to estimate every soil parameter has been increasingly known as crude and unreliable, it is still frequently used in some parts of the world due to its low cost, the possibilities of soil samples, and the fact the direct-push tests, such as the DMT and the CPT, are not locally available. The CPT and the DMT are normally considered self-standing for the soil investigation, which consists of pushing a cone and a flat blade into the ground, respectively. Compared to the CPT, the DMT has an additional loading stage using a flexible membrane located on one side of the blade at the desired testing depth. Mayne (2006) suggests that a combined use of both is a nice complement in defining general geo-stratigraphy.

The DMT is a simple, reliable, and robust soil investigation tool, and it is necessary to recognize the Marchetti's pioneering efforts in underpinning all

the subsequent works on this subject as a framework (Marchetti 1975; Marchetti 1980; Marchetti et al. 2001; Marchetti 2015). Schnaid (2008) foresaw a growing trend in favor of the use of a range of sensors incorporated within a single penetration probe. In general, instrumentation of the probe offers good opportunities for a better interpretation, although, complexity introduced by instrumentation may present challenges in probe development and even degrade probe robustness and the reliableness of the test results. Although the DMT is an easy-to-use soil investigation tool, various soil parameters are derived via a number of correlations based on only two or three pressure measurements at a single testing depth. It is reasonable to expect more measurements of the soil response can enable a better understanding or even a better interpretation of the soil parameters. With the rapid advancement in the manufacturing and electronics industry, it is feasible to have such more measurements by redesigning the probe and adding more sensors inside. This thesis aims to first identify a development route with scientific added values and practical advantages, based on an extensive literature review. Then, prototypes shall be built and tested in an iterative development process to allow in situ tests with these measurements by means of novel manufacturing techniques such as (metal) 3D printing and instrumentation system such as LabVIEW. Finally, following a good validation by comparing with the DMT and the CPT, the newly developed test is expected to improve the interpretation of soil parameters as well as opens the way for further development of more advanced testing procedure and interpretation methods.

1.1 Outline of this thesis

Chapter 2 looks into the state of the art on the DMT, the modified DMT, and the DMT-CPT relationships. The first two sections explore the main findings of the DMT, upon which the review of the modified DMT discussed in Section 2.3 provides not only a qualitative description of the prior devices but also a data analysis to identify possible problems. In the light of this analysis, Section 2.4 investigates the possible influence of the stress relief phenomenon on the test results.

Chapter 3 presents a laboratory prototype of the iDMT. The details of the methodologies and the results in the prototype development and calibrations are discussed, followed by a simple calibration chamber test.

Chapter 4 presents the iDMT apparatus and the test procedure based on

the iterative designs through prototyping. The rationales behind the design and the test procedures are discussed in details. This chapter can be regarded as a self-standing manual for the iDMT.

Given the insights obtained in the review and the observation of the test results, Chapter 5 attempts to interpret the iDMT results. Section 5.3 proposes an analytical approach to estimate the iDMT contact pressure p_c. Section 5.4 presents a numerical investigation on the piston expansion, from which the iDMT equivalent "p_1" pressure can be found. Based on the proposed approaches, the results of an in situ testing campaign using the iDMT, the DMT, and the CPT are analyzed and discussed to evaluate the capabilities of the iDMT in estimating soil parameters.

Chapter 6 summarizes the contributions made by the previous chapters and the recommendations for future work.

Chapter 2

The flat dilatometer test (DMT)

The flat dilatometer test (DMT) was designed and developed by Marchetti in Italy. The original articles published by Marchetti (1975) and Marchetti (1980) provide a detailed description of the test and a series of empirical correlations between test results and common geotechnical parameters based on the data from over 40 sites. Following this pioneering work and experience mainly gained in North America and Europe, a comprehensive study of the DMT was covered in a report for Technical Committee 16, ISSMGE (Marchetti et al. 2001). Recently, a report in the DMT'15 conference covering a number of significant findings and practical developments in the period of 2001 to 2015 was published to complement the previous TC 16 report (Marchetti 2015). These three key papers are not only "milestones" in reviewing the literature but also underpin the further development of both technical aspects and theoretical understandings.

This chapter presents the state of art of the DMT by reviewing research findings from Silvano Marchetti as well as many other researchers who delve into soil investigation not only using the flat dilatometer but also the modified dilatometers.

2.1 Apparatus and operative aspects

2.1.1 The DMT equipment components

General description

In addition to the field equipment required during the dilatometer blade installation, such as the push rods for transferring the thrust from the penetrometer

as shown in Fig. 2.1(c) to the dilatometer blade, the DMT apparatus comprises five main components:

- Dilatometer blade
- Control Unit
- Pneumatic-electrical cable
- Gas pressure source
- Electrical ground cable

(a) (b) (c)

Figure 2.1: (a) main DMT equipment components excluding the penetrometer and the push rods (reprinted from Marchetti et al. (2001)), (b) the DMT blade (reprinted from Marchetti et al. (2001)), and (c) the truck-based penetrometer pusher with 200-kN capacity

These components are shown in Fig. 2.1(a,b). The dilatometer blade is made of stainless steel and has a circular, expandable, flexible membrane on one side. During the tests, the membrane can be expanded by means of internal gas pressure supplied by the gas pressure source (normally a gas tank). The gas pressure is manually regulated by a control unit equipped with a pressure regulator, pressure gage(s) and vent valves.

In terms of measuring system, an electrical circuit consisting of the dilatometer blade, electrical ground cable, pneumatic-electrical cable, and an audio signal in the control unit is used to indicate two fixed displacement levels of the membrane center: 0.05 mm and 1.1 mm, and the corresponding instants to read the pressure values from the pressure gage(s) by eye.

The dilatometer blade and its working principle

Concerning the nominal size, the dilatometer blade is 95 mm in width, 15 mm in thickness and 50 mm in length of the lower tapered section of the tip. With a cutting edge at the end of the blade tip, the dilatometer blade can be directly pushed to penetrate the soil by a thrust safely up to 250 kN.

The standard circular flexible membrane is 60 mm in diameter and 0.20 mm in thickness, though a thicker membrane may be used in case of membrane tears in certain soils like glacial tills. Note that in the early days there were also thinner membranes used, having 0.1 mm in thickness, which results in less influence from the stiffness of the membrane. Nevertheless, this type of thin membranes was eventually abandoned due to a higher risk of damage. The flexible steel membrane is expandable by applying internal pressure and can return to its original position by de-pressurization after reaching a central displacement of 1.1 mm. Therefore, it is important to mention that the flexible membrane is not ideally flexible as it is fixed around its edges and considering its thickness, inflexibility to some extent is reasonably expected near the edges. The cavity in the soil, as a result of the membrane expansion, is of an approximate spherical-cap shape. The contact area between the membrane and the soil is de facto smaller than a circle with a diameter of 60 mm. Additionally, note that over-inflating the membrane beyond 1.1 mm of center displacement can cause the loss of flexibility, and the membrane will not come back to its original position without suction in free air.

In principle, the dilatometer blade works as an electric switch by means of membrane movement. In Fig. 2.2, this working principle is illustrated when this "switch" is off as the membrane is in an intermediate position. This "switch" is on under either of the following circumstances:

- the membrane rests against the feeler at the top of the sensing disk,
- the membrane moves outward by 1.1 mm at its center, which enables the contact between the stainless steel cylinder and the sensing disk.

Meanwhile, an audio buzzer signal and a galvanometer signal are activated under both conditions to remind the operator of taking the corresponding pressure readings.

Given a normal order of the testing steps, the membrane is in contact with the sensing disk as soon as soil pressure applies externally, typically within 20 to 40 cm below the ground surface. Then, by increasing the internal pressure

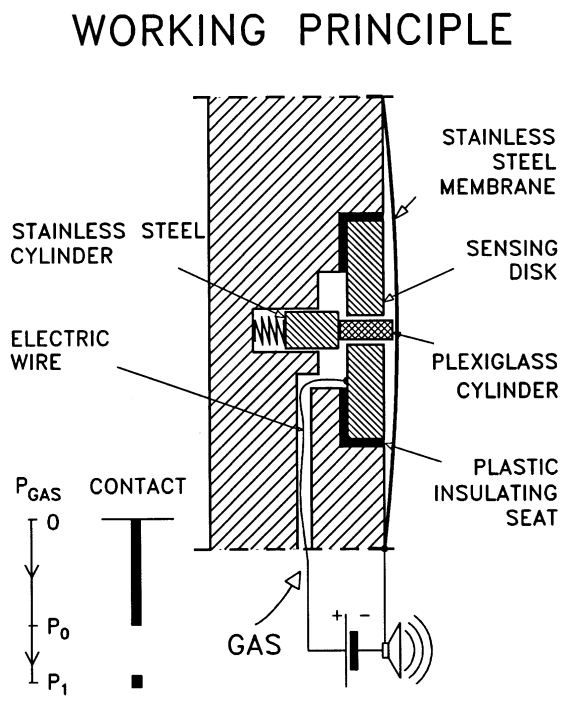

Figure 2.2: The dilatometer blade working principle (reprinted from Marchetti et al. (2001))

to counterbalance the external soil pressure, the membrane initiates its expansion, losing the contact with the sensing disk. This leads to the loss of electrical continuity and prompts the operator to read the A-pressure. The membrane is thus in an intermediate position until the central displacement reaches 1.1 mm when the stainless steel cylinder is in contact with the sensing disk. This reactivates electrical continuity to prompt the operator to read the B-pressure at 1.1 mm displacement. Note that the contact between the membrane and the sensing disk consists of a feeler with a nominal elevation of 0.05 mm above the surface of the sensing disk, so the central displacements of the membrane are 0.05 mm and 1.1 mm at the instants losing/gaining the contact.

Using such a '"switch" principle, the movement of the membrane is indicated at two central displacement levels and pressures are read by the pressure gage(s) in the control unit at the ground surface. Therefore even without any instrument inside the dilatometer blade, the DMT can provide a displacement controlled test.

(a) (b)

Figure 2.3: Apparatus: (a) the standard control unit; (b) the new control unit with automated data acquisition (photo courtesy of Diego Marchetti)

The control Unit

The control unit, as shown in Fig. 2.3(a), typically consists of valves to control gas flow and vent the system, single/dual pressure gage(s), quick connects to pressure source (normally a gas tank) and the pneumatic-electrical cable, an electrical ground cable connection, an audio buzzer signal and a galvanometer signal which can be activated by the circuitry constituted by the dilatometer blade.

In terms of gas flow and pressure control, the control unit employs four valves: main valve, micrometer flow valve, toggle vent valve, slow vent valve. The main valve is used as a positive shut-off between the gas source and the control unit. To manually control the rate of flow during the test, the micrometer flow valve is normally used rather than the main valve. The toggle vent valve can quickly vent the system pressure to the atmosphere. The slow vent valve allows the operator to vent the system slowly enough for taking an optional pressure reading during the deflation (*C*-pressure). Although this manual control unit is prevalent, a new control unit with automated data acquisition has been developed recently as shown in Fig. 2.3(b).

2.1.2 Test procedure

Preliminary checks prior to testing

ASTM Standard D6635-15 (2015) suggests that the dilatometer blade used for in situ testing shall firstly be in good visual external condition, namely, a clearance less than 0.5 mm under a 150 mm straight edge placed along the blade parallel to its axis, and a deviation less than 2 mm from the penetrating edge to the axis of the rods.

The pneumatic-electrical (p-e) cable should be threaded through a suitable number of push rods and the adapter prior to testing. Contamination of the p-e cable should be prevented with the caps on the cable ends. To check any leak in the cable or the control unit, p-e cable and the pressure source are attached to the control unit, then set the pressure regulator of the pressure source to about 3 MPa (4-6 MPa suggested by ASTM Standard D6635-15 (2015)). With the flow control valves closed, any pressure drop observed in the gage would indicate a leak in either the control unit or the p-e cable.

To check the circuitry, the other end of the p-e cable shall be connected to the dilatometer blade, the ends of the electrical ground cable are connected to the control unit and the dilatometer blade. With the center of the membrane gently pressed down, activation of the electrical/audio signal would indicate the circuitry is okay.

Membrane stiffness calibration

Marchetti et al. (2001) pointed out that the membrane stiffness calibration is not, strictly speaking, a calibration but a tare determination. Because the flexible steel membrane is fixed around its edges, pressures are required to overcome membrane stiffness to reach the two prefixed displacements at the membrane center, namely, A position at 0.05 mm and B position at 1.10 mm. Note that the neutral position of the flexible membrane is between A position and B position, correspondingly, ΔA and ΔB are defined and recorded as the positive pressures for overcoming the membrane stiffness in the air, though the negative pressure is, in fact, required to pull back the membrane to the A position.

To obtain ΔA and ΔB, a syringe is used to manually generate a positive or negative pressure. Specifically, the negative pressure is generated by quickly pulling back the syringe and holding for sufficient time (at least 5 s) to al-

low equalization, then the syringe piston is slowly released and ΔA on the low-range gage is read at the instant that the electric (buzzer or galvanometer) signal is stopped. Using the same syringe, positive pressure is generated by slowly pushing the piston into the syringe and ΔB on the low-range gage is read at the instant that the electric (buzzer or galvanometer) signal is reactivated. Eurocode7 (1997) suggested acceptable values of ΔA and ΔB are in the following ranges: 5kPa $\leqslant \Delta A \leqslant$ 30kPa and 5kPa $\leqslant \Delta B \leqslant$ 80kPa.

Furthermore, the determination of ΔA and ΔB are necessarily conducted immediately prior to a sounding, and immediately following a sounding. ASTM Standard D6635-15 (2015) suggested that if the final values of ΔA and ΔB differ from the initial values by an amount significant to the interpretation of the data, then the equipment shall be replaced/repaired and the sounding shall be repeated.

The DMT test

The DMT test generally comprises two stages: dilatometer blade installation via quasi-static push at a constant rate; and then a sequence of pressure readings at prescribed displacements during the membrane movement, based on the "switch" mechanism mentioned in Section 2.1.1. Although the general procedure is almost identical in different standard testing methods (Marchetti et al. 2001; ASTM Standard D6635-15 2015; Eurocode7 1997), the specific time requirements in each step can be different. A comparison of the specific time requirements in each step is provided in Table 2.1. The general descriptions of the DMT testing procedures are given as follows:

1. There are four gas valves used during the DMT field operation. The micrometer flow valve, the toggle vent valve and the slow vent value are regulated by the DMT operator for different purposes in the following steps. The main valve remains open during the whole test since it is a switch between the gas source and the blade control system.

2. With both of the vent valves open and the micrometer flow valve closed, the blade should be advanced vertically by means of quasi-static push at a constant rate to the desired test depth. The electrical/audio signal may start at 20 to 40 cm below ground surface as the membrane is pressed flush against the feeler by the soil pressure. After reaching the desired test depth, immediately unload any thrust on the push rods.

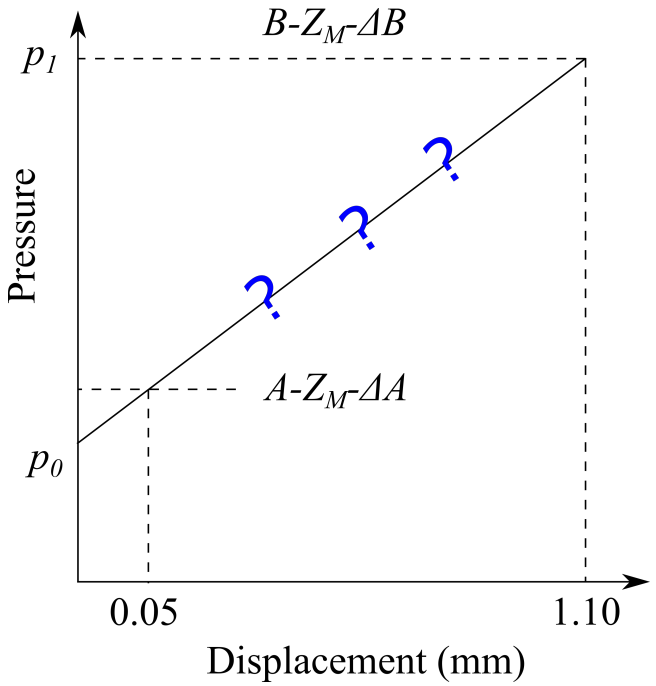

Figure 2.4: p_0 estimation via the linear extrapolation

3. Following the end of the dilatometer blade installation, the operator closes the vent valves and slowly opens the micrometer flow valve to pressurize the membrane. The gage pressure at the instant the electrical/audio signal stops (0.05 mm central membrane displacement) is recorded as the *A*-pressure reading, as shown in Fig. 2.4.

4. Without stopping the pressurization, the expansion of the membrane continues until the signal returns (1.1 mm central membrane displacement). The gage pressure at this instant is *B*-pressure reading.

5. If an optional pressure reading during the deflation (*C*-pressure) is not to be taken, the operator shall immediately open the toggle vent valve to quickly de-pressurize the membrane and close the micrometer flow valve to stop gas flow. Then he/she may advance the dilatometer blade one depth increment deeper or withdraw the dilatometer blade if it is at the end of the sounding.

6. If the *C*-pressure is to be taken, a well-controlled de-pressurization process using the slow vent valve rather the much faster toggle vent valve shall be conducted. At the instant the signal returns (0.05 mm central membrane displacement), the gage pressure is recorded as the *C*-pressure reading. Note that a fast de-pressurization may fail the soil in front of the

membrane and yield a poor reading.

Once the field pressure readings are taken during the DMT tests, proper corrections are necessary for membrane stiffness, gage zero effect and feeler pin elevation. The corrected pressures p_0 and p_1 are thus given as follows:

$$p_0 = 1.05(A - Z_M + \Delta A) - 0.05(B - Z_M - \Delta B) \tag{2.1}$$

$$p_1 = B - Z_M - \Delta B \tag{2.2}$$

where ΔA and ΔB = membrane stiffness corrections determined by membrane calibration, Z_M = gage reading when vented to atmosphere, and $Z_m = 0$ if both calibration and DMT readings are taken with the same gage.

It is important to note that the "contact pressure" p_0 is, in actuality, not measured at the instant of contact but obtained via the linear extrapolation illustrated in Fig. 2.4, given the nominal elevation of the feeler pin as 0.05 mm above the sensing disc. Marchetti and Crapps (1981) explained that the use of the feeler pin is to improve the definition of the instant when the electrical continuity is interrupted. However, this requires an assumption of the linear pressure-displacement relationship for the soil response during the membrane expansion. It is impossible to check the validity of this assumption using a DMT that has no instruments for recording a complete pressure-displacement curve.

The dissipation test

In the DMT test, pore-water pressures cannot be directly measured. Yet in low permeability soils (such as clays and silts), the time required for the dissipation of the blade-penetration induced excess pore-water pressure is significantly longer than that for the DMT test. This difference enables the estimation of in situ horizontal consolidation parameters by means of the A-method dissipation test or the A_2-method dissipation test.

The A-method dissipation test requires a timed sequence of A-pressure reading at the desired test depth. Specifically, the steps of this method are shown below:

1. Halt the dilatometer blade penetration at the desired test depth, release the thrust and start a stopwatch. Then, immediately, pressurize the membrane to obtain the A-pressure reading and read the elapsed time at the

Table 2.1: Comparison of the DMT testing rates required in each step

Procedure	TC16 report, ISSMGE by Marchetti et al. (2001)	ASTM Standard D6635-15 (2015)	Eurocode7 (1997)	ISO standard 22476-11:2017(E) (2017)
Blade advancement speed	20 mm/sec	10 to 30 mm/sec	10 to 30 mm/sec	10 to 30 mm/sec
Depth increment	100 to 200 mm	150 to 300 mm	150 to 300 mm	100 to 200 mm
A-pressure reading	about 15 s	within 15 to 30 s	less than 20 s	within approx. 15 s
B-pressure reading	about 15 to 20 s	within 15 to 30 s§	less than 20 s	within approx. 15 s
C-pressure reading	45 to 60 s	15 to 30 s	null	approximately 30 s
Each complete test sequence⁕	35 to 45 s	35 to 90 s	about 1 minute	33 to 50 s

note: each timer starts at the end of the previous step, except §.

⁕: 1-increment dilatometer penetration + *A*-*B* membrane expansion + immediate deflation.

§: the *B*-pressure reading should be obtained 15 to 30 seconds after beginning the gas flow.

instant of the A-pressure. Once the recording is complete, vent the system preventing further membrane expansion.

2. Repeat this membrane pressurization and de-pressurization step to take a timed sequence of A-pressure readings for the time-dissipation curve. The time interval between two successive A-pressure readings is normally increased by a factor of two.

3. As soon as it is convenient in the field, plot the *A-log t* diagram which normally assumes a sigmoid shape. The dissipation test can be stopped when the inflection point can be clearly identified from the *A-log t* diagram. The time at the point of inflection T_{flex} is then used to interpret the coefficient of consolidation in the horizontal direction.

Compared with the *A-method* dissipation tests measuring the total stress against the blade, the A_2*-method* dissipation test attempts to measure the pore-water pressure directly and interprets soil horizontal consolidation parameters based on the time-dissipation curve. This method assumes that a complete DMT test (A-B-C pressure readings) opens an elliptical cavity adjacent to the membrane, then the following timed sequence of A-pressure readings are a measure of the pore-water pressure in this cavity. The specific steps are given as follow:

1. Unload the thrust once the desired test depth is reached and start a stop-watch. Then, immediately perform a complete DMT test and note that the C-pressure reading of this test is the first point of the dissipation curve.

2. Immediately re-pressurize the membrane to obtain an A-pressure reading, and then vent the system to prevent further membrane expansion. Repeat this process to get an additional timed sequence of A-pressure readings. The time interval between two successive A-pressure readings is normally increased by a factor of two.

3. As soon as it is convenient in the field, plot the A-$\sqrt{t}$ diagram until having sufficient data points to determine A_{50} at 50% dissipation. Then t_{50}, the time corresponding to A_{50}, is used to interpret soil horizontal consolidation parameters.

However, the assumption of saturation of the soils along with the pore water filled in the membrane-opened cavity cannot be checked by any means

in the DMT. Thus a more accurate approach by directly measuring the pore-water pressure is considered favorable.

2.2 Interpretation of the test results

2.2.1 The DMT Indices

The starting point of the interpretation of the DMT is to identify three "intermediate" DMT indices, namely, material index I_D, horizontal stress index K_D and dilatometer modulus E_D.

Material index I_D and soil type identification

The material index is the ratio of a pressure increment $(p_1 - p_0)$ to the horizontal effective stress $(p_0 - u_0)$:

$$I_D = \frac{p_1 - p_0}{p_0 - u_0} \tag{2.3}$$

where u_0 is the pre-insertion in situ pore-water pressure.

According to Marchetti (1980), I_D is mainly used to indicate soil type as follows:

clay	$I_D < 0.6$
silt	$0.6 < I_D < 1.8$
sand	$I_D > 1.8$

It is important to note that the soil type identification based on I_D is different from common soil classification systems based on physical (textural) characteristics such as grain size and plasticity. So one may get confused about the descriptive terms such as sand, silt, and clay in the I_D-based system since it de facto reflects the mechanic behavior of soils rather than the textural characteristics. Moreover, the I_D-based soil type identification is resemblant to the CPT-based soil behavior type (SBT) classification system which has been increasingly used in recent years (Robertson 2016; Robertson 1990).

Horizontal stress index K_D

The horizontal stress index K_D can be regarded as the coefficient of earth pressure at rest K_0 amplified by the dilatometer penetration (Marchetti et al. 2001).

It is essentially the horizontal effective stress $(p_0 - u_0)$ normalized by the pre-insertion in situ vertical stress σ'_{v0}:

$$K_D = \frac{p_0 - u_0}{\sigma'^{i}_{v0}} \tag{2.4}$$

where $i = 1$.

Marchetti (2015) points out one advantage of the DMT K_D over the CPT parameters is that the normalization exponent i for K_D is equal to 1 while the normalized cone tip resistance requires i = 0.5 to 1, thus the estimation of an additional unknown soil variable i depending on soil type and in situ state is avoided. This can be justified by a much higher linearity of p_0 with testing depth (mean effective stress) compared with that of the CPT cone resistance. The non-linear relationship between the CPT cone resistance and testing depth (mean effective stress) is due to the arching phenomenon resulting from the cone penetration (Hughes and Robertson 1985). In contrast, the dilatometer having a rectangular cross section with an aspect ratio = 95/15 ≈ 6.3 produces much less arching effects than the circular-cross-section cone.

Dilatometer modulus E_D

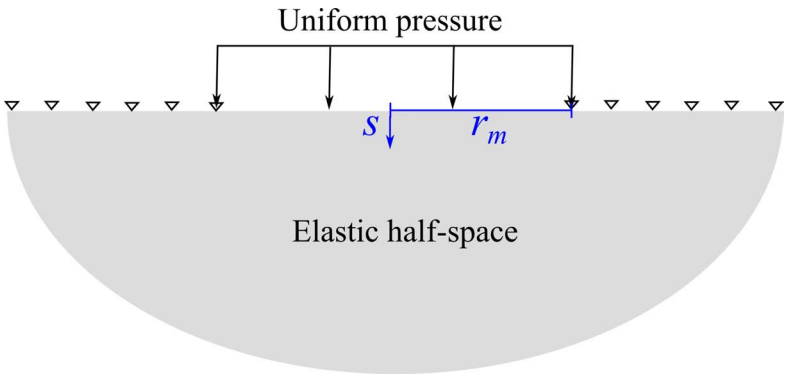

Figure 2.5: Modelling the dilatomter membrane expansion

With the pressure difference $\Delta p = p_1 - p_0$ computed from the DMT, Marchetti (1980) derives a modulus of elasticity of the soil from Δp using the analytical solution provided by Gravesen (1960). The assumption is that the space surrounding the dilatometer blade can be regarded as two elastic half-spaces in contact along the plane of symmetry of the blade. Fig. 2.5 shows this modeling of the dilatometer membrane expansion. Based on the solution provided by Gravesen (1960), the settlement calculation to this problem is given by:

$$s(r) = \frac{4}{\pi}(\frac{1-\nu^2}{E})(p_1 - p_0)r_m\sqrt{1-(\frac{r}{r_m})^2} \tag{2.5}$$

where $s(r)$ = settlement at radius r, r_m = radius of the loaded area, E = Young's modulus, ν = Poisson's ratio.

For the case of the DMT flexible membrane expansion, $s(r = 0)$ = 1.1 mm, r_m = 30 mm and the ratio $E/(1-\nu^2)$ is defined as the dilatometer modulus E_D. Then E_D is given by:

$$E_D = E/(1-\nu^2) = 34.7(p_1 - p_0) \tag{2.6}$$

It is important to note that this derivation for E_D assumes that there is a uniform stress applied to the soil by the flexible steel membrane in the DMT. However, the reality is that the membrane is circumferentially fixed on the blade, so that the membrane flexibility close to the circumference must be enormously reduced. Thus, this difference can only be taken into account in the empirical correlations related to E_D.

2.2.2 Soil unit weight

Marchetti and Crapps (1981) developed the chart, as shown in Fig. 2.6 to roughly estimate soil unit weight based on the I_D and E_D values. The lines A, B, C, and D in Fig. 2.6 are given by:

$$E_D = 10^{n+m\log I_D} \tag{2.7}$$

where n and m are give in Table 2.2.

Table 2.2: Coefficients of the lines to determine soil unit weight

	m	n
A	0.585	1.737
B	0.621	2.013
C	0.657	2.289
D	0.694	2.564

In addition, Ouyang and Mayne (2016) developed an empirical expression relating soil unit weight with the DMT parameters for soft to firm inorganic clays (normally consolidated (NC) to lightly overconsolidated (LOC)

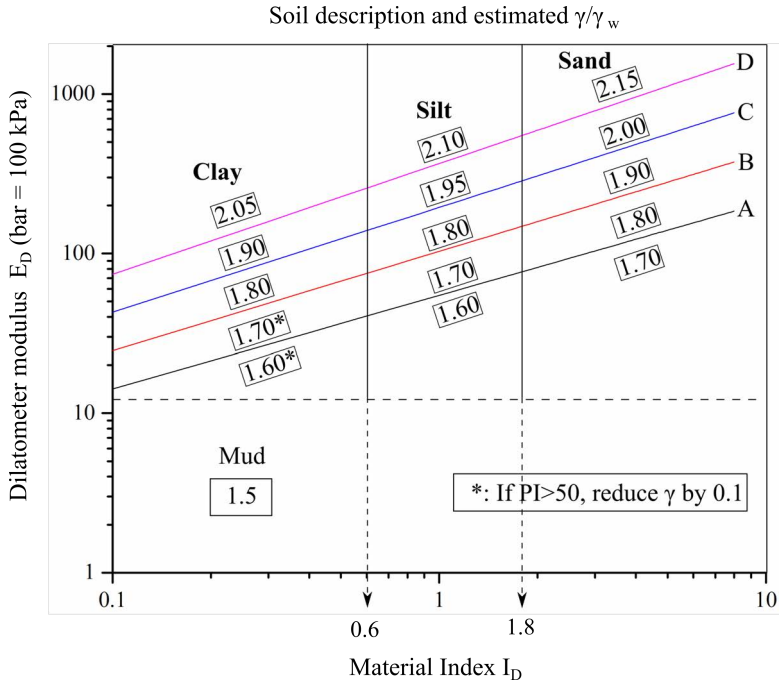

Figure 2.6: DMT chart for soil unit weight estimation (after Marchetti and Crapps (1981))

soils) based on the DMT data and the lab data from undisturbed samples on 31 clays.

$$\gamma_t = \gamma_w + 0.22 m_{p0} \tag{2.8}$$

where γ_t = the soil total unit weight, γ_w = the unit weight of water, and m_{p0} is defined as follow (intercept = 0):

$$m_{p0} = \frac{\Delta p_0}{\Delta z} \tag{2.9}$$

where p_0 = the DMT contact pressure and z = the test depth.

Concerning only soft to firm inorganic clays, this approach may show more accurate estimation for these clays than using the rough estimation based on Fig. 2.6.

2.2.3 Soil stiffness

Generally, stiffness is the gradient of the stress-strain line of a loaded and deformed material. In terms of a soil, this stress-strain line may be linear, then soil stiffness can be easily determined as the slope of the stress-strain line. Nevertheless, the stress-strain line is more likely to be non-linear in common

geotechnical problems (Atkinson 2000), thus soil stiffness needs to be described either as a secant modulus or a tangent modulus which may be given by:

$$\text{tangent stiffness} = \frac{d\sigma}{d\epsilon} \tag{2.10}$$

$$\text{secant stiffness} = \frac{\Delta\sigma}{\Delta\epsilon} \tag{2.11}$$

where σ = stress and ϵ = strain.

Furthermore, soil stiffness is a complicated phenomenon and dependent on stress history, strain level in the soil, stress level in the soil, drainage characteristics and so on. Thus, any single stiffness related soil parameter must be defined under certain conditions. For example, it is common to address stiffness of the soil skeleton in the presence of pore-water pressure in the voids of the soil skeleton, using effective stress $\sigma^{'}$ discovered by Terzaghi (1936) and given by:

$$\sigma^{'} = \sigma - u \tag{2.12}$$

where u is the pore-water pressure.

The membrane expansion during the DMT testing competes against a resistance of the surrounding soils. Thus, E_D is essentially a secant horizontal cavity expansion elastic modulus as pressure measurements are made at two fixed displacement levels. To use E_D in geotechnical applications, many attempts have been done to determine the correlation with various typical stiffness related parameters such as one-dimensional drained tangent modulus M, secant modulus at 50% strength in drained triaxial testing ($E^{'}_{50}$), unload-reload modulus ($E^{'}_{ur}$), initial shear modulus (G_0) and recently in situ stiffness decay curve ($G - \gamma$ curve, γ = shear strain). These stiffness-related parameters are key to the solutions when investigating and/or modeling stress related deformations in geotechnical problems (Cox and Mayne 2015).

Constrained modulus M_{DMT}

The one-dimensional (vertical) drained tangent modulus M has been correlated to E_D with the correction factor R_M which is in function of I_D and K_D (Marchetti 1980). The difference of many aspects between M and E_D are only taken into account in the single correction factor R_M, such as the vertical loading direction of M versus the horizontal loading direction of E_D; the drained condition of M versus the undrained condition of E_D in clays; and the stress information contained in M but not in E_D. In consequence, the resulted corre-

lation is purely empirical and the DMT determined one-dimensional (vertical) drained tangent modulus M_{DMT} is given by:

$$M_{DMT} = R_M E_D \tag{2.13}$$

$$R_M = \begin{cases} 0.14 + 2.35 \log K_D, & \text{if } I_D \leqslant 0.6 \\ 0.5 + 2 \log K_D, & \text{if } I_D \geqslant 3 \\ R_{M,0} + (2.5 - R_{M.0}) \log K_D, & \text{if } 0.6 \leqslant I_D \leqslant 3 \\ & \text{where } R_{M,0} = 0.32 + 2.18 \log K_D \\ 0.32 + 2.18 \log K_D, & \text{if } K_D \geqslant 10 \\ 0.85, & \text{if } R_M \leqslant 0.85 \end{cases}$$

Despite the recognition of the empirical nature of the correlation, M_{DMT} is generally found to be consistence with M from high-quality oedometer tests (Lacasse 1986; Iwasaki et al. 1991). In sands, recovering undisturbed samples and estimating soil compressibility are difficult and involves huge expense, so a comparison is more commonly made in terms of predicted settlement versus measured settlements. The one-dimensional settlement calculation formula is given by:

$$S_{1-DMT} = \sum \frac{\Delta \sigma_v}{M_{DMT}} \Delta z \tag{2.14}$$

where the vertical stress increment $\Delta \sigma_v$ is given by Boussinesq's solution (Boussinesq 1885).

Note that Eq. 2.14 is recommended by Marchetti et al. (2001) to predict the settlement in sands as well as the primary settlement in clays. Positive and convincing findings based on the DMT-predicted settlement have been reported by Schmertmann (1986), Monaco et al. (2006), and Failmezger (2015) in different soils.

One may express his or her doubts on the high accuracy of the DMT settlement prediction as important factors such as the loading direction is different between the DMT test and the engineering applications (e.g.: the shallow foundation) and thus have to be considered empirically. Marchetti (2015) argued that the main point of using the DMT for settlement prediction is the use of K_D which can take stress history information into account. The in situ stress

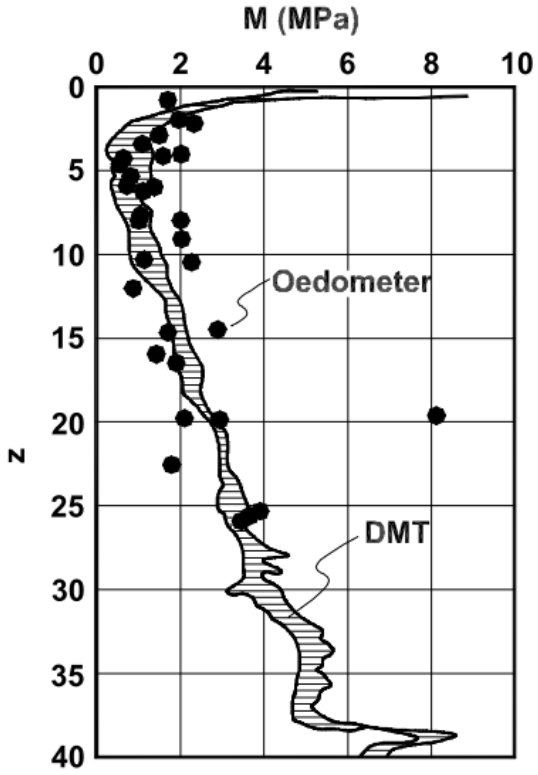

Figure 2.7: Comparison between M determined by DMT and by high-quality oedometers, Onsøy clay, Norway, reprinted from Lacasse (1986)

history is indispensable in these calculations and not many alternatives of K_D for interpreting the soil stress history are available.

Lacasse (1986) compared the constrained modulus M_{DMT} from the DMT and the high-quality oedometer tests in Onsøy clay in Norway, which indicates very good agreement, as shown in Fig. 2.7.

In situ stiffness decay ($G - \gamma$) curve

The initial small strain modulus G_0 is given by:

$$G = \rho V_S^2 \tag{2.15}$$

where $\rho =$ total soil mass density and $V_S =$ shear wave velocity.

Using elasticity, the "operative shear modulus" at working strain G_{DMT} can be given by:

$$G_{DMT} = \frac{1-2\nu}{2(1-\nu)} M_{DMT} \tag{2.16}$$

note that M_{DMT} is a drained modulus, thus $\nu = 0.5$ for undrained condition

cannot be used with Eq. 2.16.

Hardening-soil (H-S) model application via the DMT-based modulus

With M_{DMT} obtained from Eq. 2.13 and derivation based on elasticity, the drained Young's modulus is given by:

$$E^{'} = \frac{(1+\nu)(1-2\nu)}{1-\nu} M_{DMT} \tag{2.17}$$

if $\nu = 0.2$ for a soil, $E^{'} = 0.9 M_{DMT}$.

Nevertheless, in terms of stiffness parameters required in common geotechnical numerical modelings, at least two variants of Young's modulus are necessary to describe the non-linear stress-strain behavior of soils. If one has only the DMT data rather than lab triaxial testing data, Monaco and Marchetti (2004) and Schanz et al. (1999) presented a DMT-based approach using H-S model developed by Schanz and Vermeer (1998). Specifically, the secant modulus in drained triaxial testing for a mobilization of 50% the maximum shear strength $E^{'}_{50}$ and unload-reload modulus $E^{'}_{ur}$, as the two necessary stiffness parameters for the H-S model, can be approximately derived from M_{DMT} using the following expressions:

$$E^{'}_{50} \cong M_{DMT} \tag{2.18}$$

$$E^{'}_{ur} \cong 3 \text{ to } 4 M_{DMT} \tag{2.19}$$

Note that Eq. 2.18 shall have better accuracy than Eq. 2.19, since at least $E^{'}_{50}$ and M_{DMT} are both for primary loading stress path while $E^{'}_{ur}$ reflects the unloading and reloading stress path. Therefore, it is of great interest to improve the correlation for $E^{'}_{ur}$ via incorporating unloading and reloading stress path in an improved DMT testing approach which, however, requires equipment modification of the flat dilatometer.

2.2.4 Stress history

Sands

Marchetti (2015) pointed out that CPT alone or DMT alone is insufficient to estimate the stress history information in sands, namely the overconsolidation ratio (OCR) commonly defined as the ratio of the maximum past vertical stress

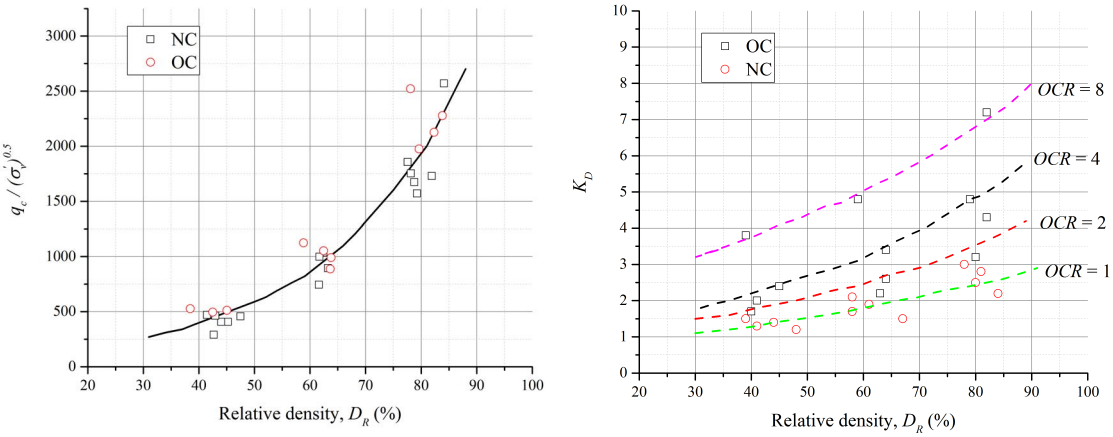

(a) Sensitivity of the CPT to OCR

(b) Sensitivity of the DMT to OCR

Figure 2.8: Comparison of the effects of stress history between the CPT and the DMT (NC = normally consolidated, OC = overconsolidated, after Lee et al. (2011))

to the present vertical effective stress. Lee et al. (2011) performed a series of CPTs and DMTs on Busan sand prepared in the calibration chamber, with the primary aim of investigating the effects of stress history. Fig. 2.8 shows the comparison of the effects of OCR and the effects of relative density (D_R). In a nutshell, the CPT cone resistance (normalized by $(\sigma_v')^{0.5}$) is mainly sensitive to D_R and insensitive to OCR while K_D reflects not only the effects of D_R but also the effects of OCR. This higher sensitivity to OCR of K_D has also been observed not only in the calibration chamber (Jamiolkowski and Lo Presti 1998) but also in the field (Marchetti 2010; Schmertmann 1986). Thus, a multi-parameter approach is required to estimate OCR in sands by separating the effects of D_R from the "mixed" soil response in the field testing.

Monaco et al. (2014) established an OCR $- M_{DMT}/q_c$ correlation based on the CPT and the DMT results before the construction of a trial embankment and after the removal of this embankment four years later. This correlation agrees with the guideline proposed by Marchetti et al. (2001) (M_{DMT}/q_c =5 to 10 in NC sands; M_{DMT}/q_c = 12-24 in OC sands) and is given by:

$$OCR = 0.0344(M_{DMT}/q_c)^2 - 0.4174(M_{DMT}/q_c) + 2.2914 \tag{2.20}$$

Clays

For uncemented cohesive soils ($I_D < 1.2$), Marchetti (1980) provided an empirical correlation relating OCR to K_D:

$$OCR = (0.5K_D)^{1.56} \tag{2.21}$$

Thus, for NC clays with OCR=1, K_D gives a value of 2, which has been confirmed in many genuinely NC (no cementation, aging, and structure) clay deposits (Marchetti et al. 2001). Additionally, Eq. 2.21 is supported by a parametric study by Finno (1993) based on strain path method for relatively low OCR values. Yu (2004) performed a finite-element validation of the K_D and the OCR relationship which indicates that Eq. 2.21 can be used with reasonable confidence in most conditions except when OCR > 8 . The numerical evaluation by Kouretzis et al. (2015) shows that the $K_D \approx 2.5$ for a NC estuarine clay and a fitting expression relating OCR to K_D is given by:

$$OCR = 0.58e^{0.23K_D} \tag{2.22}$$

The OCR estimated using this equation are found slightly smaller than that from Eq. 2.21 when $K_D < 10$.

Fig. 2.9 shows how well the OCR - K_D correlation from Marchetti (1980) fit with various experimental data. Although the correlation can stand for the general trend, scatter cannot be avoided at all. It is handy to use the correlation in practice, but caution shall be exercised to see that OCR can vary from 2 to 7 when $K_D \approx 7$.

Marchetti (2015) concluded that the OCR correlation has both "empirical" and "theoretical" roots. The lower bound K_D value for NC clays is about 2. If $K_D > 2$ is found in a geologically NC clay, it is reasonable to assume the existence of aging, structure or cementation. Furthermore, Bałachowski and Kurek (2015) confirms the high sensitivity of the DMT K_D index to the stress history in the interpretation of the DMT soundings in the pre-treated sand and the compacted sand using vibroflotation method in Gdynia port. Emad (2015) also points out that the DMT is more useful than the CPT for determining the overconsolidated nature of sandy soils compacted using the vibro compaction method at the Crescent of Palm Jumeirah in Dubai.

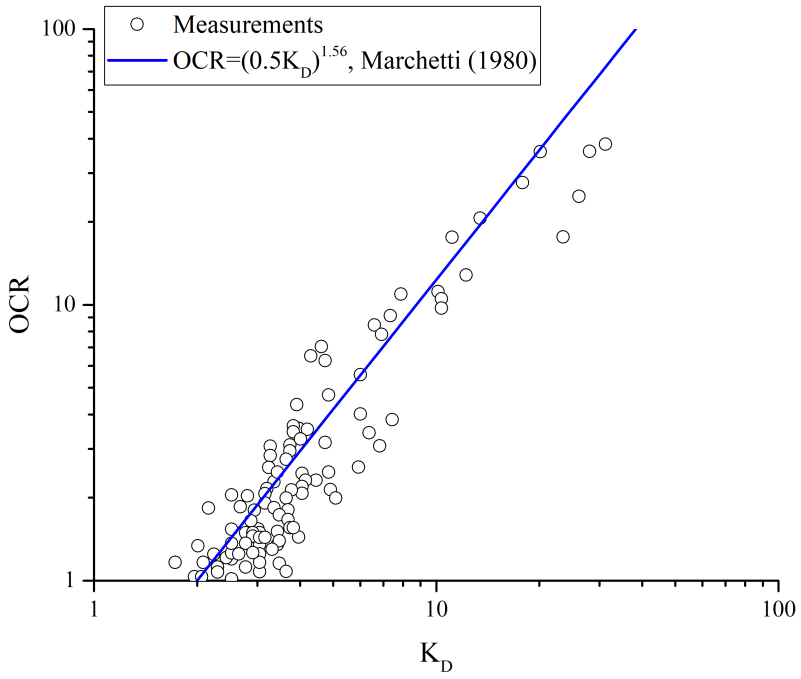

Figure 2.9: Correlations between OCR and K_D for clays with $I_D < 1.2$: experimental data from Marchetti (2015), Chang (1991), Lacasse and Lunne (1988), Mayne (1987), and Marchetti (1980), adapted from Marchetti (2015)

2.2.5 Undrained strength C_u

Once OCR is estimated out of K_D in cohesive soils, Marchetti (1980) proposed that undrained strength C_u can be estimated by the average value $(C_u/\sigma_v')_{NC} = 0.22$ provided by Mesri (1975) and the relationship between the normalized strengths of normally consolidated and overconsolidated clays and the OCR given by:

$$(\frac{C_u}{\sigma_v'}) = (\frac{C_u}{\sigma_v'})_{NC} \cdot OCR^m \tag{2.23}$$

where the average value of $m = 0.8$ is used for the simple shear strength of many clays (Ladd et al. 1977).

Thus, the following equation is derived by Marchetti (1980) for average "textbook" clays.

$$C_u = 0.22\sigma_{v0}'(0.5K_D)^{1.25} \tag{2.24}$$

Numerical studies performed by Yu (2004) and Finno (1993) and experimental results from other testing means presented by Powell and Quarterman (1988) and Lacasse and Lunne (1988) generally support this $C_u - K_D$ relationship.

Fig. 2.10 shows a comparison between C_u obtained from unconsolidated

undrained triaxial compression or unconfined compression test and C_u obtained by Eq. 2.24 using the DMT. Despite reasonable agreements between the observed values and the calculated values, it seems that the use of Eq. 2.24 may result in underestimation of C_u. This shall relate to the average value of $(C_u/\sigma'_v)_{NC}$ in Eq. 2.23, which suggests that a value higher than 0.22 for the Tokyo (Komatsugawa) site where Kamei and Iwasaki (1995) recovered the soil samples and performed the triaxial tests.

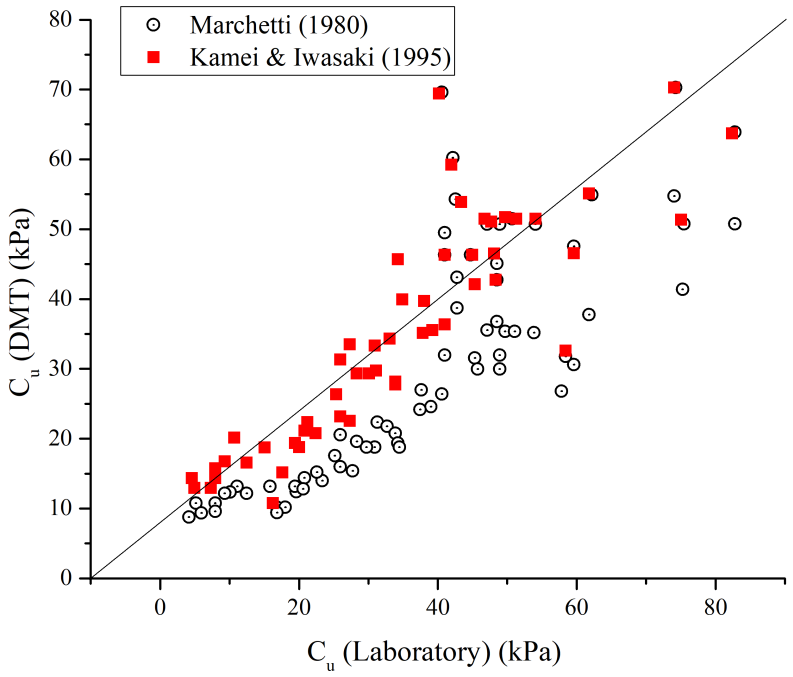

Figure 2.10: Comparison of undrained shear strength C_u from the DMT with the that from the triaxial tests, after Kamei and Iwasaki (1995)

2.2.6 K_0 in clays

Based on testing results on uncemented clays in Italy, an empirical formula between the coefficient of earth pressure at rest K_0 and the horizontal stress index K_D is proposed by Marchetti (1980) and given by:

$$K_0 = (\frac{K_D}{1.5})^{0.47} - 0.6 \tag{2.25}$$

Several attempts have been made to directly correlate K_0 and K_D as well, however, slight different correlations are found in local soils. Powell and Uglow (1988) performed a series of DMT tests in soft normally consolidated clays to heavily overconsolidated stiff clays in the UK. From geological point of view, a

significant difference is found between "young" clays (less than 70,000 years) and "old" clays (greater than 60 million years). An empirical correlation for "young" clays in the UK is presented by them as follow:

$$K_0 = 0.34 K_D^{0.55} \tag{2.26}$$

Similarly, Lacasse and Lunne (1988) and Larsson and Eskilson (1989) conducted a number of DMT tests in Norway and Sweden, respectively, and provided their local $K_0 - K_D$ correlation for Scandinavia's clays which are in a similar form with Eq. 2.25.

Taken these data of local experience into account, Kulhawy and Mayne (1990) proposed a general form for K_0:

$$K_0 = (\frac{K_D}{\beta_k})^{0.47} - 0.6 \tag{2.27}$$

where β_k depends upon soil type and geologic origin, such as $\beta_k = 1.5$ for insensitive clays (original Marchetti correlation); $\beta_k = 2$ for sensitive clays; $\beta_k = 0.9$ for fissured clays; $\beta_k = 3.0$ for glacial tills.

Other than using correlations of empirical nature, Yu et al. (1993) carried out a finite-element analysis using a linear elastic-perfectly plastic Tresca soil model. The numerical results show that $K_0 - K_D$ relationship is sensitive to the rigidity index of the soil R. Thus, although the numerically predicted K_0 and the K_D predicted values of K_0 are similar for some clays, it is possible to find a considerable difference between the two for some heavily overconsolidated soils such as London clay in the UK and Boom clay in Belgium.

Nevertheless, Marchetti et al. (2001) suggested that an approximate estimation of K_0 based on Eq. 2.25 may be sufficient in many geotechnical applications, considering the inherent difficulty of precisely measuring K_0. Fig. 2.11 from Burghignoli et al. (1991) compares K_0 from the DMT using Eq. 2.25 with the that from the self-boring pressuremeter test (SBPMT). Considering that the SBPMT is likely to be the in situ test with the least soil disturbance and the closest measurements of K_0, the slight underestimation of K_O using the DMT is still acceptable in geotechnical practice as said by Marchetti et al. (2001).

2.2.7 Friction angle and K_0 in sands

As a strength parameter, friction angle in sandy soils is of major interests as cohesion is normally negligible. In practice, it is a necessary input for the

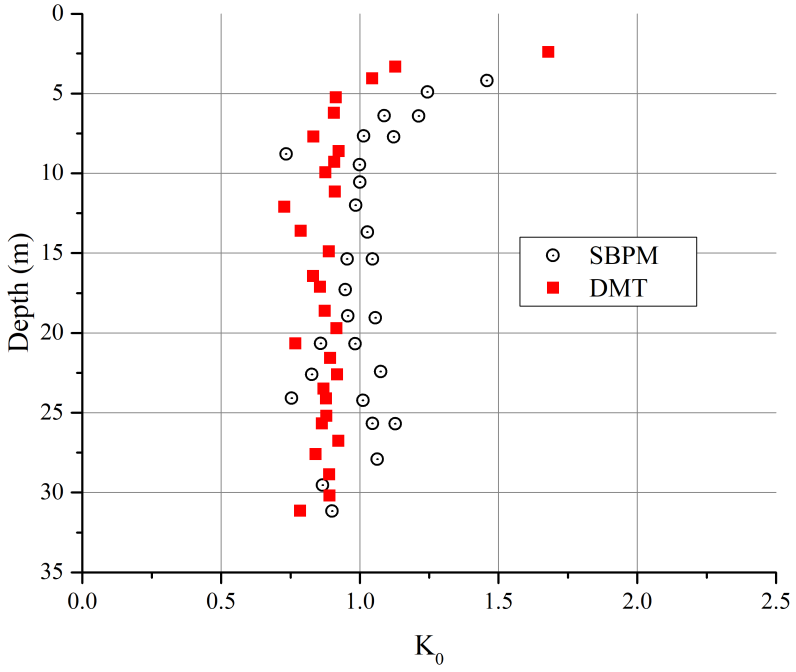

Figure 2.11: Comparison of K_0 from the DMT with the that from the self-boring pressuremeter test (SBPMT) in clays, after Burghignoli et al. (1991)

calculation of foundation bearing capacity, axial pile response and retaining wall. Normally in these practical problems, the dissipation rate of excess pore-water pressure, generated during the course of shearing, is much greater than the rate of loading. So the effective stress friction angle $\phi^{'}$ can be sought for the design from the DMT which also has drained soil behaviors during the test.

Derivation of K_0 and $\phi^{'}$ when thrust is measured during the DMT

Durgunoglu and Mitchell (1975) describes a theoretical solution (D&M theory) for rigid wedge penetration problem at shallow depth, for the study of Apollo lunar exploration program. Schmertmann (1982) and Schmertmann and Crapps (2016) uses this solution in an iterative way to find the plane strain effective friction angle $\phi^{'}_{ps}$ from a "known" K_D and the DMT blade penetration resistance q_D during the DMT penetration with a trial value of K_0, considering the width/thickness ratio of the dilatometer blade = 6.33. Specifically, with the plane strain effective friction angle $\phi^{'}_{ps}$ determined, the following equation is used to derive the equivalent axisymmetric effective friction angle $\phi^{'}_{as}$:

$$\phi^{'}_{as} = \frac{\phi^{'}_{ps} - (\phi^{'}_{ps} - 32^{\circ})}{3} \tag{2.28}$$

Knowing the ϕ'_{as}, it is possible to determine K_0 using the following equation based on the results of DMT and CPT in large triaxial chambers.

$$K_0 = \frac{40 + 23K_D - 86K_D(1 - \sin\phi'_{as}) + 152(1 - \sin\phi'_{as}) - 717(1 - \sin\phi'_{as})^2}{192 - 717(1 - \sin\phi'_{as})} \tag{2.29}$$

Then, we can compare the values of K_0 determined using Eq. 2.29 with the trivial value of K_0 in the first step to perform an iterative calculation until the two is approximately the same.

Derivation of K_0 and ϕ' when adjacent CPT data is available

If a parallel CPT data is available near the DMT test, one can also derive ϕ' based on the method of first deriving K_0 from K_D and q_c, then using the D&M theory proposed by Durgunoglu and Mitchell (1975) or its graphically equivalent means developed by (Marchetti 1985; Marchetti 1997). Note that the estimation of K_0 uses the following equation based on a number of calibration chamber tests in sands (Baldi et al. 1986).

$$K_0 = 0.376 + 0.095K_D + cq_c/\sigma'_{v0} \tag{2.30}$$

where $c = -0.005$ in "seasoned" sand, $c = -0.002$ in "freshly deposited" sand. Thus this empirical equation is only a rough estimation of K_0 and involves some subjectivity.

Fig. 2.12 shows the $q_c - K_0 - \phi'$ chart according to the D&M theory. Note that the lower bound and the upper bound of K_0 for each ϕ' line is given by the Rankine active stress coefficient ($K_A = (1 - \sin\phi')/(1 + \sin\phi')$) and the Rankine passive stress coefficient ($K_P = (1 + \sin\phi')/(1 - \sin\phi')$), respectively.

Derivation of ϕ' directly from the DMT

Campanella and Robertson (1991) provides an estimation of CPT cone resistance from the DMT K_D based on data of parallel CPT-DMT tests in the calibration chamber testing and in the field testing. The average of this relationship is given as:

$$\frac{q_c}{\sigma'_{v0}} \approx 33K_D \tag{2.31}$$

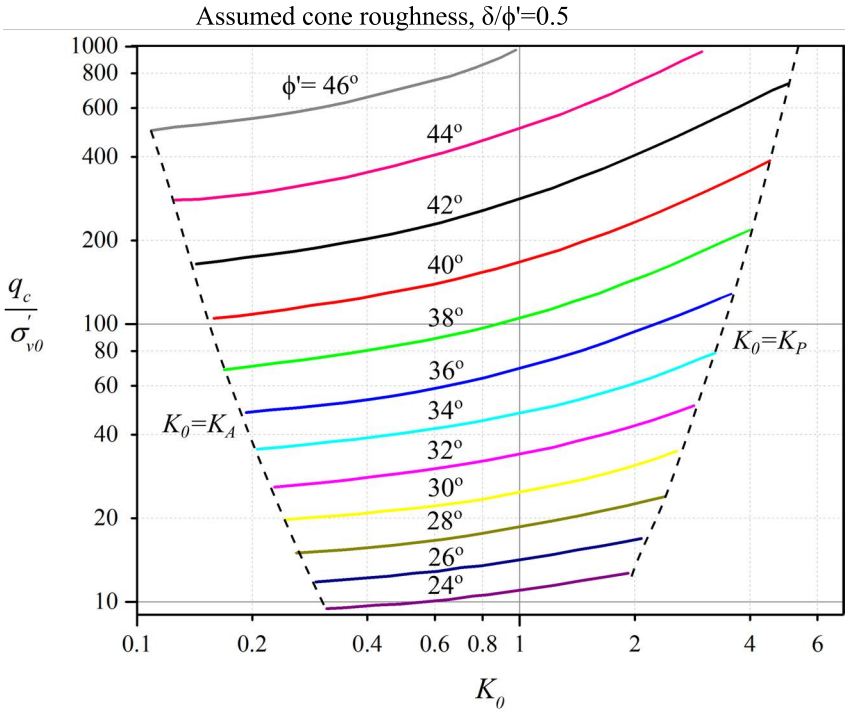

Figure 2.12: Reconstructed graphical representation of $q_c - K_0 - \phi^{'}$ values (Marchetti 1985)

In this way, it allows a comparison of $\phi^{'}$ by specifically assigning different K_0 value. Marchetti (1997) assigned three typical K_0 values: $1 - \sin\phi^{'}, 1, \sqrt{K_P}$ in the calculation and the results show the low sensitivity of $\phi^{'}$ to K_0. Thus, a recommended lower bound estimate of $\phi^{'}$ (typical magnitude of underestimation is between 2° to 4°) is given by:

$$\phi^{'} = 28^{\circ} + 14.6^{\circ} \log K_D - 2.1^{\circ} \log^2 K_D \tag{2.32}$$

Mayne (2015) confirms that Eq. 2.32 is a reasonable estimation of $\phi^{'}$ by comparing the DMT results with six series of undisturbed samples of clean sands acquired using special field drilling methods, primarily one-dimensional freezing technologies or special piston tube samplers. Fig.2.13 shows the measurements from triaxial test and different K_D expressions, which confirms the lower bound proposed by Eq. 2.32 for estimating sand strength from the DMT.

2.2.8 Coefficient of consolidation

Either the A_2-method dissipation test or the A-method dissipation test is conducted in a DMT sounding, it is possible to estimate the coefficient of consolidation c_h. Marchetti and Totani (1989) provided the following equation for the

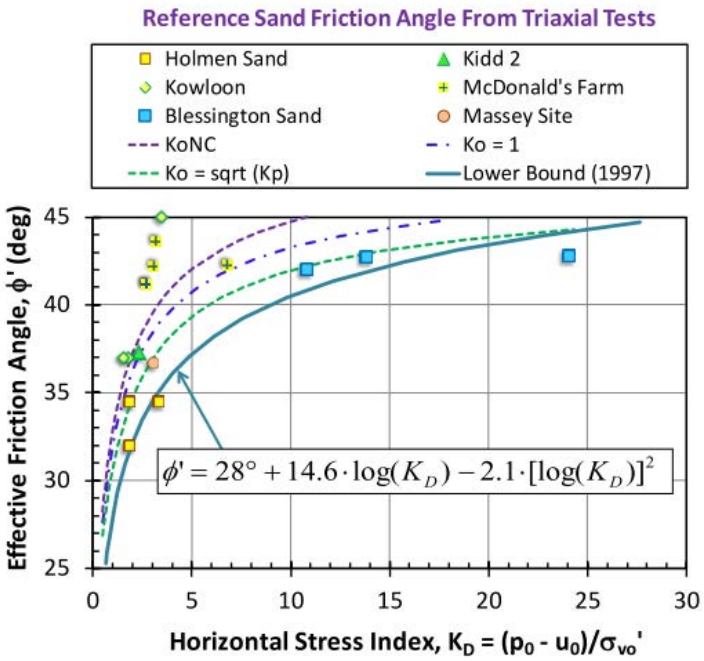

Figure 2.13: Sand friction angle ϕ' from triaxial compression tests compared with K_D expressions by Marchetti (1997), after Mayne (2015)

coefficient of consolidation in overconsolidated soils $c_{h,OC}$ using the A-method dissipation test:

$$c_{h,OC} \approx 7\,cm^2/t_{flex} \tag{2.33}$$

where t_{flex} is the time corresponding to the contraflexure point identified in the $A-\log t$ curve that is aforementioned in Section 2.1.2. The constant $7\,cm^2$ in Eq. 2.33 was determined by experimental calibration and can be several times lower if normally consolidated soils are investigated.

Rather than measuring the total pressure, the A_2-method dissipation test assumes the contact pressure is equivalent to the pore-water pressure adjacent to the membrane in soft clays. Robertson and Campanella (1988) provided the following equation to estimate c_h in soft NC to LOC clays (i.e. $I_D \leqslant 0.6$ and $K_D \leqslant 5.0$):

$$T_{50} = \frac{c_h \cdot t_{50}}{R^2} \tag{2.34}$$

where $T_{50} \approx 4$, $R = 20.57\,\text{mm}$, t_{50} = the time for 50% dissipation.

2.3 Modified dilatometer test

Following the pioneering concept of spade-like testing probes, many attempts have been made to modification of the standard flat dilatometer originally introduced by Marchetti (1980) to meet different needs in soil investigation. The most simple and straightforward modification is allowing automatic control and measurements to replace the manual steps in the standard Marchetti DMT such as the one developed by Failmezger (2015).

To better understand the measurements and the interpretation of the standard DMT, continuous measurements of the applied pressure and the membrane displacement are necessarily involved in the modifications of adding displacement and pressure measuring means in the dilatometer (Campanella and Robertson 1991; Fretti et al. 1992; Kaggwa et al. 1996; Deepthi De Silva 2000; Liu et al. 2016; Stetson et al. 2003; Motan and Khan 1988).

In efforts to deal with difficult soils, modifications of the standard dilatometer were also performed. The "Newcastle DMT" was developed for the application in glacial tills by using a rigid piston instead of a flexible membrane to load the soil (Akbar and Clarke 2001). The "ΔDMT" was developed to facilitate in situ measurements of a reservoir mud under more than 40m of water by incorporating a differential pressure sensor (Lee et al. 2013). The"mIDMT" was designed to assess the elastic behavior of shallow cohesive sediments by using smaller size probe, continuous measurements and automatic control (Barry et al. 2012). The "Dual DMT" was developed for in situ testing in fibrous peats by employing two membranes as loading means: the first membrane is the same as that in the standard dilatometer while the second membrane is mounted in the upper part of the blade which has an enlarged thickness of 30 mm compared to 15 mm in the standard one (Rahardjo et al. 2004).

Since soil stress-strain behavior is highly non-linear over the whole range of loading except at very small strains less than about 0.001%, soil stiffness modulus, as the gradient of the stress-strain curve, depends on the strain and stress levels (Atkinson 2007). In terms of the DMT, M_{DMT} is regarded as an operational modulus for the application such as settlement prediction. However, in reality, any calculation using a single operational modulus can only be accurate if the strain and stress levels in soils are relevant to that of M_{DMT}. Therefore, many attempts have been made to include small unload-reload loops for estimation of the unload-reload modulus (E_{ur}) (Bellotti et al. 1997; Benoit and Stetson 2003; Fretti et al. 1992), or enable a larger loading capability such as the

use of a rigid piston with an expansion up to 3 mm (Colcott and Lehane 2012).

Although the standard practice in the DMT does not include pore-water pressure measurements, knowing pore-water pressure information cannot only allow a direct way to estimate flow parameters of the soils but also enable the effective stress analysis. Depending on the purpose of the pore-water pressure measurements, the modified dilatometers can be divided into two types: measuring only the dilatometer penetration pore-water pressure (Liu et al. 2013; Stetson et al. 2003; Schnaid et al. 2016); measuring both the penetration pore-water pressure and the membrane/piston expansion pore-water pressure (Campanella and Robertson 1991; Akbar and Clarke 2001).

To systematically review these modified dilatometers, descriptive analysis of the apparatus modification is presented in Section 2.3.1 and quantitative investigation on testing data is provided in Section 2.3.2.

2.3.1 Review of the modified dilatometers

Modification of the soil loading means

During the DMT tests, soils are loaded in two stages: the dilatometer penetration stage and the membrane expansion stage. In principle, the modification of the apparatus may change either or both of the loading stage(s). The criterion to distinguish is that if the modified apparatuses comply with the nominal dimensions of the standard dilatometer, then only the membrane expansion stage is involved. Note that the nominal dimensions of the standard dilatometer are 95-mm width and 15-mm thickness, with an approximate 16° cutting edge (50-mm length of the tapered Section) (Marchetti et al. 2001).

In terms of the modifications made on the probe dimensions and thus the penetration stage, the dual dilatometer developed by Rahardjo et al. (2004) and the mIDMT developed by Barry et al. (2012) fall into the same category but in different directions. The dual dilatometer has a second membrane located in the upper part of the dilatometer blade which has a thickness of 30 mm compared to 15 mm-thickness of the lower part. Rahardjo et al. (2004) performed a series of field trials in soft soils and peats, and indicated that a thicker blade gives more reasonable results than the standard blade since the thicker blade displace the soil in larger strain and hence the measurement is more sensitive. Despite that Rahardjo et al. (2004) can justify his favorable assessment of the dual dilatometer in soft soils and peats, the change in soil disturbance during the blade penetration due to different blade thickness is unknown, thus

new correlations are necessarily required for the use of the dual dilatometer. In contrast, the mIDMT has only a blade thickness of 1 mm, compared to the thickness of 15 mm in the standard DMT, to minimize the soil disturbance of the probe penetration and a flexible membrane with a diameter of 24 mm for the purpose of assessing elastic behaviors of cohesive sediments at depth less than 25 cm. The design of the mIDMT follows the concept of the standard dilatometer but the modifications were made for solving marine-geology problems, rather than geotechnical ones.

Concerning the modifications made on the membrane stage, replacement of the flexible membrane with a rigid piston was carried out by both Akbar and Clarke (2001) and Colcott and Lehane (2012). Akbar and Clarke (2001) employed the rigid piston in the Newcastle dilatometer to avoid the membrane fragility in glacial tills. By using the rigid piston in a non-instrumented blade, the modified dilatometer developed by Colcott and Lehane (2012) allows a displacement up to 3 mm. The derivation of dilatometer stiffness values (E_D) in both findings use the equation for a rigid circular footing situated on an elastic half-space which is given by:

$$E_D = \frac{\pi}{4} \frac{\Delta p(1-\nu^2)}{s/D} \tag{2.35}$$

where s = the piston displacement, D = the piston diameter, Δp = the applied pressure.

However, this equation can only be approximate if any E_D-based correlation from the standard DMT is to be used because the modeling of the dilatometer membrane expansion as shown in Fig. 2.5 assumes restrained surface external to the loaded area which is not the case in the derivation of Eq. 2.35.

Modification of the displacement measuring means

The standard DMT measures pressures at prescribed displacements of 0.05 mm and 1.1 mm at the center of the membrane using a short circuit mechanics. In addition, it is assumed that the pressure-displacement relation is linear provided that the displacement is below 1.1 mm, and then linear elasticity theory is employed to interpret the soil stress-strain behavior during the membrane expansion. However, it is known that soil stress-strain behavior is generally highly non-linear. Thus, many researchers working on modified dilatometers are committed to attaining continuous pressure and displacement measure-

ments rather than simply adopting the assumption of a linear relationship.

Campanella and Robertson (1991) and Fretti et al. (1992) chose spring arms with strain gages to obtain the displacement measurements at the membrane center. Strain gages or strain arms were also used in apparatuses developed at the University of Adelaide (Kaggwa et al. 1996), University of Hong Kong (Deepthi De Silva 2000) and University of Newcastle (Akbar and Clarke 2001) while the Newcastle dilatometer is distinguished by using a rigid piston as the loading means instead of a flexible steel membrane. In the later version of the Newcastle DMT, a system of a Hall-Effect sensor along with a magnet target was used to measure the displacement of the rigid piston (Akbar et al. 2005; Aziz and Akbar 2017). However, the output signals from the strain gages or the Hall-Effect sensor in these apparatuses were all amplified on the ground surface, so the signal noise from the environment can be significant to the unamplified signal when a long cable has to be used for the tests at a large depth. To solve this issue, Stetson et al. (2003) used strain gages together with a displacement-tunable electronic oscillator to produce a sinusoidal output voltage varying in frequency, which can mitigate the influence of signal noise in the modified dilatometer developed at the University of New Hampshire. Furthermore, the compliance test is necessary if the strain gages or strain arms are used, since any compression of the membrane together the actual compliance of the strain gages (arms) at different pressures needs to be determined for a correction to get actual pressures affecting soils in a test.

Besides the aforesaid direct measuring means, the displacement can be indirectly determined by measuring the volume of the pressurized medium based on Boyle's law which is given by:

$$P_0 V_0 = P_1 (V_0 + \Delta V + V_{displaced}) \tag{2.36}$$

where P_0 = the initial pressure, P_1 = the current pressure, V_0 = the initial medium volume, ΔV = the medium volume actively displaced by the system. The medium volume displaced by the loading means $V_{displaced}$ can then be used to calculate a displacement according to the geometry of the loading means, such as a cylindrical element for a displaced piston and a spherical cap for a displaced membrane. Nevertheless, note that Eq. 2.36 only applies to the condition with constant temperature.

Based on this indirect displacement measuring means, Colcott and Lehane (2012) used oil as a medium to displace the piston via a manually controlled

hydraulic system to carry out tests within a depth of 3 m and Barry et al. (2012) used air as medium to expand the membrane via an automatic control system for tests at a depth less than 25 cm. It is interesting to find out these cases are all restricted for shallow depth of the ground. This may be due to the system capacity limitation as lower ΔV (negative) is normally required for testing at greater depth, and the presence of a number of potential sources of error, such as temperature and system compliance (i.e. diameter change of the plastic or nylon tubing at higher pressure).

To conclude, either direct or indirect displacement measuring means is possible in a modified dilatometer, the choice of which depends on the purpose of the tests. For typical geotechnical problems, it is preferable to adopt the direct means for greater system capacity and accuracy for tests at depth of at least 10 m. But for the direct means, the sensor signals shall be amplified near the blade so as to mitigate the influence of the noise, especially for when a long electrical cable is required for tests at great depth. However, for a larger membrane/piston displacement than the normal 1.1 mm, no direct measuring means has been used due to the limited space inside the dilatometer blade while the non-instrumented dilatometer developed by Colcott and Lehane (2012) is capable of a 3 mm piston displacement. Therefore, a compromise had always been made in the design of all these prior modified dilatometers.

Addition of the pore-water pressure measuring means

Ideally, pore-pressure measurements shall be made at the center of the membrane to obtain the dilatometer penetration pore-water pressure as well as the membrane/piston expansion pore-water pressure. Campanella and Robertson (1991) modified the standard dilatometer membrane to have a mini filter on the face with a small water cavity and a pore-pressure sensor attached behind. Given the fragility of the flexible membrane and the reduction of membrane flexibility due to this modification, this modified dilatometer was only used as a research dilatometer to enhance the understanding and the interpretation of the standard DMT. Akbar and Clarke (2001) used a rigid piston instead of the flexible membrane in glacial tills and proposed a pore-pressure cell directly installed in the rigid piston, however, it was acknowledged later that this pore-water pressure cell was not able to perform consistently and thus had been eliminated (Hassan Khan 2012). Thus the only results of this kind are from Campanella and Robertson (1991), which shows no excess pore-water pres-

sure generation in clean sands but significant excess pore-water pressure in soft clays during the penetration and membrane expansion. Nevertheless, it is noted that the design of attaching the pore-pressure sensor and the porous element to the expendable and easy-damaged membrane is only feasible for a research dilatometer but not sufficiently robust and practical for a routine in situ testing device.

Alternatively, the pore-pressure measurements can be expediently made nearby the membrane/piston, which however can only provide the dilatometer penetration pore-water pressure measurements. Liu et al. (2013) and Stetson et al. (2003) modified the dilatometers to have in situ pore-water pressure measured nearby the membrane rather than at the center of the membrane for the sake of easier fabrication. Schnaid et al. (2016) developed a pore-pressure dilatometer which replaces the membrane with a porous element to study the partial drainage conditions in intermediate soils such as silts. This allows pore-water pressure to be recorded during the dilatometer penetration and the dissipation test when the blade is stopped. However, the absence of a membrane or piston in this pore-pressure dilatometer results in difficulties using this probe solely for interpretation of soil parameters. Thus, a combined use of the pore-pressure dilatometer and the standard dilatometer at adjacent locations is a necessity in soil investigation.

2.3.2 Data analysis

Regression analysis of pressure-displacement curves

The use of linear elasticity is one of the advantages of the standard DMT interpretation, so the soil modulus can be obtained in a straightforward and convenient way. It is assumed that the relation between the applied pressure and the displacement at the center of the membrane is linear regardless of the soil conditions. Therefore, pressures are allowed to be measured at only two prescribed displacements. Given such a small membrane expansion, the linear pressure-displacement relationship appears reasonable. However, one must notice that the membrane expansion stage is conducted after the dilatometer penetration stage which opens a cavity in the ground and thus definitely involves the plastic behavior of the soils. Therefore, to better understand the real soil behavior during the membrane/piston expansion stage, full and continuous pressure-displacement curves obtained by modified dilatometers are discussed in this Section.

19 curves from published data from Akbar and Clarke (2001), Akbar et al. (2006), Bellotti et al. (1997), Campanella and Robertson (1991), Colcott and Lehane (2012), Deepthi De Silva (2000), Fretti et al. (1992), Kaggwa et al. (1996), and Stetson et al. (2003) in different types of soils are digitized and analysed using linear regression with the least squares method to investigate how well the data fits a linear relation. Then, the goodness of the linear fit is given by the coefficient of determination (R^2) and shown in Fig. 2.14.

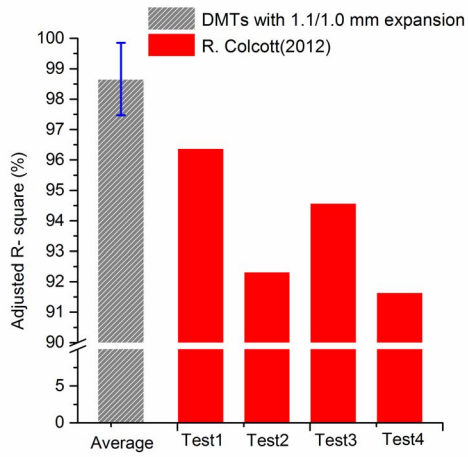

Figure 2.14: R^2 values of the pressure-displacement curves

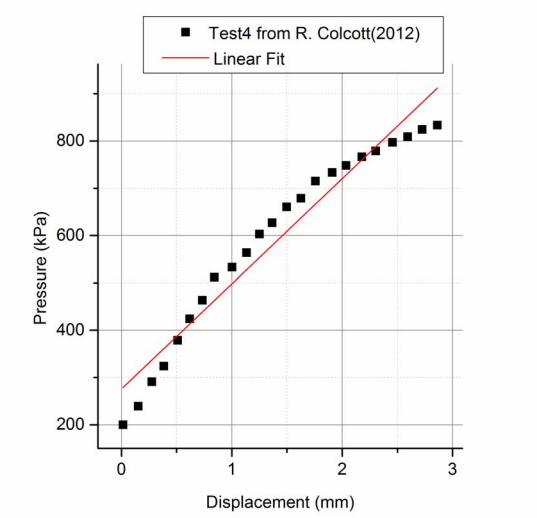

Figure 2.15: Linear fit of the Test 4 curve of Colcott and Lehane (2012)

As far as different modified dilatometers are concerned, the different maximum displacement at the center of the membrane/piston is taken into account. The 1.1 mm, used in the standard dilatometer, is also prescribed in the modified dilatometers developed by Liu et al. (2016), Stetson et al. (2003), Akbar and Clarke (2001), Deepthi De Silva (2000), and Kaggwa et al. (1996). In line with the older version of the standard dilatometer (Marchetti 1980), the apparatuses developed by Campanella and Robertson (1991) and Fretti et al. (1992) used 1.0 mm as the maximum displacement. Different from the others, Colcott and Lehane (2012) fabricated a modified dilatometer allowing the rigid piston to expand up to 3 mm which is significantly larger. Therefore, a comparison is made between 4 tests from Colcott and Lehane (2012) and 15 tests from the others. As shown in Fig. 2.14, the R^2 values computed from 4 curves of Colcott and Lehane (2012) are found relatively lower than the average value of 98.57% for other modified dilatometers. At first sight, all of them can be considered acceptable for using the linear theory in practical engineering design if only

the R^2 values are looked upon. For example, the test 4 performed by Colcott and Lehane (2012) has the lowest R^2 of 91.7% which seems "high" enough to justify the assumption of a linear relationship. However, as shown in Fig. 2.15, the curve tends to flatten with an increase in displacement which indicates that a limit pressure is likely to be approached if the displacement continues raising.

From a statistical point of view, both the R^2 values and the residual values shall be investigated to estimate the goodness of the fit. The residual is defined as a difference between the observed value and the fitted value (Residual = Observed value - Fitted value). Thus, statistically, the data points of a good linear fit shall be randomly dispersed in a residual plot that illustrates the residual values versus the fitted values.

Based on this criterion, although the pressure-displacement curves generally show good R^2 values, residuals of all regression analyses don't have the required randomness to support a linear model. Fig. 2.16 shows six exemplary residual plots with a pattern of inverted-U shape commonly found other than randomly dispersed data, suggesting that a non-linear regression would provide a better fit than the linear regression. This phenomenon shall justify the non-linear nature of the soil stress-strain relationship.

Furthermore, no recognized difference was found between the apparatuses using a rigid piston and a flexible membrane. The data from modified dilatometers capable of performing expansion larger than 1.1 mm in displacement is still very limited, so further research is needed such as a suitable non-linear regression model.

Analysis of the unload-reload loop

Performing a small unload-reload loop during the membrane expansion or contraction is technically infeasible with the standard DMT, but a number of attempts have been made using the modified dilatometers since the assessment of elastic modulus can be enhanced by assuming that a small unload-reload loop is elastic. The unload-reload loops in the modified dilatometers are resemblant to those in pressuremeter which is a cylindrical probe designed to apply uniform pressure to the walls of a borehole by means of a flexible membrane. Theoretically, the pressuremeter unload-reload loops were better studied by many researchers and a systematic review was provided by Mair and Muir Wood (1987). Wroth (1982) pointed out that the unload-reload loops have to be

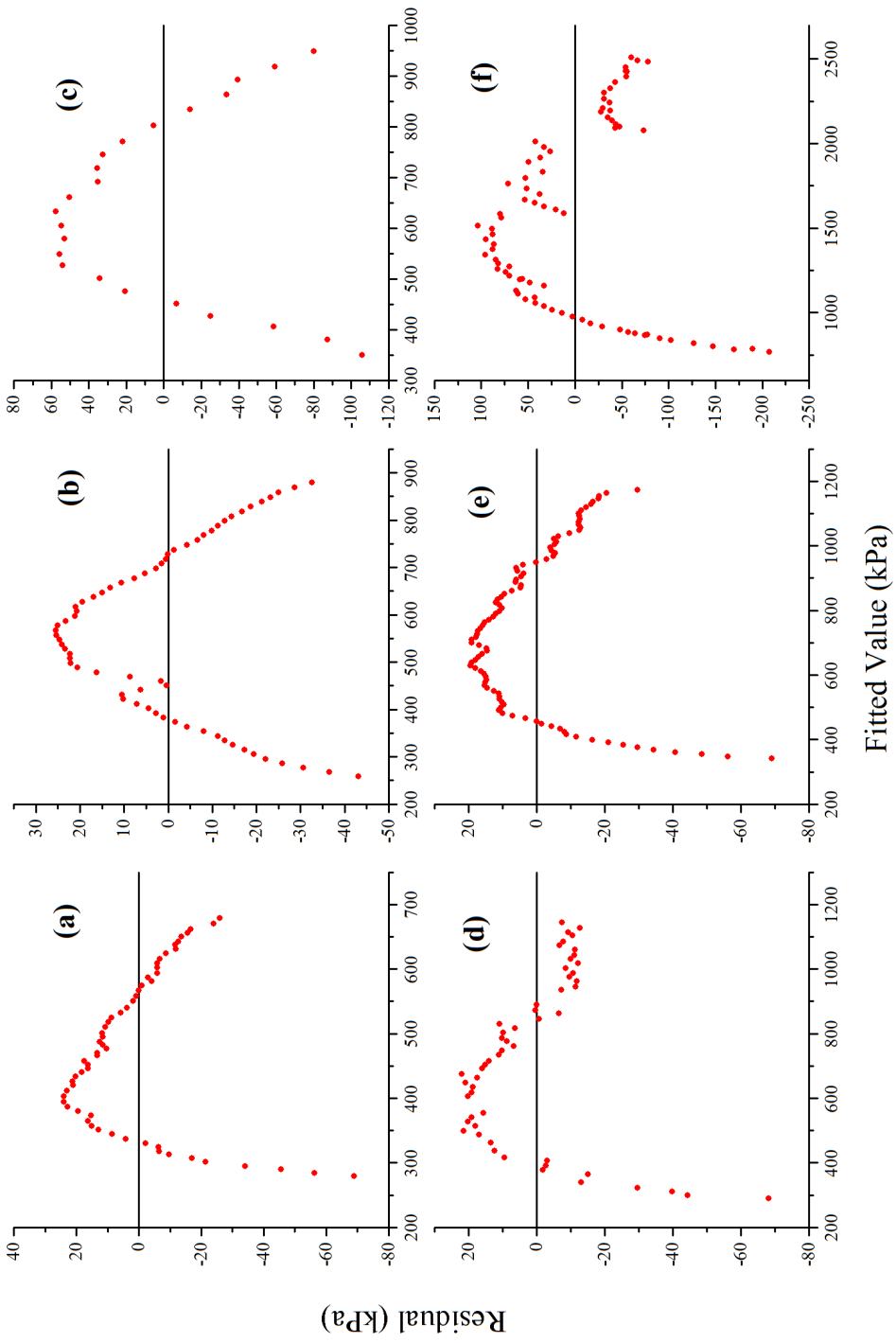

Figure 2.16: Residual plots: (a) The maximum displacement of rigid piston: 1.1mm, from Akbar et al. (2006), (b) The maximum displacement of flexible membrane: 1.0mm, from Campanella and Robertson (1991), (c) The maximum displacement of rigid piston: 3.0mm, from Colcott and Lehane (2012), (d) The maximum displacement of flexible membrane: 1.0mm, from Fretti et al. (1992), (e) The maximum displacement of flexible membrane: 1.1mm, from Kaggwa et al. (1996), (f) The maximum displacement of flexible membrane: 1.1mm, from Bellotti et al. (1997)

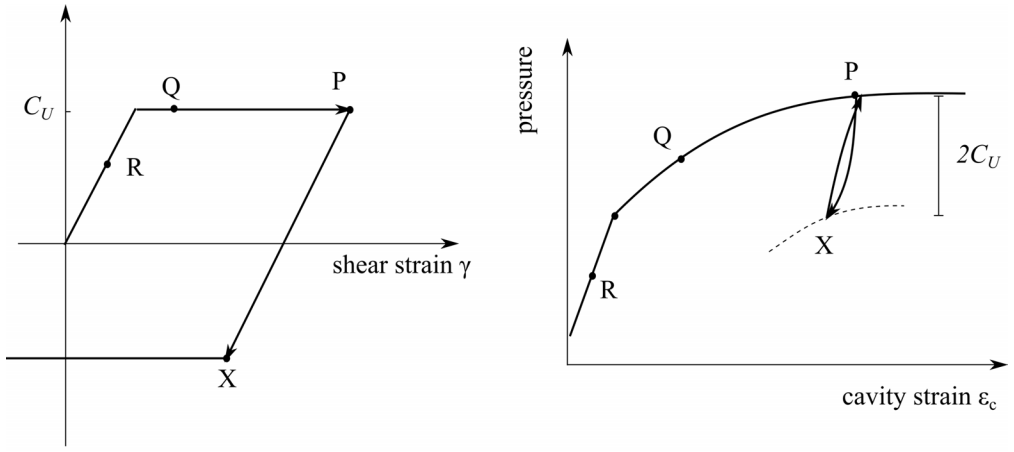

(a) shear stress-strain curve

(b) pressuremeter expansion diagram

Figure 2.17: Elastic-perfectly plastic soil response of the pressuremeter unload-reload loop, after Wroth (1982)

sufficiently small to be treated as elastic. In terms of an ideal elastic-perfectly material, the allowable size of an unload-reload loop can be estimated as two times undrained shear strength in clays ($2C_U$). Fig. 2.17 shows that unloading from point P is elastic until point X where the shear stress is reduced by $2C_U$ and the state of failure in the opposite direction is reached. Moreover, hysteresis of the unload-reload loops generally exists in the pressuremeter curves and the modified dilatometer curves. This indicates that the derived parameters such as soil modulus are dependent on the amplitude of the unload-reload loop and a higher modulus can be estimated from a smaller pressuremeter loop (Mair and Muir Wood 1987).

Nevertheless, concerning the unload-reload loops in the prior modified dilatometers, the pressure or displacement amplitudes may be even individually different in a single test. For example, Bellotti et al. (1997) performed three unload-reload loops, at the displacements of 0.25 mm, 0.50 mm and 0.75 mm, per test in a calibration chamber. Both the pressure amplitude and the displacement amplitude of each unload-reload loop increase with increasing displacement. Significant hysteresis can be seen from the loop at 0.75 mm which has the largest amplitude in both pressure and displacement.

Taken these differences in the pressure/displacement amplitude and the displacement level where the loop is performed into account, it is at least difficult to compare published data of the unload-reload loops with accuracy. However, an approximate comparison is still made using the DMT indices and the calculated unload-reload modulus E_{ur} which is given by (Bellotti et al.

1997):

$$E_{ur} = C(p_u - p_r)/(d_u - d_r) \tag{2.37}$$

where p_u = pressure at crossover; p_r = pressure at bottom of the loop; d_u = displacement corresponding to p_u; and d_r = displacement corresponding to p_r; $C = 38.2$.

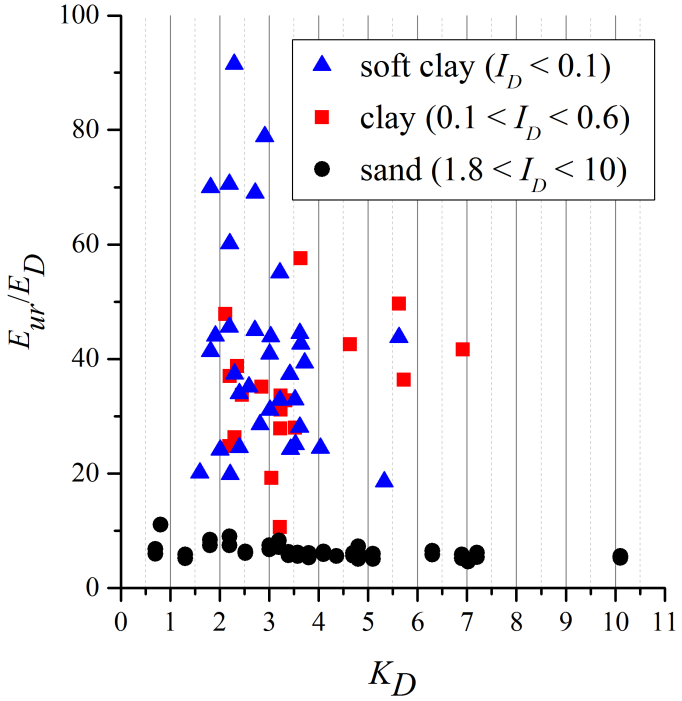

Figure 2.18: Ratio E_{ur}/E_D versus K_D for various soil types identified by I_D

Thus, a $E_{ur}/E_D - K_D - I_D$ chart is constructed using the data from Bellotti et al. (1997), Benoit and Stetson (2003), and Fretti et al. (1992), as shown in Fig. 2.18. Recognizable trends are: (a) E_{ur}/E_D is mostly in the range of 4 to 10 for clean sands, 10 to 60 for clays and 18 to 90 for soft clays, though it is lack of information for silts; (b) The largest variation of E_{ur}/E_D is found in soft clays, then in clays, smallest in clean sands; (c) Considering the correlation between K_D and the OCR in Eq. 2.21, E_{ur}/E_D tends to decrease with the OCR in both clays and soft clays; (d) It is nearly impossible to obtain E_{ur} by multiplying E_D by a constant in clays and soft clays where it varies significantly. However, it appears interesting to find that E_{ur}/E_D in clean sands has an average of 6.2 and a standard deviation of 1.17. This result is qualitatively in line with the constant ratio of E'_{ur} in drained triaxial tests to M_{DMT} given in Eq. 2.19.

Concerning further research in terms of the unload-reload loops in the modified dilatometers, precisely and accurately controlling the shape and the loca-

tion of the unload-reload loop is a necessity.

2.4 The dilatometer penetration stage

2.4.1 Review of the numerical and analytical analysis

Generally, installation of in situ testing apparatuses in the ground imposes a complex loading on the soil except for the self-boring pressuremeter which produces minimal installation disturbance. However, for the sake of economics and efficiency, direct-push technology approaches such as the CPT and the DMT are more appreciated in practice. In the CPT, the measurements are only taken during the cone penetration, thus soil parameter interpretation is based on the probe installation process, which deals with complex and mixed soil behaviors such as the combination of soil stiffness and soil strength information. In the standard/modified dilatometer test, the interpretation of some soil parameters is more straightforward and probably more accurate, such as the dilatometer lift-off pressure p_0, which provides a direct link with the in situ horizontal stress and the pressure difference $(p_1 - p_0)$ required for the membrane expansion allows the estimation of a secant soil stiffness without the need of separating soil strength behaviors. Nevertheless, the dilatometer penetration stage occurs before taking the measurements, thus the empirical nature of the understanding of this stage may lead to errors. A number of theoretical attempts were therefore made to investigate the dilatometer penetration stage using numerical and analytical approaches.

The geometry of the dilatometer blade is explicitly three dimensional. The penetration stage is essentially a cavity expansion process resulting from the dilatometer wedge which is 50 mm in length, 95 mm in height and 15 mm in thickness at the other end of the cutting edge. However, this 3-dimensional object was treated as two dimensional during various flat cavity expansion models for the sake of simplicity in the analysis (Liu et al. 2016; Marchetti 1980; Yu 2004; Yu et al. 1993; Zhou et al. 2015). Marchetti (1980) proposed that the dilatometer penetration can be regarded as the enforcement of two vertical rigid strip footing into the soil, however, no solution to this problem was provided, as shown in Fig. 2.19. Yu (2004) and Yu et al. (1993) utilized this plane strain model with cohesive soils idealized as an elastic-perfectly plastic material that obeys the Tresca yield criterion in a series of finite element simulations. The results indicate that p_0 is a function of initial horizontal stress,

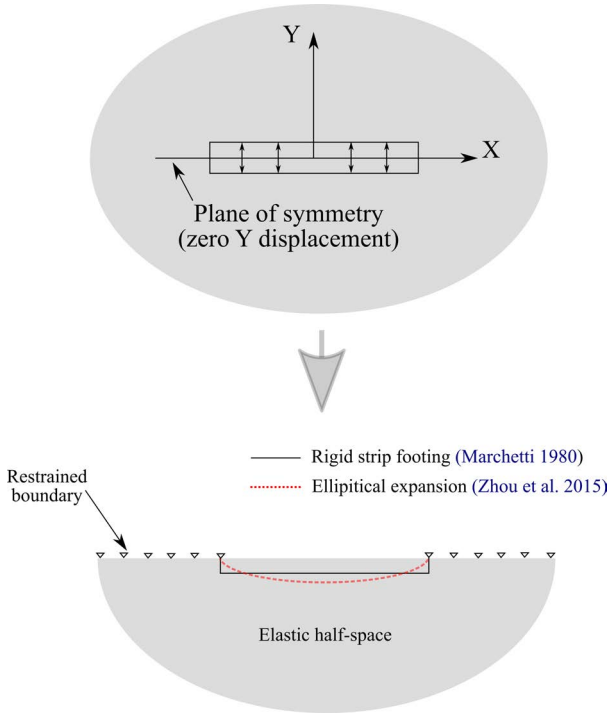

Figure 2.19: Modelling dilatometer penetration as expansion of flat cavity (adapted from Marchetti (1980) and Zhou et al. (2015))

undrained shear strength, and rigidity index of the soil which is given by:

$$I_R = G/S_u \tag{2.38}$$

where G = elastic shear modulus; S_u = undrained shear strength. The normalized lift-off pressure $(p_0 - \sigma_{h0}/S_u)$ increases significantly with an increasing I_R.

Although the flat expansion model proposed by Marchetti (1980) is able to work in a numerical simulation, it involves singular points at the dilatometer edges where the displacement is in discontinuity. This discontinuity of displacement jump prevents finding an analytical solution within the framework of continuum mechanics since soils at singular points have to be broken. To solve this problem two-dimensionally, Zhou et al. (2015) developed an alternative approach using an elliptical cavity boundary to avoid discontinuity at the two end points of the strip footing, as shown in Fig. 2.19. This way, in terms of the lift-off pressure p_0, a closed-form solution in an elastic soil and an upper-bound solution in an elastic–perfectly plastic soil that obeys the Tresca yield criterion were obtained by Zhou et al. (2015) and Liu et al. (2016), respectively. However the results are found to be sensitive to I_D as the elastic solution re-

quires I_D less than 0.8 and the elasto-plastic solution is only suitable when I_D falls between 0.2 to 1.2, which excludes sandy soils with I_D larger than 1.8.

The major shortcoming of the two-dimensional treatment for the dilatometer cavity expansion modeling is the neglect in the wedge-shape penetration that is explicitly a three-dimensional problem. Finno (1993) presented a three-dimensional numerical solution to the dilatometer penetration problem in a saturated cohesive soil using the strain path method developed by Baligh (1985). Kouretzis et al. (2015) made an attempt to numerically simulate the dilatometer penetration into saturated estuarine clays with a three-dimensional (3D) finite-element model. Both attempts allow the dilatometer penetration process being considered more realistically since the course of opening a wedge cavity by the cutting edge of the dilatometer was simulated explicitly. This can be quite important to quantify the amplification of horizontal soil stress during the dilatometer penetration, as discussed in the following Section.

2.4.2 The wedge cavity expansion effects

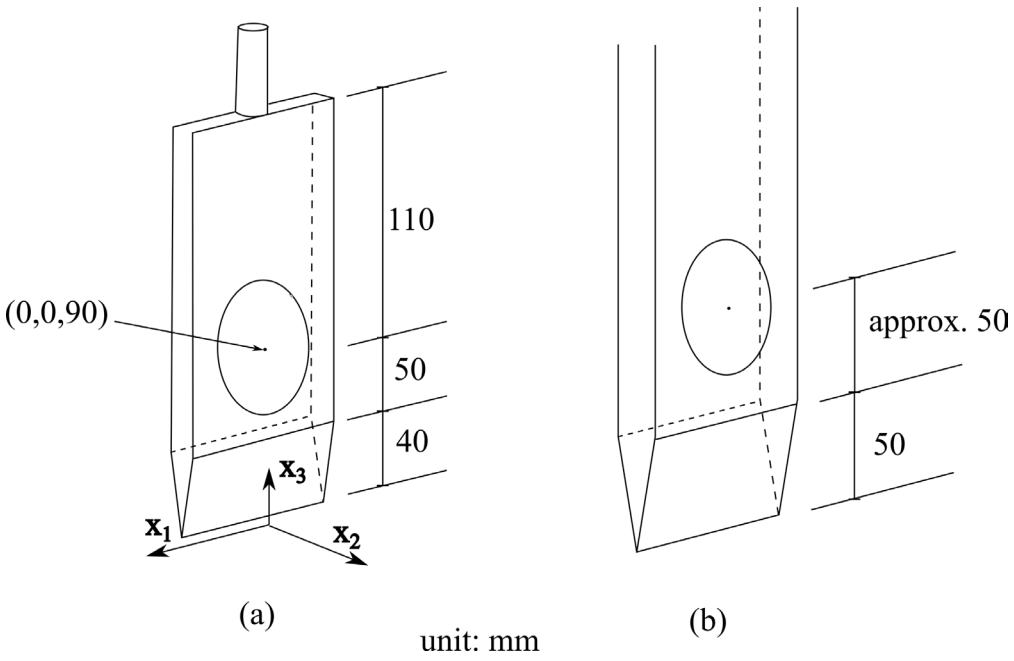

Figure 2.20: Geometry of the dilatometer used in the numerical simulation: (a) after Finno (1993), (b) constructed based on the descriptions in Kouretzis et al. (2015)

The wedge cavity expansion is a complex loading process resulting from the geometry of the dilatometer. Fig. 2.20 shows the geometry of the dilatometer

Table 2.3: Critical-state parameters adopted in the calculation by Finno (1993)

Friction angle ϕ	30°
Slope of isotropic compression lineλ	0.14
Slope of isotropic rebound lineκ	0.023
Poisson's ratio ν	0.3
Bounding surface parameter	5
Initial void ratio e_0	0.6
The coefficient of earth pressure at rest K_0	0.65
Overconsolidation ratio OCR	1.3

used in the numerical simulations. In line with earlier versions of the dilatometer in the 1980s, Finno (1993)'s dilatometer has a 40 mm tapered Section and a distance of 90 mm from the membrane center to the tip. But the geometry adopted by Kouretzis et al. (2015) is consistent with the nominal dimensions proposed by Marchetti et al. (2001), which has a 50-mm tapered section but no specific requirements related to the distance from the membrane center to the tip, though an approximate measure of 50 mm can be taken in the figure. Owing to this geometrical difference, variations to some extent in the stress and strain between the two are reasonably expected.

In Finno (1993)'s approach, a deformation field produced during the DMT blade penetration is assumed independent of the strength of the surrounding soil and the soil strains are found by means of differentiating the stream functions in accordance with this deformation field. Then the total stresses are calculated from equilibrium. To evaluate the effective stress in the soils, Finno (1993) used an anisotropic bounding surface model which requires inputs of multiple critical-state parameters given in Table 2.3.

Based on the coordinate system given in Fig. 2.20, the published data is digitized and analyzed. Concerning the expansion of the membrane is in the direction of x_2, the strain components of $\epsilon_{22}, \epsilon_{12}, \epsilon_{23}$ along a line at $x_1 = 0$, $x_2 = 0.5$ are shown in Fig. 2.21. It can be seen that both ϵ_{22} and ϵ_{23} show a gentle decline in the strain level when the dilatometer shoulder has been passed during the penetration, while ϵ_{12} remains zero during the whole probe penetration process. This may be regarded as a strain reversal occurring at the dilatometer shoulder as it is the geometrically transitional point. Furthermore, Fig. 2.22 shows the computed total stress and the effective stress along a line at $x_1 = 0$, $x_2 = 1$. The stresses in the soil increase as the soil passes the dilatometer tip to a maximum at the dilatometer shoulder, thereafter the stresses reduce to 0.6 times the maximum value that is approximately constant

Table 2.4: Modified Cam-clay parameters, after Kouretzis et al. (2015)

Slop of the critical state line	1.4
Slope of virgin consolidation line	0.8
Slope of the recompression/swelling lineκ	0.08
Poisson's ratio ν	0.33
Initial specific volume 1+e_0	4.0
Dry unit weight	6.62 kN/m^3
Permeability	10^{-8}m/s

across the membrane. Therefore the soil cylinder in contact with the membrane when the dilatometer is stopped for a test has already undergone unloading in the horizontal direction. This stress relief process is dominant in the form of pore-water pressure as the reduction in total stress is significantly greater than that in effective stress.

The 3D finite-element model in Kouretzis et al. (2015)'s approach is characterized by the use of a smooth rigid surface which slides together with the dilatometer during the penetration and allows soil nodes to conform to blade penetration without severe element distortion compromising the accuracy of the solution. Using the modified Cam-clay model to perform a coupled stress–flow analysis, Kouretzis et al. (2015) adopted the parameters given in Table 2.4.

It is found that the excess pore-water pressure development in the vicinity of the blade, rather than the effective soil stresses, accounts for the majority of the total stress acting on the membrane for the low permeability soils such as the investigated soft estuarine clay. Specifically, Fig. 2.23 shows the excess pore-water pressure contours diagram along with the average horizontal stresses plot. The excess pore-water pressure near the shoulder of the blade is found significantly higher than that of other locations during the DMT blade penetration. Regardless of the soil permeability variation from 10^{-6} m/s to 10^{-10} m/s, the pore-water pressure, effective stress and total stress generally show their peak values exactly when the blade shoulder moves past the soil cylinder, considering a distance of 0.05 m between the blade tip and the blade shoulder. Thereafter, the soil cylinder in contact with the membrane when the dilatometer is stopped for a test has already experienced unloading to some extent. Yet it appears that the horizontal stresses still undergo stress reduction at this soil cylinder rather than being constant.

Therefore, what can be generally concluded from both numerical results is that the soils next to the membrane during the DMT sounding shall undergo

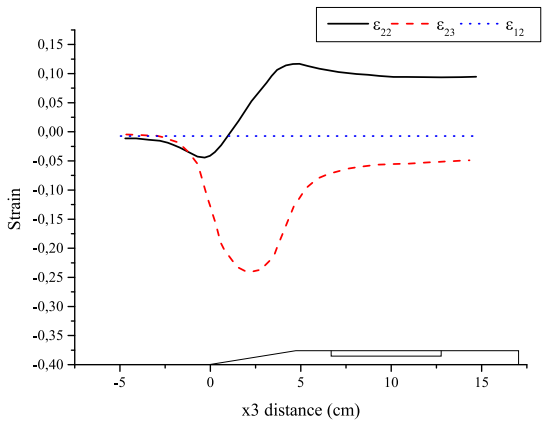

Figure 2.21: Computed strain components (adapted from Finno (1993))

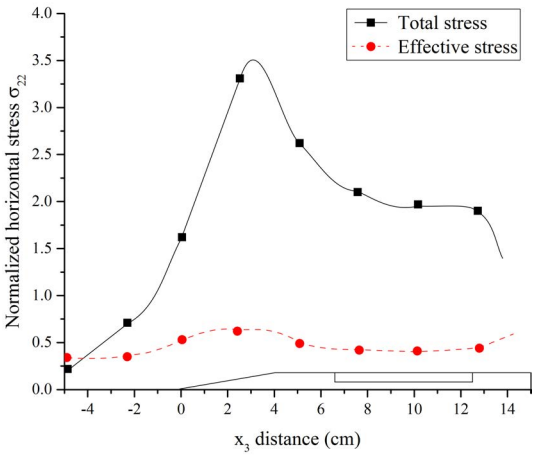

Figure 2.22: Computed horizontal stresses: normalized by initial effective overburden pressure (adapted from Finno (1993))

unloading to some extent in the horizontal direction. Thus it is reasonable to assume a reloading soil reaction against the membrane expansion, which immediately follows the dilatometer penetration stage. This soil response is supposed to be seen from the initial part of the pressure-displacement curves of the modified dilatometer(s). Furthermore, it is interesting to find that both numerical results support the hypothesis from Mayne (1987) that p_0 in clay is an approximate measure of the total pore-water pressure induced during penetration of the dilatometer. Since the pore-pressure response of clay is influenced by the in situ OCR, p_0 (or its normalized form of K_D) can be used to profile the stress history.

2.4.3 The thrust measurements

Schmertmann (1982), Schmertmann (1984), and Schmertmann and Crapps (2016) suggested that the thrust measurements made during the DMT sounding can provide various advantages such as a useful, real-time soil stratigraphy, an estimation of the blade penetration resistance q_D, use of "advance knowledge" to estimate the change in readings at the subsequent test depth and protection of the equipment. Concerning the interpretation, the addition of thrust measurements can help improve the estimation of the plane strain, drained, soil friction angle ϕ'_{ps} and the evaluation of liquefaction potential. Thus it is suggested that the many benefits of the thrust measurements are worth the extra time and expense, without compromising any regular DMT measurements.

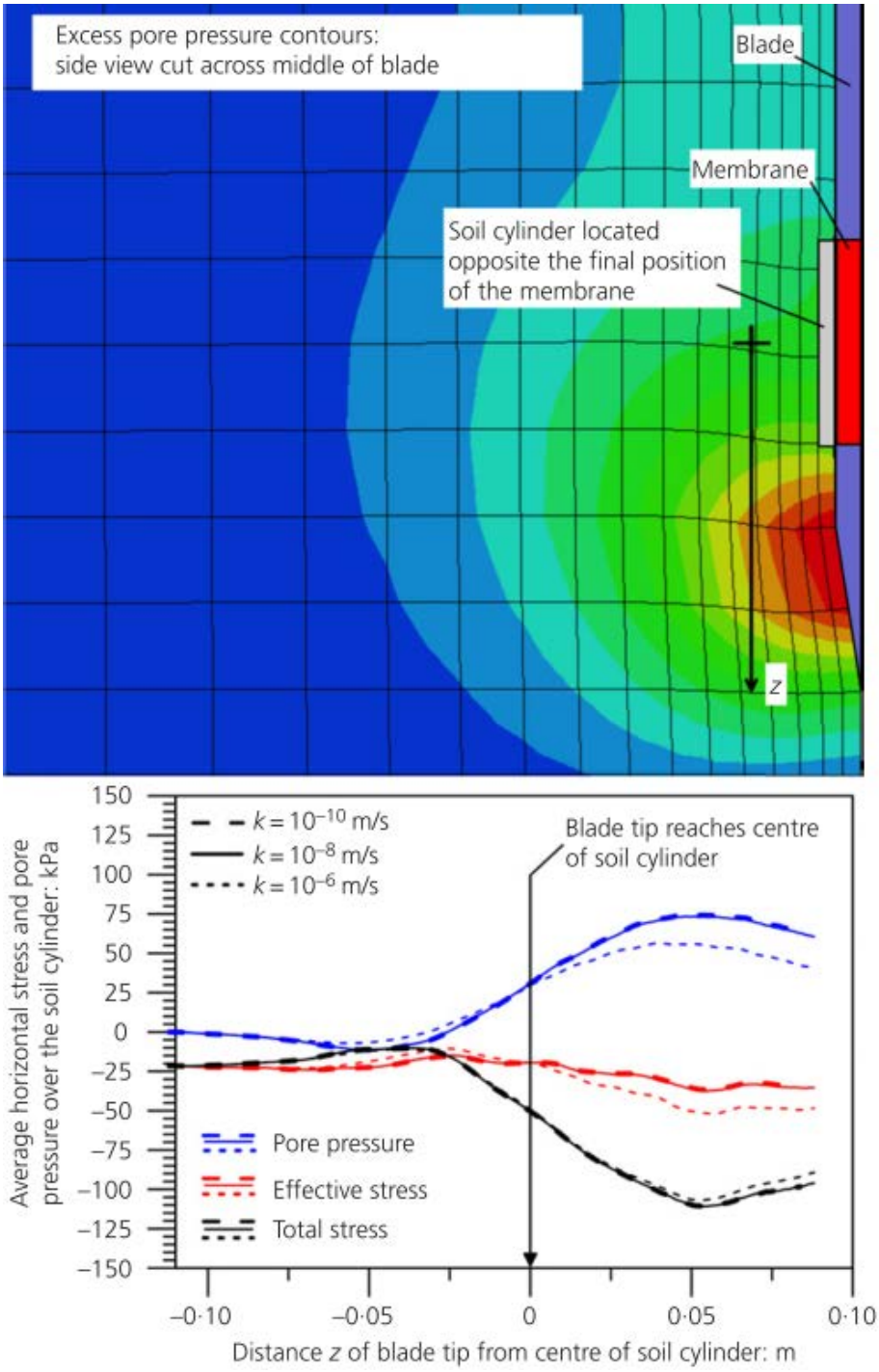

Figure 2.23: Evolution of horizontal stress and pore-water pressure averaged over a cylinder of soil located opposite the final position of the membrane (reprinted from Kouretzis et al. (2015))

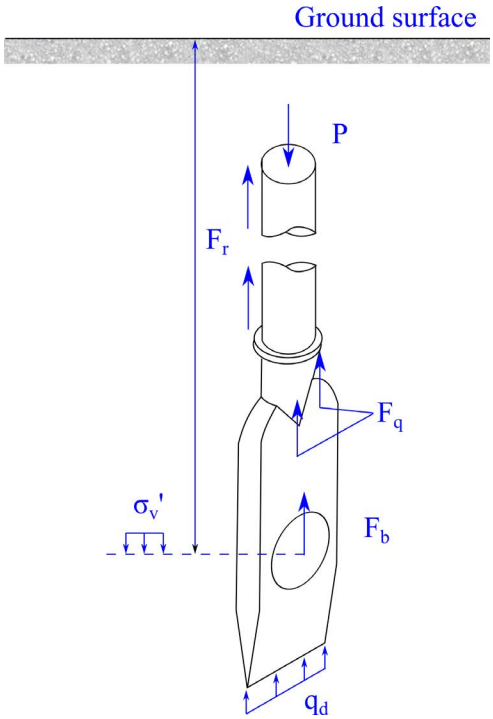

Figure 2.24: Vertical forces on the DMT blade and rods (adapted from Schmertmann and Crapps (2016) and Schmertmann (1984))

Ideally, the thrust shall be directly measured just above the blade using a load cell, like that of the cone tip load cell in the CPT. However, this creates significant extra cost for redesigning of the blade-rod connector. Alternatively, the thrust can be measured above the ground at the top of the string of rods, which is much more practical if existing systems are to be adapted. This way the DMT penetration resistance q_D can be estimated using the equilibrium equation that is given by:

$$P + W - F_r - F_q - F_b - q_D(bw) = 0 \tag{2.39}$$

where P = the thrust measurements at the top of the string of rods; W = buoyant weight of DMT rods and blade; F_r = side shear force along DMT rods; F_b = side shear force on blade; F_q = parasitic end bearing loading on the additional projected bearing area; b = blade thickness; w = blade width.

It is important to note that using Eq. 2.39 to estimate q_D involves several assumptions in the calculation. The major assumption is that friction on the rods can be neglected if a friction reducer is used just above the blade, namely $F_r = 0$. This assumption is conservative but has been proven reasonable for sounding in sand provided that testing depth is less than 15 m (Bullock 2016;

Campanella and Robertson 1991). When calculating $F_q = q_D A_p$, q_D is used with A_p the additional projected bearing area of the blade neck and the friction reducer. However, the real bearing pressure at the blade neck and the friction reducer is likely less than q_D, thus producing a conservative q_D estimation due to this assumption. In the estimation of F_b, negligible friction along the 15 mm blade edges is assumed and p_0 is used as the average effective normal stress acting on both sides of the blade. Assuming excess pore-water pressure is zero in sands, F_b is given by:

$$F_b = (p_0 - u_0)\tan(\phi^{'}/2) \times \text{blade area} \tag{2.40}$$

where friction angle at the interface between sand and a smooth steel is assumed as $\phi^{'}/2$.

Concerning conservatism of the aforementioned items in Eq. 2.39, Schmertmann and Crapps (2016) argues that the conservative and non-conservative assumptions tend to cancel each other while the generally conservative friction angle determined from q_D indicate an overall conservatism in q_D.

In terms of interpretation using the thrust measurements, $\phi^{'}_{ps}$ can be determined from q_D and the DMT data, which has been presented in Section 2.2.7. By comparing adjacent CPT and DMT tests in large calibration chamber and in the field, Schmertmann (1982) and Campanella and Robertson (1991) both give an approximate relationship between the penetration resistances:

$$q_D = (1.1 \pm 0.1) q_c \tag{2.41}$$

This relationship may be of use in the applications which require a combined use of the CPT and the DMT data while only the DMT data is available, such as the evaluation of liquefaction potential. Marchetti (2016) suggested the combined use of the CPT normalized con tip resistance Q_{cn} and the DMT K_D to estimate liquefaction potential. Thus in principle, it is possible that the use of q_D may do equally well as that of Q_{cn}, at least the uncertainty of inherently variable sandy deposits between an adjacent CPT and a DMT can be avoided.

2.5 DMT-CPT relationships

In terms of the direct-push approaches adopted in in situ testing in practice, the CPT developed in the Netherlands in the 1930s by Barentsen (1936) and the

DMT developed in Italy in the 1970s by Marchetti (1975) have become popular in many places around the world. Robertson (2009a) reviewed data of nearby CPT and DMT soundings as well as existing correlations for geotechnical parameters to find approximate correlations between the normalized parameters.

2.5.1 The CPT parameters

Electrical cone penetrometer measures force on cone and friction sleeve using strain gage load cells (ASTM D5778-95 2000). Then the cone resistance q_c and the friction sleeve resistance f_s are readily calculated as the force on the cone divided by the cone base area (typically 10 cm^2, or 15 cm^2) and the force on the friction sleeve divided by the area of the friction sleeve (typically 150 cm^2, or 225 cm^2).

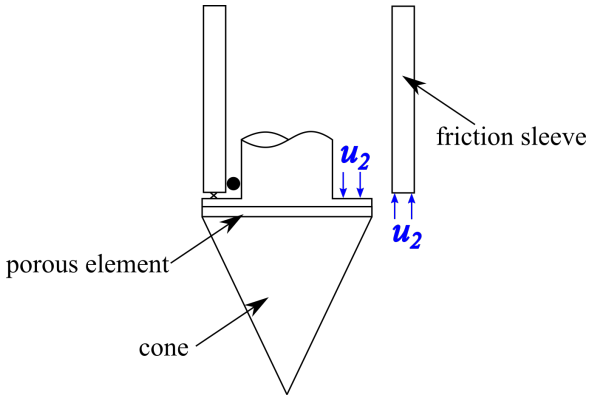

Figure 2.25: Schematic diagram of unequal area effects of the cone (adapted from Campanella et al. (1982))

In fine-grained soils, it is likely that the excess pore-water pressure $\bar{u} \neq 0$, then q_c must be corrected for pore-water pressures acting behind the cone tip that reduces the measured cone resistance. Fig. 2.25 shows this "unequal area effects" and the corrected cone resistance q_t should be used as the actual penetration resistance mobilized at the cone tip and is given by (Campanella et al. 1982):

$$q_t = q_c + u_2(1 - a) \tag{2.42}$$

where u_2 = pore-water pressure generated immediately behind the cone tip, a = net area ratio determined from lab calibration with a typical value between 0.70 and 0.85 while $q_c = q_t$ in sandy soils where $\bar{u}$ is zero.

To correlate with the DMT parameters K_D and I_D, which are normalized,

the aforementioned CPT parameters need to be normalized. Robertson (1990) suggested using the following normalized CPT parameters for the correlations:

$$Q_{t1} = (q_t - \sigma_{v0})/\sigma'_{v0} \tag{2.43}$$

$$F_r = [f_s/(q_t - \sigma_{v0})] \tag{2.44}$$

where Q_{t1} = normalized cone penetration resistance, F_r = normalized friction ratio, in %.

Similar to the DMT I_D to identify soil type based on the mechanical behavior of the soil, Robertson (1990) proposed the following equation for a soil behavior index (SBT) I_C:

$$I_C = [(3.47 - \log Q_{t1})^2 + (\log F_r + 1.22)^2]^{0.5} \tag{2.45}$$

Then, I_C can be used to identify soil types based on the following criterion:

clay	$2.95 < I_C$
silt mixtures	$2.05 < I_C < 2.95$
sand	$I_C < 2.05$

2.5.2 DMT – CPT Relationships

Considering the strong similarities between I_C and I_D in identifying different soil types, Robertson (2009a) proposed a simple relationship between the two:

$$I_D = 10^{1.67 - 0.67 I_C} \tag{2.46}$$

or

$$I_C = 2.5 - 1.5 \log I_D \tag{2.47}$$

A boundary of $I_C = 2.6$ and $I_D = 1.0$ was suggested to separate sand-like soils and clay-like soils for different equations of the CPT-DMT correlations.

In clay-like soils, where $I_C > 2.6$ and $I_D < 1.0$, K_D and E_D can be predicted based on the following equations suggested by Robertson (2009a).

$$K_D = 0.3(Q_{t1})^{0.95} + 1.05 \tag{2.48}$$

$$E_D/\sigma'_{v0} = 5Q_{t1}. \tag{2.49}$$

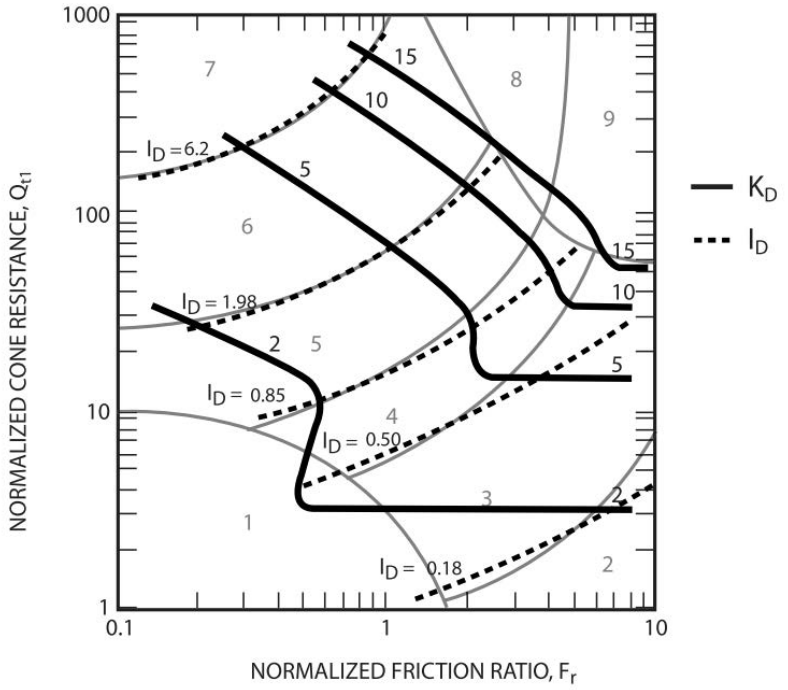

Figure 2.26: Proposed contours of DMT K_D and I_D on the CPT normalized SBT Q_{t1}-F_r chart (reprinted from Robertson (2009a))

In sand-like soils, where $I_C \leqslant 2.6$ and $I_D \geqslant 1.0$, an additional factor α varies with soil type, relative density, age and stress history, and with an average of 5 and a range from 2 to 10, has to be introduced in the following equations for the estimation of K_D and E_D:

$$K_D = (\alpha/34.7)Q_{t1}/[10^{1.67-0.67I_C}] \text{ when } I_C \leqslant 2.6, \tag{2.50}$$

$$E_D/\sigma'_{v0} = \alpha Q_{t1}. \tag{2.51}$$

Fig. 2.26 shows how the DMT parameters K_D and I_D can vary with the CPT parameters Q_{t1} and F_r in an SBT chart. However, it is important to note that the presented CPT-DMT relationships by Robertson (2009a) are only approximate but at least underpin a framework for comparison between the two most important direct-push field testing techniques. Fig. 2.27 illustrates a practical example from Robertson (2009a) where the well-captured trend and the extent of approximation can be both recognized.

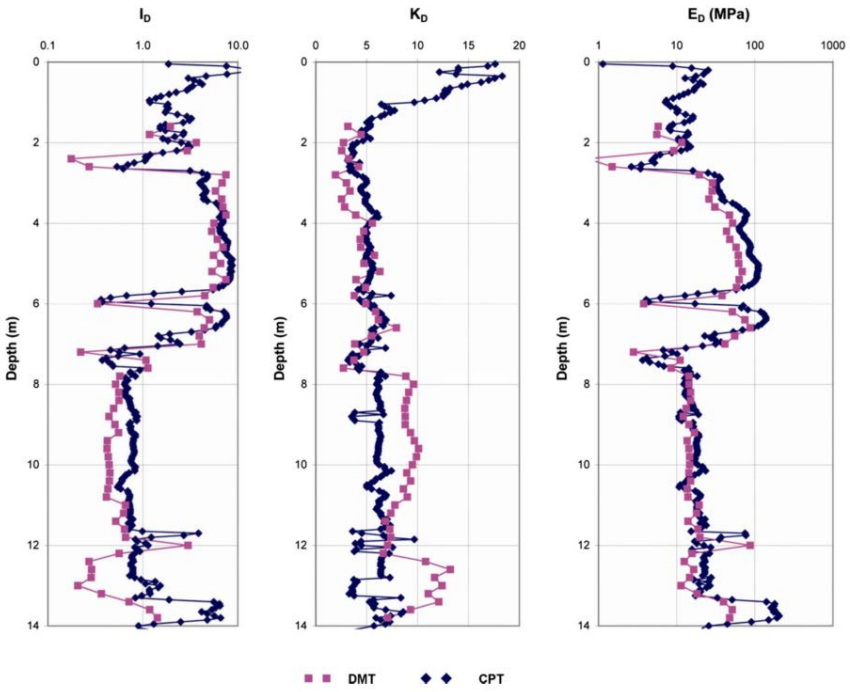

Figure 2.27: Comparison between measured DMT parameters I_D, K_D, and E_D with depth and predicted parameters using the CPT at Moss Landing site, California (reprinted from Robertson (2009a))

2.6 Discussion and conclusion

The pioneering design of the DMT by Marchetti (1975) and Marchetti (1980) aims to insert the dilatometer blade in the ground with soil disturbance as low as possible and then correlate the normalized membrane measurements (the DMT indices) to the pre-insertion in situ soil parameters. In this chapter, the review of the DMT is characterized with respect to several aspects.

Detailed review of the DMT apparatus with its operative aspects, see Section 2.1, and interpretation of the DMT results, see Section 2.2, is provided based on enormous efforts made by researchers and engineers using the DMT in soil investigation in the last 30 years. The DMT has repeatedly shown that it is a reliable and accurate site characterization tool, especially in acquiring C_u, OCR, and K_0 in clays; $\phi^{'}$, OCR and K_0 in sands if thrust measurements or adjacent CPT data is available; and the oedometer modulus M (thus the settlement prediction in sands and the primary settlement prediction in clays).

The modified dilatometers have been developed to serve different purposes such as automatic data acquisition, a better understanding of the standard DMT, dealing with difficult soils or achieving soil stiffness at additional

strain levels. A categorized review of the modifications, see Section 2.3.1, and data analysis of the pressure-displacement measurements from the modified dilatometer tests, see Section 2.3.2, are presented to understand the standard dilatometer readings in a more analytical approach. Taking the drainage condition as an example, it can only be measured by the modified dilatometer that in soft clays large excess pore-water pressures are generated, which thus dominate the dilatometer readings; in clean sands, the tests are performed under drained conditions where effective stresses are dominant; and in intermediate soils (e.g. silt-sand tailings) application of the standard DMT testing protocol can result in errors due to the partial drainage condition. Furthermore, the data analysis out of the literature not only sheds light on the non-linear nature of the pressure-displacement measurements but also, together with the aforementioned review, opens the way for the development of a newly modified dilatometer that is introduced in Chapter 3 and Chapter 4.

Although the pre-insertion soil parameters are literally correlated to the membrane measurements, the dilatometer penetration stage plays a crucial role since the membrane measurements highly depend on the process of the dilatometer penetration. In saturated cohesive soils, it is possible to address effects of the dilatometer penetration by means of numerical and analytical approach, a review is provided in Section 2.4.1. A horizontal stress relief phenomenon is discovered in these analyses, see Section 2.4.2, owing to the wedge shape of the dilatometer. The largest horizontal stress, dominant by excess pore-water pressure, is found at the dilatometer blade shoulder which is the geometrically transitional point of the blade surface. This results in soil reloading process at the start of the membrane expansion, which possibly leads to an erratic interpretation of the results. To solve this issue, a new interpretation technique is required and further discussed in Chapter 5. Moreover, the thrust measurements during the dilatometer penetration, discussed in Section 2.4.3, can indeed provide added value such as another type of continuous soil stratigraphy and the interpretation of $\phi^{'}$ in sands, thus is considered worth the efforts of modification.

Based on the aforementioned review on the DMT and the modified DMT, it is possible to identify a development route which can bring both scientific added value and practical advantages. First, rather than only the pressure readings at 0.05 mm and 1.10 mm, the full pressure-displacement curve is necessary to better consider, not only the non-linear soil behaviors as discussed in Section 2.3.2, but also the determination of the DMT contact pressure p_0. Since

in the DMT, the p_0 pressure is back-extrapolated from the pressure readings at 0.05 mm and 1.10 mm and is of paramount importance in the DMT interpretation of almost all soil parameters. Due to the numerical results discussed in Section 2.4.2, the stress relief phenomenon may significantly influence the determination of p_0, which may thus result in errors in using the correlations to derive soil parameters. To eliminate this influence, the full pressure-displacement curve has to be measured, and a new approach is required to determine the p0 pressure based on the full curve. In addition, a larger displacement is favored when we measure the full pressure-displacement curve to investigate the non-linear soil response since the strain level is not constant in different soils.

Despite many technical difficulties in the measuring process, pore-water pressure measurements are of particular interest to geotechnical engineers. In terms of the DMT and the iDMT, the pore-water pressure measurements allow not only a check on the assumption of the drainage condition (undrained or drained) in the interpretation but also are an improvement of the interpretation in partially draining soils. Moreover, it is possible to perform effective stress analysis based on the measured pore-water pressures during the membrane/piston expansion. However, this requires a departure from the standard DMT procedure since the penetration pore-water pressures during the DMT installation are expected to dominate the following membrane/piston expansion process.

After all, it is hard to ignore the advantages brought by the automation of the control & DAQ system. The current DMT standards require the operator to control the expansion rate manually and read the pressure measurements by eye. Automation of this manual process can prevent human errors and save labor cost. Therefore, these are considered as important points in the development route of the iDMT.

An increasing trend of the combined use of the DMT and the CPT in routine site characterization. The correlations between the two, discussed in Section 2.5, paves the way for the further use discussed in Chapter 5.

Chapter 3

The instrumented dilatometer: a laboratory prototype

3.1 Introduction

It is preferred to reduce risk and uncertainty involved in developing a new apparatus to be tested in the ground by first verifying the design in laboratory. Besides, the device design and the software development are both necessarily iterative processes with an ultimate aim to improve the functionality and the utility of the design and the code until issues and bugs have been reduced to an acceptable level.

Concerning the specific modifications to be made, instrumentation is necessary and a main point of interest to enable more measurements of soil behavior during the dilatometer testing process. This fits into a growing general trend, predicted by Schnaid (2008), in favor of the use of a range of sensors incorporated within a single penetration probe. Therefore, a laboratory prototype for the instrumented dilatometer test (iDMT) was developed for a proof-of-concept study excluding the impractical in situ installation process of the dilatometer in the laboratory.

As previously discussed in Chapter 2 the pressure-displacement curves in the existing modified DMTs are in essence non-linear due to the pattern of inverted-U shape spotted in the residual plots using a linear regression, though values of R^2 may be even higher than 90%. Generally, the non-random regression residuals can be caused by a missing variable, a missing higher-order term of a variable, or a missing interaction between terms already in the model. So it is considered necessary to have the measurements of a full pressure-

displacement curve to address this issue and underpin the development of new interpretation technique to reduce these errors. Moreover, it is necessary to recognize non-linearity of soil stiffness, the soil stiffness changes with the strain in soils by orders of magnitude, so the predication of a modulus can only be accurate if the strain in a soil is appropriate to the strain relevant to the secant modulus E_D from the DMT. The measurements of a full pressure-displacement curve in a larger displacement range in the iDMT can otherwise enable the estimation of soil modulus at different and larger strain levels and allow tangent modulus to be estimated as well, rather than only a single secant modulus. Therefore, it is useful to instrument the dilatometer blade for the sake of fewer errors in the interpretation and more soil stiffness information.

The existing modified dilatometers are able to provide either full pressure-displacement curves with the displacement up to 1.1 mm by means of equipping the dilatometer with sensors or a larger displacement range with a non-instrumented dilatometer such as the one developed by Colcott and Lehane (2012). This modified dilatometer can apply a rigid piston expansion of 3 mm while the piston displacement is indirectly determined by measuring the volume change of the oil pumped into the dilatometer. As mentioned in Chapter 2 this indirect measuring means can bring a number of potential sources of error, for example, it is impractical to calibrate the system compliance at all possible working pressures since the measured volume values are sensitive to the expansion of the tubing conveying the oil under pressure to the modified DMT blade. Moreover, some direct displacement measuring means may also require compliance calibration such as the strain gauges which were normally exposed to the pressure environment in the prior modified dilatometers. Therefore, considering a direct measuring means without the need to calibrate the compliance, non-contact displacement sensors (e.g. inductive sensor and capacitive sensors) are preferable since the sensing element can be shielded in a case without the influence of pressure variation. Thus, no calibration is required to determine the actual compliance of the sensor itself, which is a necessity for the strain arm measuring system. However, the difficulty of using the non-contact displacement sensor directly in the standard dilatometer or the prior modified dilatometers is the significant redesign of the blade required to house the instruments and the connections.

The DMT has been usually regarded as a displacement-controlled test since pressure readings are taken at two fixed displacement levels and time ranges given in Table 2.1 are used to regulate the course of membrane expansion. This

process requires manual operations of the pressure valves, while the testing results are assumed as operator-independent (Marchetti et al. 2001). Now with the full continuous and real-time pressure-displacement measurements available, it is viable to develop an electrical steering system to enhance the control means, such as allowing an automatic error-sensing feedback from the pressure and/or displacement measurements, and avoid any possible "human error".

Therefore, the first idea is to fabricate an instrumented dilatometer with a non-contact displacement sensor and an electrical steering system. Nevertheless, the first prototype was not successfully produced by machining which was found technically difficult due to insufficient space inside the blade for machining operations, given a mere 15 mm of blade thickness and a large expansion (such as more than 2 mm) alongside a non-contact displacement sensor.

3D printing, a term used synonymously with additive manufacturing, creates an objective adding material layer by layer, which then provides opportunities to fabricate objects, which are difficult for traditional subtractive manufacturing (ASTM Standard F2792-12a 2012; Barnatt 2014). Although 3D printing already has a number of ground-breaking applications in many fields, it is surprising to see its limited use in geotechnical testing. The following sections of this chapter present design considerations, development, calibrations of a 3D printed prototype of the instrumented dilatometer and its use in a simple calibration chamber.

3.2 Prototype development

3.2.1 Design

The instrumented dilatometer was designed with the following objectives:

1. Non-linear soil behaviors can be taken into account.
2. A comparison with the standard DMT results shall be possible.
3. The probe fabricated is robust enough to bear the testing pressure.
4. Continuous pressure-displacement measurements are recorded automatically.
5. An electro-pneumatic controlling system can adjust the applied pressure based on real-time feedback of pressure and displacement measurements.

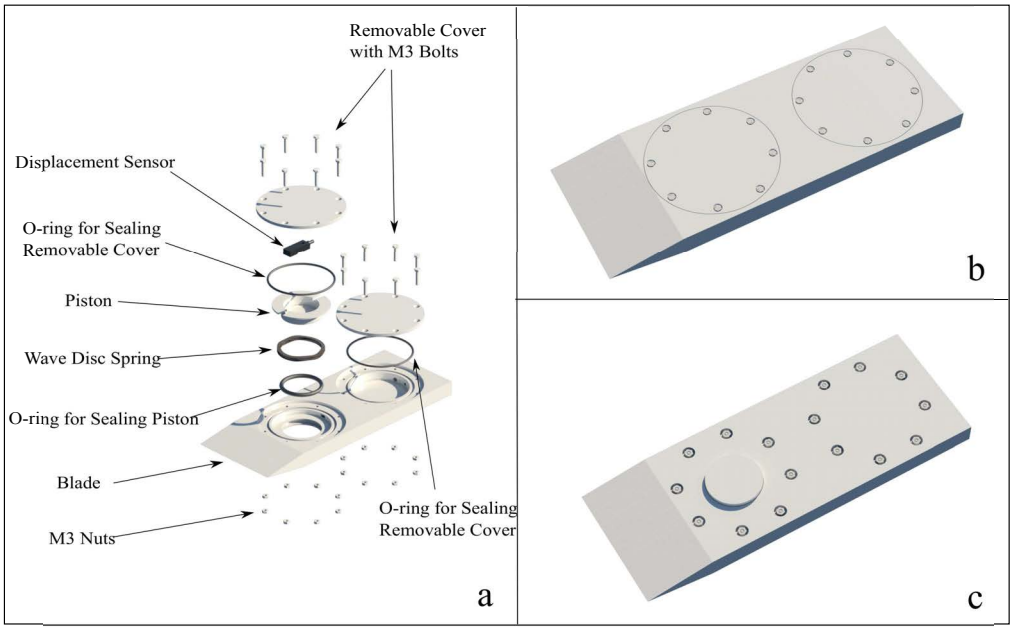

Figure 3.1: Schematic CAD-generated diagrams of the instrumented DMT blade (a) preassembly; (b) assembly in the top view; and (c) assembly in the bottom view

To achieve the goal of measuring non-linear soil behavior, larger soil deformation than that is possible with the membrane expansion in the DMT is normally required. This presents difficulty to continue using the flexible membrane since the edges of the membrane are fixed to the blade which causes difficulties to further increase the maximum displacement of the membrane due to the membrane stiffness and its boundary effects. Therefore, a rigid piston is favored in the new instrumented dilatometer design, as a rigid piston can protrude further out of the blade surface to tackle with non-linear soil response. Specifically, the design uses a 40-mm diameter piston instead of a 60-mm diameter flexible steel membrane and has an ideal piston displacement up to 2.5 mm. Note that although a larger diameter piston, such as a 60-mm one, may be preferred for the sake of requiring smaller pressure and testing bigger soil "sample", the 40-mm diameter was adopted since the conservative design can make the 3D printed prototype more robust, especially when it would be fabricated in new materials and tested without resemblant precedents.

To allow a comparison between the iDMT prototype and the standard DMT, the instrumented dilatometer blade is 15-mm thick, 95-mm wide, 50-mm long for the lower tapered section of the tip, which complies with the nominal di-

mensions of the standard dilatometer. This would enable at least a comparison of measurements between a 40-mm diameter rigid piston and a 60-mm diameter flexible membrane.

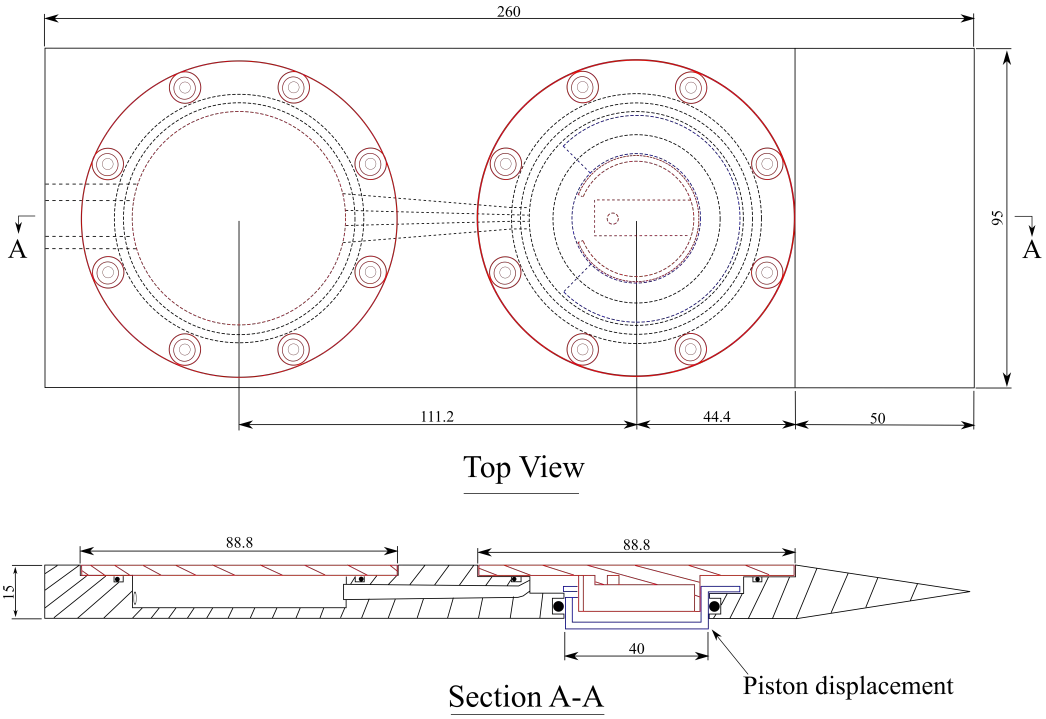

Figure 3.2: 2D schematic of the instrumented dilatometer

Fig. 3.1 shows a 3D model of the instrumented dilatometer generated in CAD-software and how it is assembled. The design involves a main instrumented dilatometer blade body, a piston and two removable covers in 3D printed material and other components in various materials. A flat wire compression spring (wave spring), situated between the piston and the main blade body, helps keep the piston in line with the blade surface at rest condition. O-rings, lodged in the specifically-dimensioned grooves, assure a watertight contact between different parts. With the M3 bolts going through the clearance holes and the corresponding nuts fitting the pockets on the other side of the blade, the two removable covers are fixed to the blade. In this way easily damaged threads in 3D printed materials can be avoided. Fig. 3.2 shows the details of this design in a top view and a section view.

An inductive displacement sensor (made by Balluff, model BAW-R03) with an accuracy of $\pm 35.0\,\mu$m is installed just below the piston to measure the piston movement. In terms of the working principle of the inductive sensor, an alternating electro-magnetic sensing field is emitted by a coil in the sensor, the impedance of the coil is changed when a metal target, such as the iDMT piston,

moves within the sensing field. Due to this principle, the inductive displacement sensor is contact-less and can save significant space in the iDMT. In this prototype development, a thin steel membrane is attached below the piston as the metal target for the measurements of the inductive displacement sensor. A pressure sensor (made by Honeywell, model MLH) with an accuracy of ± 8.75 kPa is located at the exit port of an electrical pressure regulator (made by Proportion, model QB2) because of the pressure sensor size constraint, though it would be ideal to measure the pressure near the piston.

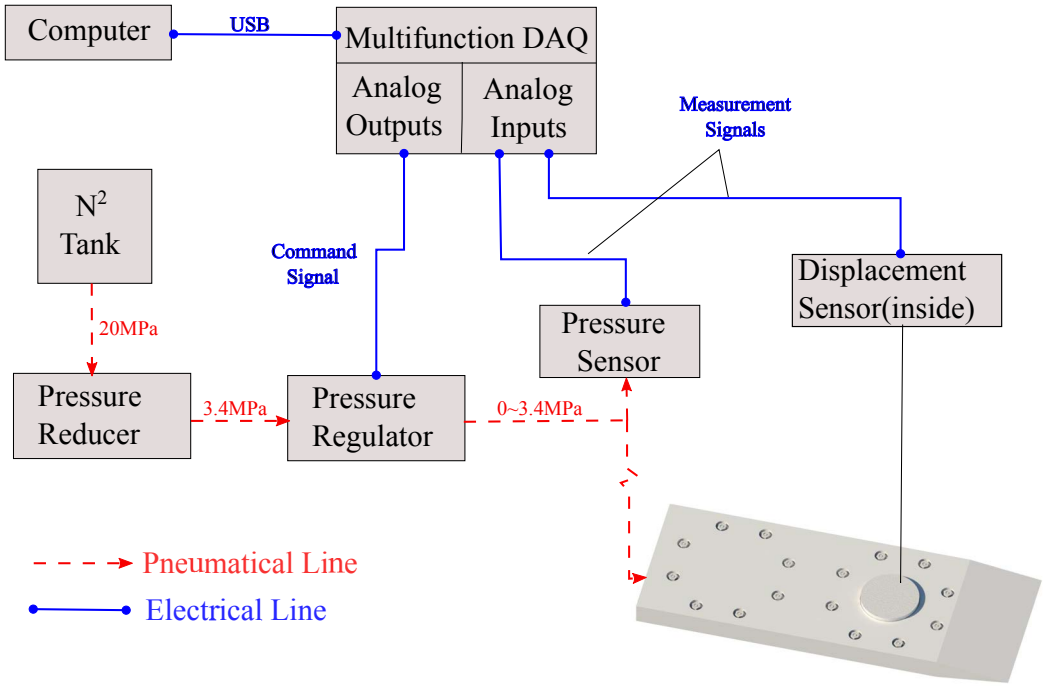

Figure 3.3: Schematic diagram of overall instrumented DMT system.

Fig. 3.3 demonstrates an overall schematic of the electro-pneumatic control and data-acquisition (DAQ) system for a pressure-controlled test, which can automatically record the measurements and electrically regulate the pressure. The computer control program is developed in LabVIEW (National Instruments); thus, the testing procedure can be controlled by a computer, such as incorporating unload–reload loops and varying loading/unloading rate. The interface between the hardware and the software is a multifunction data acquisition (DAQ) device (made by National Instruments, model USB-6009).

Furthermore, a drop in nitrogen pressure in an insulated system generally allows the gas expanding to create a cooling effect, according to Joule–Thomson effect (Rqebuck et al. 1935). Although the iDMT system is not insulated, it is possible to spot the cooling effects, such as condensation of water, near the

pressure reducer that has a pressure drop from about 20 MPa to 3.4 MPa and the pressure regulator that has a pressure drop from about 3.4 MPa to the applied pressure in the test. However, it is easy to effectively prevent this influence on the instruments by just having a section of extra tubing at the exit port of the pressure regulators. Not to mention the pressure sensor has a large compensated and operating temperature range of -40°C to 125°C, which eliminates the influence of the cooling effects.

3.2.2 3D printing of the instrumented dilatometer

For the purpose of manufacturing a prototype not only used as a visualization model but also as a device to be calibrated and tested, it was decided to use the laser sintering (LS) process in 3D printing technology to fabricate the blade in alumide which is a metallic grey, aluminum-filled polyamide 12 powder. During this process, polyamide 12, which has a lower melting point than aluminum, is sintered to produce a solid object. This process is significantly more economical than direct metal laser sintering (DMLS) which needs very high power lasers to work with metal powders (Barnatt 2014). Alumide is characterized by its high stiffness among the non-metallic materials used in 3D printing. The main properties of alumide are shown in Table 3.1 (EOS 2012).

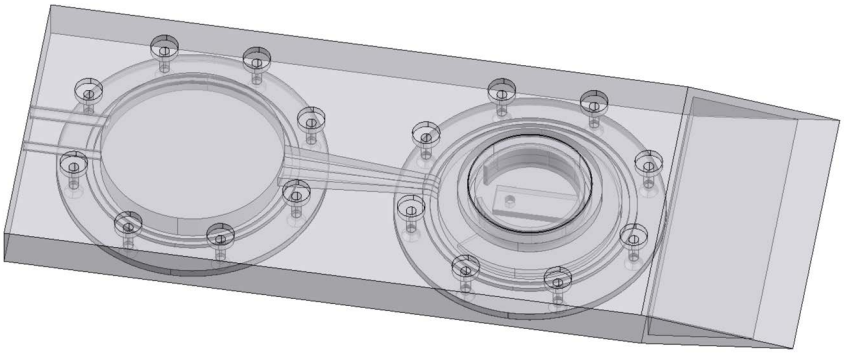

Figure 3.4: Schematic diagram of the instrumented DMT blade in a x-ray visual style

Fig. 3.4 illustrates the model in an x-ray visual style to show the inside details of the blade, which presents a challenge for traditional subtractive technology to work inside the compact dimensions of the blade, in particular, the limited thickness of 15 mm. For instance, the insufficient space of the two chamber openings, as well as the irregular tunnel connecting the chambers,

Table 3.1: Main properties of Alumide (EOS 2012)

Density (kg/m^3)	1360	Tensile Modulus (MPa)	3800
Tensile Strength (MPa)	48	Flexural Strength (MPa)	72
Flexural Modulus (MPa)	3600	Strain at break (%)	4

Table 3.2: Comparison of the design and the 3D printing dimensions

	Design dimension (mm)	Printing dimension (mm)	Error (%)
Blade width	95	95.77	+0.81
Blade thickness	15	15.24	+1.6
Blade length	260	257.92	-0.80
Piston diameter	40	40.04	+0.10
Removable cover A diameter	88.8	88.31	-0.55
Removable cover A thickness	3.0	3.08	+2.67
Removable cover B diameter	88.8	88.47	-0.37
Removable cover B thickness	3.0	3.06	+2.0

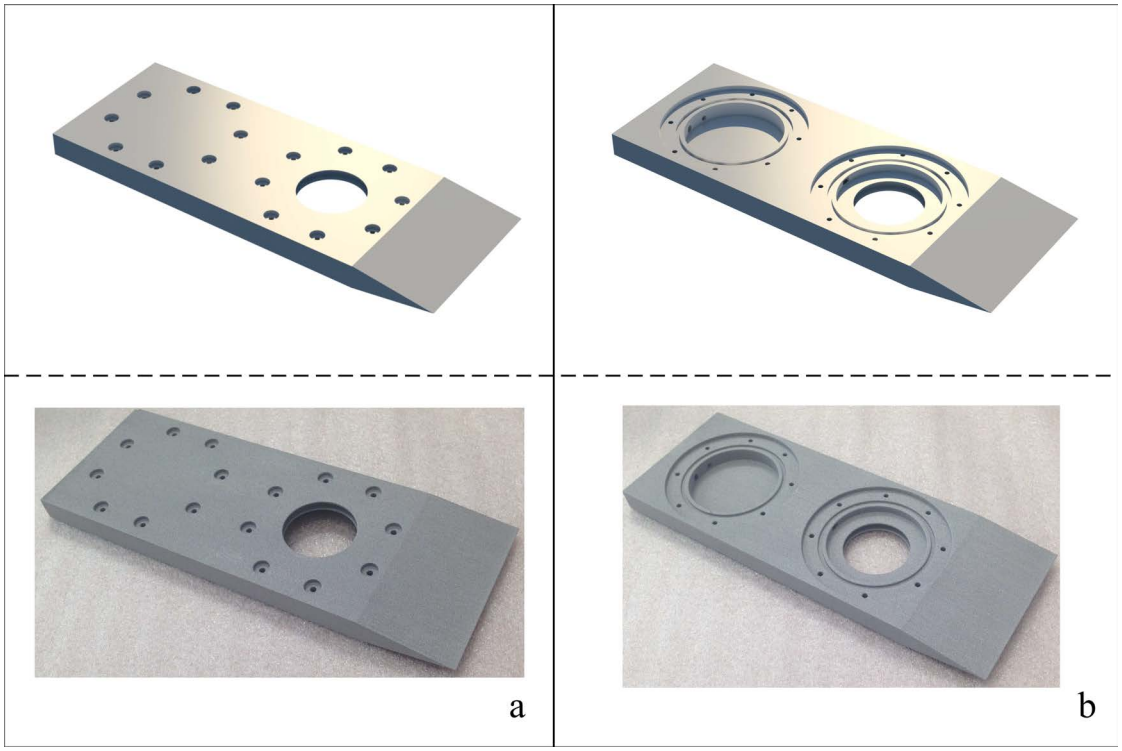

Figure 3.5: 3D printed DMT blade body in the top view(right) and the bottom view(left)

does not allow the use of standard drilling tools during the operation. By comparison, 3D printing does not suffer from any of the geometrical limitations encountered during these traditional processes. Once the 3D model is sent to either a desktop LS printer or a professional LS printer, the prototype can be obtained rapidly, within 1 day. However, the desktop LS printer that costs approximately $5,000 appears not to be robust enough to print objects with an accuracy of less than 1.0 mm, which is not satisfactory for the prototype. A professional LS printer with a price tag of about $250,000 (in 2014) can guarantee a better dimensional accuracy of 0.3% (with a lower limit of 0.3 mm); nevertheless, users normally do not purchase such a professional printer but request a 3D printing service, so the cost of printing this prototype is around $300.

Fig. 3.5 and Fig. 3.6 show the separate components of the blade in both the 3D model (up) and the 3D printed result (down). A comparison of the design and the printing product in dimensions as a proof of accuracy is shown in Table 3.2. It is noted that the error in blade thickness is slightly larger than that of other dimensions, which is possibly because of the fact that the model is printed layer by layer in the orientation along the axis of thickness.

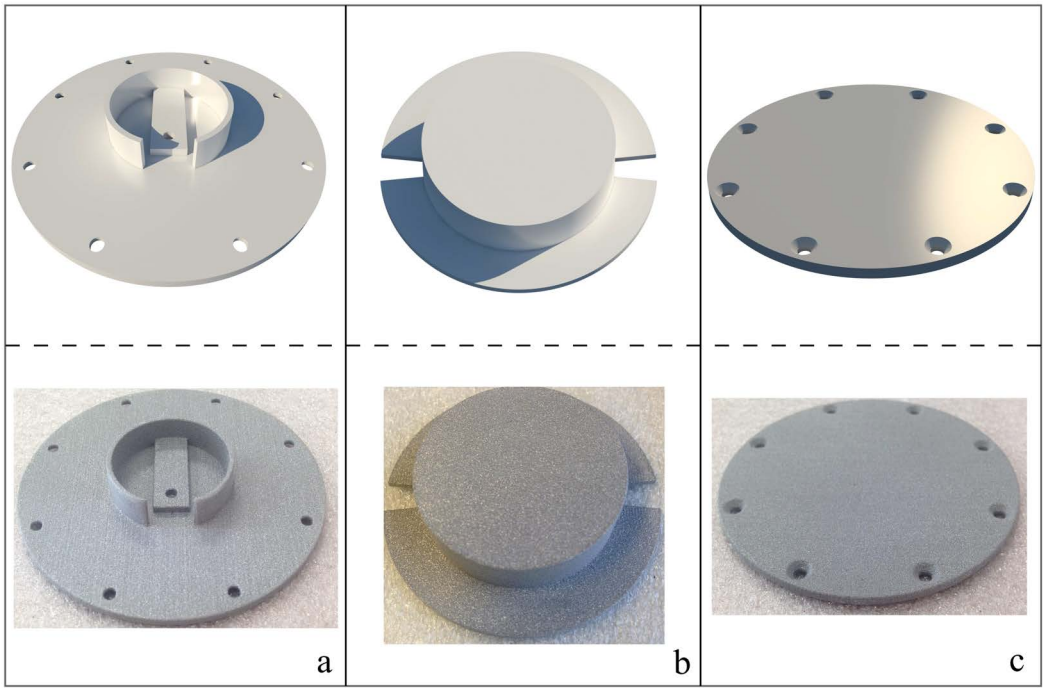

Figure 3.6: 3D printed components of an instrumented DMT blade: (a) removable cover A; (b) Piston; (c) Removable cover B.

3.2.3 LabVIEW program for the control & data acquisition (DAQ) system

LabVIEW concepts

LabVIEW (Laboratory Virtual Instrument Engineering Workbench) is a graphical programming language from National Instruments (NI) that uses icons instead of lines of text to create applications (*LabVIEW 2016 Help*). LabVIEW is featured by its execution order based on data flow, as opposed to the common sequential order of commands in text-based languages.

A LabVIEW program consists of a user interface, termed as the front panel, and graphical codes, termed as the block diagram. The block diagram uses graphical representations of functions to control the front panel objects (i.e. controls and indicators), which resembles a flowchart.

The choice of using LabVIEW over other languages for the control & DAQ system development is its easier interfacing to instruments via an NI DAQ platform without the need to write the driver and possibilities provided by parallel programming which allows multiple tasks (i.e. multiple while loops) performed in parallel. In the case of the iDMT control & DAQ system, recording different types of measurements and controlling the system based on the

real-time feedback of these measurements at the same time can thus be carried out using multiple loops in parallel.

The state machine for the control & DAQ program

The state machine is one of the fundamental LabVIEW architectures in applications where distinguishable states exist. The state is defined as the status of the program when it is working through the problem. Ideally, the state machine allows unlimited states along with unlimited triggering events associated with these states in a LabVIEW program. The given advantage of this is that all possible situations along with the corresponding reactions in the tests can be taken into account and programmed in the state machine in advance. In terms of the iDMT, the states could be the blade penetration status, the loading status, the unloading status and the pressure or displacement holding status. This way the whole complex testing program is broken down into these relatively small, focused states to ensure easier coding and maintenance. The nexus between the states relies on user input, such as start/end of the iDMT test and adjustment of the loading/unloading rate, or in-state calculation, such as displacement/pressure or its rate reaching a threshold, to determine the next state to execute.

In general, the algorithm of a state machine can be represented by a flowchart, which describes a solution model to a given problem. Hence, the operation of the iDMT test can be first outlined in a flowchart and then elaborated in a LabVIEW program based on that flowchart. In the instance of the iDMT, a general-purpose flowchart is shown in Fig. 3.7(a). This flowchart intends to generally show different states the iDMT may use, together with its corresponding schematic pressure-displacement diagram illustrated in Fig. 3.7(b). Note that the LabVIEW programming code for each state, e.g. the loading state or the unloading state, is placed in a module and thus can be easily merged into the complete program. Therefore, in principle, an iDMT test with any combination of states can be easily programmed and implemented.

3.3 Calibrations

Calibration of the iDMT can be regarded as a simulation in known and controlled boundary conditions, in a comparison with the measurements in the tests, which has to be performed for obtaining the correct soil response. The

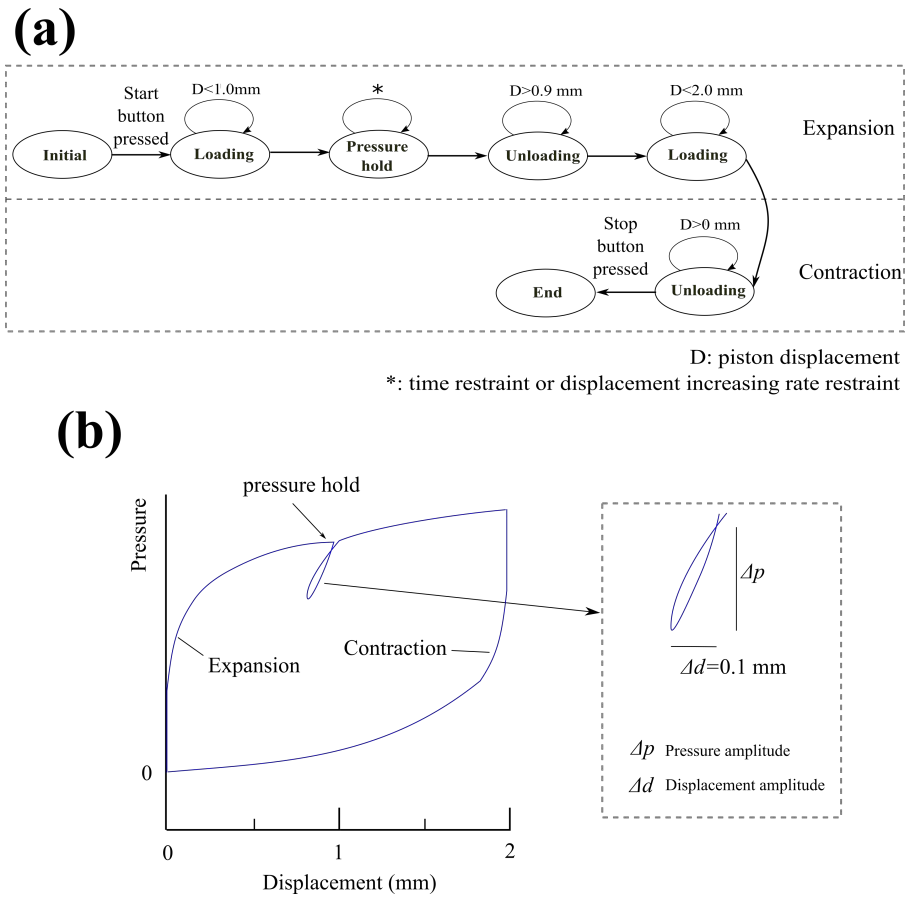

Figure 3.7: An example: (a) a general-purpose flowchart for the iDMT test, (b) and its corresponding schematic pressure-displacement diagram

iDMT calibration consists of two types: calibration of the instrument recording system and simulation of the tests in the air.

First, in terms of accuracy, precision and zero offsets of the iDMT system, all instruments are required to be checked periodically, which includes the pressure sensor, the displacement sensor, the electrical pressure regulator, the DAQ and the power supply. These calibrations of the first type form the basis of the ensuing calibrations and the iDMT tests, ensuring that correct data from instruments are logged or output properly.

Nevertheless, further calibrations are required for obtaining correct data from the iDMT tests since the raw data from the iDMT tests consist of not only soil response but also the force exerted by the springs, the friction of the O-ring and the system compliance. Therefore a second calibration procedure is indispensable to take these factors into account by means of simulating the tests in a known boundary condition. The simulation is performed in the air as no soil response is measured, thus the soil response — the corrected pressure-

displacement curve can be produced by subtracting this calibration data in the air from the raw pressure-displacement curve in soils. In principle, two sources of calibrations shall be taken into account, namely compliance of the piston displacement measuring system which is the ability of the system to resist deformation induced by a pressure change; and a tare determination of the force exerted by wave spring and the friction of the O-ring.

Concerning the system compliance, in the conventional in situ testing tools using strain arms for measuring the displacement of the flexible membrane, such as the instrumented dilatometer developed by Stetson et al. (2003) and the pressuremeter (and the cone pressuremeter) developed by Houlsby and Schnaid (1994), compliance of the strain arms along with that of the flexible membranes can have an appreciable influence on the testing results because this compliance refers to any compression of the membrane and of the strain arms due to the applied pressure. Different from these prior in situ testing probes, compliance of the piston displacement measuring system in the new iDMT is negligible since the 3600 MPa modulus of the rigid piston, as shown in Table 3.1, allows only inconsiderable compression when the applied pressure is below 1 MPa for this proof-of-concept probe testing, and the sensing element in the inductive displacement sensor is shielded in the rigid case which permits insignificant compression as well. This was checked by measuring deflection of the covers when a pressure of 1 MPa was applied, which shows zero displacement using a dial gauge with an accuracy of 5 μm.

Thus the second calibration procedure for the iDMT is only about the tare determination which consists of the force exerted by wave spring together with the friction of the O-ring at a piston displacement level.

3.3.1 Calibration of the instrument recording system

Calibration of the instrument recording system is essential as any error in a single instrument can lead to malfunction of the whole closed-loop control system, let alone correct measurements. This section specifically addresses a piston-displacement calibration and zero-offset calibrations, while routine calibrations for checking the absolute accuracy of the instruments are not discussed herein and shall be referred to the manuals provided by the manufacturers.

Zero-offset calibration

The aim of the zero-offset calibration is to determine the zero output at the local temperature and atmosphere. In the case of the iDMT, this is more concerned to the strain-gage-based sensors (e.g. the pressure sensor) than the inductive displacement sensor that is less and barely influenced by the temperature and the pressure in the typical operating range of in situ testing. Therefore the pressure zero-offset calibrations shall be performed for each particular site prior to the iDMT tests.

Fig. 3.8 shows typical results of the zero-offset calibration of the pressure sensor. The raw data was de-noised using a low-pass filter with a cut-off frequency of 2 Hz determined using the built-in spectrum analyzer in LabVIEW. Note that the noise generally comes from the cable transmission and the process of analog to digital conversion. The average value of the de-noised data is 0.99532 V, which is then used as the baseline in the ensuing data reduction.

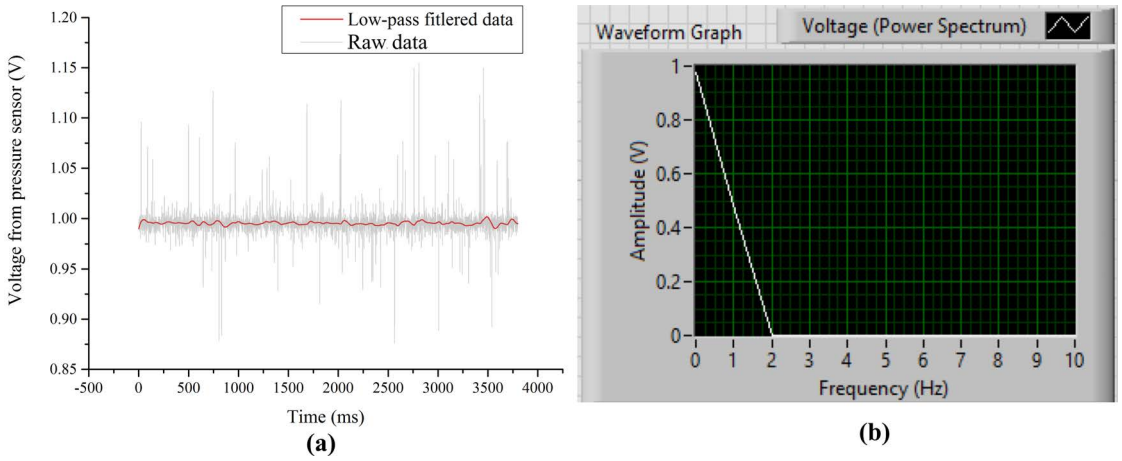

Figure 3.8: An example of the zero-offset calibration: (a) raw data versus low-pass filtered data and (b) spectrum analysis

Piston-displacement calibration

The piston-displacement calibration is conducted using a dial gauge (made by Sylvac, model μ233) having an accuracy of 5 μm and a full range of 12.50 mm, fixed by a custom-built rack to measure the piston displacement. During this calibration, both the analog voltage output of the displacement sensor and the digital displacement output of the dial gauge were recorded at the same sampling rate, so the relationship between the voltage measurements and the piston displacement can be readily described using a curve fitting technique.

Fig. 3.9 shows typical results of this piston-displacement calibration with the displacement up to 2.48mm and a 3-order polynomial fit with fixed intercept at zero was found having a coefficient of determination $R^2 > 0.99$ while the accuracy slightly decreases as it approaches the zero and full extent. The 3-order polynomial function is given by:

$$s = 0.259V - 0.019V^2 + 0.0017V^3 \tag{3.1}$$

where s = the piston displacement, V = voltage output of the displacement sensor. In addition, given the probability values ($p-$values) of the fit function are all lower than 0.05, the 3-order polynomial fit is considered statistically significant. Furthermore, this calibration was repeated 3 times and the repeatability is found good since the average difference is lower than 0.01 %.

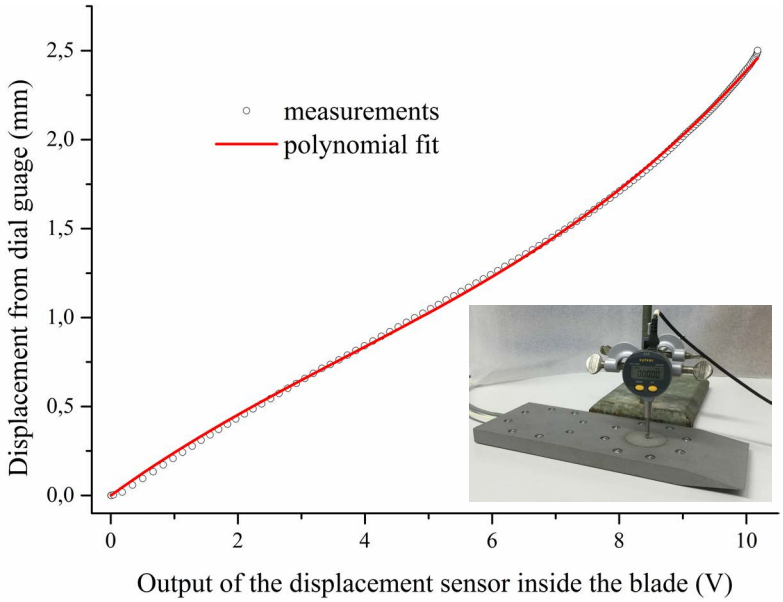

Figure 3.9: Piston-displacement calibration.

Note that although the displacement measurements in Fig. 3.9 were only taken at the piston center, four tests were carried out with the dial gauge located at different points on the piston. Fig. 3.10 shows no significant difference between the testing results and thus the displacement at the piston center (point A) can reasonably indicate the piston displacement.

Moreover, distinguished from the prior modified dilatometers using a piston, a larger expansion of approximate 6.2% of the piston diameter is allowed in this prototype having a 40-mm diameter together with a 2.48-mm displacement, which thus can possibly evaluate non-linear soil behaviors.

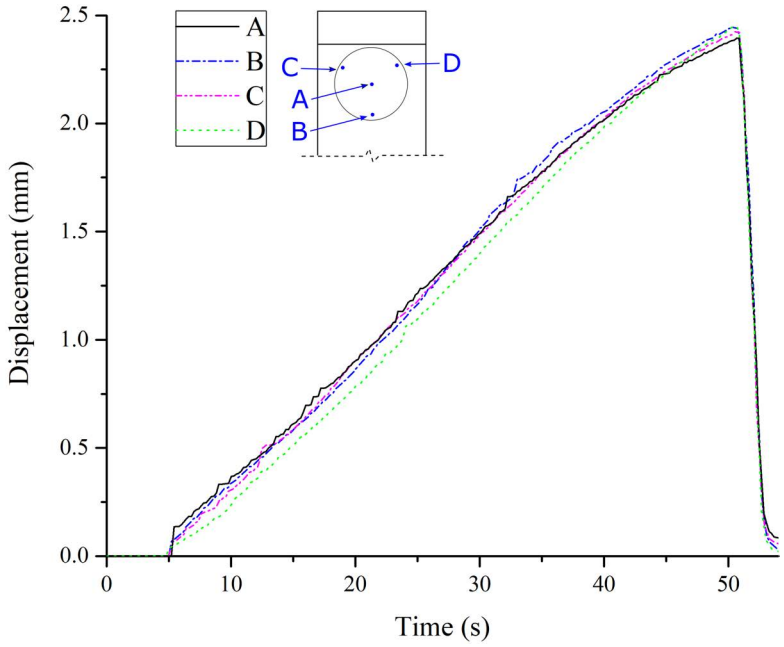

Figure 3.10: Piston displacement measured at different locations

3.3.2 Simulation of the iDMT tests in the air

Pressure-controlled or displacement-controlled?

In addition to the calibration of the instrument recording system, the second calibration procedure (the tare determination) has to be carried out to check and determine the system compliance, the force exerted by the wave spring and the friction of the O-ring, the magnitude of which may vary with a different testing protocol. In principle, the iDMT control system allows the testing protocol comprising either a pressure-controlled procedure or a displacement-controlled procedure since the system can be configured to apply a pressure on the piston based on an input and to adjust the applied pressure based on the difference between the input and the real-time pressure and/or displacement measurements.

Concerning the pressure-controlled procedure, two parameters are required to configure prior to testing: the desired pressure levels to attain and the inflation/deflation rate. Then the pressure-controlled procedure can be conducted by increasing/decreasing pressure in increments until reaching the desired pressure levels. However, the required pressure at a particular displacement in the iDMT test cannot be predicted beforehand and may even vary possibly with orders of magnitude in different soils. Thus it is more favorable to adopt the displacement-controlled procedure by increasing/decreasing displacement

in increments until reaching the desired displacement since the piston displacement range in different tests is normally identical.

In this iDMT prototype using an electrical pressure regulator, the displacement controlled procedure was tried by defining the system input as a displacement increment to attain in a given period of time. Nevertheless, this presents difficulties in configuring the corresponding pressure increment, which varies significantly between the field tests and the calibrations in the air. For instance, the adopted electrical pressure regulator has a maximum pressure capacity of 3.4 MPa and an accuracy of $\pm$ 17.235 kPa ($\pm$ 0.5% full capacity), which is mostly enough for precisely performing typical field tests. But considering a calibration with the pressure up to about 200 kPa, the smallest pressure increment carried out at the accuracy of $\pm$ 17.235 kPa is obviously too large for a regular displacement increment. Fig. 3.11 shows a calibration performed in this way. As a result, the smallest pressure increment results in overshooting a displacement increment with about 0.14 mm. By investing in a pressure regulator with better accuracy, such as having dual or even multiple controllers for different pressure ranges, it is likely to improve this testing procedure with displacement increments, but the excessive cost (at least two orders of magnitude higher than that of the single controller in 2016) of such equipment may not be worthwhile for the proof-of-concept study described in this chapter.

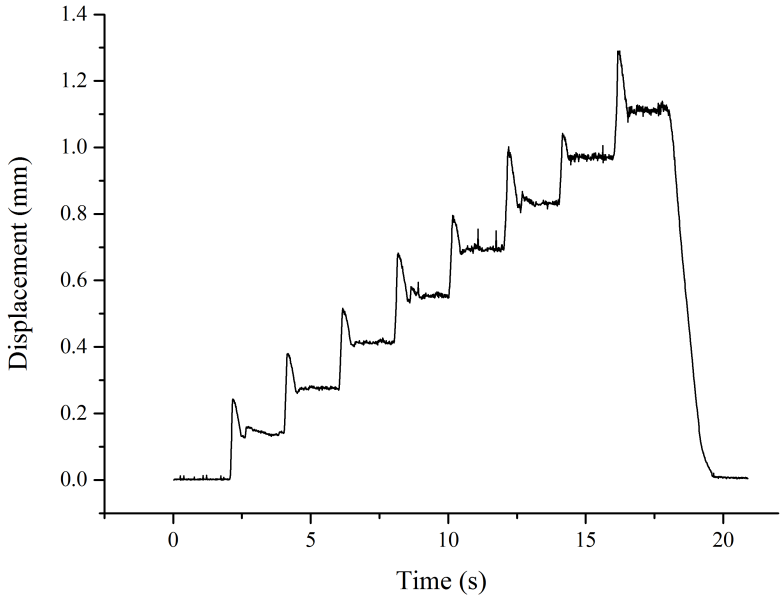

Figure 3.11: A calibration with displacement increments

Therefore the pressure-controlled procedure is chosen, and the operator is allowed to manually adjust the pressurization/de-pressurization rate based on

the real-time feedback of the measurements of the piston displacement and the applied pressure.

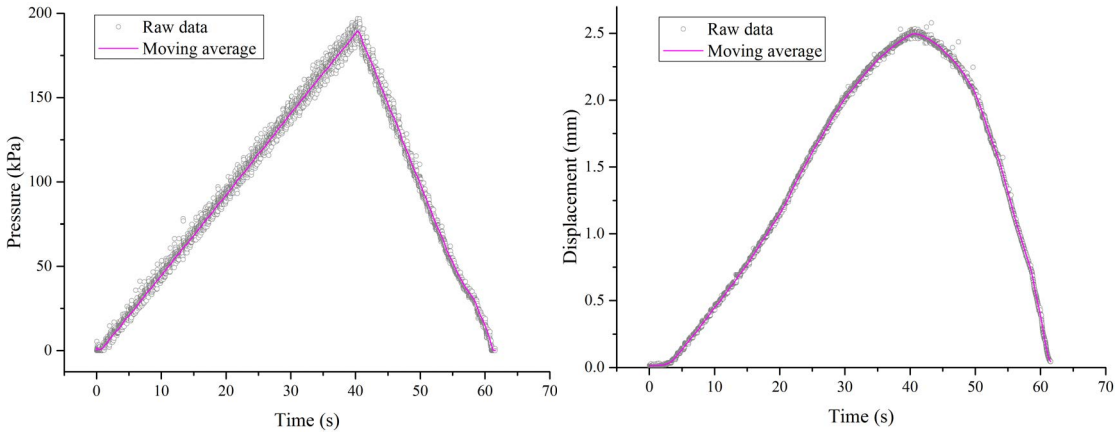

(a) The applied pressure (b) The piston displacement

Figure 3.12: Data reduction of the pressure and displacement measurements

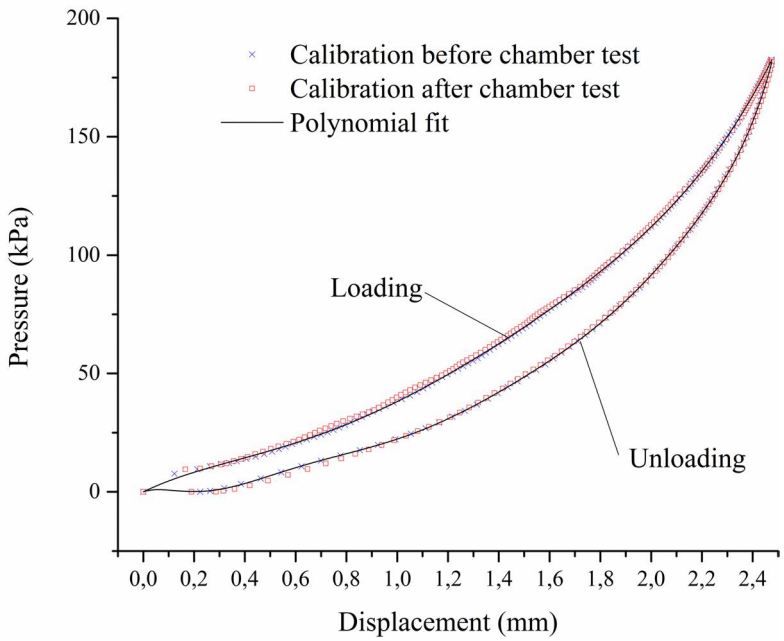

Figure 3.13: Wave spring stiffness and O-ring friction calibration.

In the first place a calibration with monotonic loading and monotonic unloading in the air with constant rate (5 kPa/s for the pressurization rate and -10 kPa/s for the de-pressurization rate) was carried out for the sake of simplicity. Fig. 3.12 illustrates the raw measurements of pressures and displacements against the testing time, where moving average of the 10-point raw data is used as a reliable statistical estimate of the level of random signals within the signal

precision span. Fig. 3.13 shows the pressures plotted against displacements of this calibration performed before a calibration chamber test, which is discussed in the following section and another calibration after the calibration chamber test. Hysteresis can be found in the pressure-displacement curves, which is due to different system responses in loading and unloading. Thus two different polynomial functions are fitted respectively to the loading curve and the unloading curve and given by:

$$P_{loading}(s) = 41.1s - 12.6s^2 + 10.1s^3 \tag{3.2}$$

$$P_{unloading}(s) = 30.1s - 24.7s^2 + 16.4s^3 \tag{3.3}$$

where s = the piston displacement (mm).

Moreover, repeatability of this type of calibrations is found to be consistently good as no significant differences are spotted between the calibrations performed before and after the calibration chamber test.

Unload-reload loop

Calibrations are also essential in order to obtain the corrected unload-reload loop in the pressure-displacement curve. Given that the pressure amplitude of the small unload-reload loops is normally less than 100 kPa, the compression of the rigid piston is negligible. So only the response of the wave spring and the O-ring is to be determined.

Since this calibration aims to simulate the test procedures adopted in the in situ testing, it is necessary that both location and size of the unload-reload loops are the same in the calibration and the in situ tests. Generally, either the pressure amplitude and the pressure where unloading starts or the displacement amplitude and the displacement where unloading starts is concerned. However, the response of the wave spring and the O-ring is only related to the piston movement rather than the pressures. So it is appropriate to match the displacement amplitude and the location in displacement of unload-reload loops in calibration to that in in situ tests. Note that the pressurization/de-pressurization rate of the unload-reload loops is configured as 60 kPa/min and -60 kPa/min, respectively, which is smaller than that of the main loop to reduce possible hysteresis. Though it is likely that the unload-reload loop will be different with different pressurization/de-pressurization rate, the cali-

bration remains valid so long as the same procedure is implemented in in situ tests.

The main purpose of conducting an unload-reload loop is to enable estimation of the unload-reload modulus which is assumed to be purely elastic provided the loop is sufficiently small to keep the soil response within the elastic domain. Therefore, the calibration aims to determine the correction required for deducing an unload-reload soil modulus from the raw data. Fig. 3.14 shows three unload-reload loops performed in different amplitudes and at different locations in a calibration. The pressure-displacement paths of the three unload-reload loops are found to be slightly different from the original pressure-displacement path of loading. Hysteresis of the unload-reload loops is generally small and negligible.

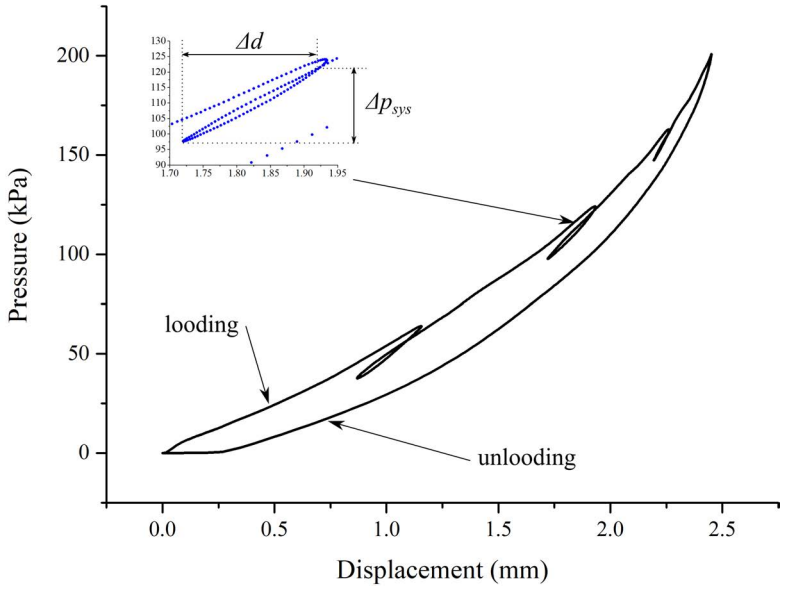

Figure 3.14: A calibration with unload-reload loops

Since the displacement amplitude Δd of the unload-reload loops is the same in calibration and in in situ tests, the calibration de facto determines the pressure change induced by the system Δp_{sys}, then the pressure amplitude of soil response can be obtained by subtracting Δp_{sys} from the raw pressure amplitude Δp_{mea} measured in a soil. Note that Δd and Δp_{sys} of the unload-reload loop is defined in the sub-figure of Fig. 3.14 where two apexes of the loop are referred. Thus, the soil unload-reload modulus E_{ur} is given as follow:

$$E_{ur} = \frac{\Delta p_{mea} - \Delta p_{sys}}{\Delta d} \approx \frac{\Delta p_{mea}}{\Delta d} - f'_{loading}(s) \tag{3.4}$$

where $f'_{loading}(s)$ is the derivative with respect to the piston displacement s

of the 3-order polynomial fit function $f(s)$ given in Eq. 3.2. This approximation assumes that the slope of the secant line $\Delta p_{sys}/\Delta d$ is close to the slope of the tangent line at the point where unloading starts, provided that the unload-reload loop is small.

3.4 Calibration Chamber Testing

Considering the proof-of-concept purpose and the iterative design needed for the entire development phase, this iDMT prototype was not devised for in situ testing which requires a pricey and robust probe fabrication. Nevertheless, a simple calibration chamber test with a comparison with the DMT is thus an expedient solution if a soil is to be tested.

3.4.1 Soil material and equipment

The calibration chamber test was performed with a dry Mol sand sample, which is a uniform fine quartz sand with a mean grain size (D_{50}) of 0.195 mm, a uniformity coefficient (C_u) of 1.60, a maximum void ratio (e_{max}) of 0.918, and a minimum void ratio (e_{min}) of 0.586 (Karg 2007).

The testing was carried out using the calibration chamber system illustrated in Fig. 3.15. The corresponding boundary condition is zero radial strain, zero bottom strain, and zero top stress. It is noted that both blades are wished-in-place to allow a comparison without the course of blade penetration, which implies both blades were in place before the sample preparation completed by a pluviation from a bottom sieve of a stationary funnel. The axial symmetrical distribution of the sample and the symmetrical layout of the blades allows a comparison of the results.

3.4.2 Results and comparison

The standard DMT test is performed based on the standard test method without the procedure of penetration. The membrane stiffness calibration is performed three times obtaining consistent results: $\Delta A = 11\,kPa$, $\Delta B = 22\,kPa$, where ΔA, ΔB = corrections determined at the displacement of 0.05 mm and 1.1 mm, respectively. The repeatability of ΔA and ΔB is important in this case since this calibration chamber system only allows a relatively low soil pressure on the membrane which is of the same order of magnitude with ΔA and ΔB. A

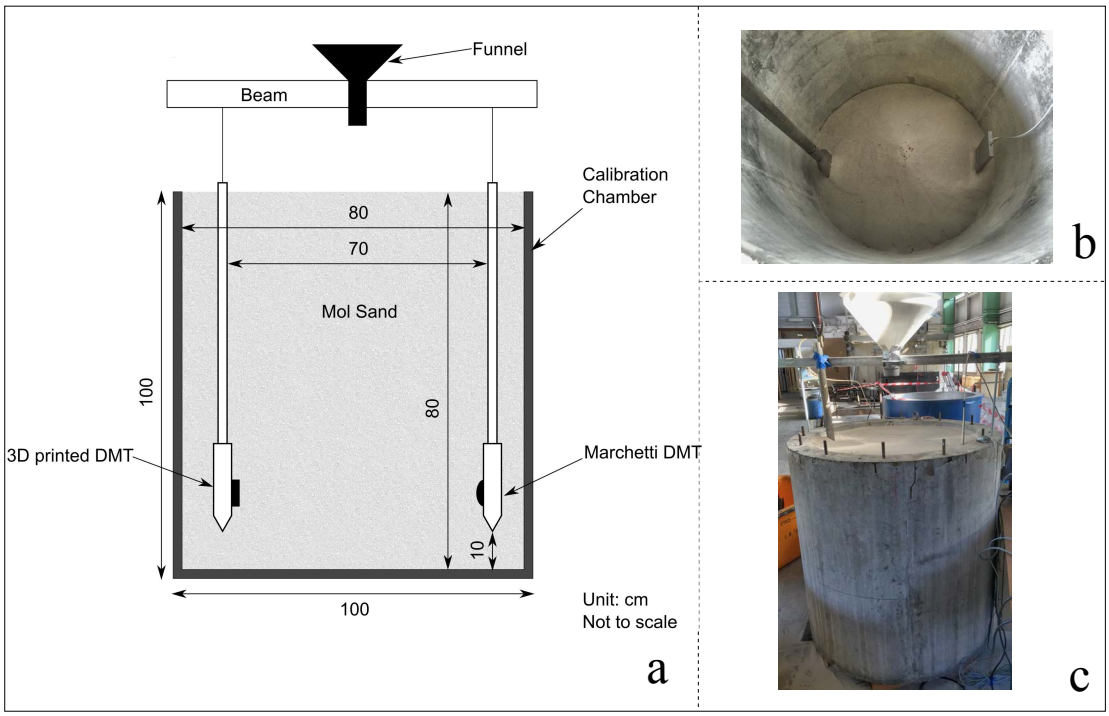

Figure 3.15: Calibration chamber system: (a) schematic view, (b) wished-in-place blades during pluviation, and (c) sample preparation completed.

more advanced calibration chamber allowing the application of stress boundaries can allow the soil pressure on the membrane at least one order higher than the corrections which results in a better accuracy, which however is not financially worthwhile in this case. Concerning the DMT testing results, the B-pressure of 40 kPa was read from the pressure gauge. Yet the A-pressure is mere -5 kPa and obtained in the same way as that of ΔA by generating negative pressure through a piston. This is not a standard practice in the DMT field testing procedure because of the relatively low soil pressure against the membrane in this case, resulting from the wished-in-place condition of the blade and the boundary conditions in the calibration chamber. Then based on Eq. 2.1 and Eq. 2.2, the corrected pressures p_0 = 5.4 kPa and p_1 = 18 kPa.

The iDMT calibration chamber test is conducted with the pressure-controlled procedure and the pressurization/de-pressurization rate of the main loop is 450 kPa/min and -900 kPa/min, which is different from 60 kPa/min and -60 kPa/min of the small unload-reload loop, respectively. This is due to the much smaller pressure amplitude and the consideration of reducing potential soil creep in the small unload-reload loop. Overall, the piston expansion stage takes about 1 min. This is approximately within the same order of magnitude of the time limits of the DMT membrane expansion, as shown in Table 2.1,

which generally takes 30 s to 60 s. Nevertheless, considering the difference between the piston expansion and the membrane expansion, the expansion rate of the two is not supposed to be necessarily the same.

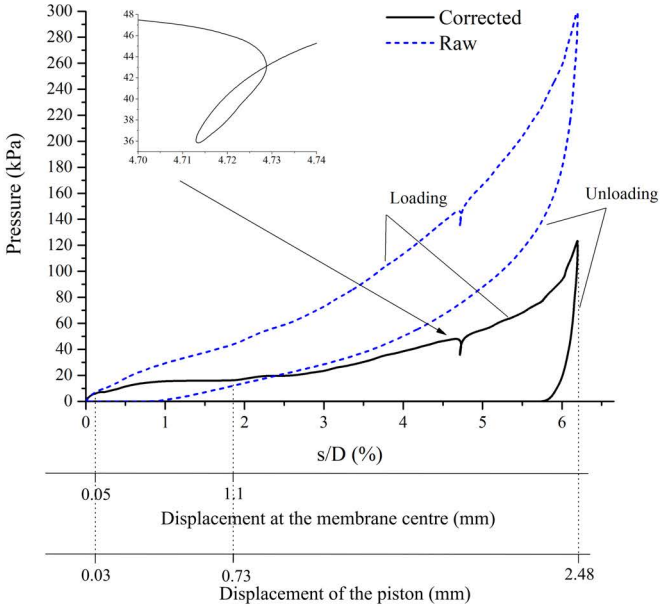

(a) the iDMT raw measurments along with the corrected curve

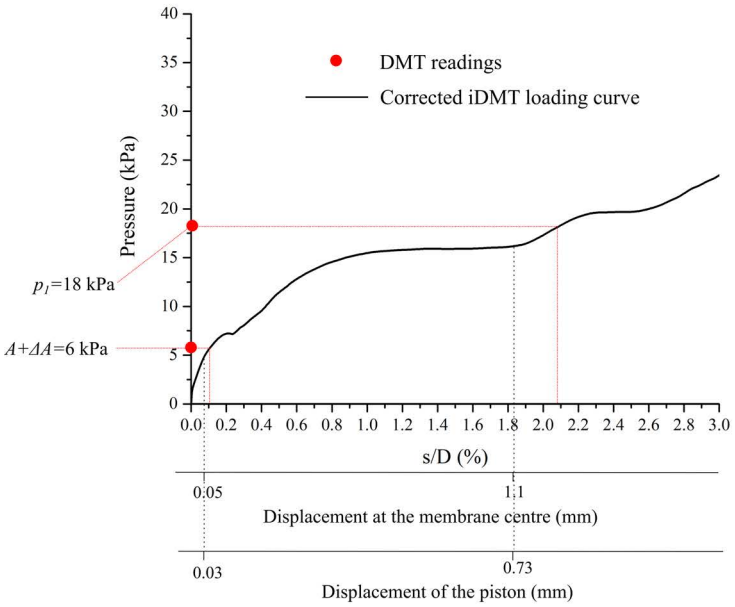

(b) the exploded view and the DMT readings

Figure 3.16: Calibration chamber testing results of a dry Mol sand

Fig. 3.16 shows the raw measurements and the corrected data from the iDMT test as well as from the standard DMT. Considering the difference be-

tween the 40-mm diameter piston and the 60-mm diameter membrane and the purpose of comparing the two kinds of data in one figure, pressures are not only plotted against the respective displacement s but also the normalized ratio of s/D, where s = the piston displacement or the membrane center displacement, and D = the piston/membrane diameter. As far as the data from the new iDMT is concerned, the corrected curve, which was produced by subtracting the calibration of wave spring resistance and O-ring friction from the raw curve, is shown along with the raw curve. It is seen that the iDMT results are consistent with expectations for a loose sand. During the loading, the soil near the piston is compressed to a denser state and the non-linear pressure-displacement behaviors are mainly caused by the rearrangement of the grains. Because this rearrangement of the grains is irrecoverable on unloading, the soil appears much stiffer in the unload–reload loop than in the loading.

The DMT $(A + \Delta A)$-pressure of 6 kPa and the p_1-pressure of 18 kPa are obtained at the membrane displacement of 0.05 mm and 1.1 mm, which are corresponding to s/D ratios of 0.083 % and 1.83 %, respectively. Note that the DMT $(A + \Delta A)$-pressure is in use in this case for a more appropriate comparison, rather than the p_0-pressure that is not measured but derived from a linear extrapolation. So a pressure of 5.1 kPa and a pressure of 16.2 kPa are read from the iDMT corrected curve at the s/D ratios of 0.083 % and 1.83 %, respectively. And s/D ratios of about 0.1 % and 2.18 % are found corresponding to the DMT p_0-pressure and the DMT p_1-pressure, respectively. The divergence between the DMT pressures and the iDMT pressures may be considered large with the difference being up to about 18 % in pressure and 20 % in the s/D ratio. But considering the low-pressure levels and the difference in the geometries of loading elements, the difference is acceptable and this comparison provides a basic evaluation of the proof-of-concept iDMT prototype.

Furthermore, the magnified view in the inset of Fig. 3.16 shows the small unload–reload loop carried out in the calibration chamber testing. Using Eq. 3.4, the soil unload-reload modulus $E_{ur} = \Delta p_{mea}/\Delta d - f'_{loading}(s) = 40$ MPa. E_{ur} may be considered as a measure of elastic stiffness of this soil sample while $E_D = 34.7(p_1 - p_0) = 0.51\,MPa$ may mainly involve irrecoverable plastic behavior considering that it is a loose pluviated sand sample.

It is noted that the force exerted by wave spring and the friction of the O-ring are important as they stand for the amount of 60.7 % of maximum total pressure. Because such a large correction is performed, the calibration for determining the force exerted by wave spring and the friction between different

parts was repeated after the calibration chamber test. As shown in Fig. 3.13, the repeatability of the two calibration curves is good but with a slight deviation in the initial pressure range and this deviation is within the accuracy range of the pressure sensor: ± 8.5 kPa (± 0.25 % of full scale). Therefore, it ensures that the large correction required does not cause significant errors in correcting the raw data.

Generally, with the pressure level up to about 298.9 kPa during the test, the new iDMT made in alumide shows promising results in performing in situ tests at least at shallow depth in soft clay that typically require a pressure within the same order of magnitude. In case a higher pressure is required, more robust and pricey material such as stainless steel along with DMLS technology or other alternative metal 3D printing techniques shall be used instead of economical alumide together with LS technology.

3.5 Conclusion

This chapter presented the design and fabrication of an iDMT laboratory prototype, followed by calibrations and a calibration chamber test. The use of 3D printing technology not only successfully completes the iDMT blade fabrication, which is difficult achieved using traditional subtractive manufacturing but also sheds light on using this novel technology in geotechnical testing such as improving laboratory and in situ devices. The use of 3D printing technology allows a larger displacement of the piston to 2.48mm than that of previous modified DMTs and the standard DMT. Additionally, the use of a computer control and data acquisition system permits the continuous pressure and displacement measurements. With these developments, calibrations and calibration chamber tests in a loose sand have been performed. Preliminary data indicate that the new iDMT prototype has the potential to produce pressure-displacement measurements to a larger strain level than the current standard DMT to evaluate non-linear soil behavior. On the other hand, the testing also proves the feasible use of 3D printed apparatus in soil testing, and the assembled LS products can withstand at least a pressure of 298.9 kPa. This experience may inspire engineers to make potential innovative improvements on geotechnical testing apparatus.

Furthermore, this lab prototype and the calibration chamber test represents the first stage of the iDMT's stepwise development, where experience is gained for the design and fabrication of the probe as well as for the software develop-

ment of the electro-pneumatic control & DAQ system. Most functions of the iDMT system were first tested with this lab prototype by trial and error, even including the ones that didn't make it to the field prototype such as the implementation of the displacement controlled procedure as shown in the Fig. 3.11.

It is interesting to note that in the lab prototype first an attempt was made to use the strain gauge to measure the displacements, which was used by the prior modified dilatometer devices described in the literature. It was easy to install the strain gauge, but the calibration results are poor since the strain gauge system itself as a sensing element is subjected to deformation induced by the applied pressure, which results in different calibrations at different pressure levels. Therefore, it was decided to use the contact-less type of sensors, in this case, the Balluff inductive displacement sensor, to allow the sensing element being shielded in a rigid case.

The sealing of the iDMT blade is important, as only a waterproof device can allow accurate measurements of the pressures. Although different sealing techniques were tried, such as the special coupling for the wires passing and the slide ring for the piston sealing, it was found that the simple techniques, in fact, gave the best results. In the end, the O-rings are used for sealing the piston and the covers, the epoxy is adopted to seal the gap where the wires pass out of the blade. Moreover, debugging the electro-pneumatic control & DAQ software written in LabVIEW is important not only for the correct test procedure but also for the sake of safety. So, this is also done with the lab prototype in-house rather than with the expensive field equipment.

The presented work in this chapter is an early iteration of the iDMT prototype and further work for in situ tests is discussed in detail in Chapter 4.

Chapter 4

The iDMT apparatus and test procedure

4.1 Introduction

Generally speaking, instrumentation of the probe offers good opportunities for a better interpretation, although, complexity introduced by instrumentation may present challenges in probe development and even degrade probe robustness. Thus, at the start, a laboratory prototype of the instrumented dilatometer was developed and tested, which has been described in Chapter 3. Though this proof-of-concept prototype allows the full pressure-displacement measurements of the piston loading and unloading in a calibration chamber, the blade is in place before the sample preparation, and so the blade penetration procedure is excluded. Therefore, it is not robust enough to carry out in situ tests as well as measure pore-water pressure in the ground, which is nevertheless considered as the primary goal of the iDMT development.

Fortunately, manufacturing techniques grow very fast in this day and age, for such as metal 3D printing allows making complicated and robust parts that are challenging to be machined or cast – and, in some cases, enables the production of parts that are otherwise impossible by any traditional means. That being said, there have been only a handful of cases taking advantage of these novel and easily accessible manufacturing techniques to develop geotechnical laboratory testing device such as 3D printing a leak-free cell in a biaxial testing system (Yuan et al. 2016), and even fewer cases can be found for in situ testing apparatuses.

With the experience gained from the lab prototype mentioned in Chapter 3

and with the aid of a novel metal 3D printing technique, the development of a more robust instrumented dilatometer with more measurements of soil response from in situ testing is described in this chapter.

4.2 General principles of the iDMT

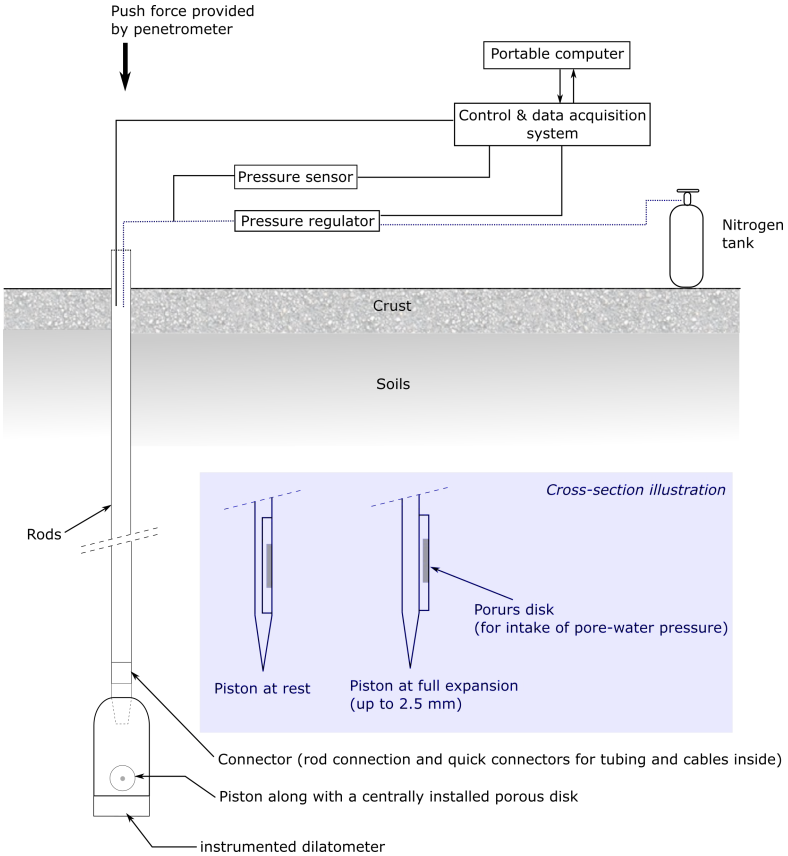

Figure 4.1: Basic principles of the iDMT test

In terms of the general working principle, the DMT blade originally introduced by Marchetti works as an electrical switch (on/off) without using any complex instrument (Marchetti 1975). This pioneering design enjoys the benefits of simplicity and does the job of obtaining pressure readings at two displacement levels at the membrane center: 0.05 mm and 1.1 mm. However, redesign of the blade and the system is technically needed if more accurate measurements of soil response are required.

The basic layout and principles of the iDMT test are shown in Fig. 4.1. Similar to the DMT tests, the instrumented dilatometer can also be installed vertically at various depths in the ground by means of direct ”static” push.

Then, a horizontal expansion stage follows the installation stage in the iDMT. But rather than a membrane expansion in the DMT, it is a rigid piston competing against the surrounding soil by means of internal gas (i.e. Nitrogen) pressure in the iDMT. Uniform displacement of the soil occurs as the rigid piston displaces up to about 2.5 mm. Continuous measurements of the applied pressure, the piston displacement and the pore-water pressure via a pore-water filter located at the piston center are all recorded in a field portable computer/laptop via the data acquisition system. Using these measurements, full pressure-displacement curve and pore-water pressure measurements can be produced to enable the effective stress analysis that is not possible in the standard DMT test. The iDMT tests are applicable to common soils, i.e., sands, silts, and clays, as long as the dimensions of grains are small compared to the piston diameter. The relative size between the piston diameter and the grain may be considered as small if smaller than 1/30, which is found by the 60-mm diameter membrane of the DMT and the maximum grain size of 2 mm of very coarse sand given by ISO standard 14688-1:2002 (2002). Note that this is a conservative estimation for the iDMT piston based on the DMT membrane since the fixed membrane edge must result in a smaller contact area with the soil than the total membrane area, which is not the case for the rigid piston.

Based on these iDMT principles, major modifications compared with the DMT system include replacing the flexible membrane with a rigid piston, instrumentation of the blade and an electro-pneumatic system allowing automatic control and continuous measurements. Furthermore, the iDMT test procedure is devised to allow a comparison with the standard DMT test results as well as the use of the well-established DMT correlations with common soil parameters.

4.3 Apparatus of the iDMT test

Common field equipment in geotechnical site characterization can be used for installing the instrumented dilatometer in the ground. Fig. 4.2 shows the field equipment used in this study: a truck-based penetrometer together with push rods which are usually adopted in the standard DMT tests as well as in the CPT tests. Alternatively, one may also use a drill rig to provide the thrust force to penetrate the instrumented dilatometer in the ground. Excluding the ordinary field equipment, the iDMT test apparatus comprises three main components:

- instrumented dilatometer
- electro-pneumatic pressure control system
- cables and pressure source

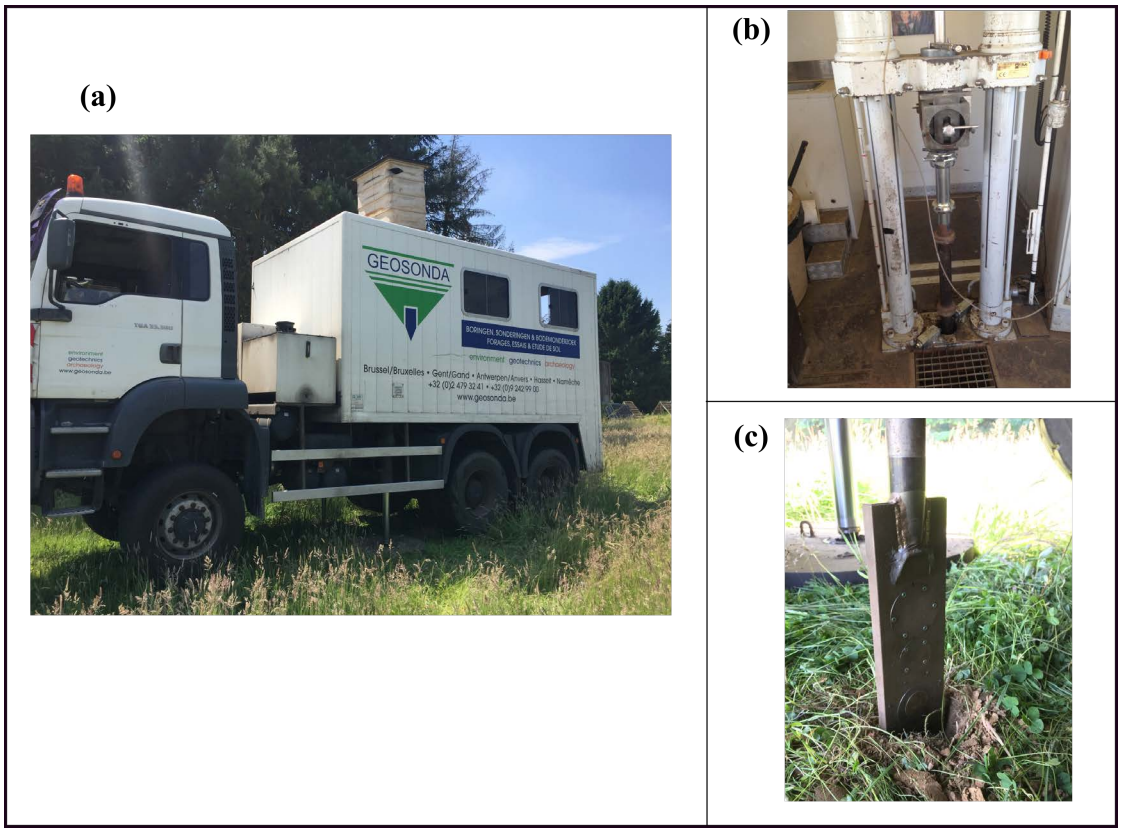

Figure 4.2: The field equipment required for the iDMT installation in the ground: (a) the (CPT) truck, (b) truck-based penetrometer and (c) the instrumented dilatometer ready for the installation

4.3.1 Instrumented dilatometer

Design

The starting point of the instrumented dilatometer design is that the external dimensions shall comply with the nominal dimensions of the standard dilatometer which are 95 mm width and 15 mm thickness, with an approximate 16° cutting edge (50 mm length of the tapered section). And the relative distance between the piston center and the instrumented dilatometer tip is kept the same with that between the membrane center and the DMT blade tip. Note

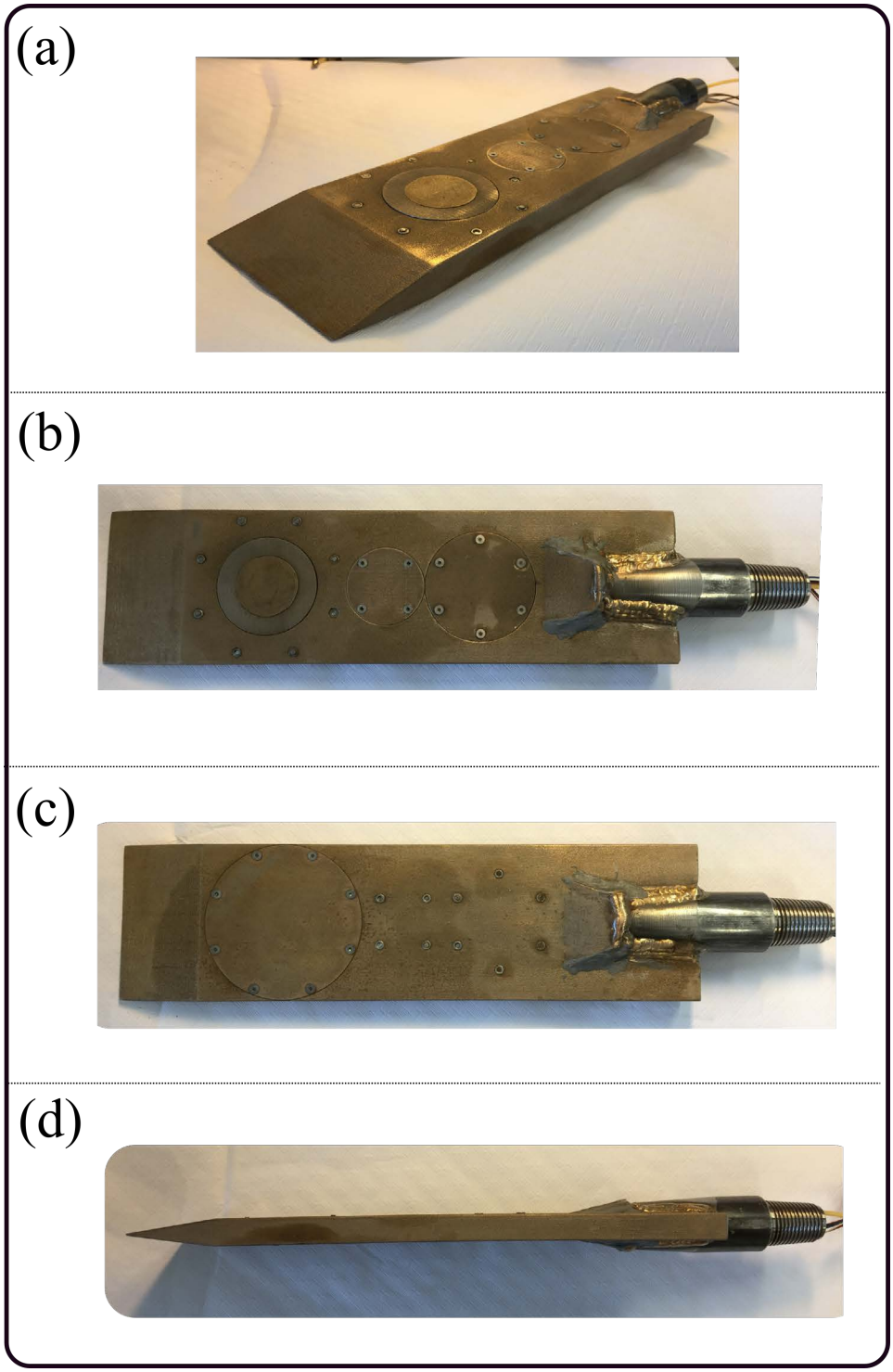

Figure 4.3: The instrumented dilatometer in: (a) angled view, (b) top view, (c) bottom view and (d) side view

that the total length of the standard dilatometer is not considered as a nominal dimension by Marchetti (1980) and Marchetti et al. (2001) but is specified between 220 mm to 230 mm by ISO standard 22476-11:2017(E) (2017). A longer

dilatometer normally shall not influence the test results as long as the wedge-shaped section of the blade below the membrane remains unchanged since the disturbance of the soil adjacent to the membrane is mainly subject to this section that opens a flat cavity during the penetration. This is supported by the numerical results from Kouretzis et al. (2015), where the standard dilatometer is modeled with an infinite length defined by a sliding surface. Stetson et al. (2003) also used a modified dilatometer with a length of 260 mm, which does not show divergence in test results owing to the different dilatometer length. In the case of the instrumented dilatometer, the total length is 350 mm.

Fig.4.3 illustrates the instrumented dilatometer in different views. In the top view, the major visual difference with the standard dilatometer is the use of a 60 mm diameter circular rigid piston in the instrumented dilatometer, rather than a 60 mm diameter circular flexible membrane used in the standard dilatometer blade. This rigid displaceable piston is in line with the blade surface at rest condition and comprises a porous disk mounted flush at its center, which allows intake of pore water. This porous disk, made of sintered bronze with an average pore size of about 10 μm, is 38 mm in diameter and 2 mm in thickness. The use of this rigid displaceable piston as the loading element is favored in this design since:

- With a displacement up to about 2.5 mm, the rigid piston can protrude further out of the blade surface, while the standard DMT only allows 1.1 mm of a central membrane displacement. Because Marchetti et al. (2001) suggests that any membrane expansion larger than 1.1 mm may permanently deform the membrane and change its calibration.

- Even if the flexible membrane is able to conduct a larger displacement, it is not possible to assume a uniform loading condition any more since the edges of the flexible membrane are fixed to the dilatometer. In terms of the rigid piston, a uniform displacement assumption is still valid with a displacement up to about 2.5 mm or even more.

- Practically, it is easier and more robust to install a pore-water filter (e.g., porous disk) on the rigid piston than on a thin (0.02 mm thickness) flexible membrane. Moreover, the stiffness behavior of the membrane – the source factor of the calibration – is changed by any modification of the membrane and under further calibration requirement concerning the system compliance.

- The calibration of the membrane may change during a sounding due to soil abrasion (wrinkles and deep scratches). While the calibration of the rigid piston system is more consistent throughout a sounding since the source factors of the calibration are inside the blade.
- The rigid piston can be used in a larger variety of soil types (e.g. glacial tills, gravels) because of its robustness, especially in soils where the membrane may be easily scratched or even damaged.

Moreover, the diameter of the rigid piston is not necessarily the same as the 60-mm diameter of the flexible membrane, so a smaller piston is also viable to increase the probe robustness. However, this can reduce the range of soils suitable for testing since the soil grains need to be small compared to the piston diameter.

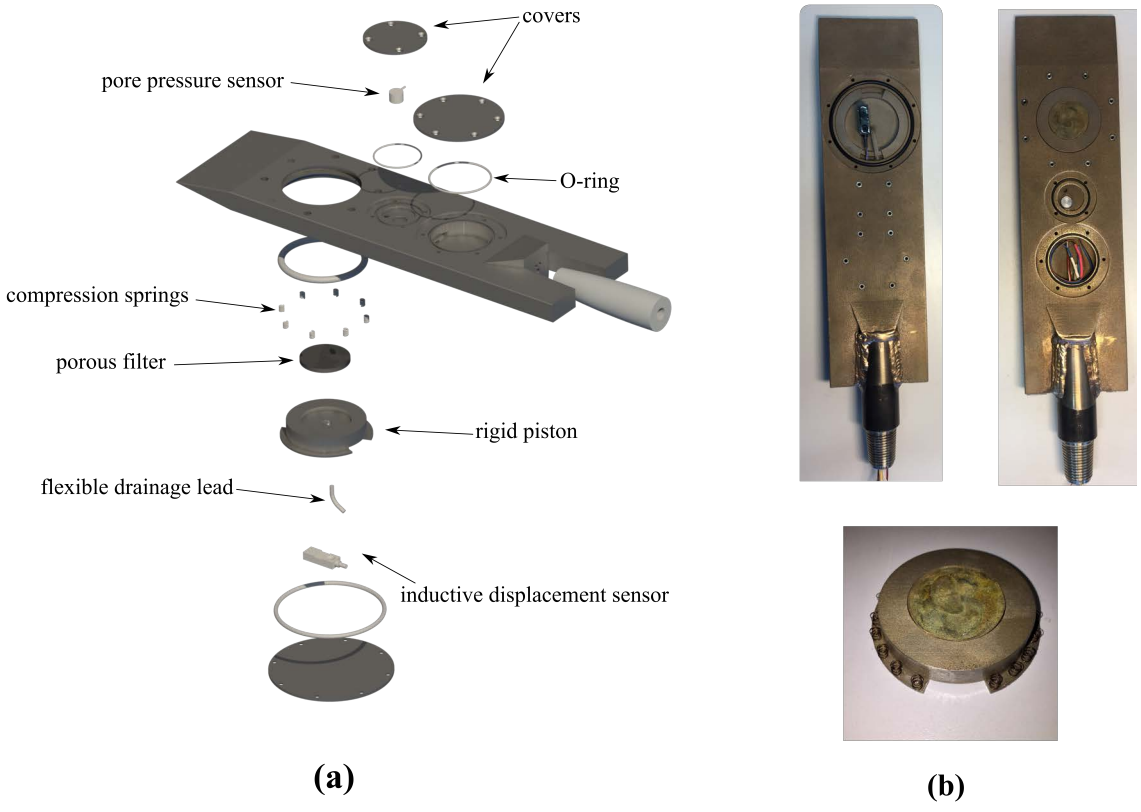

Figure 4.4: (a) Exploded CAD view of the instrumented dilatometer, (b) unveiled instrumented dilatometer (not to scale)

Alongside with the bottom view in Fig. 4.3, three covers in different sizes are spotted for sealing different chambers. Fig. 4.4 shows a CAD-generated ex-

ploded view and an unveiled view of the instrumented dilatometer regarding the parts underneath the three covers. Specifically, the main blade body comprises 3 chambers, wherein 3 covers along with O-rings lodged in specifically dimensioned grooves are used to seal the chambers and shield the elements within the chambers from outside influence.

In the chamber close to the blade tip, an inductive distance sensor (made by Balluff, model BAW-R03) is installed to measure the piston movement up to 3 mm. The piston itself is the metal target influencing the sensor output with its movement. Note that this piston comprises a porous disk mounted at its center, which allows intake of pore water. An array of compression springs are evenly distributed on the flange of the piston to keep the piston in line with the first blade surface at rest condition, as shown in Fig. 4.4(b). This is different from the wave spring used in the iDMT laboratory prototype since the stiffness of the wave spring significantly increases with the shaft diameter, which results in an undesirable larger correction.

The adjacent chamber is a pore-water pressure cell comprising a pore-water pressure sensor (made by Keller, Model 4LC) to measure a pressure range of 0 (vacuum) to 1 MPa (relative to vacuum). The channel for conveying pore water between this pore-water pressure cell and the pore-water filter in the piston consists of a flexible drainage lead and a 3D printed tunnel. Prior to in situ tests, this cell together with the drainage lead, the tunnel, and the pore-water filter must be saturated with viscous silicone oil to reduce the possibility of saturation loss. This way, a fixed and stable environment is created to have a consistent performance of the pore-water pressure measurements. The third chamber of the instrumented dilatometer is necessarily configured to house circuitry and to provide space during assembly and maintenance.

Additionally, note that the small pockets of the instrumented dilatometer in the top and bottom view are used to keep the nuts and the bolts in place to fix the chamber covers at the other side of the blade. The nuts and bolts are designed to be flush with the surface of the instrumented dilatometer when tightened properly.

Fabrication

Given the complexity inside the instrumented dilatometer, the fabrication is at least challenging for traditional manufacturing means. With standard machining tools, the irregular tunnels and the hidden grooves inside the blade are

difficult to built. In a comparison, metal 3D printing does not suffer any of the aforesaid geometrical limitations and reduces the production time with orders of magnitude. However, objects normally require a minimal thickness (1 to 3 mm depending on material) to be metal 3D printed, even thicker to form a suitable stiffness and strength since the process is creating an object by laying down successive layers of material. So, certain 3D printed parts with small thickness cannot safely withstand the pushing thrust during the penetration, such as the threads on the rod-blade connector. Therefore, a hybrid of manufacturing technologies is used in the instrumented dilatometer fabrication: the main blade body and the rigid piston are metal 3D printed; the rod-blade connector is machined; then the main blade body and rod-blade connector are welded together. This hybrid method is de facto a compromise between the traditional machining process and the metal 3D printing technique, which not only enables the fabrication of the iDMT probe that is too complex for the traditional machining but also fortifies the parts such as the threads which are less robust in case of fabricating with the 3D printing techniques.

There are various methods of metal 3D printing. The goal of this project is to fabricate the parts sufficiently robust in an accurate manner, at low cost. So, it was decided to use the binder jetting technique to produce a matrix metal material — 420 stainless steel infiltrated with bronze. The binder jetting technology is originally developed at MIT (Sachs et al. 1990), but only becoming one of the commercial 3D printing technologies around 2010. Binder jetting in 420 stainless steel infiltrated with bronze typically involves the following steps: printing, curing, sintering and infiltration, and finally cooling down (ExOne 2014). The printing is a process of a liquid binder selectively deposited to join stainless steel (alloy 420) powder particles, and this process is repeated layer by layer to form a complete object. This object is then cured in an oven to enable the handle-ability. Following the curing, the objects are sintered and infiltrated with bronze (90% Cu and 10% Sn) above 1100°C. In the last step, the object is cooled down in an annealed way to increase its ductility and ease the welding. The finished object composes of 60% stainless steel and 40% bronze infiltrant, with the main properties shown in Table 1. It is worth mentioning that the whole production process of the instrumented dilatometer parts takes only 2 days, costs approximately €300 excluding VAT, which is by no means feasible using traditional machining or casting techniques. In terms of geometrical accuracy of the finished products, the main blade body has a width of 94.8 mm (-0.21% error), a thickness of 15.5 mm (+3.3% error) and a length

of 349 mm (-0.29% error); the rigid piston is 60.3 mm (+0.5% error) in diameter. The error (in percentage) of the blade thickness is generally one order of magnitude larger than the rest, due to the fact that the layer by layer printing orientation is along the axis of thickness, and a single layer thickness is 0.1 mm.

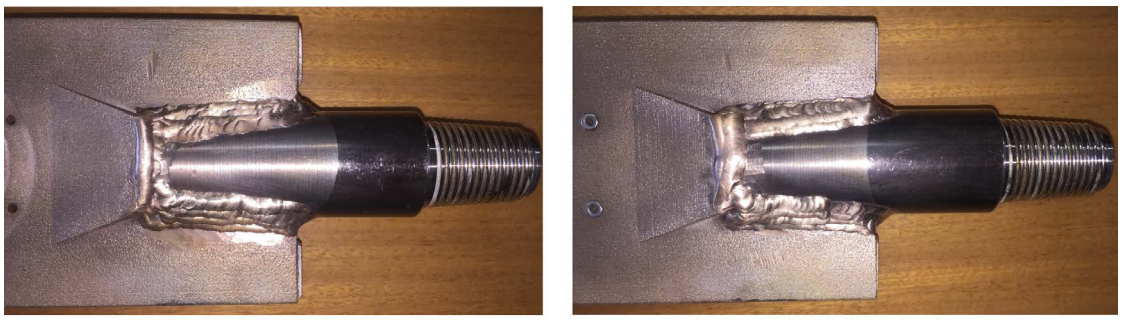

(a) **(b)**

Figure 4.5: Both sides of the welded section of the instrumented dilatometer

As the rod-blade connector is machined from a push rod, the key to the success of the hybrid manufacturing is a good welding process to bond two distinct parts together. In this case, a tungsten inert gas (TIG) welding process is conducted by layer-by-layer depositing silicone-bronze ($CuSi_3$) filler and allowing a slow cooling down process to the atmosphere temperature between two successive layers. These cooling down intervals allow the heat generated during the TIG welding to be dissipated evenly to prevent any crack formation due to the different thermal properties between the 3D printed parts and the machined parts. Fig. 4.5 shows the welding part of the instrumented dilatometer where layers of the ($CuSi_3$) filler can be spotted right on the surface.

Following this welding procedure, a penetrant testing (PT) was performed to inspect if there is any invisible surface-breaking defect developed during the welding. The PT generally involves the following steps: cleaning; applying the penetrant, removal of the penetrant, applying the developer to draw the penetrant from defects out onto the surface to form a visible indication and post cleaning. Concerning this welding, no defects or imperfections were found by the PT, which indicates a good welding.

4.3.2 Electro-pneumatic pressure control system

Fig.4.6 shows the electro-pneumatic pressure control system comprising components deployed alongside with a penetrometer on the ground surface and the sensors installed in the instrumented dilatometer. The instrumented dilatome-

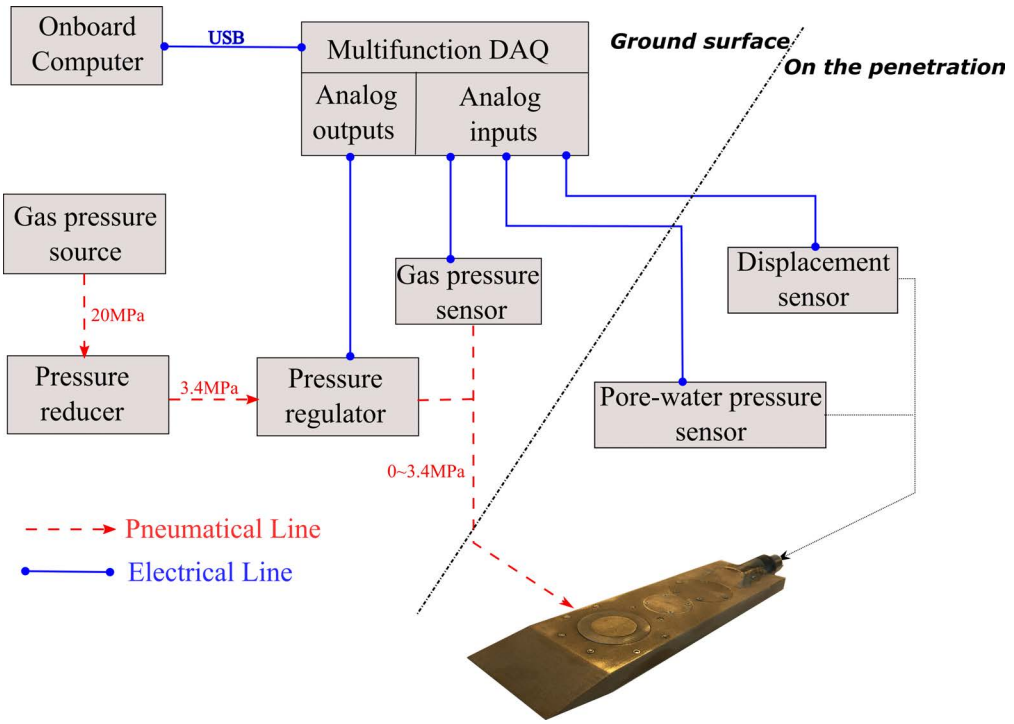

Figure 4.6: Schematic diagram of the instrumented dilatometer electro-pneumatic pressure control system

ter allows direct measurements of the piston displacement and pore-water pressure at the piston center, while the applied pressure is measured on the ground surface using a sealed gauge pressure sensor (made by Honeywell, model MLH). By providing real-time feedback of these measurements to the control system, the electrical pressure regulator (made by Proportion, model QB2) can automatically adjust the applied pressure using a proportional integral derivative (PID) mechanism to construct different loading path, such as constant rate of stress or constant rate of strain. Meanwhile all measurements are recorded in a portable computer via a data acquisition (DAQ) device (made by National Instruments, model USB-6009), which facilitates an onsite real-time check of the data.

In the iDMT system, the sensors deliver analog outputs and the electrical pressure regulator receives analog input. So, an Analog-to-Digital Converter (ADC) is employed in the DAQ to record the sensor measurements in digital format for further processing with in the computer, while a Digital-to-Analog Converter (DAC) is also necessary for the DAQ to convert the desired pressure value to an analog signal for the electrical pressure regulator. Thus the resolution of the whole system depends on the DAQ resolution which is given as

follows:

$$Resolution = \frac{Range}{2^{Bits} - 1} \tag{4.1}$$

where Bits = 12 for the DAC and Bits = 16 for the ADC.

Thus, the resolution of the pressure control, the total pressure measurements, the pore-water pressure measurements and the displacement is 8.42 kPa, 0.53 kPa, 0.02 kPa and 0.05 μm, respectively. However, it is important to understand that accuracy of the measurements and of the pressure control is different from the resolution, and the resolution can be several orders better than the accuracy. According to the data sheet of each individual instrument, the accuracy of the pressure control, the total pressure measurements, the pore-water pressure measurements and the displacement is $\pm$17.5 kPa, $\pm$8.75 kPa, $\pm$2.5 kPa, $\pm$35 μm, respectively.

4.3.3 Cables and gas pressure source

In terms of the standard DMT tests, an electrical ground cable and a pneumatic-electrical cable having a wire inside constitute a complete circuit along with the push rods and the dilatometer. Rather than a simple on/off switch circuit like this, the instrumented dilatometer requires a more complex circuit design that is given in Fig. 4.6. Excluding the cables between the instruments on the ground surface, two electrical cables, and a gas tube are required to run inside the push rods, which are normally packed in a reel prior to the assembly for field testing as shown in Fig.4.7(a,b). Quick connectors are specifically built to ease the connections with the still part on the ground surface as well as the part on the penetration.

The gas pressure source of the iDMT tests can be the same as that for the standard DMT tests, which is typically a gas (compressed nitrogen or compressed air) tank equipped with a pressure regulator, as shown in Fig. 4.7(c). In the case of the iDMT test, the regulated output pressure is 34.47 MPa that is equivalent to the maximum output pressure of the electrical pressure regulator. Although the capacity of this pressure level is supposed to be able to address most soil conditions based on the DMT experience from Marchetti et al. (2001), higher pressure can be required for very stiff soils. That said, it is always possible to use an electrical pressure regulator with greater capacity while main concerns are related to the budget and how often one may use that high-pressure range.

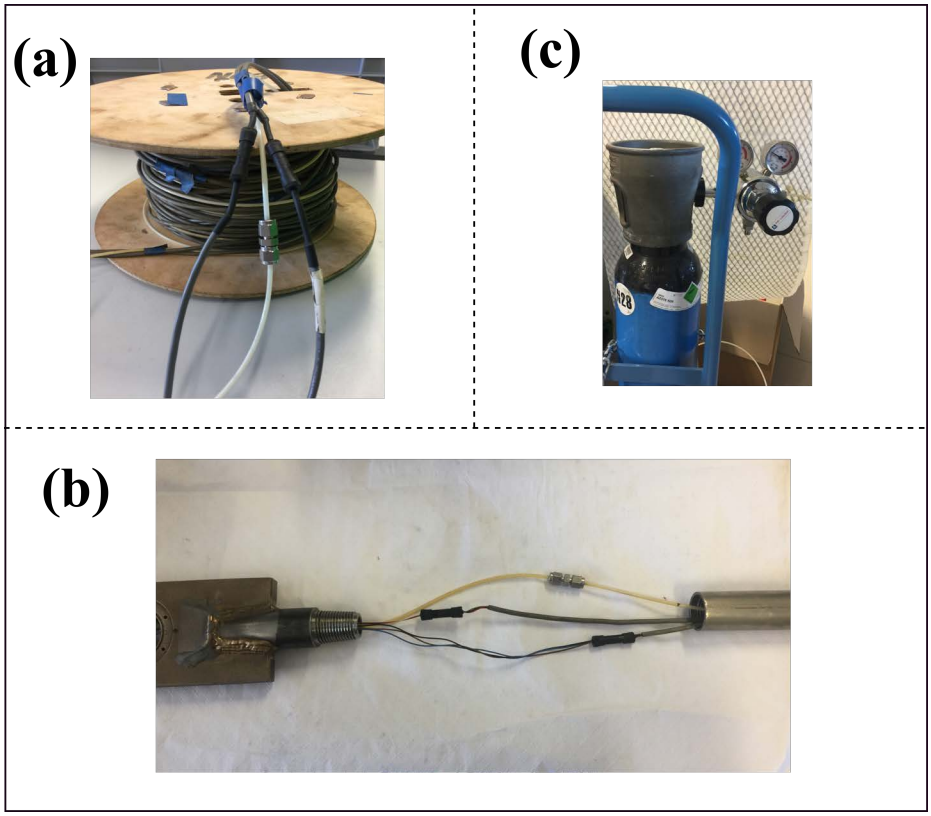

Figure 4.7: (a) Cable reel for the pneumatic tube and electrical cables along with the quick connectors on the ground surface; (b) the quick connector near the instrumented dilatometer and (c) the gas (nitrogen) pressure source.

4.4 A pseudo displacement-controlled algorithm

4.4.1 Algorithm description

As mentioned before, a short circuit mechanism is used to signal the central membrane displacement at 0.05 mm and 1.10 mm in the DMT. The standard DMT testing methods introduced in ASTM Standard D6635-15 (2015), ISO standard 22476-11:2017(E) (2017), Marchetti et al. (2001), and Eurocode7 (1997) generally provide time limits, as shown in Table 2.1, for taking pressure readings at the two displacement levels. This way the pressurization rate is controlled by manually regulating the applied pressure and shall be varied with the anticipated pressure readings: faster in stiff soils and slower in soft soils. Strictly speaking, this process may be only regarded as a pseudo displacement-controlled procedure as this operation requires first an anticipation of the pressure readings and then manually regulate the flow valve to adjust the pressurization/de-pressurization rate in order to comply with the

time limits given in the standards. In other words, the average velocity of the membrane movement (the rate of change of the membrane displacement as a function of time) is controlled by the DMT, but the actual velocity at a give time is operator-dependent since the DMT does not measure continuous displacements.

With the new instrumented dilatometer, it is possible to automatically adjust the pressurization/de-pressurization rate based on the real-time feedback from the measurements which include the piston displacement, the applied total pressure, the pore-water pressure and the penetration thrust. This is enabled by using the state machine architecture in LabVIEW aforementioned in Section 3.2.3, which is thus operator-independent.

Given the difference in many aspects between the iDMT test and the standard DMT test, the iDMT test procedure is not necessarily the same as that of the DMT. Nevertheless, at the current initial stage of the iDMT research, it is reasonable to follow the DMT test procedure to not only allow the use of the well-established DMT correlations with common soil parameters but also measure in comparable soil conditions. Therefore, in terms of the pseudo displacement-controlled procedure, the time limits for the DMT test provided in Table 2.1 can be translated to the upper bound and the lower bound in velocity. In the in situ testing, the actual velocity is measured in real time since the piston displacement together with the testing time are both continuously measured and recorded. Then running the algorithm as shown in Fig. 4.8 maintains the velocity in a pre-determined range, which then realizes the pseudo displacement-controlled procedure similar to the DMT test procedure. Note that the execution rate of this algorithm in LabVIEW (the timed loop) is set as every 100 ms, which assures stable and smooth results of the pressure control. The details of the algorithm programmed in LabVIEW are provided in Appendix A.

4.4.2 Calculation of the piston velocity

The loading stage of the iDMT test and the standard DMT test can both be regarded as deforming a volume of soils by means of a cavity expansion. The extent of the expansion is usually quantified as the piston displacement and the displacement at the membrane center, respectively. However, a comparison between the two is not allowed in this way.

Therefore, the volume of the expanding cavity is considered better as a

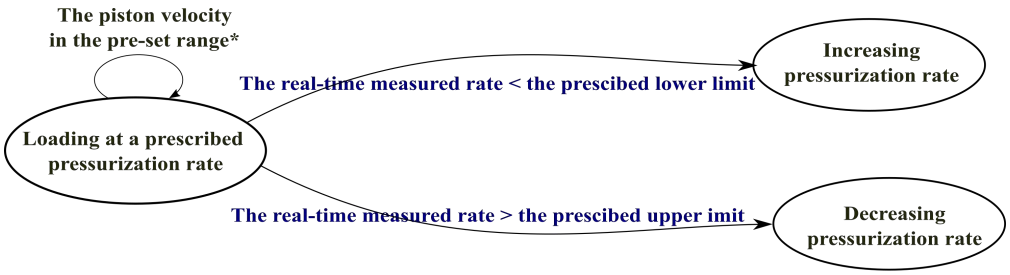

* the pre-set range is converted from the DMT time limits

Figure 4.8: Flow chart snippet for the pseudo displacement-controlled algorithm

common and comparable variable. As shown in light magenta in Fig. 4.9, the expansion of the flexible membrane is modeled as an expanding spherical cap, and the expansion of the rigid piston is modeled as an expanding cylindrical element. The volume of this spherical cap is expressed as:

$$V_m = \frac{1}{6}\pi h(3a^2 + h^2) \tag{4.2}$$

where V_m is the membrane volume, h is the membrane displacement at the center, a = 3 cm (the membrane radius).

The volume of the cylindrical element can be expressed as:

$$V_p = \pi r^2 h' \tag{4.3}$$

where V_p is the piston volume, r is the piston radius and h' is the piston displacement.

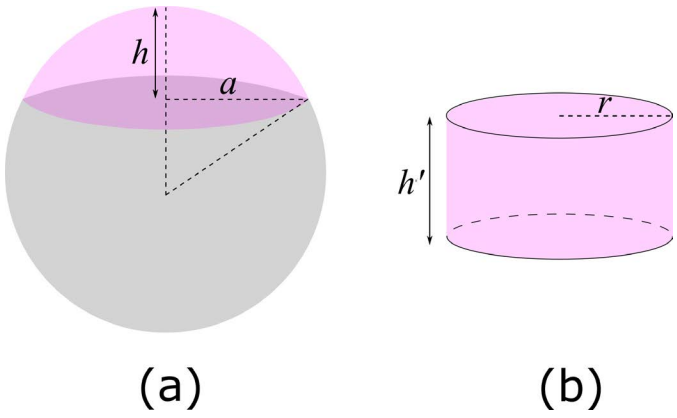

Figure 4.9: Expanding cavity volume of (a) a flexible membrane and (b) a rigid piston

In terms of the maximum loading capacity, the flexible membrane (a = 30 mm, h = 1.1 mm) and the rigid piston (r = 30 mm, $h^{'}$ = 2.5 mm) allow a maximum cavity volume of 1555.7 mm^3, 7068.4 mm^3, respectively. In case of a smaller piston with a diameter of 40 mm, the maximum cavity volume is 3140 mm^3.

In the DMT, the pressurization rate is normally controlled by acquiring sequential pressure readings within required time ranges. Taking the difference between the popular standard testing methods into account, as shown in Table 2.1, the time generally required for a complete expansion sequence (A-pressure and B-pressure) is within 30 s to 60 s. Similarly, the time required for a slow, controlled de-pressurization for the C-pressure is within 15 s to 60 s, which varies a lot between different testing standards. This pressurization/de-pressurization rate requirement with respect to the time limits can be expressed as a volume-per-time range of 26 mm^3/s to 52 mm^3/s for a pressurization and 26 to 104 mm^3/s for a controlled de-pressurization. Then, the time required for a full 60 mm-diameter piston expansion to 2.5 mm and a full reduction to zero displacement can be derived from the volume-per-time ranges as 136 s to 272 s and 68 s to 272 s, respectively. Nevertheless, an immediate de-pressurization is performed in the typical iDMT soundings, rather than a controlled de-pressurization since there is no such need of measuring pore-water pressure via the C-pressure when the direct pore-water pressure measurements at the piston center are available.

4.5 Calibration

Generally, the methodology used in calibration of the iDMT test is the same as that of the iDMT laboratory prototype described in Chapter 3, which includes two types of calibration to obtain a correct soil response from the iDMT: calibration of the instrument recording system, and determination of the internal resistance during the piston movement in known and controlled boundary conditions. The first one ensures that correct data from instruments are logged, and the latter is required for the interpretation of soil response during testing. The iDMT calibration results along with the difference with the aforementioned lab-prototype calibration are described in this section.

In terms of calibration of the instrument recording system, the piston-displacement calibration is firstly performed to measure the output of the non-contact displacement sensor in function of the displacement of the target

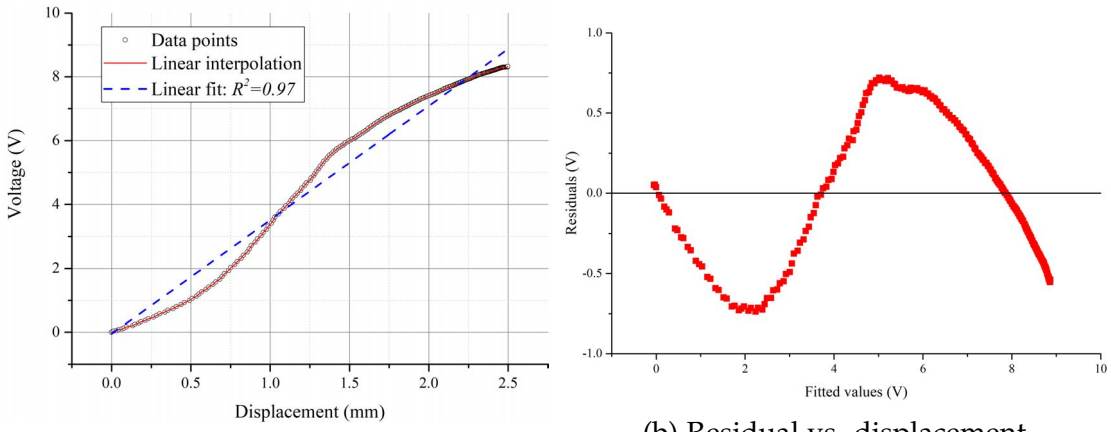

(a) Piston-displacement calibration

(b) Residual vs. displacement

Figure 4.10: Piston-displacement calibration

(piston) made of the non-standard material (420 stainless steel infiltrated with bronze). The piston displacement is measured using a dial gauge (made by Sylvac, model μ233) at the same sampling rate as the inductive displacement sensor, which is similar to the set-up shown in Fig. 3.9. Fig. 4.10 illustrates the relationship between the voltage output of the sensor and the piston displacement measured by the dial gauge. Note that this voltage-displacement relationship is generally dependent on the type of metal used. Based on the sensor manual, the curve is supposed to be linear if the target is made of 100% stainless steel, while in the case of a matrix metal made of 60% 420 stainless steel and 40% bronze, a non-linear relationship is spotted. Despite that a high coefficient of correlation of 0.97 can be obtained by the best fit line, the linear fit is inappropriate for the non-random residual plot as shown in Fig. 4.10. Note that this non-linear nature is related to the material property of the matrix metal made of 60% 420 stainless steel and 40% bronze and thus constant during the tests. Therefore, instead of the linear fitting, interpolation is adopted to estimate the displacement value at any given voltage, using the two adjacent known data points. It is worth mentioning that this piston-displacement calibration is found highly repetitive by having identical results in three independent calibrations.

Furthermore, zero-offset calibration determining the value at zero loads shall be performed routinely in the field prior to each field test since ambient temperature or atmosphere pressure shift can result in errors. Thus the zero-offset calibrations are necessary for all transducers in the instrument recording system, including the displacement sensor, the total pressure sensor, and the pore-water pressure sensor. One may refer to the example given in Section 3.3.1

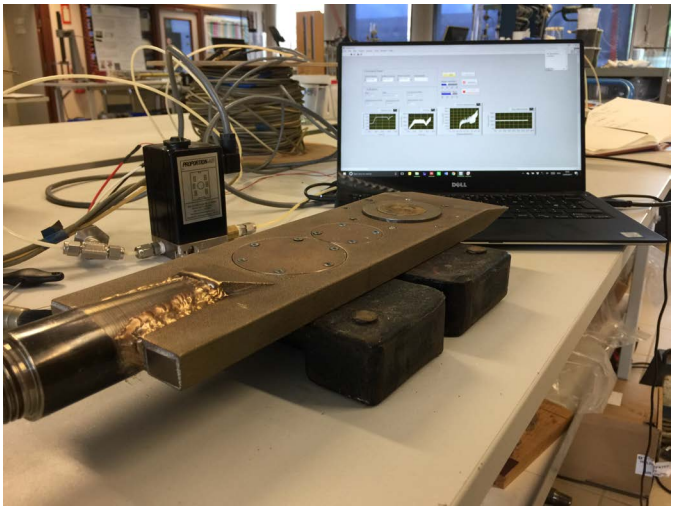

Figure 4.11: Calibration set-up in the air

for the zero-offset calibration of the total pressure sensor.

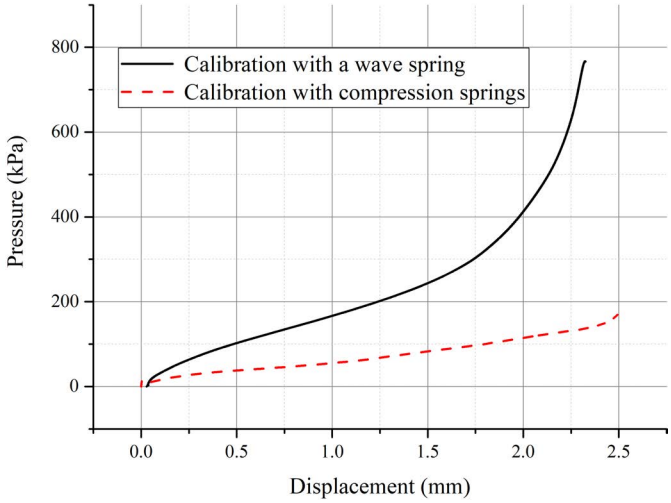

Figure 4.12: Loading curves of calibrations with compression springs or a wave spring

Considering that the raw data from field tests consists of not only the soil response but also the system internal resistance which is the sum of the force exerted by the compression springs, the friction of the O-ring and the system compliance, calibrations mimicking the in situ testing procedure in the air are needed, as shown in Fig. 4.11. Although it is possible to use a wave spring with the 40-mm diameter piston described in Chapter 3, a larger wave spring is required for a 60-mm diameter piston, which results in significantly larger pressure to counterbalance the force of the wave spring especially when the displacement is larger than 2.0 mm.

Fig. 4.12 shows the loading curves in calibrations with a wave spring or compression springs inside the instrumented dilatometer. The loading curve produced with the compression springs requires only about 180 kPa pressure to achieve 2.5 mm piston displacement while the other one with the wave spring needs over 750 kPa to reach only 2.3 mm. Considering that the loading curves in the calibrations are to be subtracted from the raw data, smaller correction is obviously preferred, so compression springs are used in the instrumented dilatometer.

Figure 4.13: Loading-unloading loop of a calibration in the air

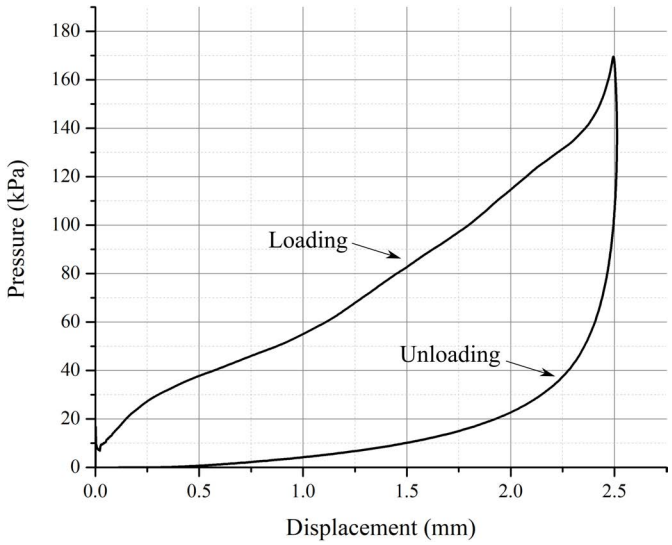

In the standard DMT test procedure, a slow de-pressurization process can be carried out for pore-water pressure information from the *C*-pressure reading. In the iDMT test procedure, de-pressurization is normally conducted instantly since pore-water pressure can be directly measured at the piston center. Although only the loading curve is concerned, Fig. 4.13 shows a complete calibration with monotonic loading and unloading, which indicates a non-linear hysteric loading-unloading loop. This may be an issue since hysteresis can be either rate-dependent or rate-independent. Thus, a study with three different pressurization rates was performed, which includes the maximum, the minimum and the mean pressurization based on the aforementioned piston velocity calculation, which is given in Table 4.1.

Fig. 4.14 shows the three loading curves in different pressurization rates. Considering a $\pm$ 8.5 kPa accuracy of the instrument system, no significant difference between the loading curves is found. This confirms that the loading curve is rate-independent in the given pressurization range. With this calibra-

Table 4.1: The pressurization rates

	Maximum	Mean	Minimum
Pressurization	52 mm^3/s	39 mm^3/s	26 mm^3/s

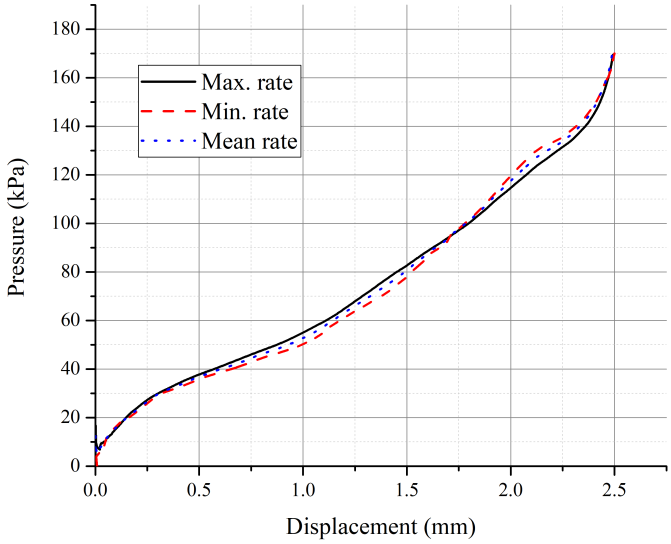

Figure 4.14: Compression spring stiffness and O-ring friction calibrations

tion data available, the soil response — the corrected pressure-displacement curve can be readily produced by a subtraction from the raw field data. Together with the development of the pore-water pressure, these corrected measurements are supposed to reasonably enable a better interpretation of soil properties than that of the standard DMT having pressure readings at only two displacement levels.

Furthermore, as described in Chapter 3, the estimation of the soil stiffness can be enhanced by performing small unload-reload loops in the iDMT tests. Fig. 4.15 illustrates the simulation of such test procedure in the air, which can be regarded as a calibration to correct the field data. The size of unload-reload loops is controlled by a predefined displacement magnitude which is 0.1 mm in these calibrations. In addition, a pressure holding phase generally precedes the unload-reload loop to minimize the influence of creep on measurements of the unload-reload loop. Fig.4.15 shows 5 loading curves with small unload-reload loops performed at different displacement levels. However, it is found that the behaviors of these unload-reload loops are different from those in the lab-prototype identified in Fig. 3.14, such as considerable creep in displacement and significantly higher system modulus $E_{sys} = \Delta p_{sys}/\Delta d$. This may be due to

the difference of the friction of the O-ring in contact with the alumide and the matrix metal (420 stainless steel infiltrated with bronze). Note that magnitude of E_{sys} are in the same order of the typical soil unload-reload modulus, which indicates large corrections and low accuracy of the corrected results, so it is not suggested to include the small unload-reload loops in the iDMT test procedure.

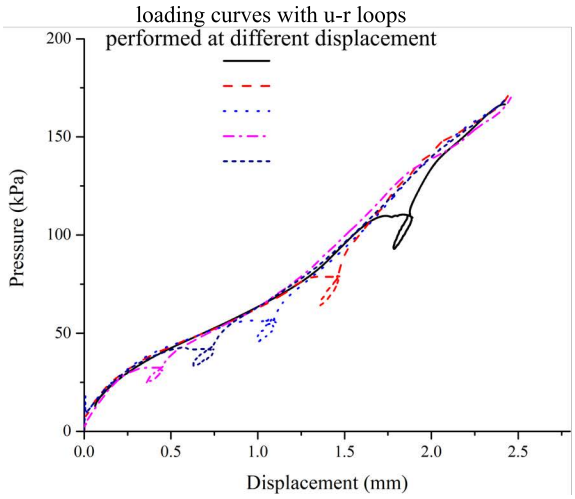

Displacement (mm)	E_{SYS} *(MPa)*
0.46	71
0.74	54
1.09	67
1.47	118
1.89	138

Figure 4.15: Small unload-reload loops in the iDMT calibrations

4.6 Test procedure

De-airing

Prior to installing an instrumented dilatometer in the ground, not only calibrations should have been carried out as discussed in Section 4.5 but also de-airing the pore-water pressure measuring system is essential to obtain good pore-water pressure measurements. Fig.4.16 shows the set-up of a vacuum container and a vacuum pump for the de-airing process. Specifically, the de-airing involves first putting the instrumented dilatometer and silicone oil in the vacuum container, where the elevation of the silicone oil must be higher than the pore-water chamber of the instrumented dilatometer (the middle chamber) in the vacuum container. Then open the valve and start the engine of the vacuum pump, one may spot air bubbles coming out the porous filter at this stage. Until the pressure readings on the vacuum pump become stable and the air bubbles turn invisible, the valve and the engine can be closed. Then the instrumented dilatometer is left in the vacuum container until the assembly with field equipment for in situ testing.

Figure 4.16: Set-up for saturating the pore-water pressure measuring system

Pre-drilling

In terms of probe installation in stiff soils such as crust or fills it is necessary to pre-drill or hand auger at least the first 1 m in depth in order to prevent damaging the instrumented dilatometer as well as underground utilities especially in urban areas.

Installation

Before installing the instrumented dilatometer in the ground, it is important to warm up the whole electrical instrument system. This warm-up period takes at least 15 min, which can help mitigate glitches and reduce the noises in the signal, especially for the inductive displacement sensor. And the penetrometer must be set up so as to obtain the thrust direction as vertical as possible.

On an iDMT sounding, the rate of penetration and the test depth interval are prescribed as 20 mm/s and 200 mm, respectively, which are the same with

the typical values for the DMT tests. In addition, the truck-based penetrometer system measures the thrust with a built-in manometer and the penetration depth with a built-in depth transducer, so a thrust profile can be obtained in real-time. However, it is preferred that this penetrometer system is integrated with the instrumented dilatometer electro-pneumatic system in further work to synchronize measurements from both systems. This was not practical during the present development phase of the iDMT tests. Once reaching the desired test depth, the thrust applied on the push rods must be released and the piston loading process follows immediately.

Piston loading

Since the instrumented dilatometer measures the piston displacement directly and continuously, either a pressure-controlled or a displacement-controlled procedure could be adopted using the electro-pneumatic system. However, the problem of using a pressure-controlled procedure is that the considerably varying strain rate may lead to different soil behaviors and it does not allow a comparison with the standard DMT test results. Equally, the displacement-controlled procedure is not practical with the current electro-pneumatic system since the procedure must be realized via adjusting the applied pressure which nevertheless requires pricey pressure controller with much higher accuracy as discussed in Section 3.3.2.

So a reasonable compromise to allow a comparison with the standard DMT test results, a pseudo displacement-controlled algorithm was devised as discussed in Section 4.4. This algorithm allows the pressurized piston moving with a velocity always in a pre-determined range that is converted from the time limits of the DMT tests. This way a comparison with the DMT test results is guaranteed. But this algorithm alone is not enough to carry out the piston loading since the piston lift-off in soils requires reaching at least a lift-off pressure $p_{\text{lift-off}}$, which must be a pressure-controlled process. Therefore there are effectively two stages of the iDMT tests: pressure-controlled stage prior to the piston lift-off, and the pseudo displacement-controlled stage. Correspondingly, there are two parameters to control the iDMT tests: the pressurization rate in the first stage and the piston velocity range in the latter.

Although in some prior modified dilatometers and the lab prototype of the iDMT described in Chapter 3 unload-reload loops are performed to enhance the assessment of elastic modulus, this is not adopted in the iDMT tests.

Since the modulus measured at the initial loading phase is already a reloading modulus that assumes elastic soil behaviors, this is discussed in more detail in Chapter 5. Furthermore, the unload-reload loops are not technically desirable because of the high E_{sys} and the time-consuming pressure holding step as discussed in Section 4.5.

Re-calibration

Although in the iDMT sounding the compression springs and the O-ring do not suffer the influence from soil abrasion which is the usual cause of a change of the flexible membrane calibration curve in the standard DMT sounding, the calibration in the air is routinely repeated after the in situ tests to check the consistence of the calibration results. The repeatability can be considered sufficiently good as long as a divergence between the two is generally smaller than 17 kPa considering the system accuracy of ± 8.5 kPa.

4.7 Conclusion

This chapter focused on the design, development and test procedure of the iDMT test. Compared to the proof-of-concept laboratory prototype described in Chapter 3, the development of this instrumented dilatometer considers not only the much-needed robustness for in situ testing but also the use of a larger diameter piston and the pore-water pressure measurements at the piston center. Generally speaking, with the updates of both the hardware design and the software algorithm, the metal 3D printed instrumented dilatometer is able to perform in situ tests in common soils such as sands, clays, silts or mixtures and permits a deeper insight into the non-linear soil response along with pore-water pressure information, which provides a potential opportunity to improve the interpretation of soil properties. The test results and the interpretation are discussed in more detail in Chapter 5.

Using the novel technique of metal 3D printing in 420 stainless steel infiltrated with bronze, the instrumented dilatometer allows not only the assembly of a 60-mm diameter piston that is larger than the 40-mm diameter piston in the prototype discussed in Chapter 3 but also the combination of a pore-water pressure measuring system which includes a pore-water pressure cell, a pore-water filter in the piston and a channel for conveying pore water between the cell and the filter. While the metal 3D printing technique enables the pro-

duction of the complex design, it is not expected to be robust in some subtle parts such as the threads of the rod-blade connector which needs to be sufficiently strong to withstand the thrust during the penetration in the ground. So a TIG welding process with $CuSi_3$ as filler was successfully tried to bond the 3D printed part and the conventional machined part together. In addition, replacing the wave spring with the compression springs allows the instrumented dilatometer to deliver a piston displacement up to 2.5 mm with only about 170 kPa pressure during the calibrations. The calibration procedure of this instrumented dilatometer is generally the same with that of the lab prototype, while the results are slightly different because of the different probe materials and the different springs.

The instrumentation system of the iDMT test for automatic control and continuous measurements is, in general, the same with that of the lab prototype, except the pore-water pressure measuring matter. The major update is more about the software aspects. An iDMT test procedure is devised using a pseudo displacement-controlled algorithm which establishes the equivalence between iDMT and DMT measurements, based on the expanding cavity volume, by comparing the displacement rate of the iDMT rigid piston with the DMT membrane displacement rate. This can potentially allow a comparison with the standard DMT test results as well as the use of the well-established DMT correlations with common soil parameters in the iDMT interpretation.

Chapter 5

Testing and interpretation of the iDMT

5.1 Introduction

The ultimate goal of developing the iDMT is to enable a more accurate interpretation of soil parameters. It is reasonable to expect that the iDMT is able to achieve this goal as soil responses such as the full pressure-displacement curve and the pore-water pressure measurements at the piston center during the piston expansion stage are measured rather than only pressure readings at two displacement levels in the standard DMT tests.

In this chapter, methodologies are proposed in the first place, which mainly includes the determination of the contact pressure based on the full pressure-displacement expansion curve and the study of the piston expansion stage. This enables the estimation of the iDMT indices which can be then used with the well-established DMT correlations for soil parameters.

A field-testing program consisting of the iDMT test, the DMT test, and the CPT tests is conducted at three sites in Belgium. Fig. 5.1 (a) shows the locations of the three sites. At each site, the field-testing program is carried out at adjacent locations by using a truck-based penetrometer to allow the probes being statically pushed to a test depth at a constant rate of 20 mm/s, as shown in Fig. 5.1 (b).

Regarding the instrumented dilatometer used in this program, an early prototype with a 40-mm diameter piston is used in the Zwijnaarde test site while the latest device with a 60-mm diameter piston and other improvements, such as a better welding at the blade-rod connector, is used in the Limelette test site

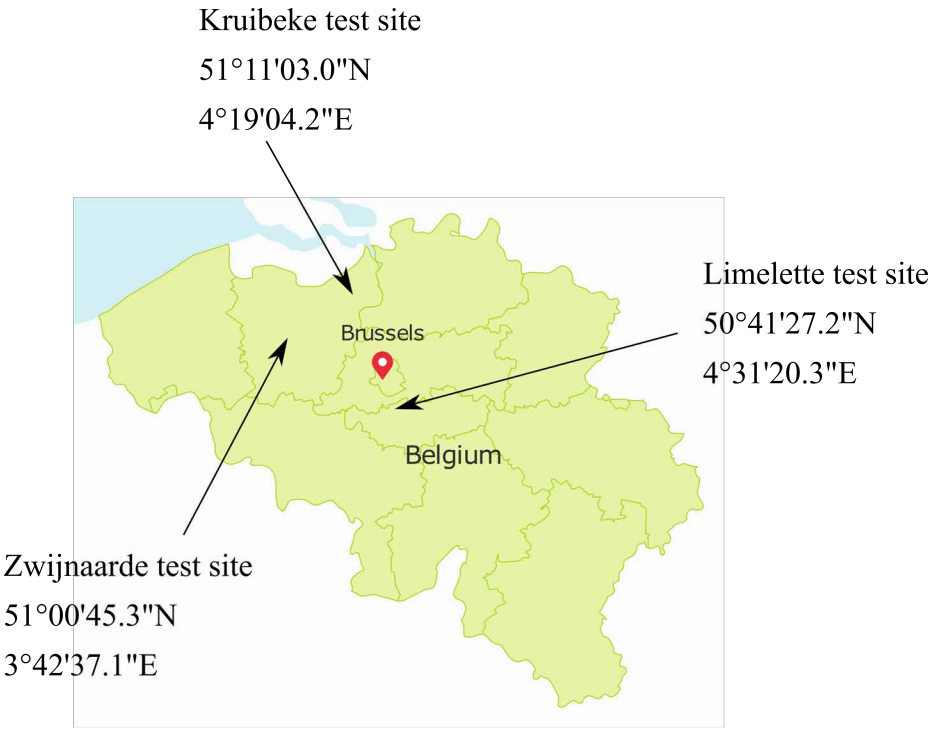

(a)

(b)

Figure 5.1: (a) Location of the test sites in Belgium and (b) the truck with penetrometer used for the field-testing program

and the Kruibeke test site.

Then, data from this testing campaign as well as from prior modified DMT tests extracted from the literature are analyzed. Although there were no undisturbed samples recovered from the sites for accurately determining the soil

parameters in lab, the validation of the iDMT interpretation resides on the comparison between the common in situ testing techniques such as the standard DMT and the CPT. This way not only an index parameter comparison among the standard DMT test, the iDMT test and the prediction based on the CPT is allowed but also the comparison between the geotechnical parameters estimated by different means may permit the further use of the iDMT for geotechnical engineering design.

5.2 The DMT contact pressure p_0

In the DMT tests Eq. 2.1 is used to determine p_0 based on the assumption of a linear pressure-displacement relationship between 0.05 mm (elevation of the feeler pin above sensing disc) and 1.10 mm, as shown in Fig. 2.4 (Marchetti et al. 2001). So the first corrected pressure reading p_0 is de facto not a measured pressure but a back-extrapolated contact pressure at a zero displacement. The linear back-extrapolation can provide accurate and repeatable p_0 as long as a linear relation of pressure-displacement is appropriate in the measured soil conditions. However, the validity of this assumption can only be checked by evaluating the full pressure-displacement curve which is not feasible with the standard DMT. It will definitely be a biased estimation if a highly non-linear pressure-displacement relation is present in a soil.

The DMT contact pressure p_0 is crucial in the DMT interpretation since it is a necessary input for all three "intermediate" DMT index parameters I_D, K_D, and E_D which are then used to derive common soil parameters. Therefore, any error related to the determination of p_0 can lead to the misinterpretation of soil parameters using the DMT. On the other hand, improving the determination of the contact pressure can effectively result in an increase in accuracy of the interpretation using the iDMT. Specifically, with continuous measurements of the applied pressure and the piston displacement in the iDMT, it is at least no more a necessity to stick to the assumption of the linear pressure-displacement relationship which may potentially bring errors that are already discussed in Section 2.3.2.

In Section 2.4.2, the wedge cavity expansion effects have been discussed by reviewing the numerical results given by Finno (1993) using the strain path method and Kouretzis et al. (2015) using the finite element method. Both works are in line with a finding that the maximum value of the total horizontal stresses of the soil elements close to the blade surface is attained near the

blade shoulder which is the geometrical transition point of the blade surface. Once this point has been passed during the penetration, the total horizontal stresses may decrease to 0.6 times the maximum value that is approximately constant at the membrane (Finno 1993); or still undergoes a continued reduction at the membrane (Kouretzis et al. 2015). The difference may be due to the larger 50 mm long tapered section of the blade used by Kouretzis et al. (2015), compared to the 40 mm one by Finno (1993). This allows us to perceive that the initial soil response during the membrane expansion stage is a reloading phase since the membrane expansion in fact follows the unloading from the penetration stage. While these numerical findings only apply in saturated cohesive soils, it is likely that the unload-reload effect also takes place in sandy soils where the same initial soil response is spotted in the measurements.

It is therefore that p_0 estimated using Eq. 2.1 is, in fact, not the "real" lift-off pressure but a conceptual contact pressure at a zero displacement neglecting the initial stiff reloading phase. In case of the reloading phase going beyond 0.05 mm, the pressure-displacement relationship is likely to be non-linear between the A-pressure and the B-pressure since the initial elastic reloading is normally much stiffer than the ensuing phase. This can possibly lead to noticeable errors using Eq. 2.1 to obtain p_0. More importantly, the rationale of using the displacement of 0.05 mm appears irrelevant to this initial reloading phase since Marchetti et al. (2001) indicates that it is to improve the definition of the lift-off of the membrane, i.e. the instant at which the electrical circuit is interrupted. Then the magnitude of 0.05 mm appears more related to engineering judgment rather than a quantitative estimation of the initial reloading phase.

Furthermore, it has been observed that the slope of the expansion curve represents some elastic-plastic response in sands and is largely controlled by the excess pore-water pressure generated during the penetration in clays (Campanella and Robertson 1991). The soils tend to behave non-linear in either case, so an approximation to some extent can be expected under the assumption of a linear relationship. To eliminate these possible errors and reasonably take account of the unload-reload effect, a new estimation technique for the contact pressure based on the full expansion curve is a necessity in the iDMT interpretation.

5.3 The iDMT contact pressure p_c

5.3.1 Review of the pressure-displacement curves in the iDMT

Using an iDMT with a pressure sensor and a displacement sensor, a full pressure-displacement curve can be obtained. However, various shapes of the curves are produced in different soils as illustrated in the review of the iDMT data. Fig. 5.2 shows two types of typical loading curves which have the common feature that an initial stiff soil response occurs at the start of the membrane/piston expansion. Specifically, in Fig. 5.2 (a), an abrupt change in slope (angular discontinuity) of the pressure-displacement curve is seen and found in most of the calibration chamber tests in sands (Bellotti et al. 1997; Fretti et al. 1992) and in a few in situ tests in sandy soils (Marchetti 1980; Akbar and Clarke 2001; Campanella and Robertson 1991; Stetson et al. 2003). Also, there is a second type of curve which does not show an apparent angular discontinuity, as demonstrated in Fig. 5.2 (b). This type of curve has not yet been observed in any calibration chamber test in sands but only in in situ tests with different types of soils (Campanella and Robertson 1991; Stetson et al. 2003; Benoit and Stetson 2003). Considering the iDMT test results in three Belgian sites and the available data in the literature, the proposed two types can generally describe most of pressure-displacement curves.

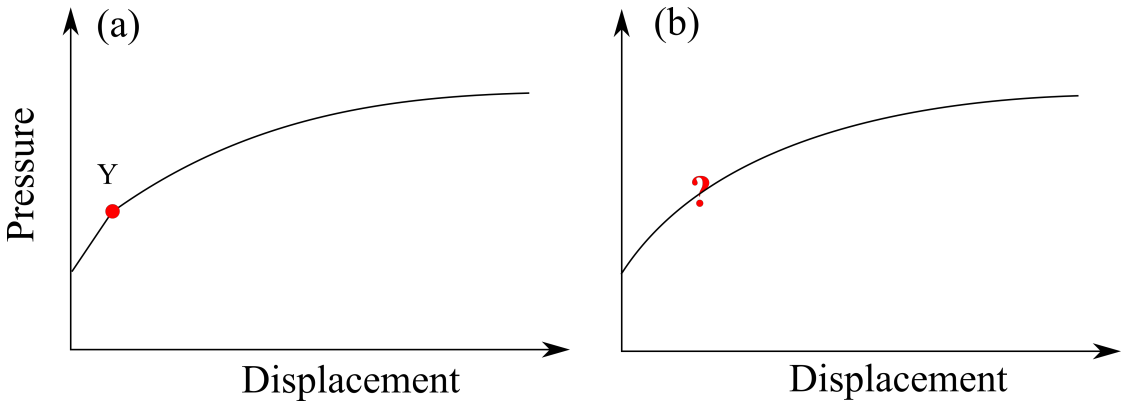

Figure 5.2: Schematic diagrams of the typical pressure-displacement curves

A clear angular discontinuity may indicate that the soils behave somewhat brittle while the gradual deforming soils are rather ductile. Generally, soils can behave either ductile or brittle. Atkinson (2007) has a very good example that soft clay is ductile when it has a relatively high-water content but, if it is highly compressed, stiff clay becomes brittle. However, the ductility and the brittleness are not soil properties that are usually being sought for in geotechnical

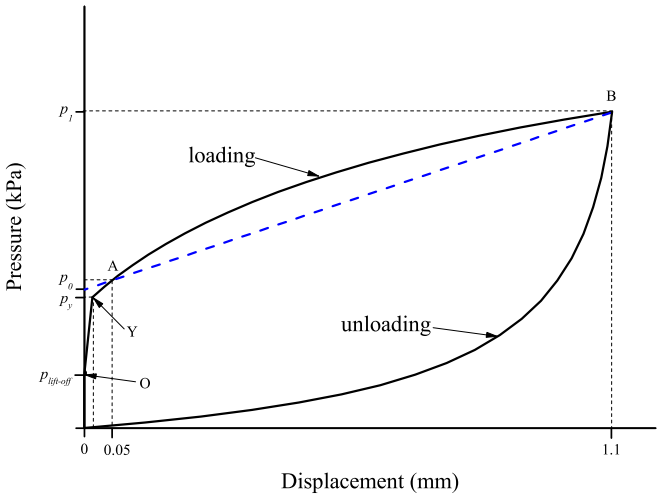

Figure 5.3: Schematic diagram of a complete pressure-displacement curve

practice and are difficult to quantify by any means. Qualitatively, the ductility and the brittleness appear to be related to the presence of microstructure in soils such as cementation in sandy soils and state parameter of the soils. The state parameter is determined by the combination of the soils' current voids ratio or water content, normal effective stress and overconsolidation ratio.

In order to examine this initial stiff soil response, a schematic pressure-displacement curve is illustrated in Fig. 5.3. There are several important points to consider during the loading phase: O, the lift-off point where the membrane starts to move; Y, the onset of yield; A, the pressure reading at the displacement of 0.05 mm; B, the pressure reading at the displacement of 1.10 mm.

As pressure readings at point A and B are obtained in the standard DMT, p_0 is derived from Eq. 2.1 based on the assumption of a linear relationship, as illustrated by the dashed line in Fig. 5.3. In other words, the post-yield curve is assumed to be linear from A to B in the standard DMT interpretation. So having a non-linear post-yield curve and/or having a large initial stiff response beyond the displacement of 0.05 mm makes this interpretation technique erratic. However, this cannot be checked without the instrumentation of the DMT.

The p_0 pressure has been interpreted in different ways when a full pressure-displacement curve is available in an iDMT. Bellotti et al. (1997) and Fretti et al. (1992) use the pressure p_y at the onset of yield while Campanella and Robertson (1991) and R. Colcott (2012) use the pressure $p_{\text{lift-off}}$ when the membrane/piston starts to move. Besides the points found in the Fig. 5.3, Akbar and Clarke (2001) adopts an empirical approach: the pressure at 0.06 mm which ap-

proximately corresponds to the intersection between the initial slope and the post-yield slope based on their database. Although p_y and $p_{\text{lift-off}}$ are readily read from the measured curve, so not influenced by the effects of the non-linearity and the initial stiff response, the use of both can give rise to errors if the DMT correlations with soil parameters are to be used. This is due to the fact that the definitions are not in line with that of the p_0 in the standard DMT — a corrected contact pressure at a zero displacements.

5.3.2 An analytical approach to estimate p_c

In terms of the iDMT conceptual contact pressure at a a zero displacement, p_c is used to distinguish from the DMT contact pressure p_0. To address the aforementioned loading curves of four types, the proposed method involves two steps to find p_c at a a zero displacement: (1) the determination of the transitional "yield" point Y to distinguish the initial reloading phase O-Y and the post-yield phase Y-A-B, as shown in Fig. 5.3; (2) the estimation of p_c based on the post-yield phase of the loading curve. Appendix B includes the MATLAB codes of this approach.

Determination of the transitional "yield" point Y

In Fig. 5.2(a), apparent angular discontinuity can be clearly identified in the red circle. Then, it is convenient to locate point Y at this exact transitional point. This kind of loading curves is typically found in calibration chamber tests with clean and uniform sand as well as in some in situ tests with soils of different types. Nevertheless, it has been found more likely in in situ tests that a clear yield point Y can not be identified since a smoothed loading curve is observed, as shown in Fig. 5.2(b). This presents difficulties to directly identify point Y, so this section focuses on the estimation of point Y in a smooth loading curve.

In the DMT/iDMT tests, an unloading phase during the blade penetration precedes an initial reloading phase during the membrane/piston expansion. A resemblant unloading-reloading phenomenon can be likewise found in the one-dimensional consolidation (oedometer) test. So the preconsolidation pressure cannot be measured directly, but can be estimated with a satisfactory degree of accuracy by means of the empirical graphical methods such as the widely used Casagrande method proposed by Casagrande (1936). Given the similarity of the unloading-reloading effect, an adapted Casagrande graphical method is considered possibly useful in the determination of point Y in a

smooth loading curve. Furthermore, it is worth mentioning that the relationship, given in Eq. 2.13, between the one-dimensional drained tangent modulus M from the oedometer test and the DMT indices has been found adequately accurate (Marchetti et al. 2001). This may somewhat justify the use of an adapted Casagrande graphical method, though the boundary condition and the loading direction are different.

In addition, implementation of a graphical method by hand is time-consuming and cannot avoid human errors. Therefore, an algorithm has been developed and programmed in MATLAB to automate this procedure. The specific steps are given as follows (One may refer to Section 5.3.3 for concrete examples in the meantime for a better understanding of this technique):

1. An arrangement of the iDMT data on a semi-log plot of the displacement with a linear scale for the x-axis and the pressure with a logarithmic scale for the y-axis. Note that this presentation is typical in iDMT curves for a clear demonstration of the stress-strain relation.

2. Curve fitting of the data points from the lift-off point till the end of loading to a power function:
$$y = ax^b + c \tag{5.1}$$

3. Estimation of the point of the maximum curvature of the fitted curve. Using the mathematical definition of the radius of curvature R, as shown in the Eq. 5.2, the R determination for a power function is obtained in the following Eq. 5.3. As the curvature is the reciprocal of the radius of curvature, the point of the maximum curvature is given by the minimum value of R.
$$R = (1 + (dy/dx)^2)^{3/2}/(d^2y/dx^2) \tag{5.2}$$
$$R = x^{2-b}[a^2b^2x^{(2b-2)} + 1)^{3/2}]/[ab(b-1)] \tag{5.3}$$

4. Determination of the bisector line from the vertical line and the tangent line at the point of the maximum curvature.

5. Extend the straight portion of the expansion curve near the end of loading.

6. The point where the lines in part 4 and part 5 intersect is used to obtain the displacement of the transitional "yield" point Y.

In the last step, the displacement of the intersection is used to deduce the yield point, which is different from Casagrande's method using the pressure of the intersection as the preconsolidation pressure. The rationale of this is that the membrane/piston expansion can be regarded as a displacement-controlled test as the soil elements are loaded until the maximum displacement that the system is capable of; while the one-dimensional consolidation test is a pressure-controlled test as the specimen is subjected to increments of pressure until the final pressure being equal to or greater than four times the preconsolidation pressure. Therefore, a large enough pressure in the DMT test is unlikely to be reached in many soils but the maximum displacement is normally multiple times higher than the displacement of the intersection.

Back-extrapolation of p_c

Once the transitional "yield" point Y is identified, the start of the post-yield phase of the loading curve is determined. Then, p_c at a a zero displacement can be back-extrapolated from a regression model fitting the post-yield loading curve. To account for a nature of non-linearity of varying rates and of asymptotic behaviors, an exponential-linear regression model is thus proposed:

$$Y = c^{'} + a^{'}X - b^{'}d^{'X} \tag{5.4}$$

where $a^{'}$ and $c^{'}$ are the parameters for a linear asymptote line representing a potential boundary as the curve potentially tends to flatten, $b^{'}$ indicates the range of non-linear part and $d^{'}$ is the rate of the non-linearity. It is noted that the model is valid when the requirement of parameter constraints is met, which is $b^{'} \geqslant 0$ and $0 < d^{'} < 1$.

Ideally, the iDMT results may be resemblant to the results of pressuremeter tests that the piston expansion reaches a limit pressure p_L, which has been spotted in some iDMT tests as well as several iDMT data from R. Colcott (2012) and Benoit and Stetson (2003). In this case, $p_L = c^{'}$ and $a^{'} = 0$. In reality, we may have a linear asymptote line instead, due to the rate effects and the possible creep behaviors. So, a liner part is proposed as the boundary in the regression model. Considering the non-linear soil response especially the high non-linearity in the initial part of the pressure-displacement curve, an exponential part is proposed. It is simple to use such a two-parameter regression as $b^{'}$ indicates the range of non-linear part and $d^{'}$ is the rate of the non-linearity. This way it is sufficiently flexible to have good fits in most

conditions.

5.3.3 An example

An example of the proposed p_c estimation technique is elaborated in this section. Then, a discussion of the regression models regarding Eq. 5.1 and Eq. 5.4 is presented by analyzing this example.

A typical case of a smoothed loading curve

In stead of using the manual graphical method like the one proposed by Casagrande (1936) to identify the point of the maximum curvature of the loading curve, a power fit is used to represent the test data of the loading curve for analytically deriving the point of the maximum curvature. Similarly, a non-linear regression model given by Eq. 5.4 is also used to back-extrapolate p_c by fitting data points of the post-yield curve. Therefore, the two regression models are of importance and thus discussed in this section by means of showing the application of the proposed p_c method on a typical smooth loading curve.

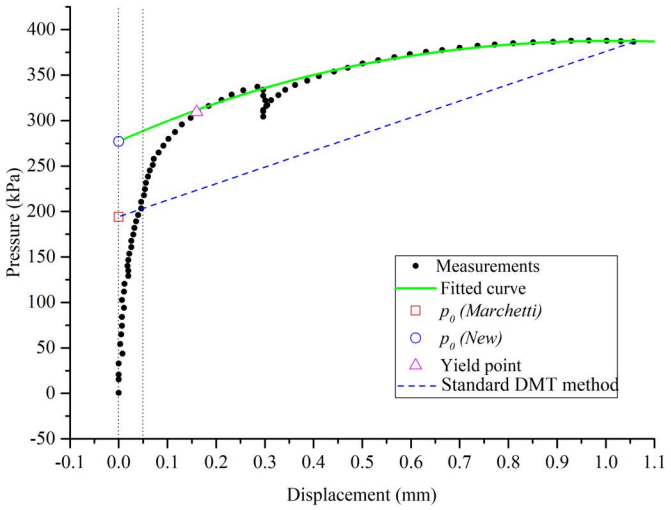

Figure 5.4: Estimation of p_0 and p_c (measurements from Benoit and Stetson (2003))

Fig. 5.4 shows the digitalized data points of the loading curve of an iDMT test performed at the depth of 13.72 m in soft varved clay by Benoit and Stetson (2003). Although the in situ tests in soft clays normally assumes undrained soil conditions, this test was carried out after the full pore-pressure dissipation so the measurements are not influenced by the dissipation of pore-water pressure

generated by blade installation in soils. This issue is concerned since the incorporation of an unload-reload loop may require a longer time to perform the test than that of the standard DMT test. The partial drainage condition, which is more difficult to interpret, rather than the undrained condition may be met if the excess pore-water pressure is not fully dissipated.

In the standard DMT method, p_0 is interpreted by a linear relation assumption via two points: the points at the displacement of 0.05 mm and 1.1 mm. Using this technique in this iDMT data, the point at the maximum displacement of 1.04 mm and the linear interpolated point at the displacement of 0.05 mm are adopted to obtain a p_0 value of 194.0 kPa. However, as shown in the graphical illustration of this method in Fig. 5.4, the line between the two points is significantly biased from the real measurements. This is due to the large initial stiff response in the loading curve which covers the range exceeding the displacement of 0.05 mm. Therefore the use of the standard DMT method is inappropriate in this case. To address this issue, the proposed interpretation technique must be applied.

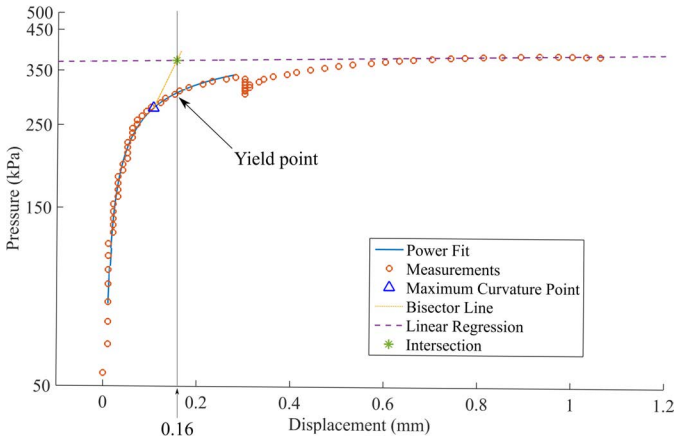

Figure 5.5: Determination of the transitional "yield" point (data points from Fig. 5.4)

As a smoothed curve is seen in this data rather than an angular discontinuity, the aforementioned algorithm based on the graphical method for determining the transitional "yield" point Y is applied in MATLAB, and the analytical procedure is illustrated in Fig. 5.5. Given the location of the intersection point, the yield point is situated at a displacement of 0.16 mm and a pressure of 309.4 kPa. Note that this displacement value is much higher than the predefined value of 0.05 mm in the standard DMT. Then, with the yield point determined, the post-yield data points (with the unload-reload loop omitted) are selected to carry out the curve fitting based on the regression model of Eq. 5.4,

estimating a p_c of 277 kPa in Fig. 5.4.

Discussion on the regression models

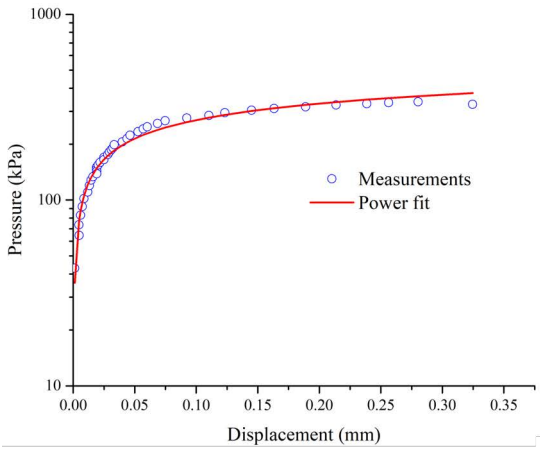

(a) Power fit of the loading curve

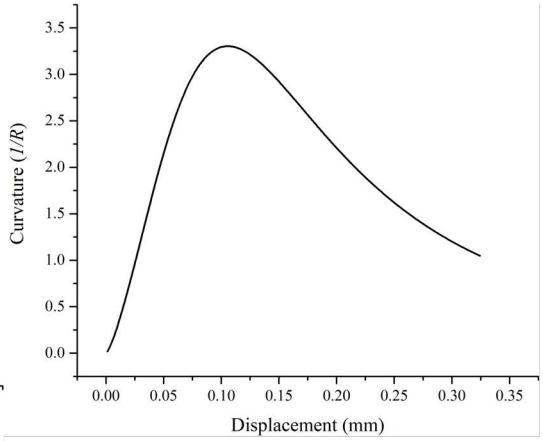

(b) curvature derived from the power fit

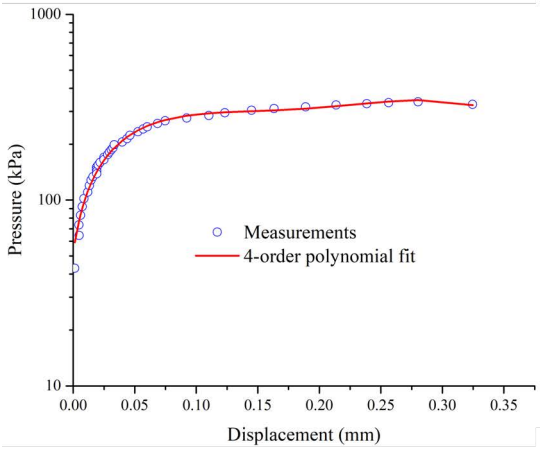

(c) Polynomia fit of the loading curve

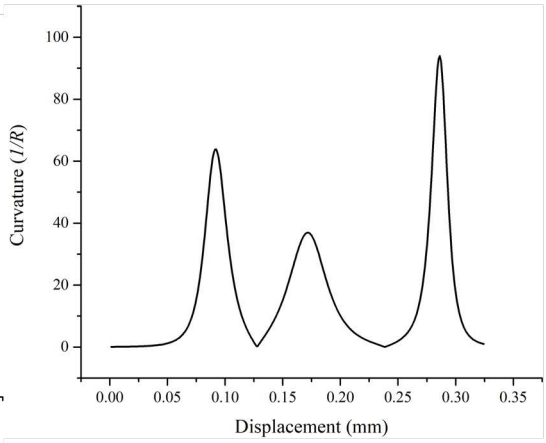

(d) curvature derived from the polynomial fit

Figure 5.6: Regression analysis for the maximum curvature: (a) Power fit of the loading curve, (b) curvature derived from the power fit, (c) Polynomia fit of the loading curve and (d) curvature derived from the polynomial fit (data points from Fig. 5.4)

In terms of the curve fitting technique for estimating the point of the maximum curvature, a number of different fitting functions are tested. But only the 4-order polynomial fit and the power fit are found adequate to give good fits to all curves. Fig. 5.6(a,c) shows an example of using both functions for the same data set. The polynomial and the power fitting results are respectively given by:

$$P = 52.4 - 230300s^4 + 174000s^3 - 46630s^2 + 5518s \tag{5.5}$$

$$P = -0.5612s^{-0.1656} + 3.252 \tag{5.6}$$

where P = pressure, s = membrane displacement at the center.

Concerning the goodness of fit, satisfying results are found in both cases. However, the objective of this regression analysis is to find the point of the maximum curvature rather than only delivering a good fit. Fig. 5.6(b,d) shows the curvature, the reciprocal of R given in Eq. 5.2, calculated from both fits. The point of maximum curvature can be easily identified from the single peak of the curvature from the power fit at the displacement of 0.11 mm. Nevertheless, the point of the maximum curvature from the 4-order polynomial fit does not stand for the general trend but de facto interpret the noise of the data points. Taking this into account, it is necessary to use the power fit but not the polynomial fit while both have good fitting results.

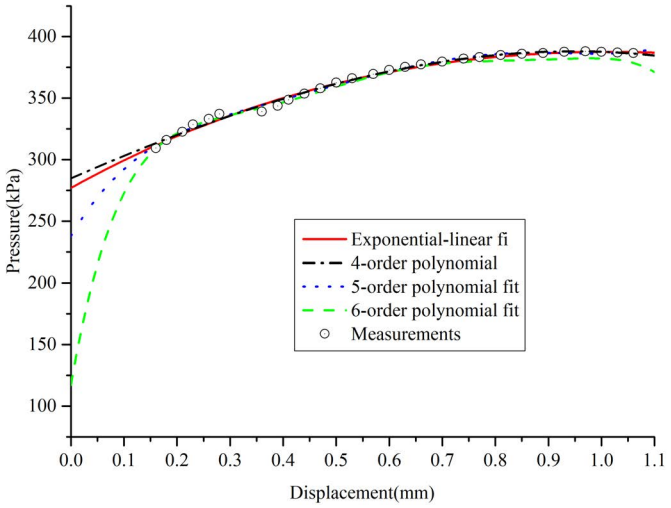

Figure 5.7: Fitting function comparison (with data points of the small unload-reload loop omitted from Fig.5.4)

Similarly, a study on the regression model for back-extrapolating p_c was carried out as well. Fig. 5.7 shows the use of the proposed exponential-linear regression model given by Eq. 5.4 and the polynomial fits with different orders. Note that the data points of the small unload-reload loop are necessarily omitted since it does not correspond to the standard test procedure. From a theoretical point of view, a small unloading during the membrane expansion shall not significantly impact the rest of the loading curve. So, this data set was still extracted from the literature to validate the proposed model.

Despite that the goodness of the fit is generally found acceptable in Fig. 5.7, the use of polynomial fits with different orders results in a significant differ-

ence in the prediction of p_c at a zero displacement. The p_c of 280 kPa estimated by the 4-order polynomial fit is found close to the p_c of 277 kPa from the exponential-linear regression model. Nevertheless, the predicted p_c decreases from 280 kPa to 120 kPa with the rise of the polynomial degree from 4 to 6. So the p_c estimation based on the polynomial fits can be erratic due to the sensitiveness to the degree of the polynomial. Although further validation is needed, the results of the exponential-linear regression model appear showing reasonable back-extrapolation for p_c and are given by:

$$P = 1393 - 343.5s - 1116(0.5931^s) \tag{5.7}$$

where P = pressure, s = piston displacement.

5.3.4 Typical applications in different soils

This section presents typical applications of the proposed p_c estimation technique in different soils. The main difference between these examples is how the transitional "yield" point is determined: either a direct identification of the yield point when spotting an abrupt change of curve slope or using the adapted Casagrande method in MATLAB in the case of a smoothed loading curve. So the applications using the data from the iDMT tests at three sites, namely Zwijnaarde, Limelette and Kruibeke in Belgium, as well as from the literature are presented and discussed. Note that this section focuses on the use of the proposed p_c estimation technique rather than giving the complete data reduction process.

p_c on smoothed loading curves

The Newcastle dilatometer test (NDMT) developed by Akbar and Clarke (2001) is featured by the use a rigid piston with up to about 1.1 mm displacement. Fig. 5.8 (b) shows a typical NDMT testing result (the corrected loading curve) in Lahore cohesive soils in Pakistan (Akbar et al. 2005).

It is interesting to point out that the pressure-displacement relationship is initially stiff and non-linear following the piston lift-off, and then gradually becomes linear with an increase in the piston displacement. This initial stiff response is possibly attributed to soil reloading as the soils were unloaded during the blade penetration stage. This initial stiff phase covers a large range of displacement till around 0.3 mm, which invalidates the use of the standard DMT

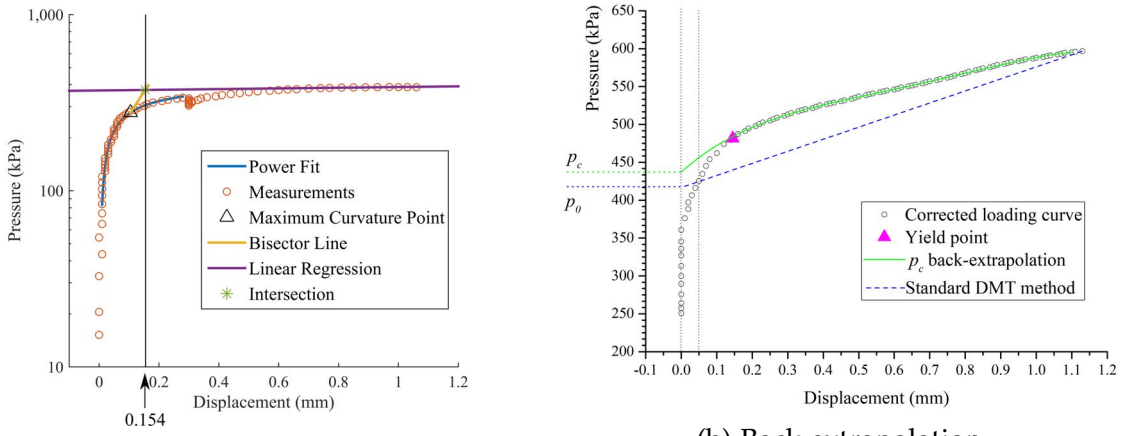

(a) The "yield" point

(b) Back extrapolation

Figure 5.8: Estimation of p_c and p_0 (measurements from Akbar et al. (2006))

method. If a line from the maximum displacement point through the 0.05 mm displacement point is constructed to estimate p_0, it is apparent that this estimation is biased as shown in Fig. 5.8 (b). Therefore, the assessment based on the full pressure-displacement curve is necessary for the contact pressure at a zero displacement. Fig. 5.8 (a) illustrates the first step of finding the displacement at the transitional "yield" point via the adapted Casagrande method, which is located at 0.154 mm. Then, the post-yield phase of the loading curve is fitted using the proposed regression model mentioned in Eq. 5.4 to estimate a p_c of 437 kPa that is higher than the p_0 of 416 kPa. The corresponding regression results are given by:

$$P = 508.25 + 100.08s - 71.52(0.00008)^s \tag{5.8}$$

Fig. 5.9 and Fig. 5.10 show two iDMT testing curves at 3.0 m and 5.8 m in depth in an iDMT sounding, respectively. This sounding was carried out in a site which composes of silty sands to sandy silts and locates at Technologiepark, Zwijnaarde in Belgium. The groundwater table is about 2.8 m below the ground surface.

With the proposed adapted Casagrande method for such smooth loading curves, the transitional "yield" points can be located at 0.277 mm and 0.278 mm in displacement in Fig. 5.9 (a) and Fig. 5.10 (a), respectively. Then, non-linear regression analysis can be conducted using Eq. 5.4, the results of which are given by:

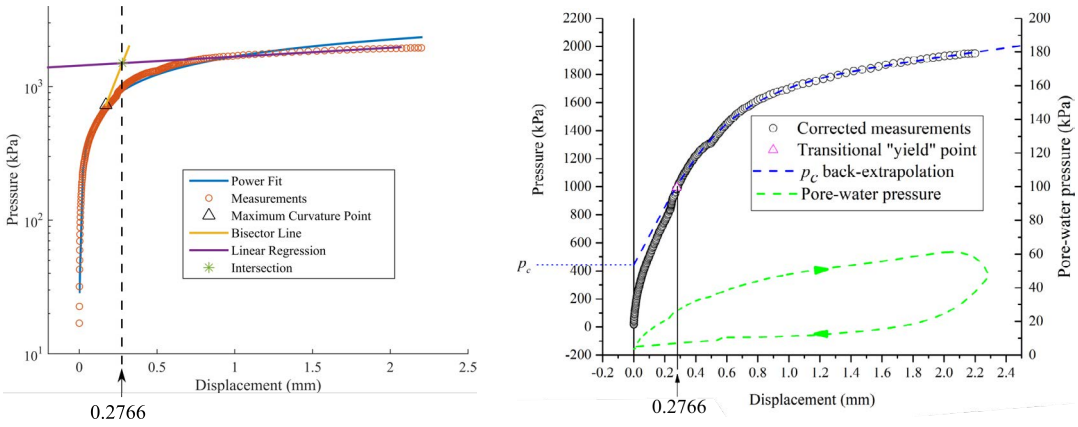

(a) The "yield" point (b) Back extrapolation

Figure 5.9: Typical estimation of p_c from the iDMT in silty sand (Zwijnaarde) at 3.0 m in depth

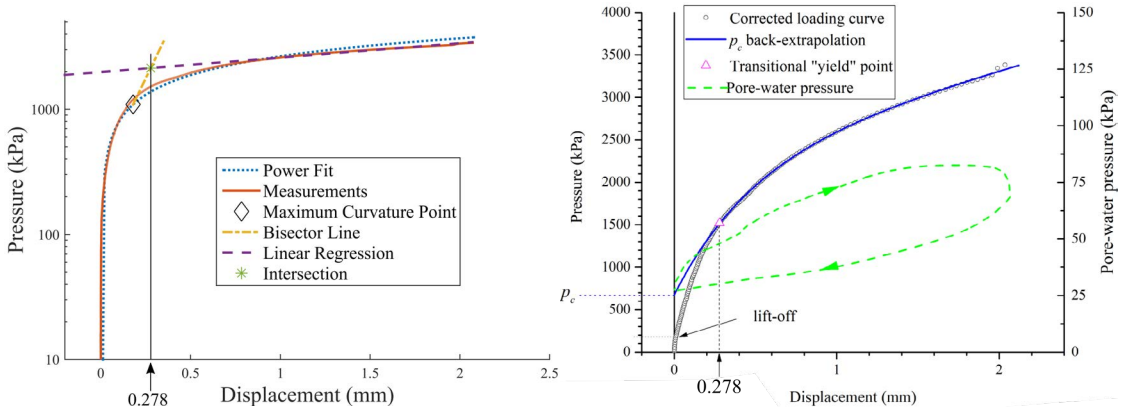

(a) The "yield" point (b) Back extrapolation

Figure 5.10: Typical estimation of p_c from the iDMT in silty sand (Zwijnaarde) at 5.8 m in depth

$$P = 2026 + 123.02s - 1583.05(0.0668)^s \tag{5.9}$$

$$P = 2259 + 536.9s - 1584.8(0.1284)^s \tag{5.10}$$

Thus, p_c of 443 kPa and 674 kPa can be estimated from Eq. 5.9 and Eq. 5.10 at the depth of 3.0 m and 5.8 m, respectively. In addition, it is worth mentioning that the pore-water pressure developments are also measured through the test at the piston center and shows a slight increase above the equilibrium water pressure during the expansion and a gentle decline before reaching the maximum displacement. This generation of excess pore-water pressure to some extent is possibly due to fines in the soils while the dissipation at the meantime

is expected as well. However, the magnitude of the pore-water pressure development is negligible compared to the total pressure of soil response, which justifies the use of total stress analysis.

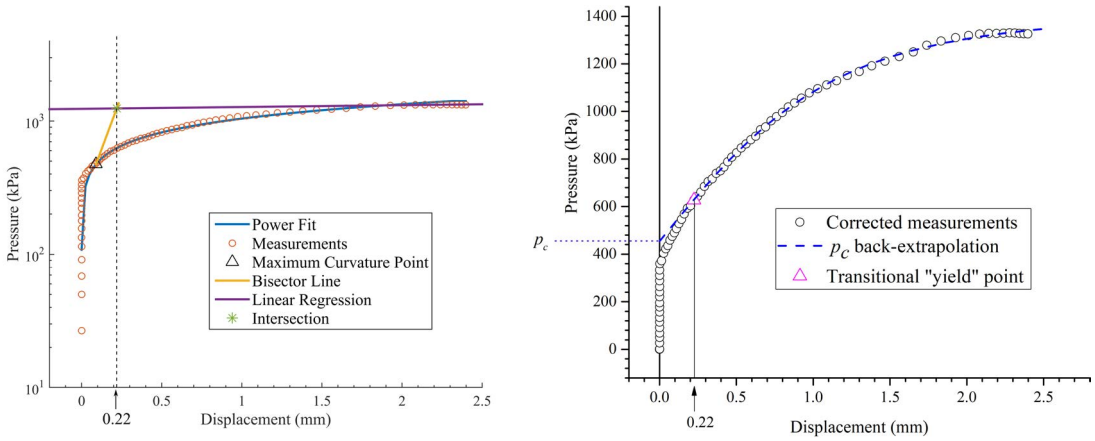

(a) The "yield" point (b) Back extrapolation

Figure 5.11: Typical estimation of p_c from the iDMT in clayey silt (Limelette) at 3.4 m in depth

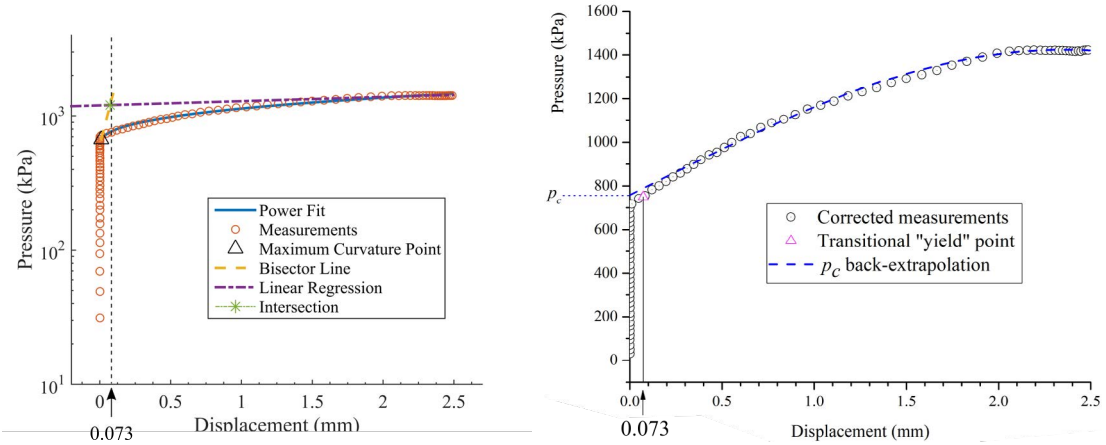

(a) The "yield" point (b) Back extrapolation

Figure 5.12: Typical estimation of p_c from the iDMT in clayey silt (Limelette) at 4.2 m in depth

Fig. 5.11 and Fig. 5.12 show two iDMT testing curves at 3.4 m and 4.2 m in depth in an iDMT sounding, respectively. This sounding was carried out at a site which composes of silty clays to clayey silts and locates at Limelette in Belgium. The groundwater table was deeper than the maximum depth of 5.8 m of this sounding, so no pore-water pressure development was measured during the tests. Similar to the previous duo cases, the adapted Casagrande method

is applied to find the transitional "yield" points at 0.22 mm and 0.073 mm in Fig. 5.11 (a) and Fig. 5.12 (a), respectively. Then, the regression formulas for p_c back-extrapolation are calculated and given by:

$$P = 1477.42 - 1022.23(0.32)^s \tag{5.11}$$

$$P = 1627 - 868.2(0.132)^s \tag{5.12}$$

As the intercepts at a zero displacement, p_c of 455 kPa and 759 kPa can then be estimated from Eq. 5.11 and Eq. 5.12 for the tests at the depth of 3.4 m and 4.2 m, respectively. Furthermore, the coefficient a' in Eq. 5.4 are found as zero in both regression analysis, which likely indicates that limit pressures p_L are approached.

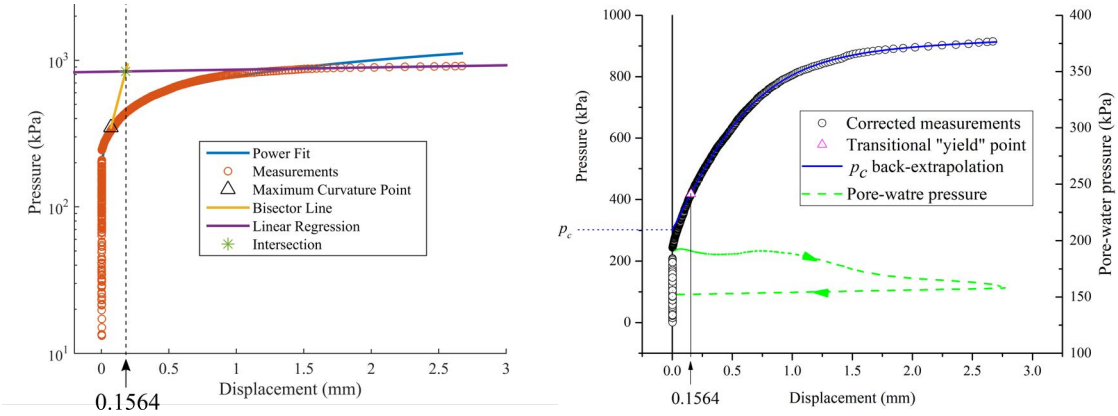

(a) The "yield" point (b) Back extrapolation

Figure 5.13: Typical estimation of p_c from the iDMT in clay (Kruibeke) at 3.8 m in depth

Fig. 5.13 and Fig. 5.14 show two iDMT testing curves at 3.8 m and 6.4 m in depth in an iDMT sounding, respectively. This sounding was carried out at a site which composes of stiff clays and locates at Kruibeke in Belgium. Similar to the foregoing cases, it is hard to directly identify the transitional "yield point" from the corrected loading curves. So, the adapted Casagrande method is used to find the transitional "yield" points at 0.156 mm in Fig. 5.13 (a) and 0.083 mm in Fig. 5.14 (a). Then, p_c of 301 kPa and 908 kPa can be estimated from respective curves at 3.8 m and 6.4 m in depth, based on the regression formulas given by:

$$P = 966.6 - 665.45(0.183)^s \tag{5.13}$$

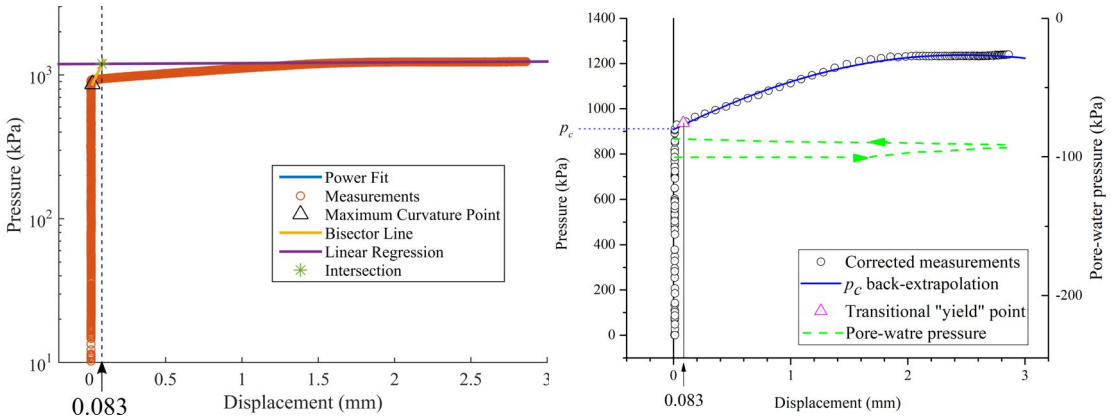

(a) The "yield" point (b) Back extrapolation

Figure 5.14: Typical estimation of p_c from the iDMT in clay (Kruibeke) at 6.4 m in depth

$$P = 1305.1 - 396.9(0.109)^s \tag{5.14}$$

Although p_c is estimated based on the total stress analysis, pore-water pressure development accounts for a considerable part in the two tests. In the test at 3.8 m in depth, pore-water pressure $u_{\text{lift-off}}$ is close to 191 kPa when the piston is about to lift off, which accounts for 63.5% of p_c. Campanella and Robertson (1991) and Mayne (1987) pointed out that the initial contact pressure in normally consolidated clays is an approximate measure of the total pore-water pressure induced during penetration of the dilatometer blade. In terms of the stiff clays in this iDMT sounding, the large proportion of the pore-water pressure thus seems reasonable. Furthermore, the pore-water pressures in both tests decay slightly over the course of the piston expansion from 0 mm to around 0.9 mm, then the drops become faster till reaching the maximum displacement. Taking this pore-water pressure effect into account, the last flattening phase of the pressure-displacement curve may de facto result from the fact that the decline of pore-water pressure and the increase in soil effective stress cancel each other. In addition, the pore-water pressure, in general, remains constant during the unloading since immediate de-pressurization was carried out in this iDMT sounding.

p_c with apparent transitional "yield" point

As discussed in Fig. 5.2 (a), the transitional "yield" point is readily identified by the point of angular discontinuity. These apparent transitional "yield" points

are found in the testing curves produced in calibration chamber with clean and uniform sand as well as in sandy field site. Thus, it appears at least more likely to directly locate the "yield" point from testing curves in sand or sandy soils.

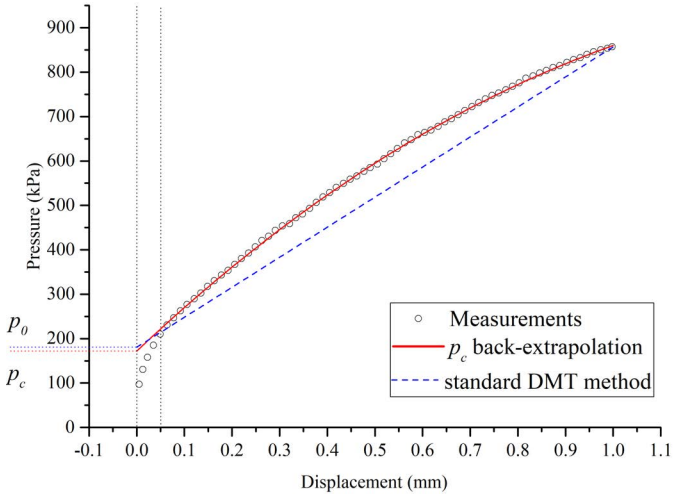

Figure 5.15: Estimation of p_0 and p_c (measurements from research DMT in the sand at 9.0 m in depth (Campanella and Robertson 1991))

Fig. 5.15 shows the results of a research DMT test at a depth of 9 m in the sand (Campanella and Robertson 1991). The research dilatometer used in this test measures the displacement at the membrane center in the range of 0 to 1.0 mm. A p_0 of 181 kPa can be obtained using the standard Marchetti method that draws a line from the point at the maximum displacement through the point at 0.05 mm displacement to a zero displacement. Nevertheless, noticeable deviations from the measurements can be seen between the standard DMT method (the dashed line) and the measurements in Fig. 5.15. In this particular case, the initial soil response occurs within the range of 0.05 mm as the "yield" point locates exactly at 0.05 mm. So, non-linearity of the post-yield curve mainly accounts for the difference between the measurements and the linear extrapolation of the standard DMT method. Using the regression model of Eq. 5.4, the best fit can be found and given by:

$$P = 1318.8 - 1146.6(0.39)^s \tag{5.15}$$

Then p_c of 172 kPa can be estimated as the intercept of Eq. 5.15 at a zero displacement, which is smaller than $p_0 = 181$ kPa.

Fig. 5.16 shows the data and analysis of a research DMT test at 11.8 m in the sand in the same sounding as the previous case. A similar approach is used since the "yield" point also locates at 0.05 mm. The best fit of the post-yield

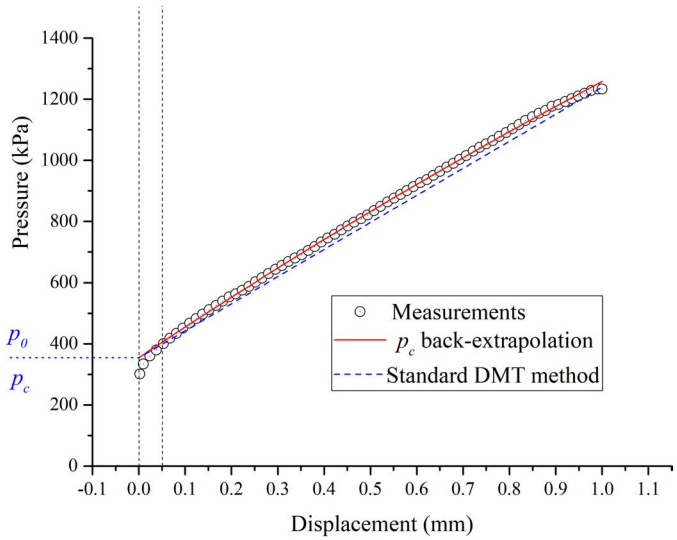

Figure 5.16: Estimation of p_0 and p_c (measurements from the research DMT in the sand at 11.8 m in depth (Campanella and Robertson 1991))

curve based on Eq. 5.4 is given by:

$$P = 4743.8 + 3.5s - 4389(0.795)^s \tag{5.16}$$

Then, it is interesting to find out that $p_c = p_0 = 355\,\text{kPa}$ in this particular case. This may be due to the high linearity of the post-yield curve and the fact that the initial stiff range is lower than the displacement of 0.05 mm, which is in accordance with the assumption of the linear pressure-displacement relationship from 0.05 mm to 1.1 mm in the standard DMT.

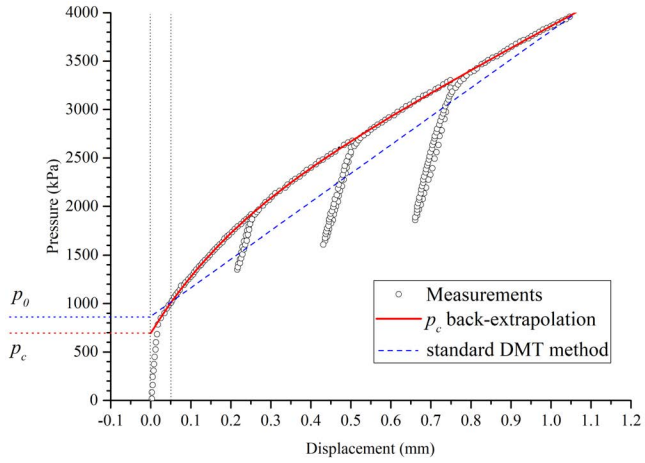

Figure 5.17: Estimation of p_0 and p_c (measurements from the research DMT on pluviated Toyoura sand samples in a calibration chamber with $OCR = 7.2$ and $D_R = 87.2\%$ (Bellotti et al. 1997))

Different from the smoothed curve of the iDMT results, the test data shown in Fig. 5.17 can be divided into various phases based on the curve shape. This feature allows the determination of the yield point by having different shapes of the initial stiff phase and the post-yield phase.

The research DMT used by Bellotti et al. (1997) measures the displacement at the membrane center and the corresponding applied pressure. Then a series of calibration chamber tests are performed on Toyoura sand. The common characteristic of these testing curves is that there is an angular discontinuity between the initial stiff response and the post-yield curve.

Fig. 5.17 shows a typical result on a specimen with an *OCR* of 7.2 and a relative density D_r of 87.2%. The yield point can be readily located at a displacement of 0.018 mm, which follows the initial stiff response. Although the initial stiff response occurring within 0.018 mm does not weigh against the use of the standard DMT method, considerable deviations between the standard DMT method and the measurements are found, which is then exclusively due to the non-linearity of the post-yield curve. Then, the post-yield data points (with the unload-reload loop omitted) are selected to carry out the curve fitting based on the regression model of Eq. 5.4, the result of which is given by:

$$P = 1645 + 2225s - 950.7(0.0085)^s \tag{5.17}$$

This allows an estimation of $p_c = 694$ kPa, while $p_0 = 857$ kPa. Along with the example given by Fig. 5.15, it appears that p_c tends to be lower than p_0 in a sand if the initial stiff response occurs within 0.05 mm and the post-yield curve is non-linear.

Fig. 5.18, 5.19 and 5.20 show three iDMT test results in a site which composes of silty sands to sandy silts and locates at Technologiepark, Zwijnaarde in Belgium. The groundwater table is about 2.8 m below the ground surface. As immediate de-pressurization is carried out, only the loading part of the measurements is corrected using the calibration data. The corrected loading curve is therefore used to interpret soil response during the loading stage. Resemblant to the previous cases in the sands, it is possible to directly identify the "yield" point on the three testing curves by finding the angular discontinuity. Nevertheless, it appears that the corrected loading curve in the iDMT consists of three distinct phases which have not been found in any modified dilatometer with the flexible membrane. This may be attributed to the large deformation applied by the rigid piston.

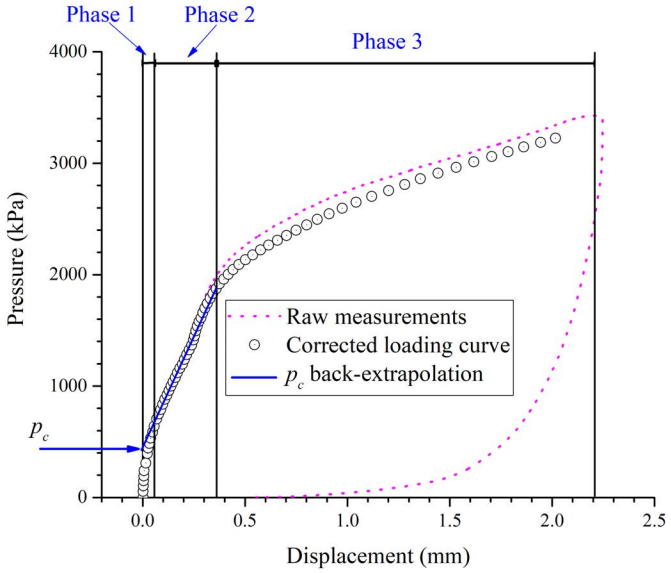

Figure 5.18: Estimation of p_c from the iDMT in silty sand (Zwijnaarde) at 6.4 m in depth

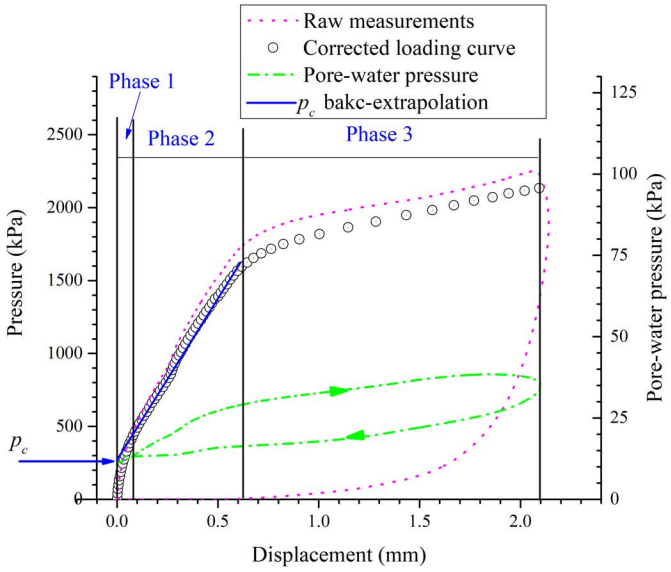

Figure 5.19: Estimation of p_c from the iDMT in silty sand (Zwijnaarde) at 4.0 m in depth

Taking Fig. 5.19 as an example, in phase 1, the piston begins to move outward when the pressure reaches around 100 kPa. Then an initial stiff piston expansion follows until the pressure-displacement relation becomes linear. This linear piston expansion may be regarded as a pseudo-elastic phase (hereinafter phase 2) prior to the phase 3 where plastic behavior becomes dominant. In this particular testing curve, phase 2 starts at around 0.08 mm and ends at the initiation of yielding at about 0.65 mm where the increase in pressure reaches

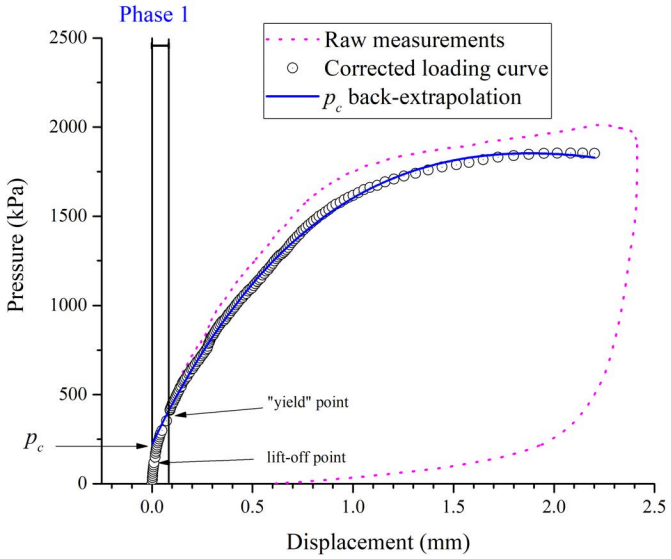

Figure 5.20: Estimation of p_c from the iDMT in silty sand (Zwijnaarde) at 2.6 m in depth

the strength of the soils adjacent to the piston. In phase 3 it appears that a limit pressure p_l is approached. This may be reasonable for this sand-silt mixture considering that the rigid piston expansion with a uniform displacement results in more significant plastic soil response than that of the flexible membrane expansion with the same displacement magnitude measured at the membrane center. Campanella and Robertson (1991) indicates that the slope of the DMT expansion curve from p_0 to p_1, i.e. E_D, represents a measure of the "elastic-plastic" response of the sand.

Therefore, linear regression is conducted for the phase 2 in Fig. 5.18 and Fig. 5.19 to back-extrapolate p_c of 421 kPa and 255 kPa at a zero displacement, respectively. This method can prevent potential errors including parts of phase 1 or 3 in the prefixed displacement range such as that of the DMT. Additionally in Fig. 5.19, the pore-water pressure is measured through the test at the piston center and shows a slight increase above the equilibrium water pressure during the expansion and a gentle decline before reaching the maximum displacement. This generation of excess pore-water pressure to some extent is possibly due to fines in the soils while the dissipation at the meantime is expected as well. However, the magnitude of the pore-water pressure development is negligible compared to the total pressure of soil response.

However, in the case of Fig. 5.20, it is not easy to identify a single point for the change from phase 2 to phase 3 since the transition is gradual. So a p_c of 241 kPa is estimated based on the regression model of Eq. 5.4 and the best fit

is given by:

$$P = 2050 - 1808.9(0.21)^s \tag{5.18}$$

5.4 The piston expansion

5.4.1 Problem formulation

The DMT membrane expansion

As already discussed in Section 2.2.1, the expansion stage of the standard DMT test can be formulated in a way to obtain an exact solution using linear elasticity. The soils surrounding the dilatometer are admitted as two elastic half-spaces in contact along the plane of symmetry of the blade, as shown in Fig. 5.21.

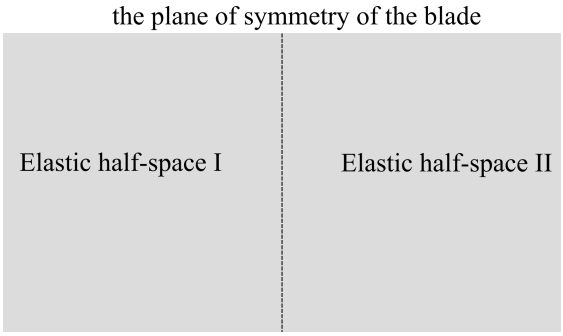

Figure 5.21: Basic Model of the ground surrounding the blade

Then, at the membrane expansion stage, an elastic half-space is subjected to the condition of zero vertical displacements external to the circular area loaded by a uniform pressure, as shown in Fig. 5.22 (a). By assuming the load as a uniform pressure, the membrane stiffness and the boundary effects are neglected and a solution can be found in Eq. 2.5. This solution is in accordance with the general form of distributed loads on the surface of an elastic half-space (Poulos and Davis 1974). Using the influence factor proposed by Mayne and Poulos (1999), the general form of this solution is given by:

$$\frac{E}{1-\nu^2} = \frac{qD}{s} I \tag{5.19}$$

where E = Young's modulus; q = the applied pressure; D = diameter of the loaded area; ν = Poisson's ratio; I = influence factor = $2/\pi$ for Eq. 2.5, which is shown in Fig. 5.22(a); s = the displacement at the center of the loaded area.

Based on this general form with the influence factor I, it is easy to compare the solutions of different cases which can be generally delineated as distributed loads on the surface of an elastic half-space. For example, as shown in Fig. 5.22(b,c), $I = 1$ when a uniform pressure is applied on a circular area; $I = \pi/4$ in case the circular area is prescribed by a uniform displacement.

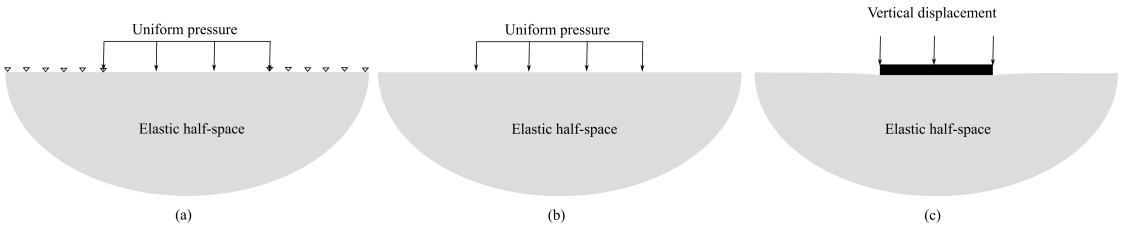

Figure 5.22: Distributed loads on the surface of an elastic half-space: (a) zero vertical displacements are prescribed to the area external to the circular area loaded by a uniform pressure, $I = 2/\pi$; (b) the circular area loaded by a uniform pressure, $I = 1$; and (c) the circular area is prescribed by a uniform displacement, $I = \pi/4$.

The iDMT piston expansion

Nevertheless, an exact solution cannot be derived using the same method for the problem of the iDMT rigid piston expansion, which is due to the presence of discontinuities (displacement jump) at the edge of the loaded area, as shown in Fig. 5.23.

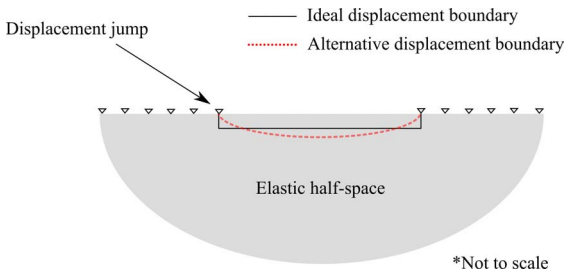

Figure 5.23: The displacement boundaries for the iDMT rigid piston expansion

In reality, the likely scenarios may depend on the soil type. In saturated cohesive soils with a relatively high-water content, such as soft clay and mud, the rigid piston expansion process may be reduced to a flow problem where the soils behave like a fluid, such as the strain path method used by Finno (1993) to model the dilatometer penetration in the fluid. In case the soils still respond as a continuous mass of elastic solid, a separation between the metal blade and the soils may happen with a small void adjacent to the piston. It is

also possible that the soils have elasto-plastic behaviors with soil failure near the piston edge. In dry soils or brittle stiff clays, soil cracking may occur with the development of a fracture or even multiple fractures. Generally, different methodologies are required to address these various kinds of soil responses on a case-by-case basis, such as solid mechanics, fluid mechanics, or fracture mechanics.

However, a precise simulation of the rigid piston expansion process can only be useful when an accurate and good simulation of the iDMT blade penetration process is completed first. This is due to the fact that the iDMT blade penetration process precedes the rigid piston expansion process. Considering that the iDMT blade penetration process opens a flat cavity with a thickness of 15 mm in the ground, the rigid piston process with a displacement up to 2.5 mm is expected to be heavily influenced by the results of the penetration process.

Therefore, it is a trade-off between case-by-case simulations involving the DMT penetration process together with the rigid piston process and a simple calculation with an approximation to some extent. Although the full simulations may provide more precise results and insights of the mechanics, the objective of investigating the piston expansion process in this chapter is to have a data-reduction process similar to that of the DMT interpretation. Considering that the analysis of the DMT membrane expansion is based on linear elasticity, it is favorable to adopt a similar approach in the iDMT interpretation to allow an extended use of the DMT correlations developed by many researchers over the past several decades. In a later stage this approach can then be extended to consider elasto-plastic soil behaviors with reasonable efforts, when the linear-elastic approach appears insufficient.

An alternative displacement boundary is proposed to allow the continuity of displacement at the piston edge and a gradual transition of displacement from the piston edge to the piston center. Fig. 5.23 shows this assumed displacement boundary characterized by a semi-ellipse. The difference in reaction of elastic soils is assumed to be small if the cavity volume resulting from the semi-elliptical boundary and the ideal cylindrical boundary is identical. Note that this assumption is simple and is expected to result in some errors. The advantage of using this alternative semi-elliptical displacement boundary is to allow a simple calculation using finite element method (FEM) to back-calculate the influence factor I.

5.4.2 Benchmark calculation

Generally speaking, to gain faith in the validity of numerical results using the newly proposed boundary, the approach must be applied at first to benchmark situations where exact solutions exist. When satisfactory results are obtained, the model can be used to problems where exact solutions are not available. In this way, albeit the solution will be approximate, the magnitude of error shall be estimated.

The benchmark, in this case, is Fig. 5.23(a) with $I = 2/\pi$, which is used for the flexible membrane expansion process in the DMT. Except for the different forms of loading, the situation of this benchmark is identical to the piston expansion of the iDMT. Fig. 5.24 shows the boundary condition used in the FEM calculation, where the infinite elastic half-space is simulated as a finite FEM mesh.

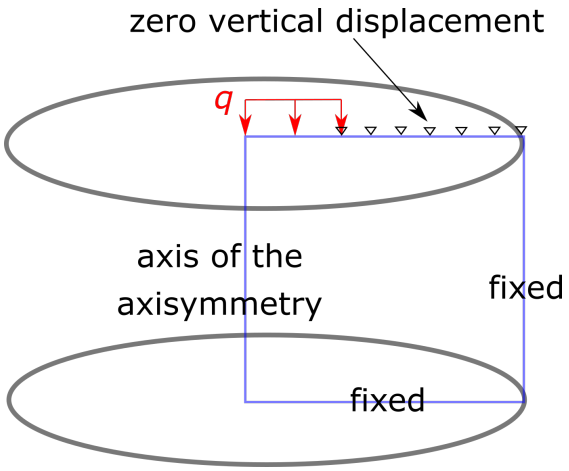

Figure 5.24: The boundary condition of the benchmark (not to scale)

Specifically, an axisymmetric FEM model is built in Abaqus software using the 6-node quadratic axisymmetric triangle (CAX6) elements. The parameters used in this calculation are given in Table 5.1.

In terms of the exact solution of Eq. 5.19, a vertical displacement at the center of the loaded area can be obtained as 1.1 mm, using the parameters shown in Table 5.1. For the FEM calculation, the linear elastic analysis is performed with the first stress invariant ($I_1 = \sigma_{11} + \sigma_{22} + \sigma_{33}$) contours and the vertical displacement contours shown in Fig. 5.25. With the zoomed in contour on the right side of Fig. 5.25(a,b), stress concentration at the edge of the loaded area and a vertical displacement of 1.096 mm at the center of the loaded area can be

Table 5.1: Input parameters of the benchmark

Young's modulus (E)	5 N/mm^2
Poisson's ratio (ν)	0.3
The uniform pressure q	0.15823 N/mm^2
Mesh size	300 mm$\times$300 mm
Radius of the loaded area	30 mm
Number of elements	703
Number of nodes	1500

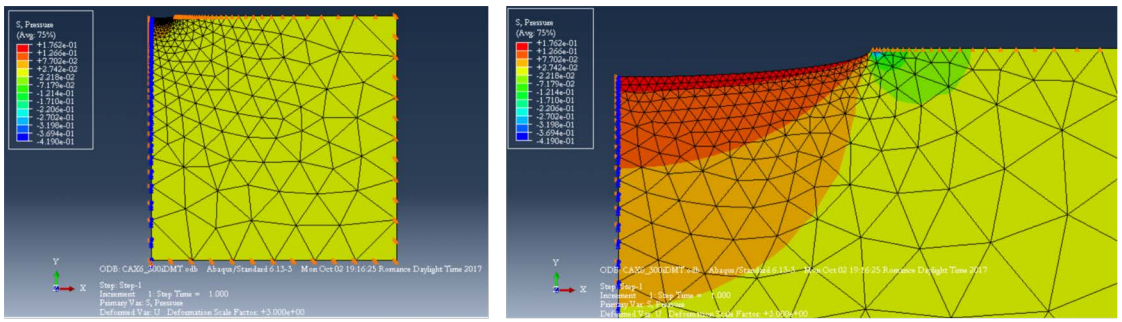

(a) the first stress invariant I_1

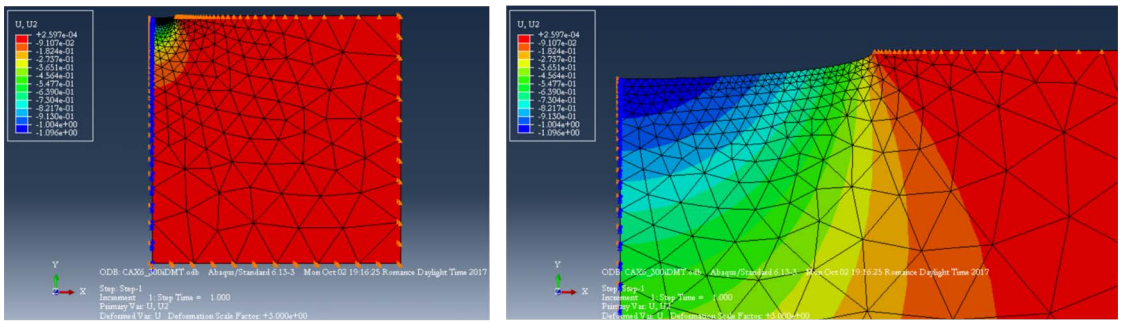

(b) vertical displacement

Figure 5.25: FEM calculation results of the benchmark (deformation scale factor: 3.0): (a) the first stress invariant I_1 contours, (b) vertical displacement contours

spotted, respectively.

Therefore, concerning the vertical displacement at the center of the loaded area, the benchmark gives a -0.36% error compared to the exact solution, which is considered good enough as the baseline for further calculations.

5.4.3 Piston expansion calculation

Fig. 5.23 shows the proposed semi-elliptical displacement boundary for the piston expansion and the prescribed displacement is given by:

$$u = s_e \sqrt{1 - x^2/r^2} \tag{5.20}$$

where s_e is the displacement at the center (the vertex of the ellipse along the minor axis) and r is the radius of the loaded area. Appendix C includes the Abaqus input codes for this calculation.

In case of a piston expansion with a uniform displacement of 1.1 mm, the alternative semi-elliptical displacement boundary has the central displacement s_e=1.65 mm, based on the assumption of the same cavity volume resulting from the ideal cylindrical boundary and the alternative semi-elliptical boundary. Then, this displacement boundary is used together with the parameters shown in Table 5.1, except the uniform pressure for the benchmark. Fig. 5.26 shows the FEM calculation results of the first stress invariant I_1 contours and the vertical displacement contours on the deformed mesh where the prescribed displacement boundary and the stress concentration at the edge of the loaded area can be seen.

Furthermore, a total vertical reaction force of 583.027 N is obtained by summing up the vertical reaction force acting on each node of the loaded area. This can be used to get an average pressure of 0.2062 N/mm^2 through dividing 583.027 N by the loaded area of 2827.43 mm^2. Then an influence factor I of 0.4885 can be back-calculated for the piston expansion calculation based on Eq. 5.19, using q=0.2062 N/mm^2, D=60 mm, and s=1.1 mm. The iDMT modulus is thus given by:

$$E_D = \frac{E}{1 - \nu^2} \approx 0.49 \frac{qD}{s} \tag{5.21}$$

where D = the piston diameter; s = the piston displacement.

With the Eq. 5.21, it is possible to seek for a relation between the flexible membrane expansion in the DMT and the rigid piston expansion in the iDMT, if the soil behavior is completely elastic. Specifically, the pressure required for a 1.1 mm central movement of the flexible membrane results in approximate 0.56 mm and 0.85 mm displacement of a rigid piston with a diameter of 40 mm and 60 mm, respectively. This result can be further used for deriving the iDMT index.

However, it is necessary to note that approximation is involved in both the

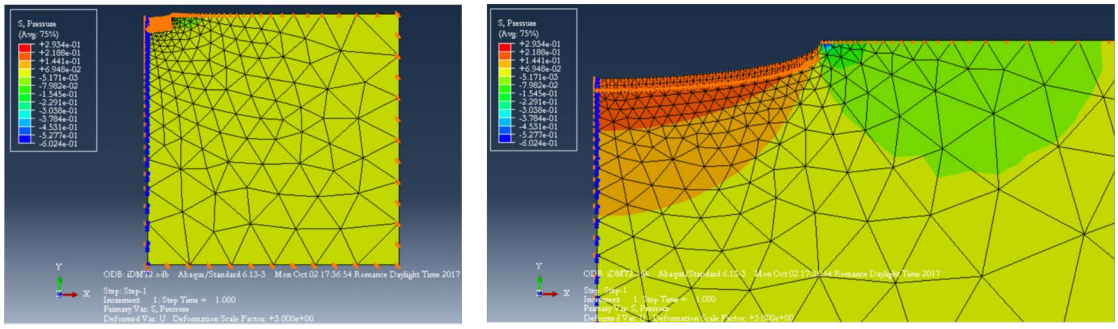

(a) the first stress invariant I_1

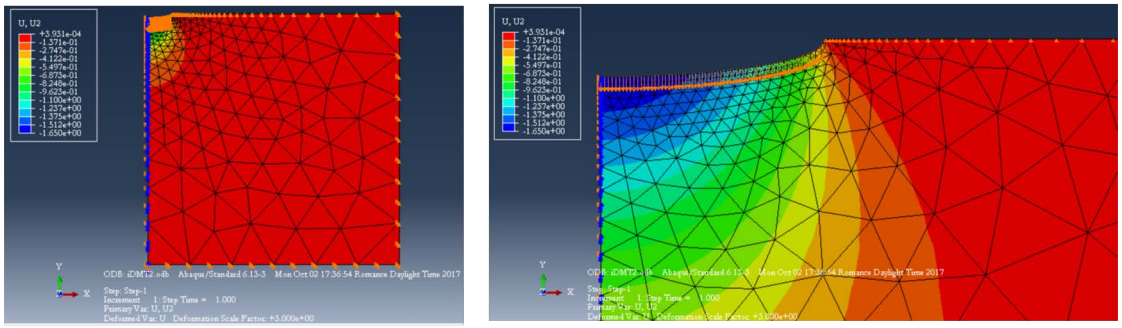

(b) vertical displacement

Figure 5.26: FEM calculation results of the piston expansion with the semi-elliptical displacement boundary (deformation scale factor: 3.0): (a) the first stress invariant I_1 contours, (b) vertical displacement contours

calculation of the piston expansion and the membrane expansion. In the piston expansion, it is the approximation of using the alternative semi-elliptical boundary to model the ideal cylindrical boundary. In the membrane expansion, the assumption of uniform pressure exerted by the flexible membrane can be inaccurate near the membrane edge that is fixed on the blade.

5.5 The iDMT indices

Calculated from p_0 andp_1, three DMT indices can be identified, namely I_D, E_D, K_D, using the aforementioned formulae established by Marchetti et al. (2001). These DMT indices are then used to derive common soil parameters. Therefore, it is of great interest to identify the iDMT indices in a similar way. In the iDMT, p_c and $p_{0.85}$ (or $p_{0.56}$ instead of $p_{0.85}$ in case of a 40-mm diameter piston) may be considered as alternatives of p_0 andp_1, so the iDMT indices are expressed as:

$$I_D = (p_{0.85} - p_c)/(p_c - u_0) \tag{5.22}$$

$$K_D = \frac{p_c - u_0}{\sigma_{v0}} \tag{5.23}$$

$$E_D = 34.7(p_{0.85} - p_c) \tag{5.24}$$

where $p_{0.85}$ for a 60-mm diameter piston can be replaced by $p_{0.56}$ for a 40-mm diameter piston. Note that the constant of 34.7 in the calculation of E_D in the iDMT remains the same as that of the DMT since the displacement of 0.85 mm of $p_{0.85}$ is already "equivalent" to 1.1 mm of p_1 based on Eq. 5.19. The soil unit weight is estimated in the same way as that in the DMT using the solution chart of E_D versus K_D (Marchetti et al. 2001).

5.6 Zwijnaarde test site

Zwijnaarde test site at Ghent University is mostly composed of sandy silts to silty sands and the groundwater table is about 2.8 m below the ground surface during this testing program. The iDMT test, the DMT test, and the CPT test are carried out at adjacent locations only 1 m apart from each other in October, 2016. The three soundings reach a depth of 7.0 m while the first 1 m soil near the ground surface is hand augured for the sake of safety concerns. Therefore the iDMT and the DMT soundings each include 30 tests with a test interval of 0.2 m. Examples of the iDMT sounding have already been presented in Section 5.3.4. Note the iDMT prototype used in this sounding has a 40-mm diameter rigid piston, so $p_{0.56}$ is considered "equivalent" to p_1 in the DMT.

In terms of the iDMT, the testing procedure aforementioned in Section 4.6 is used to minimize the difference with the DMT testing procedure to allow a comparison. In addition, during the penetration stage the thrust on top of the rods is measured by a load cell and a friction reducer is installed just above the blade to prevent damage of the equipment as well as to estimate the blade penetration resistance.

Once the piston reaches the desired testing depth, pressurization starts immediately. The pressurization continues until at least a piston displacement of 2.0 mm or a pressure of 3.4 MPa (the maximum capacity of system) is reached before an immediate de-pressurization. Though the iDMT is capable of carrying out additional small unload-reload (or reload-unload) loops to enhance estimation of soil stiffness, this is not adopted in this test to avoid influence on the comparison with the DMT. Before the penetration, the pore-water pres-

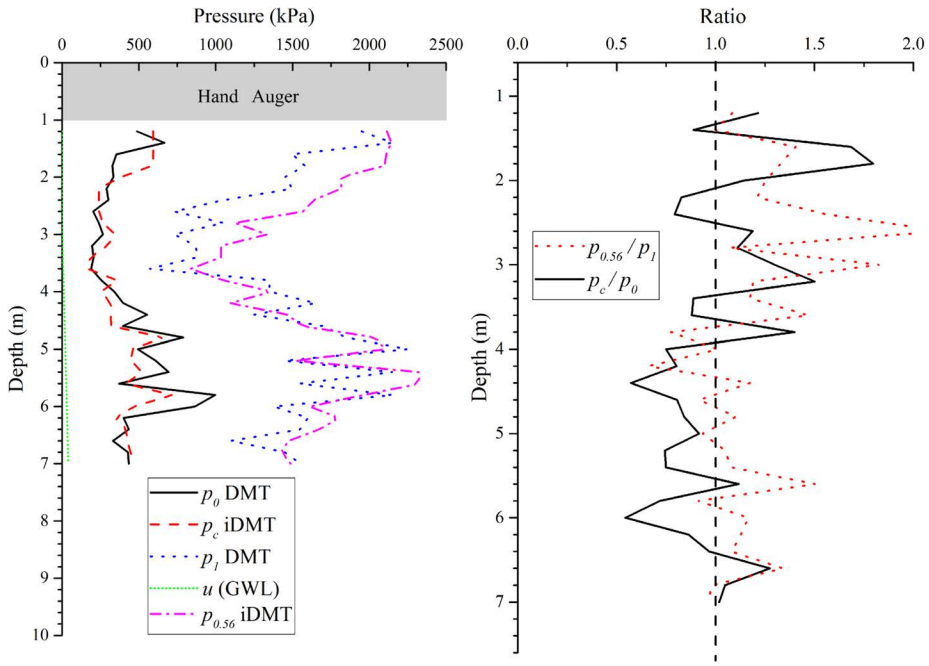

Figure 5.27: The pressure profile of the DMT and the iDMT results at Zwijnaarde test site

sure cell and the pore-water intake filter at the piston center are fully saturated using viscous silicone oil, as discussed in Section 4.6.

5.6.1 Comparison of the iDMT and DMT pressure profiles

Fig. 5.27 shows the profiles of p_1 from the DMT and $p_{0.56}$ from the iDMT in a comparison. The general trend of p_c/p_0 appears to agree with each other, with a mean ratio of 1.01. However, p_c may be significantly different from p_0 at certain depths, with a standard deviation of 0.3 for the set of p_c/p_0 values. Moreover, p_0 is found mostly larger than p_c in the depth range from 4.0 m to 6.4 m. The trends of p_1 and $p_{0.56}$ pressure profiles appear similar, with a mean $p_{0.56}/p_1$ ratio of 1.18 and a corresponding standard deviation of 0.3. The divergence is mainly attributed to greater $p_{0.56}$ values in the depth range of 1.6 m to 3.6 m. This may imply that the rigid piston competes with larger plastic soil response than the flexible membrane. Furthermore, it is necessary to pay attention to the limitation of these comparisons due to the influence from the partial drainage conditions. The scatter is also possibly attributed to the variation in soil stratigraphy which results in different soils measured at the same depth in adjacent in situ soundings.

5.6.2 Comparison of the indices K_D, E_D, I_D

Robertson (2009a) proposed CPT-DMT correlations based on a great number of sites where adjacent CPT and DMT data are available. Thus, it can predict the DMT indices (I_D, E_D , K_D) out of the CPT parameters (the normalized cone resistance Q_{t1} and the normalized friction ratio F_r). The formulas of these correlations have been given in Section 2.5. Fig. 5.28 shows the five basic CPT profiles which include the cone tip stress q_c, the sleeve friction stress f_s, the normalized CPT parameters Q_{t1} and F_r, and the SBT index I_C. In terms of soil behavior type based on I_C, the Zwijnaarde test site can be classified as a sandy site composing clean sand to silty sand from a depth of 1 m to 2.5 m and mostly sand mixtures from 2.5 m to 7 m. Furthermore, considering that I_c ranges from 1.84 to 2.51 in this CPT sounding, the correlations for sand-like soils ($I_C \leqslant 2.60$) of Eq. 2.50, 2.51, 2.46 are used accordingly to predict the DMT indices out of the CPT measurements.

Fig. 5.29 shows a comparison among the measured DMT indices, the CPT-predicted DMT indices and the iDMT indices based on the three individual soundings 1 m apart from each other. The plots for I_D and E_D are presented on log scales for a clearer illustration of the range of values. It appears that I_D and E_D based on the iDMT can give slightly larger values than that of the DMT since mostly either p_c may be smaller than p_0 or $p_{0.56}$ may go higher than p_1. Nevertheless, in general, I_D from both tests describes similar soil classification of sands and silts, and the difference between the two is considered smaller than that between the DMT measured I_D and the CPT predicted I_D. In terms of E_D in the DMT and the iDMT, the derivation simply assumes that the soils are purely elastic while in reality E_D is essentially a large strain response (Robertson 2009a; Robertson 1990). Thus, scatter to some extent resulted from elasto-plastic soil response is reasonably expected between the DMT measured E_D and the iDMT measured E_D. Predicting E_D and K_D from the CPT data requires selecting an appropriate α which depends on soil type, relative density, age and stress history. But α is not unique to all soils, thus bands bounded by α are alternatively used in the comparison plots of E_D and K_D. Robertson (2009a) suggests that α is in a range from 2 to 10, with an average of 5 for most soils. In this case, the selected α values are 2 and 8.3 for a good capture of the trends and variation in both E_D and K_D. Furthermore, the comparison of K_D between the DMT and the iDMT shows reasonable agreement, which is essentially the normalized comparison of p_c, p_0 in Fig. 5.27. The "K_D crusts"

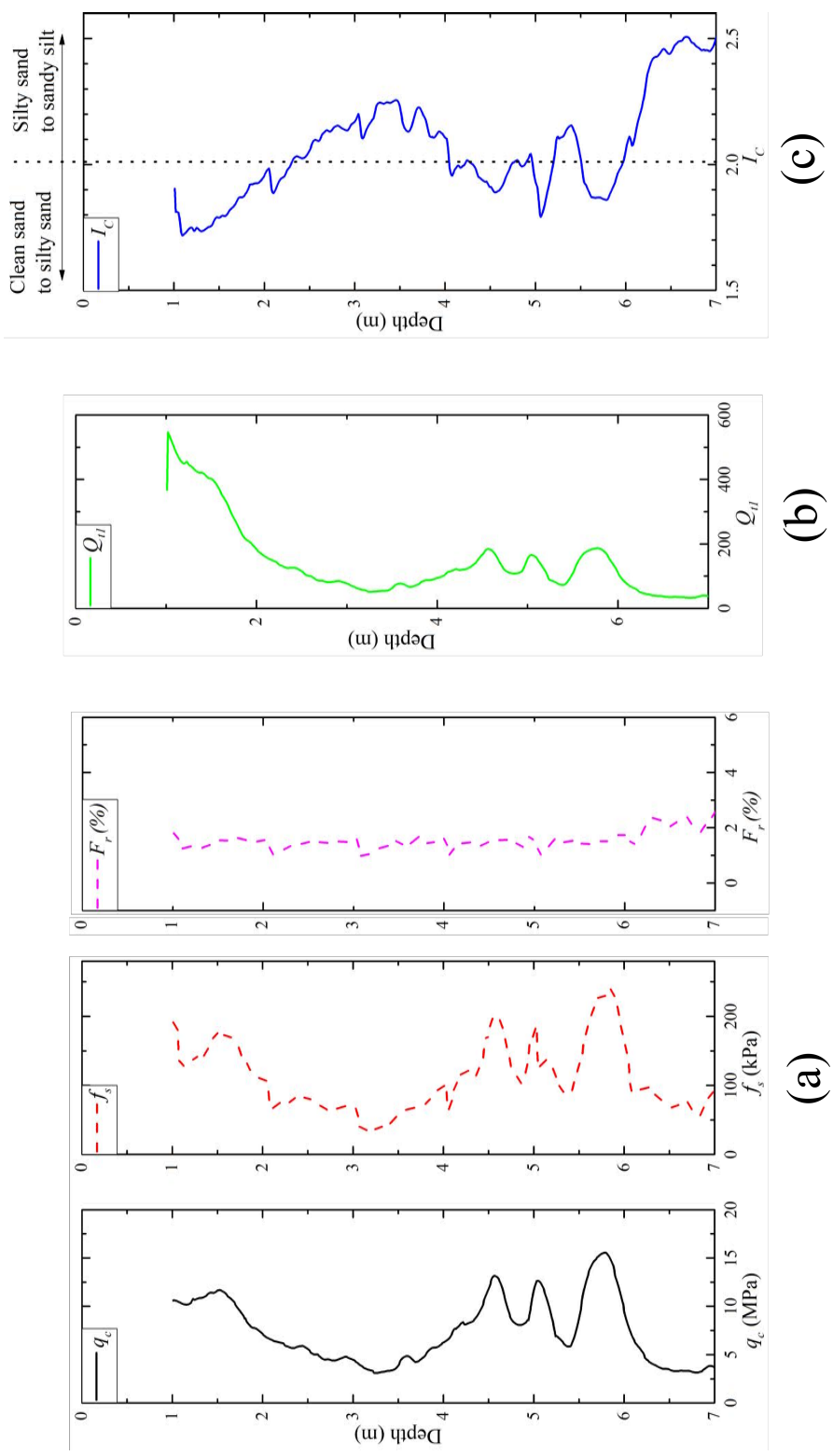

Figure 5.28: CPT profile at Zwijnaarde test site: (a) the typical CPT results, (b) the normalized CPT Q_{t1}, and (c) the CPT SBT index I_C

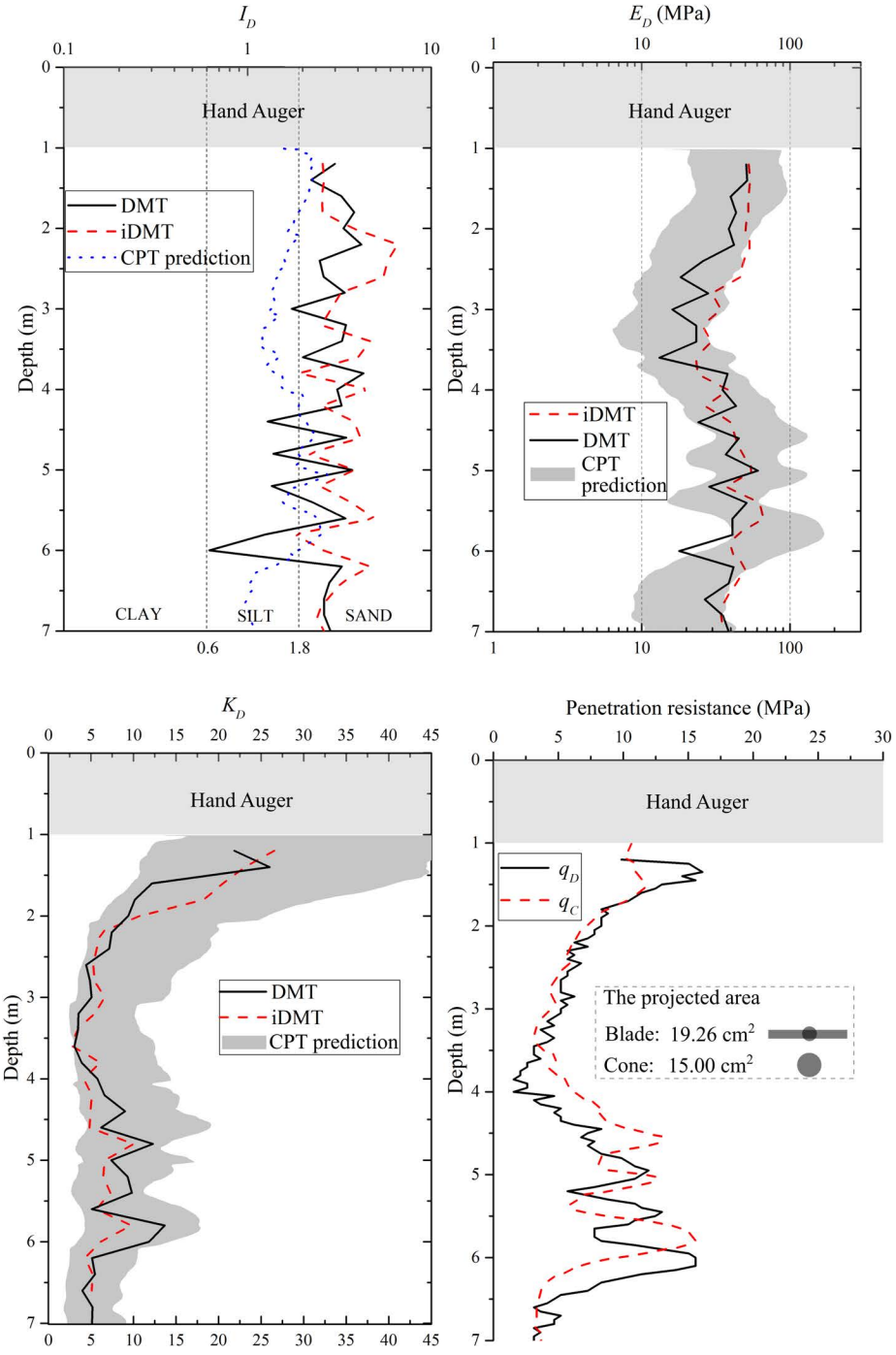

Figure 5.29: Profile of I_D, E_D, K_D and the penetration resistance from the iDMT, the DMT, the CPT results at Zwijnaarde test site

possibly resulting from shallow desiccation crusts in the sands (Marchetti 1997) are fairly captured by both K_D profile as sharp reductions are seen from 1 to 2.5 m.

In this iDMT sounding, the thrust is measured at the top of the rods with a manometer where readings were taken every 50 mm, and a friction reducer is installed just above the blade. Thus q_d is estimated by correcting the thrust using the approach devised by Schmertmann (1982). Fig. 5.29 compares the profile of the DMT q_d with the CPT q_c. An average ratio q_d/q_c of 1.09 is found to be consistent with the range of 1.1 ± 0.1 given in the literature, yet the ratios vary from 0.25 to 2.37, with a standard deviation of 0.44. This magnitude of dispersion may be due to the inherently variation of the sandy site, such as the shift of similar large variations in the depth range of around 4.5 m to 6.3 m.

5.6.3 Comparison of common soil parameters

The CPT test can normally provide a good estimation of stiffness and strength of soils. (Schnaid 2008) reviewed a great number of research findings concerning an interpretation of the CPT results. Using the recent correlation proposed by Mayne (2014) and the latest unified approach proposed by Robertson (2009b), peak friction angle $\phi^{'}$ is given by:

$$\phi^{'} = 17.6 + 11\log(Q_{t1}) \tag{5.25}$$

and undrained shear strength C_u is as follows:

$$C_u = (q_t - \sigma_v)/N_{kt} \tag{5.26}$$

where $N_{kt} = 10.5 + 7\log(F_r)$.

The CPT determined vertical drained constrained modulus M_{CPT} is given by:

$$M_{CPT} = \begin{cases} \alpha(q_t - \sigma_v), & \text{If } I_C > 2.20 \\ & \text{where } \alpha = 14 \text{ for } Q_{t1} > 14 \\ & \text{and } \alpha = Q_{t1} \text{ for } Q_{t1} \leqslant 14 \\ 0.0188(q_t - \sigma_v)10^{0.55I_C + 1.68}, & \text{If } I_C \leqslant 2.20 \end{cases}$$

Furthermore, as discussed in Section 2.2.4, Marchetti (2015) pointed out that CPT alone or DMT alone is insufficient to estimate OCR and K_0 in a sand. But with M_{DMT} from the DMT and q_c from the CPT together, it is possible to

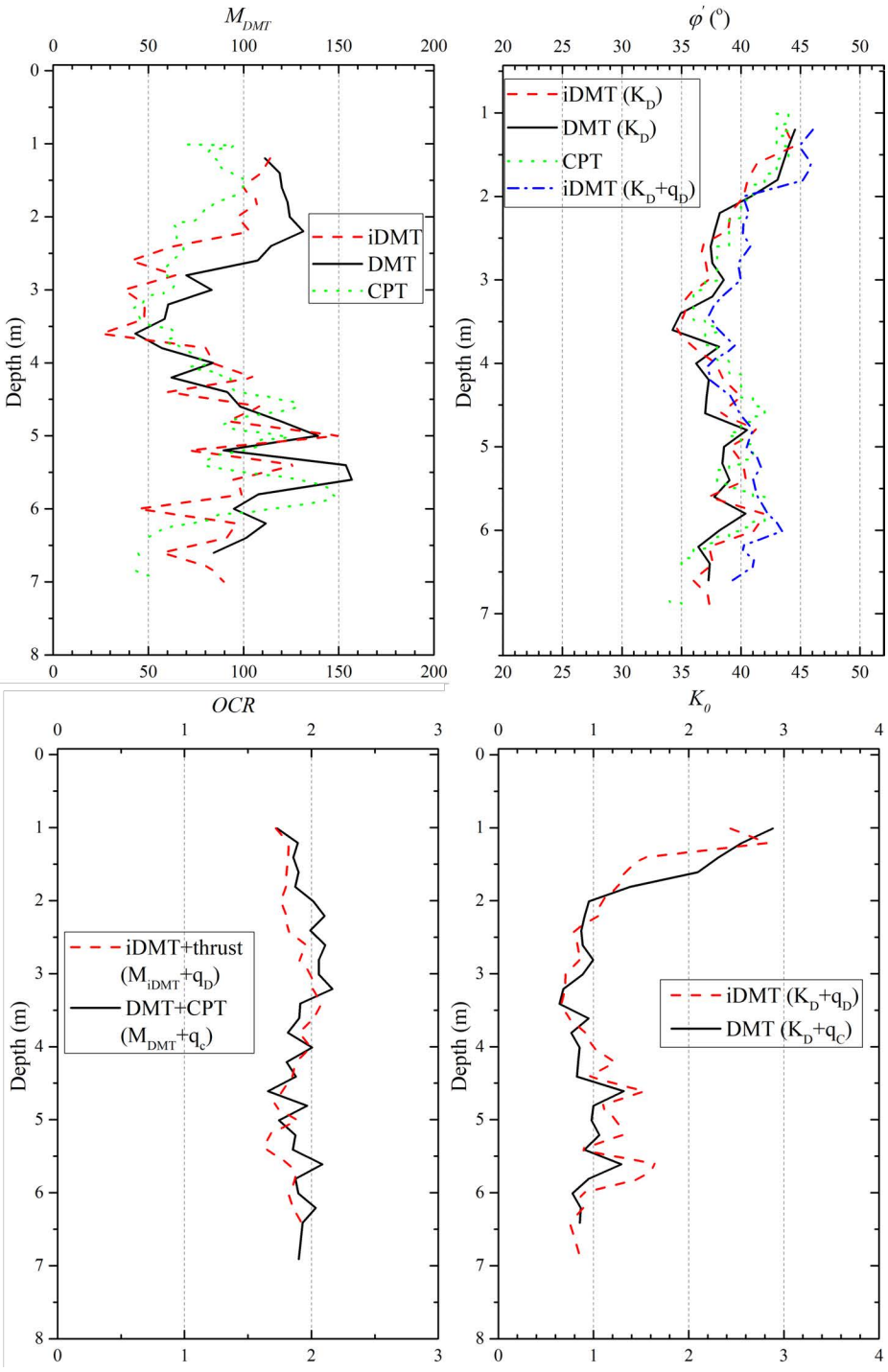

Figure 5.30: Comparison of K_0, OCR, C_u, and M_{DMT} at Zwijnaarde test site

estimate OCR and K_0 using Eq. 2.20 and Eq. 2.30, respectively.

Fig. 5.30 shows the comparison of K_0, OCR, $\phi^{'}$, and M_{DMT} estimated from the CPT, the DMT, and the iDMT. The comparison shows promising use of the iDMT results as the iDMT estimated K_0, OCR, $\phi^{'}$ are very close to the benchmark results of the CPT and the DMT. In terms of M_{DMT}, the general trends of all three tests are found the same while distinct difference mainly locates above 3.5 m where the DMT results estimate larger M_{DMT} than that of the CPT and the iDMT showing similar values. The scatter may be considered reasonable since neither the CPT, nor the DMT, nor the iDMT has soil response similar to that of the vertical, constrained, and drained soil condition. Moreover, it is interesting to find out that effective friction angles $\phi^{'}$ estimated using Eq. 2.32 from both the iDMT and the DMT are generally slightly lower than those by the CPT and the $K_D - q_D$ method mentioned in Section 2.2.7. This confirms that Eq. 2.32 is an lower bound estimation of $\phi^{'}$.

5.7 Limelette test site

The testing campaign was also carried out in silts at Limelette test site which is a well-known geotechnical experimentation site in Belgium. The soundings were performed in June 2017 when the groundwater table is normally deep (likely deeper than 10 m) in this season. All three soundings went up to exactly 6 m in depth where significant penetration thrust is required to further penetrate the deeper ground layer gravels. Considering the likelihood of silt stone, the soundings were stopped at this level, so no pore-water pressure was measured. In total 24 iDMT tests, 25 DMT tests, and 1 CPT sounding were conducted from the depth of 1.0 m to 6 m, as there were two bad iDMT tests at 2.8 m and 6.0 m in depth due to glitches in the electrical system. Note the iDMT device used in this sounding has a 60-mm diameter rigid piston, so $p_{0.85}$ is considered "equivalent" to p_1 in the DMT. During the tests, the pressurization continues until at least a piston displacement of 2.5 mm or a pressure of 3.4 MPa (the maximum capacity of a system) is reached before an immediate de-pressurization.

Fig. 5.31 shows an example of the iDMT test at a depth of 3.2 m concerning the basic data reduction process. In terms of the p_c determination procedure, one may refer to the aforementioned cases shown in Fig. 5.12 and Fig. 5.11. By subtracting the interpolated values from the calibration sheet, the corrected loading curve can be produced from the uncorrected loading curve (raw mea-

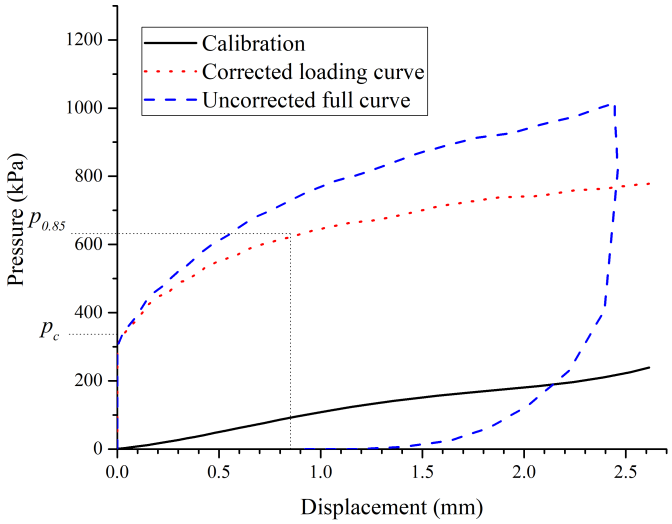

Figure 5.31: The iDMT test result at a depth of 3.2 m: comparison of uncorrected and corrected curves

surements). Then, $p_{0.85}$ can be readily read from the curve as 620 kPa, and p_c can be estimated as 322 kPa by means of the adapted Casagrande method based on the corrected loading curve.

5.7.1 Comparison of the iDMT and DMT pressure profiles

Fig. 5.32 shows the profiles of p_0, p_1 from the DMT and p_c, $p_{0.85}$ from the iDMT in a comparison. The main trend of p_c and p_0 appears to agree with each other, as the set of p_c/p_0 values show a mean p_c/p_0 ratio of 1.18 and a standard deviation of 0.39. Albeit the standard deviation appears high, it can be induced by the variation in soil stratigraphy at different locations, so a judgment of the trends is more reasonable. The trends of p_1 and $p_{0.85}$ pressure profiles appear similar, with a mean $p_{0.85}/p_1$ ratio of 1.08 and a corresponding standard deviation of 0.2. It is interesting to note that the trend of $p_{0.85}/p_1$ is mostly resemblant to that of p_c/p_o, which is not seen in the results at Zwijnaarde test site. This may be to due to the influence of the partial drainage conditions in the tests at Zwijnaarde test site. The similarity of the trends in two ratios may be more explicit when the drainage process is de-coupled from the soil response.

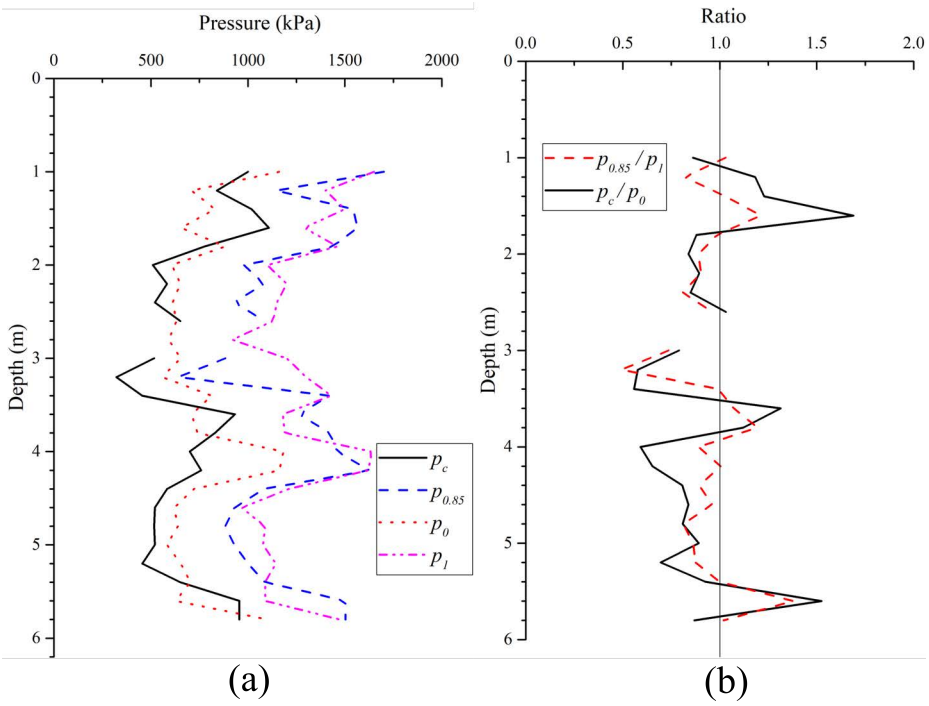

Figure 5.32: The pressure profile of the DMT and the iDMT results at Limelette test site

5.7.2 Comparison of the index parameters K_D, E_D, I_D

Fig. 5.33 has shown the five basic CPT profiles of q_c, f_s, Q_{t1}, F_r, and I_C. In terms of soil behavior type based on I_C, the Zwijnaarde test site can be basically classified as sand mixtures in the upper layer from 1.0 m to 4.26 m, overlaying silt mixtures from the depth of 4.26 m to 6.0 m. Therefore, by setting a cut-off of $I_C = 2.65$, the correlations for sand-like soils ($I_C \leqslant 2.65$) of Eq. 2.50, 2.51, 2.46 for the upper layer and the correlations for clay-like soils ($I_C > 2.65$) of Eq. 2.46, 2.49, 2.48 could be used accordingly to predict the DMT indices out of the CPT measurements.

Fig. 5.34 shows a comparison among the measured DMT indices, the CPT-predicted DMT indices and the iDMT indices based on the three individual soundings 1 m apart from each other. The prediction of K_D and E_D out of the CPT results are presented in a band for the upper soil layer to a depth of 4.26 m. The upper and the lower boundary of the band are defined by $\alpha = 5$ and $\alpha = 10$, respectively. In general, I_D describes similar soil classification of clayey silts from all three soundings, and E_D from the iDMT and the DMT both indicate values mostly within the band predicted by the CPT. The comparison of K_D between the DMT and the iDMT shows reasonable agreement, nevertheless, the CPT results tend to underestimate K_D. Similar to the results at Zwijnaarde

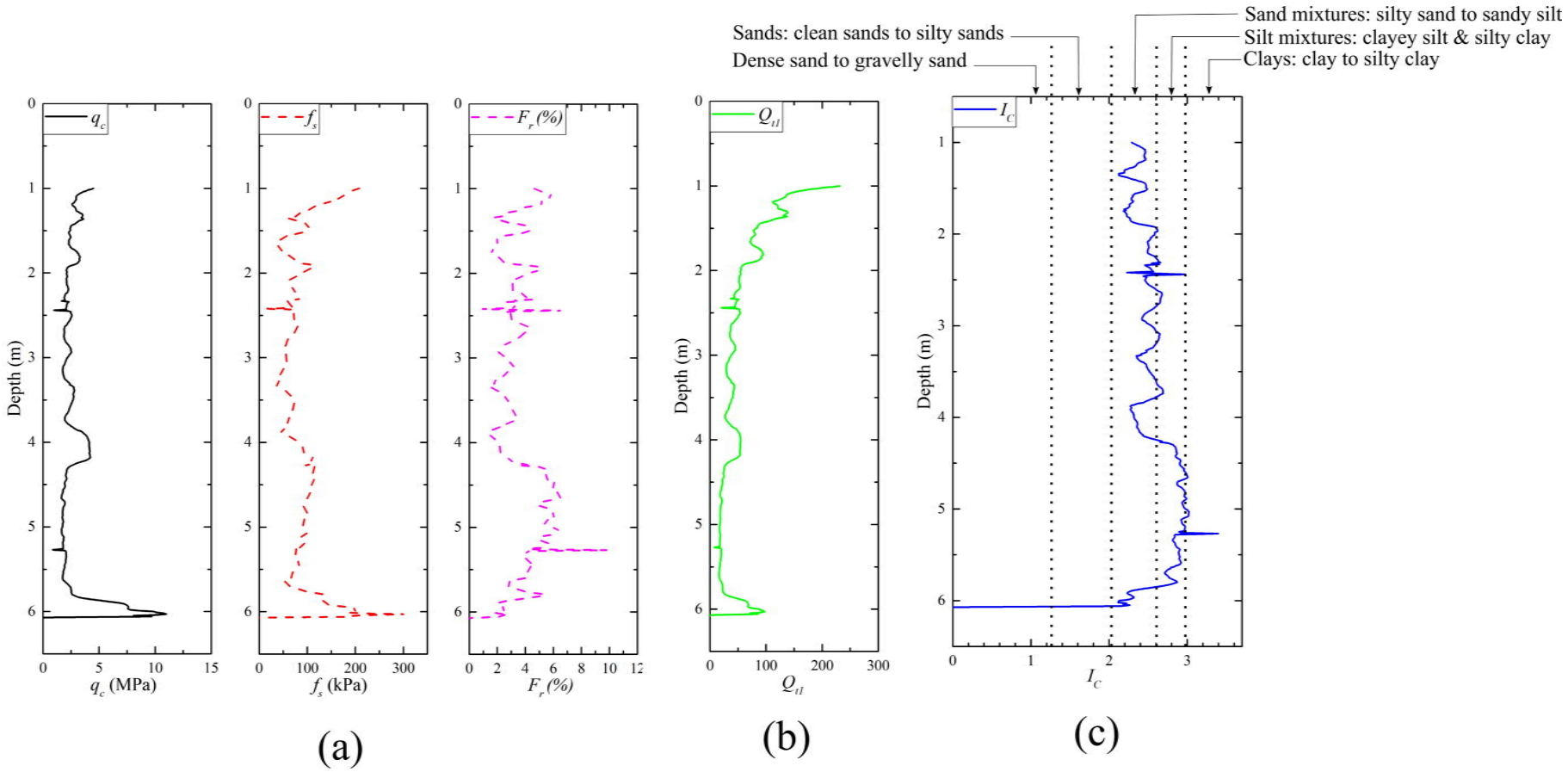

Figure 5.33: CPT profile at Limelette test site: (a) the typical CPT results, (b) the normalized CPT Q_{t1}, and (c) the CPT SBT index I_C

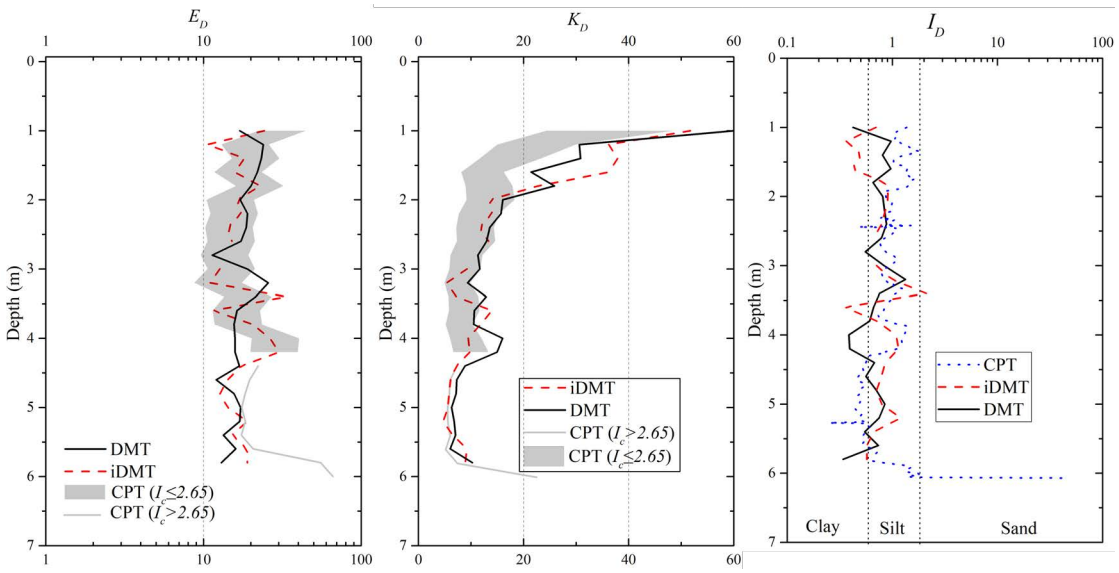

Figure 5.34: Profile of I_D, E_D, K_D from the iDMT, the DMT, the CPT results at Limelette test site

test site, the "K_D crusts" are also captured by all K_D profile as sharp reductions are seen from 1 to 2.0 m.

5.7.3 Comparison of common soil parameters

Fig. 5.35 shows the comparison of K_0, OCR, C_u, and M_{DMT} estimated from the CPT, the DMT, and the iDMT. It is worth mentioning that these in situ soundings were performed in unsaturated soils as the ground water table is deeper than the maximum test depth of 6.0 m. So, albeit C_u is sought for a comparison of the soil strength parameter, it does not necessarily indicate the shear strength under undrained condition.

In terms of strength and stiffness parameter, a comparison of the derived C_u and M profiles from the DMT, the iDMT, and the CPT indicates quite good agreement amongst not only the CPT-based relationships and the DMT-based relationships but also the DMT results and the iDMT results which both use the same relationships. Concerning the OCR, the trends of the DMT results and the iDMT results fairly agree with each other except that the DMT gives significant larger values in the thin layer near the ground surface. This is likely due to the effects of soil crust. The CPT-estimated OCR is generally smaller and thus conservative for geotechnical design, which is reasonable since that q_t is known to be insensitive to changes in OCR (Schnaid 2008). The CPT relationship for OCR is given by:

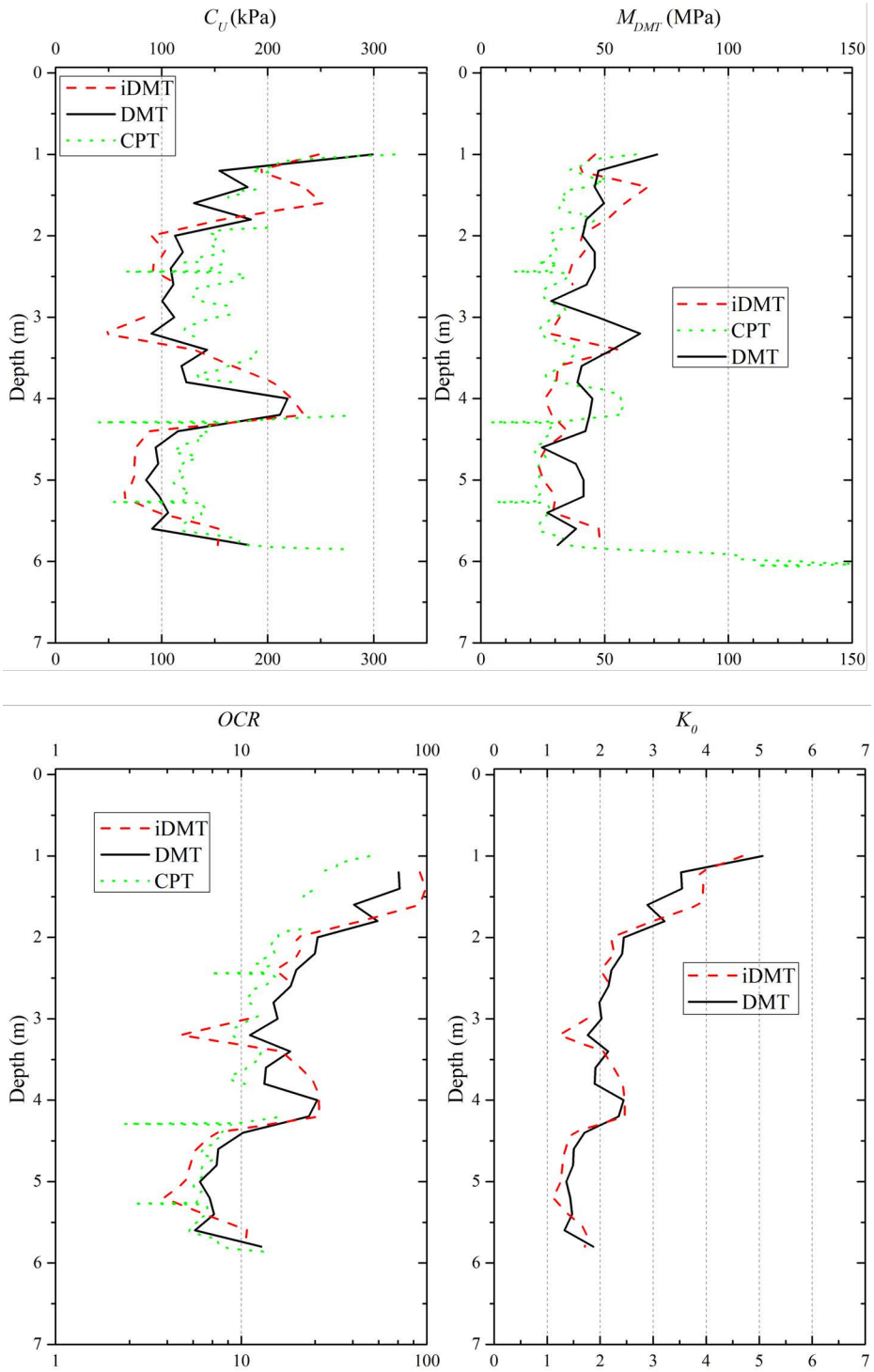

Figure 5.35: Comparison of K_0, OCR, C_u, and M_{DMT} at Limelette test site

$$OCR = [\frac{Q_{t1}^{0.20}}{0.25(10.5 + 7\log(F_r))}]^{1.25} \tag{5.27}$$

where $I_c > 2.6$ is required to use this relationship.

Regarding K_0 estimation, there are even more uncertainties from the CPT results since not only OCR but also the soil effective peak friction angle is required. Therefore, only a comparison between the DMT results and the iDMT result for K_0 estimation is shown in Fig. 5.35. The comparison shows promising results that the iDMT estimated K_0 values are at least as good as those from the DMT, while further validation may require the performance of self-boring pressuremeter test.

5.8 Kruibeke test site

An iDMT sounding and a DMT sounding were carried 1 m apart from each other at Kruibeke test site in July 2017. At an adjacent location, a mechanical CPT was performed in October 2015, the results of which are shown in Fig. 5.36. The soils at Kruibeke are known to compose of a layer of overconsolidated (OC) clays overlying a layer of heavily overconsolidated (HOC) clays (Belgian Boom clay) (Peiffer 2016). The Boom clay belongs geologically to the tertiary formation of Boom in Belgium, which has a same geological origin as the London Clay. The ground watertable is at about 1.4 m in depth.

The iDMT sounding and the DMT sounding were conducted to the maximum depth of 9.0 m where more than 55 kN is required to penetrate further into the ground. So, there were in total 40 iDMT and 40 DMT tests performed at Kruibeke test site. During the tests, the pressurization continues until at least a piston displacement of 2.5 mm or a pressure of 3.4 MPa (the maximum capacity of the system) is reached before an immediate de-pressurization. Nevertheless, starting from the test at 6.6 m onwards, the maximum pressure achieved in the iDMT tests is only 1000 kPa. This is due to a broken air tubing on the ground surface during the installation of the push rods onto the penetrometer. While a temporary fix was done on site, it was found that an applied pressure exceeding 1000 kPa could result in breakage again. Therefore, in terms of the iDMT interpretation in the depth range of 6.6 m to 9.0 m, the conceptual contact pressure p_c is estimated using the real lift-off pressures as approximate results while $p_{0.85}$ could not be reached.

In addition to the aforementioned test examples given in Fig. 5.13 and

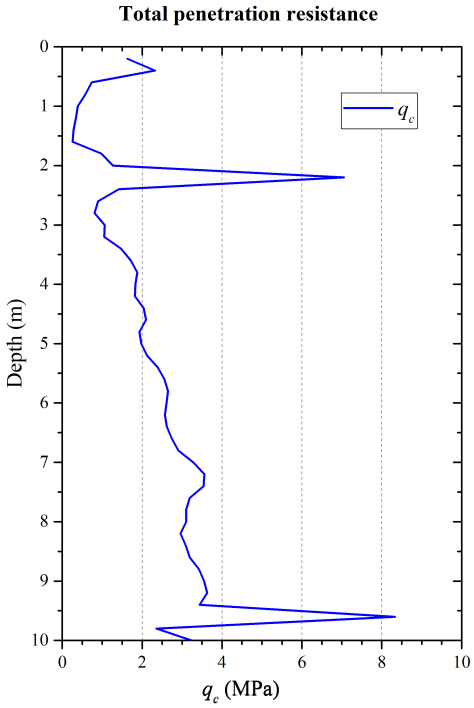

Figure 5.36: The tip resistance of a nearby mechanical CPT at Kruibeke test site

Fig. 5.14. Fig. 5.37 provides an example of the iDMT test at a depth of 6.0 m concerning the basic data reduction process. The negative pore-water pressure measurements indicate that this test is performed in an overconsolidated soil while the sensor measures the minimum pressure of its capacity at −100 kPa in the initial piston expansion up to 0.6 mm. So, pore-water pressures equal to or smaller than −100 kPa are expected in the soil at this stage. Similar to previous cases, the corrected loading curve is produced by subtracting interpolated calibration values from the uncorrected loading curve. Then, $p_{0.85}$ of 1091 kPa is readily read from the curve and p_c of 760 kPa is determined by means of the adapted Casagrande method.

5.8.1 Comparison of the iDMT and DMT pressure profiles

Fig. 5.38 shows the profiles of p_0, p_1 from the DMT and p_c, $p_{0.85}$ from the iDMT in a comparison. Although the comparison between the iDMT p_c, $p_{0.85}$ and the DMT p_0, p_1 shows very good agreement in trend, a significant difference is found at 5.6 m with a spike in both ratios of p_c/p_0 and $p_{0.85}/p_1$ to about 2.0. This is likely due to the fact the iDMT sounding starts measuring the overconsolidated clays at 5.6 m while the DMT at 5.8 m, and there is a vast increase in the pressure measurements from the upper overconsolidated soil

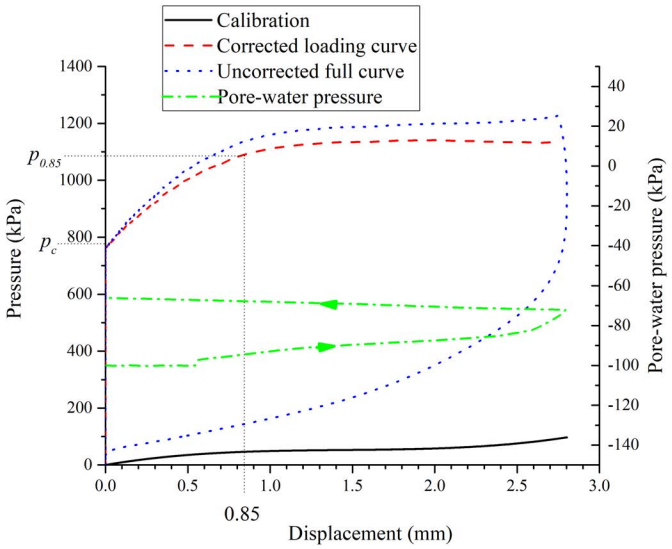

Figure 5.37: The iDMT test result at a depth of 6.0 m in an overconsolidated soil: comparison of uncorrected and corrected curves and pore-water pressure development

layer to the heavily overconsolidated Boom clay. Statistical analyzes indicated that the mean value (and $\pm$ one standard deviation) of $p_c/p_0 = 1.04 \pm 0.19$ and of $p_{0.85}/p_1 = 1.01 \pm 0.24$.

5.8.2 Comparison of the index parameters K_D, E_D, I_D

Fig. 5.39 shows a comparison between the measured DMT indices and the iDMT indices. The general trends of three index profiles are excellently captured by both tests. Specifically, I_D from both tests describes similar soil classification of a crust layer of clay on top of a silt layer from 2 m to about 5.5 m. Under this silt layer the tertiary overconsolidated Boom Clay can be found as the degree of overconsolidation is explicitly indicated by an increase in K_D. It is worth mentioning that the silt layer classified by the I_D profile at Kruibeke test site is based on the soil behaviour type (SBT) rather than the grain size criteria. So, due to stronger mechanic behaviours, overconsolidated clays can be classified as silts using the I_D-SBT criterion.

5.8.3 Comparison of common soil parameters

Fig. 5.40 shows the comparison of C_u, M_{DMT}, OCR, and K_0 estimated from the DMT, and the iDMT. In addition, C_u estimated by the mechanical CPT is also provided using Eq. 5.26 while N_{kt} cannot be calculated due to the lack of

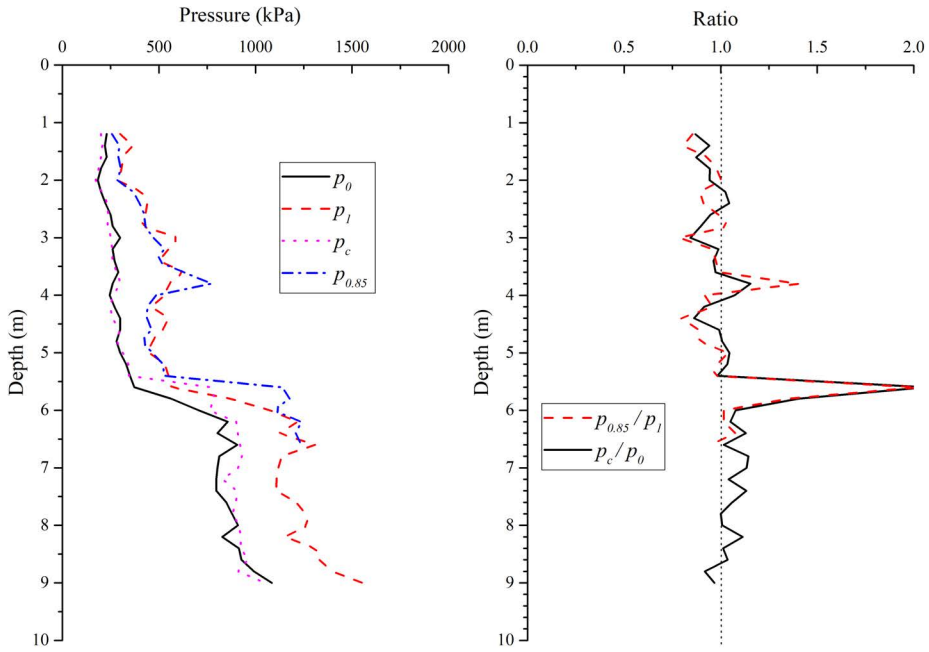

Figure 5.38: The pressure profile of the DMT and the iDMT results at Kruibeke test site

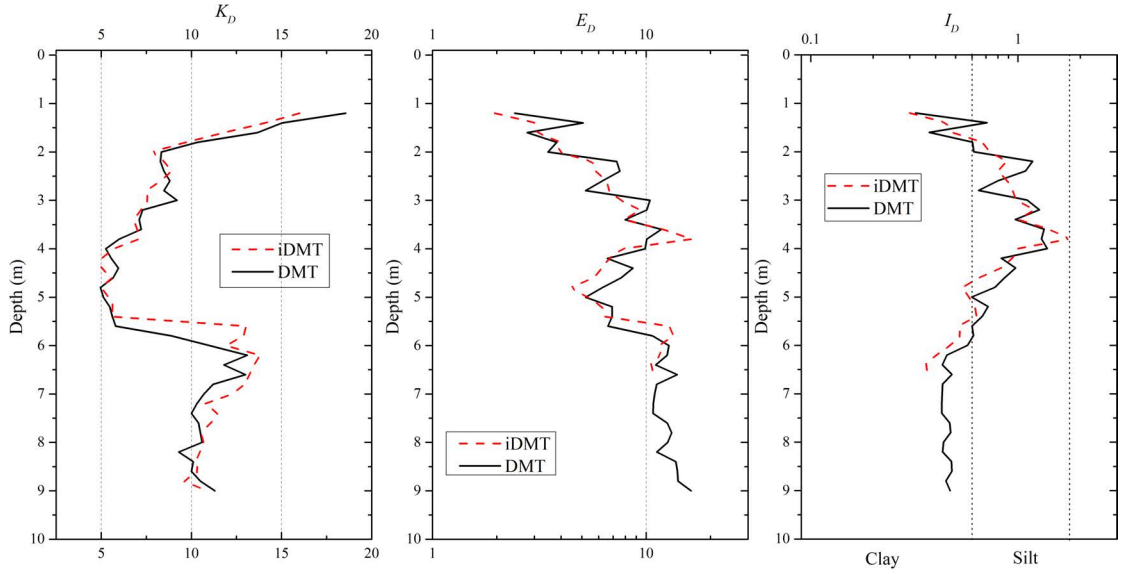

Figure 5.39: Profile of I_D, E_D, K_D from the iDMT and the DMT at Kruibeke test site

sleeve friction measurements in the mechanical cone. Schnaid (2008) suggests the range of N_{kt} empirical values is from 12 to 15. In case $N_{kt} = 15$, the undrained shear strength C_u by the CPT still suggests much larger values than that from either the iDMT or DMT. Furthermore, it is hard to identify the influence of the variation of OCR and K_0 on C_u. Taking this into account, it can be unreliable to interpret C_u from the cone resistance alone since normally the sleeve friction is supposed to be more significant than the cone resistance in clayey soils (Robertson 2012).

Considering the empirical nature of the relationship for M_{DMT}, the comparison between the iDMT and the DMT also shows excellent agreement in trends and a reasonable difference in magnitudes. Regarding K_0 and OCR estimation, the agreement between the iDMT results and the DMT is very good from the depth of 1.2 m to 5.4 m. Nevertheless, in the Boom clay layer from the depth of 5.6 m to 9,0 m, the iDMT estimated K_0 and OCR values are generally larger than the DMT results. This deviation may be due to the different loading mechanics between the rigid piston expansion and the flexible membrane expansion, but further validation on this explanation is required in this case.

5.9 Discussion on the pore-water pressure measurements

In general, pore-water pressures during the iDMT testing campaign were successfully measured at Zwijnaarde test site and Kruibeke test site, while it was not possible at Limelette test site since the groundwater table was deeper than the maximum test depth.

Fig. 5.41 shows the results in different types of soils, which includes silty sands at Zwijnaarde test site, heavily overconsolidated (HOC) Boom clays with OCR>11 and overconsolidated (OC) clays with 10>OCR>3 at Kruibeke test site.

In silty sands, as shown in Fig. 5.41(a), the excess pore-water pressure is generated during the piston expansion process. However, the magnitude of the pore-water pressures is much smaller compared to that of the total pressures, which have the peak values of about 1900 kPa of the total pressure but only around 60 kPa of the pore-water pressure. Although this does not justify a purely drained test, the measured total pressures are largely controlled by the effective stress. In addition, the dissipation of the excess pore-water

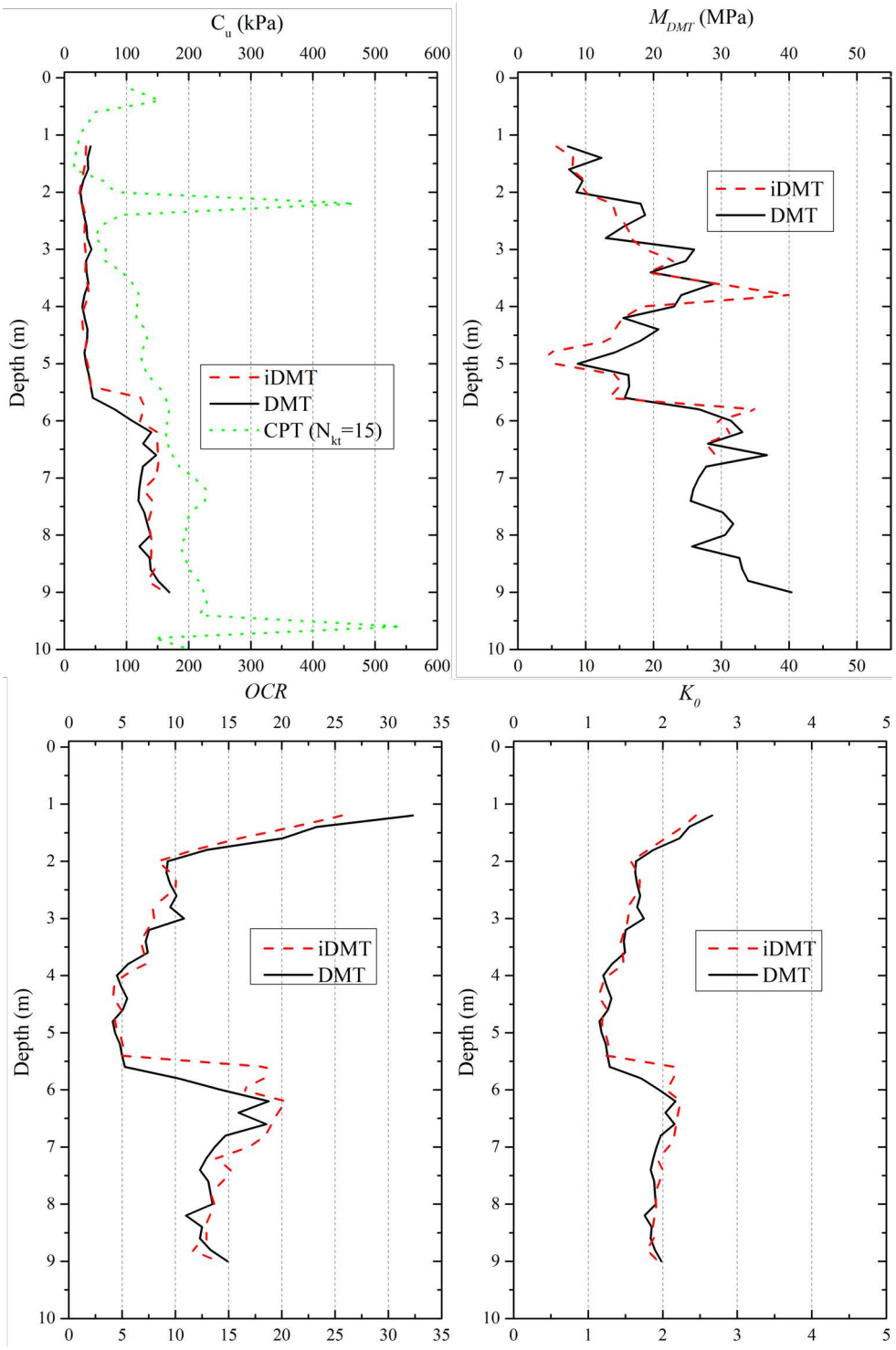

Figure 5.40: Comparison of K_0, OCR, C_u, and M_{DMT} at Kruibeke test site

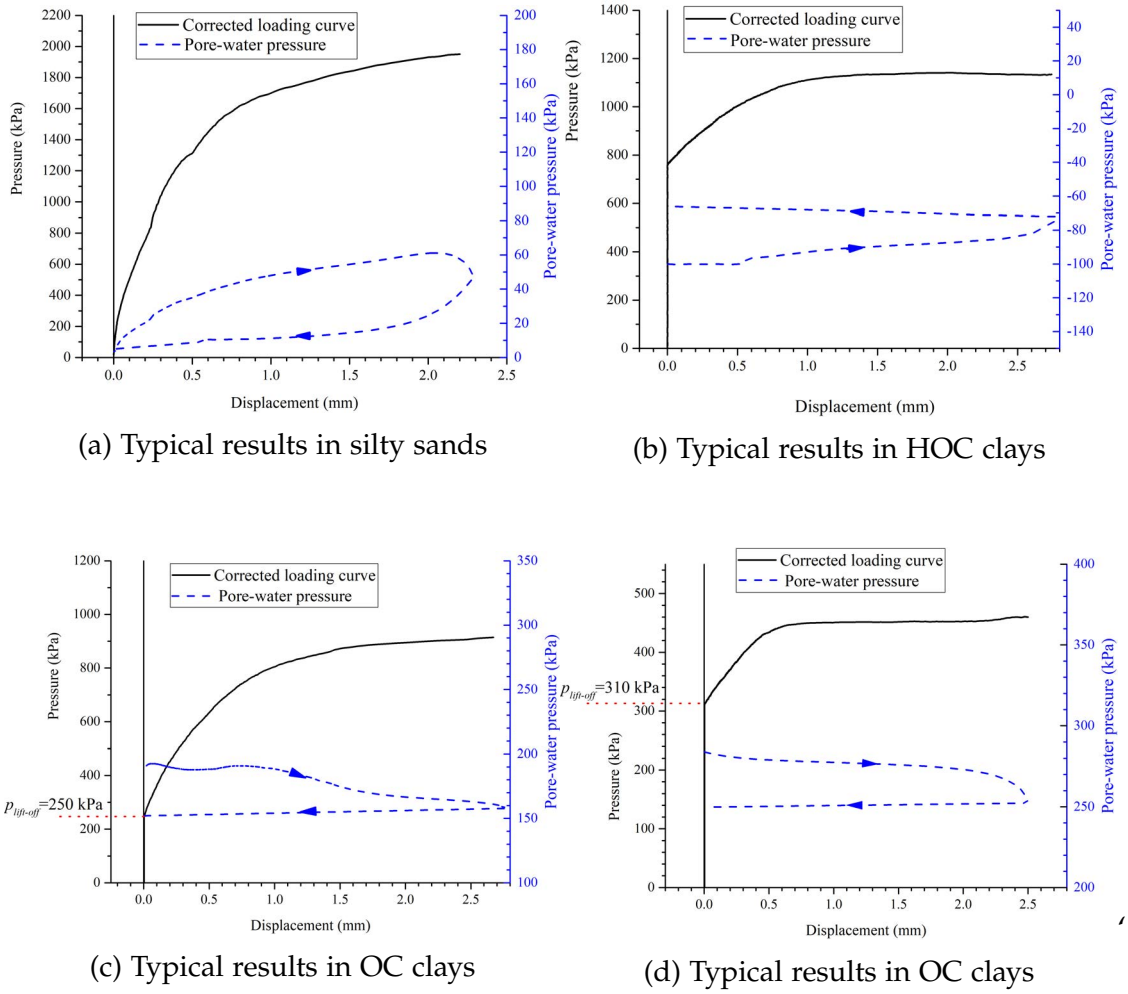

(a) Typical results in silty sands

(b) Typical results in HOC clays

(c) Typical results in OC clays

(d) Typical results in OC clays

Figure 5.41: Pore-water pressure measurements in different types of soil materials at Zwijnaarde test site and Kruibeke test site.

pressures is found fast, in spite of short unloading time due to the immediate de-pressurization process.

In an HOC Boom clay, as shown in Fig. 5.41(b), negative pore-water pressures are observed. Nevertheless, the pressure sensor used in the iDMT device measures a pore-water pressure range from -100 kPa to 900 kPa, which results in any pore-water pressure lower than -100 kPa reads as -100 kPa. Therefore, the initial phase of pore-water pressure measurements of -100 kPa in Fig. 5.41(b) may be due to a pressure lower than or equal to -100 kPa. This drawback indicates that a better pressure sensor with larger negative range is required in HOC clays. Except for this technical disadvantage, the negative pore-water pressures in HOC clays at least confirm the exhibition of soil dilatant behaviors, and the total pressure is strictly controlled by the effective stress. Furthermore, the pore-water pressure development during the piston

expansion seems to be largely influenced by the penetration pore-water pressure at least in the initial phase where -100 kPa is recorded from the beginning of the piston movement. This is reasonable considering that the blade penetration opens a flat cavity with a thickness of 15 mm while the maximum displacement of the piston is merely 2.5 mm.

The influence of the penetration pore-water pressure is also observed in the upper clay layer with relatively smaller OCR at Kruibeke test site, which is significant since the pore-water pressure accounts for a large part of the total pressure at the beginning of the piston expansion. Fig 5.41(c,d) illustrate the corrected loading curves along with the pore-water pressure measurements, where the pore-water pressures at the instant of the piston lift-off $u_{\text{lift-off}}$ account for 76.4% and 91.6% of the total lift-off pressure $p_{\text{lift-off}}$, respectively. This indicates that the penetration pore-water pressure is dominant when the piston begins its movement, and the pore-water pressure development during the piston expansion is a mixed soil response resulting from both the blade penetration and the piston expansion. With the current iDMT test procedure developed for a comparison with the DMT, it is not possible to separate the pore-water pressure induced by the piston expansion from the penetration pore-water pressure.

However, the pore-water pressure measured at the instant of the piston lift-off $u_{\text{lift-off}}$ is informative since it stands for the amount of the penetration pore-water pressure immediately before the piston expansion and is not involved in the mixed soil response once the piston departs. Fig 5.42 shows the ratios of $u_{\text{lift-off}}$ to $p_{\text{lift-off}}$ and $u_{\text{lift-off}}$ to p_c of the upper clay layer at Kruibeke test site. Note that $u_{\text{lift-off}}$ and $p_{\text{lift-off}}$ are measured simultaneously while the iDMT contact pressure p_c is derived from the full iDMT loading curve. The mean value of $u_{\text{lift-off}}/p_c \pm$ one standard deviation and the mean value of $u_{\text{lift-off}}/p_{\text{lift-off}} \pm$ one standard deviation are 0.73 ± 0.065 and 0.83 ± 0.067, respectively.

Mayne (1987) proposed that the DMT contact pressure p_0 provides an approximate measure of the total penetration pore-water pressure caused during penetration of the dilatometer blade in clay deposits. This postulation is possibly also true with the iDMT contact pressure p_c or the iDMT lift-off pressure $p_{\text{lift-off}}$ which accounts for about 73% and 83% of $u_{\text{lift-off}}$, respectively. Because $u_{\text{lift-off}}$ is presumably lower than the maximum penetration pore-water pressure (u_{max}) for the stress relief phenomenon caused by the wedge cavity expansion effects discussed in Section 2.4.2. With the soil parameters used by Finno (1993), as shown in Table 2.3, $u_{\text{lift-off}}$ is about 56% of u_{max} at the blade shoulder

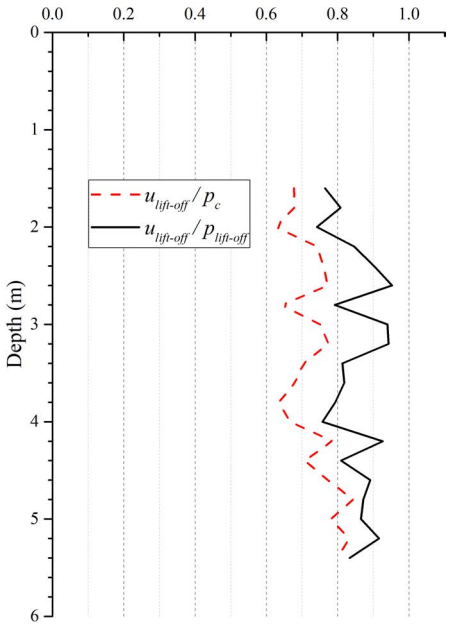

Figure 5.42: Profile of $u_{\text{lift-off}}/p_c$ and $u_{\text{lift-off}}/p_{\text{lift-off}}$ in the upper OC clay layer at Kruibeke test site

during the penetration. While Kouretzis et al. (2015) did not provide the full pore-water pressure distribution on the DMT membrane, the pore-water pressure at the closest point to the membrane center accounts for about 73% to 80% of u_{max} with varying permeabilities, as shown in Fig. 2.23. Therefore, this drop of pore-water pressure from u_{max} to $u_{\text{lift-off}}$ is likely to compensate the difference between $u_{\text{lift-off}}$ and $p_{\text{lift-off}}$ or between $u_{\text{lift-off}}$ and p_c, which allows Mayne (1987)'s postulation to be valid with the iDMT pressure p_c or $p_{\text{lift-off}}$. Note that p_c has the same conceptual root with the DMT contact pressure p_0, while $p_{\text{lift-off}}$ is, in fact, the "real" contact pressure that is measured at the instant of the piston lift-off.

5.10 Conclusion

With the hypothesis that the developed iDMT with full pressure-displacement curve and pore-water pressure measurements are able to deliver more reasonable and accurate estimation of soil parameters, the methodologies devised in this chapter include the determination of the contact pressure p_c based on the full pressure-displacement expansion curve and the study of the piston expansion stage.

Specifically, in Section 5.3, the influence of unload-reload effects during the

dilatometer penetration on the determination of p_0 in the DMT is firstly reviewed, then an analytical approach is proposed. The analytical approach programmed in MATLAB consists of determining the transitional "yield" point on the corrected loading curve and then estimating p_c using the post-yield phase of the curve via a proposed exponential-linear regression model as expressed in Eq. 5.4. Note that an adapted Casagrande method is proposed for locating the "yield" point in case that a smooth loading curve is measured.

In Section 5.4, similar to the flexible membrane expansion analysis in elasticity, an alternative semi-elliptical boundary is proposed for the rigid piston expansion in the elastic FEM analysis to prevent the broken soils (displacement jump). Given the benchmark simulation having excellent agreement with the analytical solution, Eq. 5.21 is derived for the iDMT modulus. Thus, the pressure required for a 1.1 mm central movement of the 60-mm diameter membrane results in approximate 0.56 mm and 0.85 mm displacement of a rigid piston with a diameter of 40 mm and 60 mm, respectively.

These proposed methodologies enable the estimation of the iDMT indices which can be then used with the well-established DMT correlations for common soil parameters. So, rather than establishing brand-new interpretation techniques in particular for the iDMT, the iDMT estimates the basic pressure reading of p_c, $p_{0.85}$ or $p_{0.56}$, then derives common soil parameters by inheriting the tremendous efforts made for the DMT relationships in the past four decades. Moreover, this allows a comparable situation where we can validate the use of the iDMT in many aspects by checking the results of the CPT, the DMT, and the iDMT from parallel soundings in the ground.

Therefore, an in situ testing campaign using the standard dilatometer, the instrumented dilatometer, and the cone was carried out in Belgium, as discussed in Section 5.6, 5.7,and 5.8.

The p_0 based DMT indices have proven good correlations with common soil parameters as mentioned in Chapter 2, such as the DMT horizontal stress index K_D can capture very well the stress history of clays. These well-established DMT correlations are based on the mean values of the DMT measurements and of the soil parameters, so the effects of the stress relief phenomenon, in fact, average out in the correlations.

In this testing campaign, the mean p_c values are found close to the mean p_0 values (the mean value of $p_c/p_0 \pm$ one standard deviation in three sites are 1.04 ± 0.19 in the Kruibeke test site, 1.18 ± 0.39 in the Limelette test site, and 1.01 ± 0.3 in the Zwijnaarde test site). Therefore, it is appropriate to use p_c

for evaluating the three DMT indices I_D, E_D and K_D and consequently for the DMT correlations. In terms of an individual estimation based on p_c, one can at least eliminate the effects of the stress relief phenomenon in confidence. After all, the aim is to use the correlations with less scatter as well as have a better understanding of the factors underlying the correlations.

In terms of using the iDMT $p_{0.85}$ or $p_{0.56}$ pressures for the DMT p_1 pressure, although the average values are close in this testing campaign, uncertainties exist for the difference in mechanics between the rigid piston expansion and the flexible expansion. Generally, the iDMT $p_{0.85}$ or $p_{0.56}$ pressures are not intended to replace p_1, but rather intended to allow a simple comparison between the two in the first stage of the iDMT research.

Then, a comparison is made between the measured iDMT indices, the measured DMT indices, and the CPT predicted DMT indices, which shows reasonable agreements in common soils including sands, sand mixtures, silt mixtures, overconsolidated clays, and heavily overconsolidated Boom clays. The common soil parameters such as K_0, OCR, C_u, $\phi^{'}$, and M_{DMT} can be successfully interpreted from the iDMT results with an accuracy at least as good as the DMT and the CPT.

Chapter 6

Conclusion and future work

6.1 Conclusion of the present work

The objective of the work described in this thesis is to present design, use, and interpretation of an instrumented dilatometer test (iDMT). Starting from reviewing the flat dilatometer test (DMT) and the prior modified dilatometer tests in both practical and theoretical aspects, Chapter 2 gives insights into problems such as the possible non-linear pressure-displacement measurements and the influence of stress relief phenomenon. Then in Chapter 3, a proof-of-concept study on the development and use of the iDMT prototype in the laboratory is presented. This preliminary work paves the way for standardizing the iDMT device and the iDMT test procedure to carry out in situ test in different soils in Chapter 4. With the newly developed iDMT and the test procedure, an in situ testing campaign in Belgium was carried out. To analyse the data from this testing campaign as well as from the literature, analytical and numerical approaches are proposed with the consideration of the problems identified in the review. Therefore, Chapter 5 presents the combination of the methodology, the in situ tests, and the analysis and comparison of the test results.

A thorough review of the DMT in Chapter 2 not only underpins the iDMT interpretation but also reveals that the interpretation of the DMT in common soils (sands, silts, and clays) relies heavily on the value of p_0, since the p_0 pressure is essential for identifying the DMT indices K_D, I_D, E_D and thus of paramount importance in deriving common soil parameters based on these three DMT indices. Nevertheless, the determination of p_0 fairly relies on the assumption of the linear pressure-displacement relationship. Though this assumption cannot be checked by the DMT itself, a data analysis on 19 pressure-

displacement curves from the prior modified dilatometers is provided. The analysis based on linear regression indicates that residuals of all curves don't have the required randomness to support a linear model, albeit the pressure-displacement curves generally show good R^2 values. Rather than randomly dispersed data, a pattern of inverted-U shape is commonly found, suggesting that a non-linear regression model would provide a better fit. Furthermore, a stress relief phenomenon during the DMT installation stage is discovered by reviewing two numerical simulations in saturated cohesive soils with different methods, i.e., the strain path method and the finite element method. This stress relief mainly involves a decline in the horizontal stress of the soil cylinder next to the membrane/piston when the dilatometer shoulder (the geometrically transitional point) has been passed during the penetration. Note that the p_0 pressure is inherently related to the in situ horizontal stress and therefore also related to this stress relief process. And the stress relief can in turn result in an initial reloading phase at the membrane/piston expansion stage, which is possible to invalidate the linear pressure-displacement assumption. These findings together with the review of the DMT and the modified DMT equipment opens the way for the development of the iDMT that is introduced in Chapter 3 and Chapter 4.

The use of proof-of-concept iDMT prototypes in pilot laboratory test can bridge the gap effectively between how the iDMT device is envisioned during design iterations and how it is ultimately used in the in situ tests. The prototype was fabricated in alumide using the 3D printing technique with a laser sintering process. The design uses a rigid piston instead of the flexible membrane, thus allows a larger displacement up to 2.48 mm. The use of a computer control and DAQ system based on LabVIEW permits continuous pressure-displacement measurements. Nevertheless, it is found difficult to implement an ideal displacement-controlled procedure with the current system due to the insufficient accuracy. Calibrations and calibration chamber tests in a loose sand are performed, which indicates that the iDMT prototype has the potential to evaluate non-linear soil behaviors and, on the other hand, the 3D printing technique and the LabVIEW control & DAQ system are proven feasible for device development and testing in soils.

Based on the experience gained in iterative design through prototyping, the iDMT for in situ testing in common soils, such as sands, clays, silts or mixtures, is developed. This final prototype uses a 60-mm rigid piston with a displacement up to 2.5 mm and allows the pore-water pressure measurements at the

piston centre. In terms of the fabrication, a hybrid of manufacturing technologies is used: the main blade body and the rigid piston are metal 3D printed in 420 stainless steel infiltrated with bronze; the blade tip and the rod-blade connector are machined; then the parts are welded. This hybrid method is de facto a compromise between the traditional machining process and the metal 3D printing technique, which not only enables the fabrication of the iDMT probe that is too complex for the traditional machining but also fortifies the parts such as the threads and the blade tip which are less robust in case of fabricating with the 3D printing techniques. The key to success of this hybrid method is the TIG welding process that layer-by-layer deposits the $CuSi_3$ filler to bond two distinct parts together. This methodology for developing the geotechnical testing device is not already in the literature and therefore may inspire engineers to make other potential innovative improvements. The additional merit of this development approach is that the metal 3D printing and the LabVIEW-based instrumentation enable the device and the system easily reproducible, in contrast to some prior esoteric designs presenting difficulties to reproduce with the only help of documents.

Furthermore, the test procedure for the iDMT tests is established for carrying out in situ soil investigation. It is worth noting that a pseudo displacement-controlled algorithm is devised to allow the pressurized piston moving with a velocity always in a pre-determined range that is converted from the time limits of the DMT tests. This way a comparison with the DMT test results is guaranteed. Together with the non-linear soil response along with pore-water pressure measurements, a deeper insight into soil response is permitted by the iDMT, which provides a potential opportunity to improve the interpretation of soil properties.

With the successful use of the iDMT in the field, the main approach adopted to compare the test results is an in situ testing campaign consisting of the iDMT test, the DMT test, and the CPT tests performed at adjacent locations at three sites in Belgium. In the light of tremendous efforts on the DMT correlations with common soil parameters by a great number of researchers, the iDMT interpretation aims to use these well-established formulas at the current research stage. This requires the determination of equivalent p_0 and p_1 in the iDMT, which, in turn, provides an opportunity to improve the accuracy of the equivalent pressures in the iDMT.

First, an analytical approach programmed in MATLAB to estimate the iDMT contact pressure p_c is proposed. The main procedure involves the determina-

tion of the transitional "yield" point and then the estimation of p_c based on the post-yield phase of the loading curve. This approach can cope with almost all the iDMT pressure-displacement curves regardless of degrees of the non-linearity and the initial stiff reloading phase. Generally, p_c gives slightly larger values than p_0, with statistical analyzes indicates the mean value (and $\pm$ one standard deviation) of $p_c/p_0 = 1.01 \pm 0.3, 1.18 \pm 0.39, 1.04 \pm 0.19$ for Zwijnaarde test site, Limelette test site, Kruibeke test site, respectively.

Then an investigation on the piston expansion stage using the FEM is conducted. With an alternative semi-elliptical displacement boundary, the pressure required for a 1.1 mm central movement of the membrane results in approximate 0.56 mm and 0.85 mm displacement of a piston with a diameter of 40 mm and 60 mm, respectively. Thus, $p_{0.85}$ and $p_{0.56}$ are considered as equivalent p_1 in the DMT, with statistical analyses indicates the mean value (and $\pm$ one standard deviation) of $p_{0.56}/p_1 = 1.18 \pm 0.3$ for Zwijnaarde test site, and $p_{0.85}/p_1 = 1.08 \pm 0.2, 1.01 \pm 0.24$ for Limelette test site, Kruibeke test site, respectively.

Together with p_c, the iDMT indices can be derived for estimating soil parameters. Then, a comparison is made between the measured iDMT indices, the measured DMT indices, and the CPT predicted DMT indices, showing reasonable agreements in common soils including sands, sand mixtures, silt mixtures, overconsolidated clays, and heavily overconsolidated Boom clays. The common soil parameters such as K_0, OCR, C_u, $\phi^{'}$, and M_{DMT} can be successfully interpreted from the iDMT results with an accuracy at least as good as the DMT and the CPT.

6.2 Recommendations for further work

Rather than a research dilatometer just built for a better understanding of the standard DMT, the design, development, and use of the iDMT open the way in many directions. This regards to five points given below for future research.

Field measurements versus laboratory investigations

One of the most important questions to be answered is that how accurate is the estimation of soil parameters from the iDMT. Albeit the comparison with the DMT and the CPT shows good agreements, there is always a need to find the baseline from laboratory tests on undisturbed samples. Acquiring undisturbed

samples, especially in clean sands, requires using special field drilling means such as freezing techniques or thin tube samplers. Despite that the cost of these investigations is high, triaxial testing and oedometer testing can accurately measure the common soil parameters such as OCR, C_u, $\phi^{'}$, and M_{DMT} under controlled and well-defined boundaries. With the laboratory results on the soil parameters and the iDMT performed at the same site, a comparison can be made; the relationships can be refined; faith can be gained in using the parameters determined by the iDMT for geotechnical designs.

Additions to the iDMT system

The present iDMT system comprises a sub-system of the truck-based penetrometer and the other sub-system of control & DAQ instruments. Integration of the two systems can sync the pore-water pressure measurements with the penetration depth for an additional pore-water pressure profile produced from the iDMT as well as remove the need to record the test depth manually.

Furthermore, it is of interest to combine the instrumented dilatometer with the seismic module in the SDMT. The seismic module measures the shear wave velocity (V_S) and therefore a small strain shear stiffness of the soil ($G_0 = \rho V_S^2$), where ρ = the density of soil. In principle, the iDMT non-linear pressure-displacement curves together with the G_0 modulus shall be helpful to construct the in situ $G - \gamma$ curves.

The iDMT system allows not only the implementation of the standard DMT test procedure but also the new test procedure. The study of the dynamic behaviors of soils can be of particular interests since the rigid piston in the iDMT can apply cyclic loading on the soil. This can be used to investigate a broad of geotechnical applications such as strain accumulation phenomenon and deep foundations subjected to lateral cyclic loading (e.g., offshore piles under wave loading).

The piston expansion models

In this thesis, the piston expansion process is investigated for the sake of interpreting the iDMT measurements in a way comparable to the DMT interpretation, which allows an extended use of the DMT correlations developed by many researchers over the past several decades. However, it is important to understand the presented calculation in Section 5.4 is by no means an accurate simulation of the piston expansion process. The proposed alternative elliptical

displacement boundary has the advantage of using the FEM calculation tool as part of a data-reduction process by easing the discontinuity with a gradual transition of the displacement, while it is only an approximation with limited accuracy if it is considered as a simulation. This is not only because of the approximate assumption of the same elastic reaction, when the cavity volume resulting from the elliptical boundary and the ideal boundary is identical, but also the lack of a precise simulation of the blade penetration process.

To precisely simulate the piston expansion process, one must first complete the simulation of the blade penetration process, since the blade penetration precedes the piston expansion and has a larger deformation to the soils. Finno (1993), Kouretzis et al. (2015), and Yu et al. (1993) presented different viable models for the simulation of the DMT blade penetration, though Yu et al. (1993) used a 2D FEM model that ignores the wedge cavity expansion effects described in Section 2.4.2. The consideration of the modeling approach also depends on the situations in different types of soils.

In case of saturated cohesive soils with a relatively high-water content, such as soft clay and mud, a continued investigation based on Finno (1993) is reasonable. During the rigid piston expansion, the soils are assumed to follow a definite deformation path independent of soil resistance. If inertial effects are ignored, the rigid piston expansion process is reduced to a flow problem, where soil particles move along streamlines around a fixed rigid body.

If the soil still responds as a continuous mass of elastic solid, a separation between the metal blade and the soils may happen with a small void directly adjacent to the piston. But it is necessary to reasonably determine the size of the void and discuss its possible influence on the results. Nevertheless, rather than a void, soil failure may occur near the piston edge if the soils are elasto-plastic.

In dry soils, stiff clays or other ground materials in the ground, soil cracking may occur with the development of a fracture or even multiple fractures. Fractures may be initiated at the piston edge and even propagated during the piston expansion. This requires the use of linear elastic fracture mechanics or elasto-plastic fracture mechanics, which can be investigated by means of an extended finite element method (XFEM). Nevertheless, it is necessary to determine the threshold of crack initiation, and how tough the soils can respond to the cracks.

Pore-water pressure measurements

Apart from the pore-water pressure measured at the instant of the piston lift-off $u_{\text{lift-off}}$, the present iDMT pore-water pressure measurements in saturated clays generally represent a mixed soil response from the two stages of the iDMT test: the blade penetration and the piston expansion. This is because the iDMT test procedure is configured as similar as possible to the standard DMT test procedure to allow comparable situations in the first research stage with a main purpose of validation. Note that the standard DMT procedure requires an immediate pressurization following the halt of the blade penetration at the test depth, so dissipation of the excess pore-water pressure generated during the penetration in saturated clays is by no means fast enough before the membrane expansion. Nevertheless, in a further step of the iDMT research, it is highly recommended to depart from the standard DMT procedure, which allows the main research points as follows:

- The rigid piston expansion occurs after a complete dissipation of the excess pore-water pressure generated during the blade penetration. This allows a direct measure of the pore-water pressure development induced by the piston expansion rather than a coupled reaction. Furthermore, the pore-water pressure measurements during this complete dissipation also allow an assessment of flow characteristic of the soil such as horizontal coefficient of consolidation c_h and coefficient of permeability k_h.
- In case the present iDMT system is integrated into the penetrometer system, it is possible to have pore-water pressure measurements and the penetration depth readings at the same time during the blade penetration process. Then, an additional penetration pore-water pressure profile can be created, which is similar to the pore-water pressure parameter ratio B_q in the piezocone penetration test (CPTu). Likewise, it is possible to construct an iDMT pore-water pressure index to have a better interpretation in saturated clays.

Rate effects

The possible rate effects on the iDMT test can be categorized into two situations: the iDMT test results are influenced by the partial drainage conditions in intermediate permeability soils, such as silts; and the non-negligible dynamic effect.

With the pore-water pressure measurements, it is possible to readily identify the intermediate permeability soils when the dissipation of excess pore-water pressure has considerable influence on the measured soil response during the course of the piston expansion. Albeit it can be erroneous to use the standard DMT methods for these soils, it provides an opportunity to develop new interpretation techniques specifically for this situation.

At the current research stage, the pressurization (loading) rate of the iDMT piston expansion is set in accordance with that of the DMT by considering a cavity-volume equivalence. Since the DMT membrane expansion is normally assumed as a static loading process, the dynamic and rate effects of the iDMT piston expansion are assumed negligible. However, this may be incorrect as soil creep is sometimes observed in the in situ tests. Therefore, a further study of the pressurization rates on the iDMT test results is of particular interests, which also opens the way of investigating the soils under vibration using the iDMT.

Appendix A

LabVIEW program

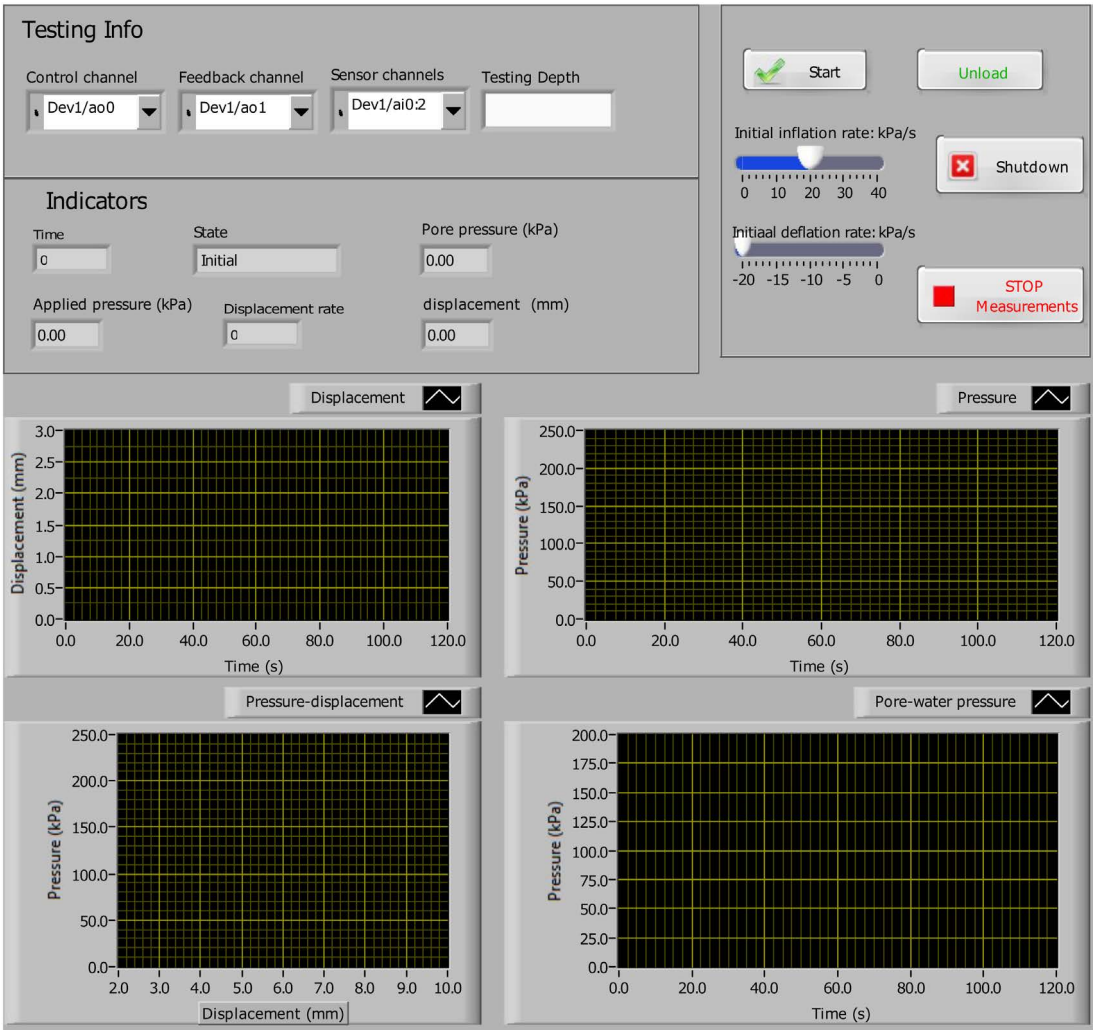

Figure A.1: Front panel of the LabVIEW program

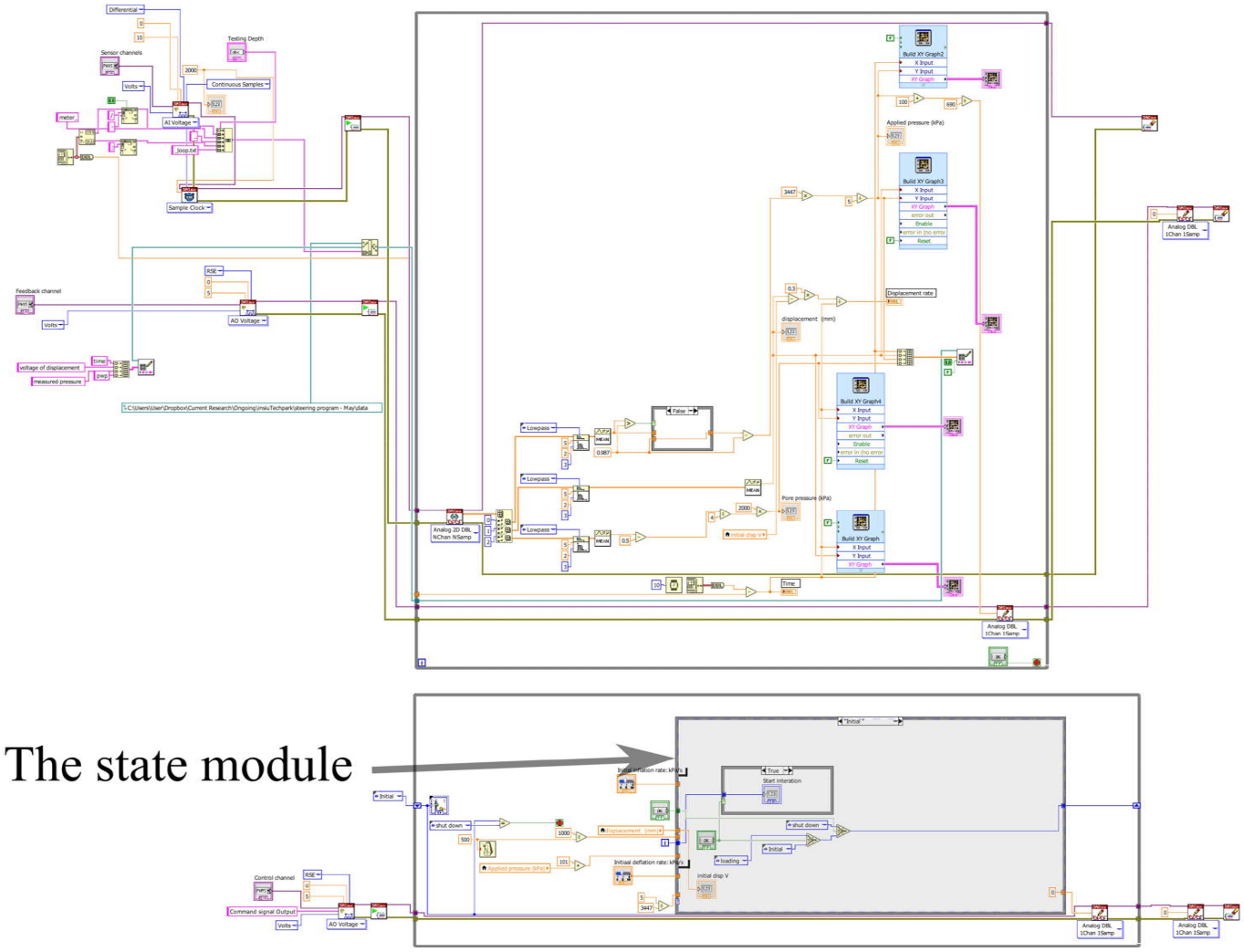

Figure A.2: The block diagram of the LabVIEW program for general purpose (The state module can be easily adjusted based on the specific needs)

(a) loading state

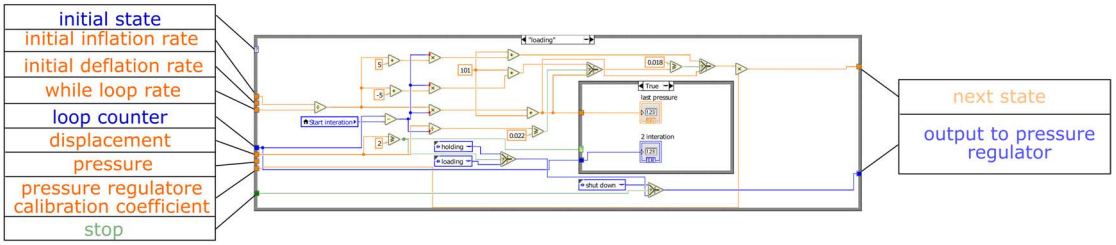

(b) pressure hold state

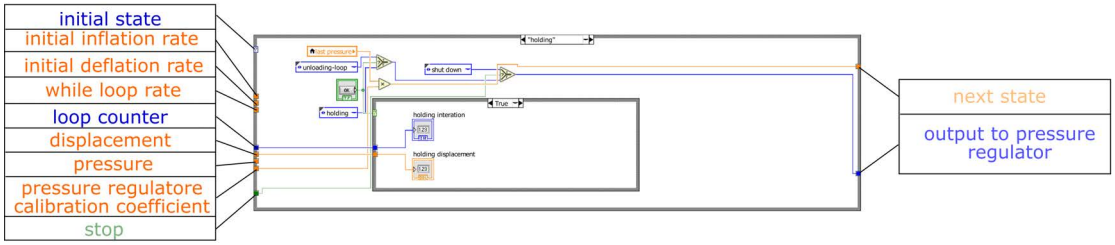

(c) unloading state

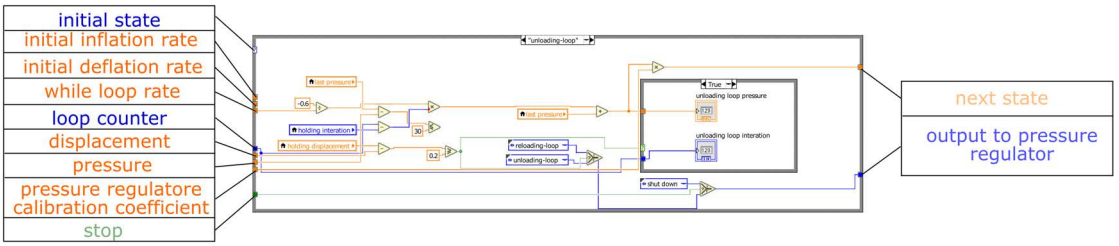

(d) reloading state

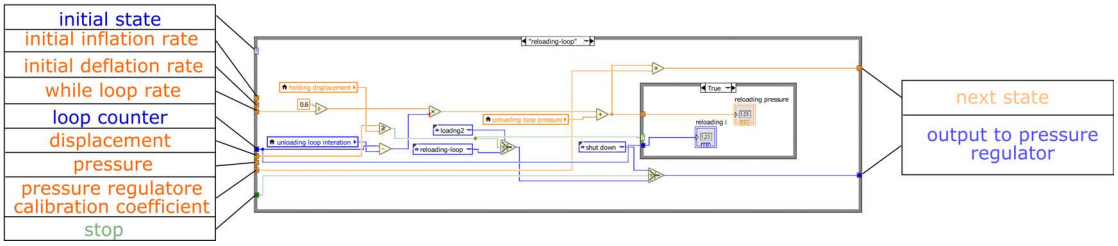

Figure A.3: Examples of the states: (a) loading state, (b) pressure hold state and (c) unloading state (d) reloading state (annotated snippets)

Appendix B

MATLAB codes for p_c estimation

```
importfile; % import the iDMT raw data
d=VarName1; % Define the first variable as the piston displacemnet
p=VarName2; % Define the second variable as the applied pressure

%First step: obtain the contact pressure using the DMT method, B ...
   = the pressure at 1.1 mm or the maximum displacement; and A is ...
   the pressure at the displacement of 0.05 mm (or the nearest ...
   point). This step is useful when the modified DMT employes a ...
   flexibel membrane, otherwise, it can be skipped.
B=p(end);
for i=1:(length(d)-1)
if d(i)==0.05
A=p(i);
break;
elseif (d(i)-0.05)*(d(i+1)-0.05) < 0
A= p(i)+(p(i+1)-p(i))*(0.05-d(i))/(d(i+1)-d(i));
break;
end
end
p0_Marchetti = A +(B-A)*(0-0.05)*(d(end)-0.05)
% Obtain r squared of the Marchetti method
SStot=0;
SSres=0;
for j=(i+1):length(p)
SStot=SStot+(p(j)-mean(p)).^2;
SSres=SSres+((A +(B-A)*(d(j)-0.05)*(d(end)-0.05))-p(j)).^2;
end
R_squared = 1-SSres./SStot
```

```
%Second step: the estimation of p_c
% 1. Select the data points
% 2. Power fit
% 3. Get the max. curvature point
% 4. Get bisector line
% 5. Linear regression
% 6. Estimation of p_c

% 1. Select the data points
%If ommiting the data points of the unload-reload loop is required
% for i=1:length(p)
%     if p(i+1)<p(i)
%         break;
%     end
% end
% da_all=d(1:i);
% pa_all=p(1:i);
% da=da_all(da_all>0);
% pa=pa_all(da_all>0);
% lg_pa=log10(pa);
lg_pa=log10(p);
da = d;

% 2. Power fit
[fitresult, gof] = createFit(da, lg_pa)

%power2 fit x=da y=lg_pa

% 3. Get the max. curvature point
syms xx yy dy ddy;
aa=coeffvalues(fitresult);
yy=aa(1).*xx.^aa(2)+aa(3);
dy=diff(yy,xx);
ddy=diff(dy,xx);
K=abs(ddy)/(1+dy.^2).^1.5;
xk=[min(da):0.01:max(da)];
ss=eval(subs(K,xx,xk));
max_curvature=max(ss)
figure;
plot(xk,ss);
xlabel('displacement');
ylabel('curvature');
disp=xk(ss==max(ss));
pre=(aa(1).*disp.^aa(2)+aa(3));
```

```
max_curvature_point=[pre disp]
x=linspace(min(da),max(da));
y=eval(subs(yy,xx,x));

% 4. Get bisector line
% tangent line
% yt=at*(xt-bt)+ct;
kt=1./eval(subs(dy,xx,disp));
kb=tan(0.5*atan(kt));

% 5. Linear regression
d_last=d(d>0.8);
lg_p_last=real(log10(p(d>0.8)));
linear_fit = polyfit(lg_p_last,d_last,1);
syms xp
eqn = kb.*(xp-pre)+disp-(linear_fit(1).*xp+linear_fit(2))==0;
lg_p_y=eval(solve(eqn,xp));
p_y=10.^lg_p_y
d_y=linear_fit(1).*lg_p_y+linear_fit(2)
figure;
semilogy(x,10.^y,'linewidth',2);
xlabel('Displacement(mm)')
ylabel('Pressure(kPa)')
axis([-0.2 2.5 10 4000]);
hold on
lg_p=real(log10(p));
semilogy(d,10.^lg_p,'o');
semilogy(disp,10.^pre,'^k','markersize',10);
xb=linspace(pre,max(lg_p)+0.01);
xl=linspace(pre+0.08,max(lg_p)+0.005);
yb=kb*(xb-pre)+disp;
yl=polyval(linear_fit,xl);
semilogy(yb,10.^xb,'linewidth',2);
semilogy(yl,10.^xl,'linewidth',2);
semilogy(d_y,10.^lg_p_y,'*','MarkerSize',10)
legend('Power Fit','Measurements','Maximum Curvature ...
    Point','Bisector Line','Linear ...
    Regression','Intersection','location','west');
hold off;
% 6. Estimation of p_c
% Fitting of post-yield curve
d_py=d(d>d_y);
p_py=lg_p(d>d_y);
%If ommiting the data points of the unload-reload loop is required
```

```
% for i=1:length(p_py)
%     if p_py(i+1)<p_py(i)
%         break;
%     end
% end
% p_py1=p_py(1:i);
% p_py2=p_py(p_py>p_py(i));
% p_py_sum=cat(1,p_py1, p_py2);
% d_py1=d_py(1:i);
% d_py2=d_py(p_py>p_py(i));
% d_py_sum=cat(1,d_py1, d_py2);
% [fitresult1, gof] = Exp_linear(d_py_sum,p_py_sum)
% coeff=coeffvalues(fitresult1);
% p0_new=coeff(1)+coeff(4)
% [d_py,p_py]=Exp_linear(x,y,2)
[fitresult1, gof] = Exp_linear(d_py,p_py) ;
p_c=10.^feval(fitresult1,0)
```

Appendix C

Abaqus Input Codes on the piston expansion analysis

Considering the large number of nodes (1500) and elements (703), detailed node and element information is omitted for readability of the document.

```
*Heading
** Job name: iDMT2 Model name: Model-1
** Generated by: Abaqus/CAE 6.13-3
*Preprint, echo=NO, model=NO, history=NO, contact=NO
**
** PARTS
**
*Part, name=Ground
*Node
1,         300.,           0.
.....................................
1500,   200.755127,   151.777649
*Element, type=CAX6
1,   94,   71,   70,  400,  401,  402
.....................................
703,  399,  382,  389, 1500, 1486, 1489
*Nset, nset=soil, generate
1,  1500,     1
*Elset, elset=soil, generate
1,  703,    1
** Section: ground
*Solid Section, elset=soil, material=Material-1
,
*End Part
```

```
**
**
** ASSEMBLY
**
*Assembly, name=Assembly
**
*Instance, name=Ground, part=Ground
*End Instance
**
*Nset, nset=loading, instance=Ground
4,   5,  37,  38,  39,  40,  41,  42,  43,  44,  45,  46,  47,  ...
   48,  49,  50
51,  52,  53,  54,  55,  56,  57,  58,  59,  60,  61,  62,  63,  ...
   64,  65,  66
67,  68,  69,  70,  71, 401, 498, 596, 656, 659, 662, 666, 668, ...
   670, 673, 674
677, 681, 685, 689, 693, 697, 701, 705, 709, 713, 717, 725, 729, ...
   733, 737, 743
751, 755, 759, 763, 767, 771, 774, 778, 782
*Elset, elset=loading, instance=Ground
1,  35,  68,  91,  93,  95,  97,  99, 101, 103, 104, 106, 108, ...
   110, 112, 114
116, 118, 120, 122, 124, 126, 130, 132, 134, 136, 138, 142, 144, ...
   146, 148, 150
152, 154, 156, 158
*Nset, nset=_PickedSet4, internal, instance=Ground
2,    5,   72,   73,   74,   75,   76,   77,   78,   79,   80,   ...
   81,   82,   83,   84,   85
86,   87,   88,   89,   90,   91,   92,   93,  499,  597,  606,  ...
   625,  627,  631,  789,  827
834,  844,  850,  858,  946,  951, 1021, 1035, 1047, 1153, 1156, ...
   1209, 1379, 1382, 1407
*Elset, elset=_PickedSet4, internal, instance=Ground
35,  69,  72,  79,  80,  82, 161, 182, 186, 190, 192, 197, 275, ...
   282, 331, 341
348, 417, 418, 455, 610, 611, 626
*Nset, nset=_PickedSet5, internal, instance=Ground
3,    4,   16,   17,   18,   19,   20,   21,   22,   23,   24,   ...
   25,   26,   27,   28,   29
30,   31,   32,   33,   34,   35,   36,  424,  427,  442,  445,  ...
   447,  450,  453,  456,  459
462,  465,  468,  471,  474,  477,  480,  856,  862,  870, 1392, ...
   1406, 1449
*Elset, elset=_PickedSet5, internal, instance=Ground
```

```
9,  10,  15,  16,  17,  18,  19,  20,  21,  22,  23,  24,  25,  ...
   26,  27,  28
195, 199, 203, 616, 625, 652
*Nset, nset=_PickedSet6, internal, instance=Ground
1,    3,   11,   12,   13,   14,   15,  410,  423,  433,  436, ...
   1427, 1429
*Elset, elset=_PickedSet6, internal, instance=Ground
4,   9,  12,  13, 637, 638
*Nset, nset=_PickedSet7, internal, instance=Ground
1,    2,    6,    7,    8,    9,   10,  409,  598, 1414, 1418, ...
   1421, 1436
*Elset, elset=_PickedSet7, internal, instance=Ground
4,  69, 630, 632, 634, 641
*Elset, elset=__PickedSurf8_S2, internal, instance=Ground
1,  68,  91,  93,  95,  97,  99, 101, 103, 104, 106, 108, 110, ...
   112, 114, 116
118, 120, 122, 124, 126, 130, 132, 134, 136, 138, 142, 144, 146, ...
   148, 150, 152
154, 156, 158
*Elset, elset=__PickedSurf8_S1, internal, instance=Ground
35,
*Surface, type=ELEMENT, name=_PickedSurf8, internal
__PickedSurf8_S2, S2
__PickedSurf8_S1, S1
*End Assembly
**
** MATERIALS
**
*Material, name=Ground
*Elastic
5., 0.3
**
** BOUNDARY CONDITIONS
**
** Name: bottom Type: Displacement/Rotation
*Boundary
_PickedSet7, 1, 1
_PickedSet7, 2, 2
_PickedSet7, 6, 6
** Name: right Type: Displacement/Rotation
*Boundary
_PickedSet6, 1, 1
_PickedSet6, 2, 2
_PickedSet6, 6, 6
```

```
** Name: sym Type: Symmetry/Antisymmetry/Encastre
*Boundary
_PickedSet4, XSYMM
** Name: top_restrained Type: Displacement/Rotation
*Boundary
_PickedSet5, 2, 2
** ----------------------------------------------------------------
**
** STEP: Step-1
**
*Step, name=Step-1, nlgeom=NO, inc=1
*Static, direct
1., 1.,
**
** BOUNDARY CONDITIONS
**
** Name: loading Type: Displacement/Rotation Using Analytical ...
   Field: AnalyticalField-1
*Boundary
Ground.4, 2, 2
Ground.5, 2, 2, -1.65
Ground.37, 2, 2, -1.64907
Ground.38, 2, 2, -1.64632
Ground.39, 2, 2, -1.64179
Ground.40, 2, 2, -1.63554
Ground.41, 2, 2, -1.6276
Ground.42, 2, 2, -1.61801
Ground.43, 2, 2, -1.60679
Ground.44, 2, 2, -1.59397
Ground.45, 2, 2, -1.57955
Ground.46, 2, 2, -1.56355
Ground.47, 2, 2, -1.54598
Ground.48, 2, 2, -1.52682
Ground.49, 2, 2, -1.50607
Ground.50, 2, 2, -1.48372
Ground.51, 2, 2, -1.45973
Ground.52, 2, 2, -1.43408
Ground.53, 2, 2, -1.40673
Ground.54, 2, 2, -1.37762
Ground.55, 2, 2, -1.34669
Ground.56, 2, 2, -1.31386
Ground.57, 2, 2, -1.27902
Ground.58, 2, 2, -1.24207
Ground.59, 2, 2, -1.20285
```

```
Ground.60, 2, 2, -1.16118
Ground.61, 2, 2, -1.11684
Ground.62, 2, 2, -1.06955
Ground.63, 2, 2, -1.01895
Ground.64, 2, 2, -0.964561
Ground.65, 2, 2, -0.905768
Ground.66, 2, 2, -0.841703
Ground.67, 2, 2, -0.771111
Ground.68, 2, 2, -0.692067
Ground.69, 2, 2, -0.601317
Ground.70, 2, 2, -0.492519
Ground.71, 2, 2, -0.349315
Ground.401, 2, 2, -0.427383
Ground.498, 2, 2, -1.64977
Ground.596, 2, 2, -0.24771
Ground.656, 2, 2, -0.54995
Ground.659, 2, 2, -0.64857
Ground.662, 2, 2, -0.732917
Ground.666, 2, 2, -0.807422
Ground.668, 2, 2, -0.874551
Ground.670, 2, 2, -0.935845
Ground.673, 2, 2, -0.992338
Ground.674, 2, 2, -1.04476
Ground.677, 2, 2, -1.09365
Ground.681, 2, 2, -1.13942
Ground.685, 2, 2, -1.18239
Ground.689, 2, 2, -1.22281
Ground.693, 2, 2, -1.26087
Ground.697, 2, 2, -1.29675
Ground.701, 2, 2, -1.33056
Ground.705, 2, 2, -1.36243
Ground.709, 2, 2, -1.39244
Ground.713, 2, 2, -1.42066
Ground.717, 2, 2, -1.44715
Ground.725, 2, 2, -1.47196
Ground.729, 2, 2, -1.49513
Ground.733, 2, 2, -1.51667
Ground.737, 2, 2, -1.53662
Ground.743, 2, 2, -1.55499
Ground.751, 2, 2, -1.57177
Ground.755, 2, 2, -1.58698
Ground.759, 2, 2, -1.6006
Ground.763, 2, 2, -1.61262
Ground.767, 2, 2, -1.62303
```

```
Ground.771, 2, 2, -1.63179
Ground.774, 2, 2, -1.63889
Ground.778, 2, 2, -1.64428
Ground.782, 2, 2, -1.64792
**
** OUTPUT REQUESTS
**
*Restart, write, frequency=0
**
** FIELD OUTPUT: F-Output-1
**
*Output, field, variable=PRESELECT
**
** HISTORY OUTPUT: H-Output-2
**
*Output, history
*Node Output, nset=loading
RF2,
*End Step
```

Reference

Akbar, A and B G Clarke (2001). "A flat dilatometer to operate in glacial tills". In: *Geotechnical Testing Journal* 24.1, pp. 51–60.

Akbar, A, S Kibria, B G Clarke, and Millpress (2005). "The Newcastle Dilatorneter testing in Lahore cohesive soils". In: *Proceedings of the 16th International Conference on Soil Mechanics and Geotechnical Engineering*. Rotterdam, pp. 651–654.

Akbar, A, H Nawaz, and B. G. Clarke (2006). "The Newcastle Dilatometer Testing in Pakistani Sandy Subsoils". In: *Proceedings from the Second International Flat Dilatometer Conference*. Washington, D.C., pp. 254–260.

ASTM D5778-95 (2000). *Performing Electronic Friction Cone and Piezocone Penetration Testing of Soils*. West Conshohocken, PA: ASTM International.

ASTM Standard D6635-15 (2015). *Standard Test Method for performing the Flat Plate Dilatometer*. West Conshohocken, PA: ASTM International.

ASTM Standard F2792-12a (2012). *Standard Terminology for Additive Manufacturing Technologies*. West Conshohocken, PA: ASTM International.

Atkinson, J (2007). *The mechanics of soils and foundations*. Second Edi. London: Taylor & Francis.

Atkinson, J. H. (2000). "Non-linear soil stiffness in routine design". In: *Géotechnique* 50.5, pp. 487–508.

Aziz, M. and A. Akbar (2017). "Interrelationships of Flat Rigid Dilatometer Parameters With Unconfined Compression Test Results Interrelationships of Flat Rigid Dilatometer". In: *Geotech. Test. J* 40.2, pp. 258–268.

Bałachowski, Lech and Norbert Kurek (2015). "Vibroflotation Control of Sandy Soils using DMT and CPTU". In: *The 3rd International Conference on the Flat Dilatometer*. Rome, pp. 185–190.

Baldi, G., R. Bellotti, V. Ghionna, M. Jamiolkowski, S. Marchetti, and E. Pasqualini (1986). "Flat Dilatometer Tests in Calibration Chambers". In: *ASCE Specialty Conference on "Use of In Situ Tests in Geotechnical Engineering"*. Blacksburg, p. 431.

Baligh, Mohsen M. (1985). "Strain Path Method". In: *Journal of Geotechnical Engineering* 111.9, pp. 1108–1136.

Barentsen, P. (1936). "Short description of field testing method with cone shaped sounding apparatus". In: *Proceedings 1st International Conference on Soil Mechanics and Foundation Engineering*. Cambridge, Mass., B/3: 6–10.

Barnatt, Christopher (2014). *3D Printing: Second Edition*. CreateSpace Independent Publishing Platform.

Barry, Mark A, Bruce D Johnson, and Bernard P Boudreau (2012). "A new instrument for high-resolution in situ assessment of Young's modulus in shallow cohesive sediments". In: *Geo-Marine Letters* 32.4, pp. 349–357.

Bellotti, Roberto, Jean Benoît, Carmelo Fretti, and Michele Jamiolkowski (1997). "Stiffness of Toyoura sand from dilatometer tests". In: *Journal of geotechnical and geoenvironmental engineering* 123.9, pp. 836–846.

Benoit, J and K P Stetson (2003). "Use of an instrumented flat dilatometer in soft varved clay". In: *Journal of geotechnical and geoenvironmental engineering* 129.12, pp. 1159–1167.

Boussinesq, J. (1885). *Applications des potentiels à l'étude de l'équilibre et mouvement des solides elastiques*. Paris: Gauthier–Villard.

Bullock, Paul J (2016). "Driven Pile Setup Testing and the Dilatometer". In: *The 3rd International Conference on the Flat Dilatometer*. Rome, pp. 73–74.

Burghignoli, A., L. Cavalera, V. Chieppa, M. Jamiolkowski, C. Mancuso, S. Marchetti, V. Pane, P. Paoliani, F. Silvestri, F. Vinale, and E. Vittori (1991). "Geotechnical characterization of Fucino clay". In: *Proc. X ECSMFE*. Florence, pp. 27–40.

Campanella, R G and P K Robertson (1991). "Use and interpretation of a research dilatometer". In: *Canadian Geotechnical Journal* 28.1, pp. 113–126.

Campanella, Richard G., D. Gillespie, and Peter K. Robertson (1982). "Pore pressures during cone penetration testing". In: *Proceedings 2nd Eurpean Symposium Penetration Testing, ESPOPT-II*. Amsterdam, pp. 507–512.

Casagrande, A (1936). "The determination of the pre-consolidation load and its practical significance". In: *Proceedings of the 1st International Conference on Soil Mechanics and Foundation Engineering*. Vol. 3. Harvard, pp. 60–64.

Chang, M. F. (1991). "Interpretation of overconsolidation ratio from in situ tests in Recent clay deposits in Singapore and Malaysia". In: *Canadian Geotechnical Journal* 28.2, pp. 210–225.

Clayton, C. R. I., N. E. Simons, and M. C. Matthews (1982). *Site investigation*. Halsted Press.

Colcott, R and B. M. Lehane (2012). "The design, development and application of a new DMT". In: *Geotechnical and Geophysical Site Characterization 4*. Pernambuco, pp. 565–570.

Cox, Crystal and Paul Mayne (2015). "Soil stiffness constitutive model parameters for geotechnical problems: A dilatometer testing approach". In: *Proceedings DMT'15*. Rome, pp. 393–400.

Deepthi De Silva, Udakara (2000). "Experimental study of a modified flat dilatometer under plane strain condition". Ph.D. Thesis. The University of Hong Kong.

Durgunoglu, H.T. and J.K. Mitchell (1975). "Static penetration resistance of soils: I - analysis; II - evaluation". In: *ASCE Specialty Conference on In-Situ Measurement of Soil Properties*. Raleigh, North Carolina: ASCE, pp. 151–189.

Emad, Sharif (2015). "Early Applications of DMT in Dubai in Two Main Projects for Natural and Artificial Earthfill Silty Sand". In: *The 3rd International Conference on the Flat Dilatometer*. Rome, pp. 135–144.

EOS (2012). *Alumide Data sheet*.

Eurocode7 (1997). "Section 9: Flat dilatometer test (DMT)". In: *Geotechnical design - Part 3: Design assisted by field testing*. ENV 1997-3, pp. 66–73.

ExOne (2014). *Data sheet of 420 Stainless Steel Infiltrated with Bronze*.

Failmezger, R. (2015). "Redesign of shallow foundations using dilatometer tests: more case studies after DMT'06 conference". In: *The 3rd International Conference on the Flat Dilatometer*. Rome, pp. 83–92.

Finno, R J (1993). "Analytical interpretation of dilatometer penetration through saturated cohesive soils". In: *Geotechnique* 43.2, pp. 241–254.

Fretti, C, D. LO Presti, and R Salgado (1992). "The research dilatometer: in situ and calibration chamber test results". In: *Riv. Italiana di Geotecnica* 26.4, pp. 237–242.

Gravesen, S (1960). *Elastic semi-infinite medium bounded by a rigid wall with a circular hole*. Tech. rep. Copenhagen: Meddelelse No. 10, Laboratoriet for Bygninsteknik, Danmarks Tekniske Højskole.

Hassan Khan, Ammad (2012). "Experimental Analysis of Flat Rigid Piston Dilatometer". Ph.D. Thesis. University of Engineering & Technology, p. 51.

Houlsby, G. T. and F. Schnaid (1994). "Interpretation of shear moduli from cone pressuremeter tests in sand". In: *Géotechnique* 44.1, pp. 147–164.

Hughes, J. M. O. and P K Robertson (1985). "Full-displacement pressuremeter testing in sand". In: *Canadian Geotechnical Journal* 22.3, pp. 298–307.

ISO standard 14688-1:2002 (2002). *Geotechnical investigation and testing – Identification and classification of soil – Part 1: Identification and description*. Geneva, Switzerland: International Organization for Standardization.

ISO standard 22476-11:2017(E) (2017). *Geotechnical investigation and testing – Field testing – Part 11: Flat dilatometer test*. Geneva, Switzerland: International Organization for Standardization.

Iwasaki, K., H. Tsuchiya, Y. Sakai, and Y. Yamamoto (1991). "Applicability of the Marchetti Dilatometer Test to Soft Ground in Japan". In: *Proc. GEOCOAST '91*. Yokohama, pp. 29–32.

Jamiolkowski, M. and D.C.F. Lo Presti (1998). "DMT research in sand. What can be learned from calibration chamber tests". In: *1st Int. Conf. on Site Characterization ISC'98*. Atlanta, Oral presentation.

Kaggwa, W S, M B Jaksa, and R K Jha (1996). "Development of automated dilatometer and comparison with cone penetration tests at the University of Adelaide, Australia". In: *Advances in Site Investigation Practice*. London, pp. 372–382.

Kamei, Takeshi and Kimitoshi Iwasaki (1995). "Evaluation of Undrained Shear Strength of Cohesive Soils Using a Flat Dilatometer." In: *SOILS AND FOUNDATIONS* 35.2, pp. 111–116.

Karg, Christian (2007). "Modelling of strain accumulation due to low level vibrations in granular soils". Ph.D. Thesis. Ghent University.

Kouretzis, G P, Y Ansari, J Pineda, R Kelly, and D Sheng (2015). "Numerical evaluation of clay disturbance during blade penetration in the flat dilatometer test". In: *Géotechnique Letters* 5, pp. 91–95.

Kulhawy, F.H. and P.W. Mayne (1990). *Manual on estimating soil properties for foundation design*. Tech. rep. Electric Power Research Inst., Palo Alto, CA (USA); Cornell Univ., Ithaca, NY (USA). Geotechnical Engineering Group, p. 250.

Lacasse, S. (1986). *In Situ Site Investigation Techniques and Interpretation for Offshore Practice*. Tech. rep. Oslo: 40019–28, Norwegian Geotechnical Institute.

Lacasse, S. and T Lunne (1988). "Calibration of dilatometer correlations". In: *Proc. Int. Sym. on Penetration Testing ISOPT-1*. Orlando, pp. 539–548.

Ladd, C C, R Foott, K Ishihara, F Schlosser, and H G Poulos (1977). "Stress deformation and strength characteristics". In: *Proceedings of the 9th International Conference on Soil Mechanics and Foundation Engineering*. Tokyo, pp. 421–497.

Larsson, R. and S. Eskilson (1989). *Dilatometerforsok i lera*. Tech. rep. Linkoping: Swedish Geotechnical Institute.

Lee, Jui-Ting, Chien-Chih Wang, Yen-Te Ho, and An-Bin Huang (2013). "Characterization of reservoir sediment under water with differential pressure-sensored flat dilatometer and piezo-penetrometer". In: *Acta Geotechnica* 8.4, pp. 373–380.

Lee, Moon-Joo, Sung-Kun Choi, Min-Tae Kim, and Woojin Lee (2011). "Effect of stress history on CPT and DMT results in sand". In: *Engineering Geology* 117.3, pp. 259–265.

Liu, Hanlong, Hang Zhou, and Gangqiang Kong (2016). "Upper-Bound Solution for Flat Cavity Expansion Model". In: *Journal of Engineering Mechanics* 142.7, pp. 1–9.

Liu, Xueyan, Dinghua Zhu, and Dajun Yuan (2013). "Improvement and application of flat dilatometer". In: *Chinese Journal of Geotechnical Engineering* 35.13, pp. 1375–1380.

Mair, R. J. and David Muir Wood (1987). *Pressuremeter testing: methods and interpretation*. London: CIRIA-Butterworths.

Marchetti, S. and D. K. Crapps (1981). *Flat Dilatometer Manual*. Tech. rep. Internal Report of G.P.E.

Marchetti, S. and G. Totani (1989). "Ch Evaluations from DMTA Dissipation Curves". In: *Proc. XII ICSMFE*. Rio de Janeiro, pp. 281–286.

Marchetti, S, P Monaco, G Totani, and M Calabrese (2001). "The flat dilatometer test (DMT) in soil investigations." In: *International Conference on In Situ Measurement of Soil Properties*. Bali, pp. 95–131.

Marchetti, Silvano (1975). "A new in situ test for the measurement of horizontal soil deformability". In: *Conference on In Situ Measurement of Soil Properties*. Raleigh, N.C.: ASCE Specialty Conference, pp. 255–259.

— (1980). "In situ tests by flat dilatometer". In: *Journal of the Geotechnical Engineering Division* 106.3, pp. 299–321.

— (1985). "On the field determination of K_0 in sand". In: *Proceedings of 11th International Conference on Soil Mechanics & Foundation Engineering*. San Francisco: Balkema, pp. 2667–2672.

— (1997). "The flat dilatometer: Design applications". In: *3rd Geotechnical Engineering Conf., Keynote lecture*. Cario, pp. 421–448.

— (2010). "Sensitivity of CPT and DMT to stress history and aging in sands for liquefaction assessment". In: *Proceedings of the CPT 2010 International*. Huntington Beach, California.

— (2015). "Some 2015 Updates to the TC16 DMT Report 2001". In: *The 3rd International Conference on the Flat Dilatometer*. Rome, pp. 43–65.

Marchetti, Silvano (2016). "Incorporating the Stress History Parameter KD of DMT into the Liquefaction Correlations in Clean Uncemented Sands". In: *Journal of Geotechnical and Geoenvironmental Engineering* 142.2.

Mayne, P. W. (1987). "Determining preconsolidation stress and penetration pore pressures from DMT contact pressures". In: *Geotechnical Testing Journal* 10.3, pp. 146–150.

— (2006). "Interrelationships of DMT and CPT readings in soft clays". In: *Proceedings from the Second International Flat Dilatometer Conference*. Atlanta, pp. 220–225.

— (2014). "Interpretation of geotechnical parameters from seismic piezocone tests". In: *Proc. 3rd Intl. Symposium on Cone Penetration Testing*. Las Vegas, Nevada, pp. 47–73.

— (2015). "Peak Friction Angle of Undisturbed Sands using DMT". In: *The 3rd International Conference on the Flat Dilatometer*. Rome, pp. 237–242.

Mayne, P. W. and Harry G. Poulos (1999). "Approximate Displacement Influence Factors for Elastic Shallow Foundations". In: *Journal of Geotechnical and Geoenvironmental Engineering* 125.6, pp. 453–460.

Mayne, P. W., Matthew R. Coop, Sarah M. Springman, An Bin Huang, and Jorge G. Zornberg (2009). "Geomaterial behavior and testing". In: *Proceedings of the 17th International Conference on Soil Mechanics and Geotechnical Engineering: The Academia and Practice of Geotechnical Engineering*. Vol. 4, pp. 2777–2872.

Mayniel, K. (1808). *Traité Experimental, Analytique et Pratique de Ia Poussee des Terres et des Murs de Revetment*. Paris: D. Colas.

Mesri, G. (1975). "Discussion of "New Design Procedure for Stability of Soft Clays," by Ladd, C. C., and Foott, R ." In: *Journal of Geotechnical and Geoenvironmental Engineering* 101.4, pp. 409–412.

Mitchell, J. K., F. Guzikowski, and W. C. B. Villet (1978). *The measurement of soil properties in-situ: present methods—their applicability and potential.* Tech. rep. University of California at Berkeley: Lawrence Berkeley Laboratory Report 6363.

Monaco, P and S Marchetti (2004). "Evaluation of the coefficient of subgrade reaction for design of multi - propped diaphragm walls from DMT moduli". In: *Proceedings of the Second International Conference on Site Characterization*. Porto, pp. 993–1002.

Monaco, P, G Totani, and M Calabrese (2006). "DMT-predicted vs observed settlements: a review of the available experience". In: *Proc. 2nd International Conference on the Flat Dilatometer*. Washington, pp. 244–252.

Monaco, Paola, Sara Amoroso, Silvano Marchetti, Diego Marchetti, Gianfranco Totani, Simonetta Cola, and Paolo Simonini (2014). "Overconsolidation and Stiffness of Venice Lagoon Sands and Silts from SDMT and CPTU". In: *Journal of Geotechnical and Geoenvironmental Engineering* 140.1, pp. 215–227.

Motan, E S and A Q Khan (1988). "In-situ shear modulus of sands by a flat-plate penetrometer: a laboratory study". In: *ASTM Geotechnical Testing Journal* 11.4, pp. 257–262.

National Instruments. *LabVIEW 2016 Help*.

Ouyang, Z and P W Mayne (2016). "New DMT method for evaluating soil unit weight in soft to firm clays". In: *Geotechnical and Geophysical Site Characterisation 5*. Gold Coast, pp. 785–789.

Peiffer, Herman (2016). "The Use of a DMT to Monitor the Stability of the Slopes of a Clay Exploitation Pit in the Boom Clay in Belgium". In: *Geotechnical and Geophysical Site Characterisation 5*. Gold Coast.

Poulos, H. G. and E. H. Davis (1974). *Elastic solutions for soil and rock mechanics*. New York: John Wiley, p. 43.

Powell, J. J. M. and RST Quarterman (1988). "The interpretation of cone penetration tests in clays, with particular reference to rate effects". In: *Proc. Int. Sym. on Penetration Testing ISOPT-1*. Orlando, pp. 903–910.

Powell, J. J. M. and I. M. Uglow (1988). "The interpretation of the Marchetti dilatometer test in UK clays". In: *Penetration Test In U.K.* Thomas Telford Ltd, pp. 29–49.

R. Colcott, B M Lehane (2012). "the design, development and application of a new dmt". In: *Geotechnical and Geophysical Site Characterization 4*. Pernambuco, pp. 565–570.

Rahardjo, Paulus P, Yunan Halim, and Lento Sentosa (2004). "Use of dilatometer and dual dilatometer test for soft soils and peats". In: *Proceedings ISC-2 on Geotechnical and Geophysical Site Characterization*. Rotterdam, pp. 775–782.

Robertson, P. K. (1990). "Soil classification using the cone penetration test". In: *Canadian Geotechnical Journal* 27.1, pp. 151–158.

— (2009a). "CPT-DMT Correlations". In: *Journal of Geotechnical and Geoenvironmental Engineering* 135.11, pp. 1762–1771.

— (2009b). "Interpretation of cone penetration tests — a unified approach". In: *Canadian Geotechnical Journal* 46.11, pp. 1337–1355.

Robertson, P. K. (2012). "The James K. Mitchell Lecture: Interpretation of in-situ tests–some insights". In: *Geotechnical and Geophysical Site Characterization 4*. Pernambuco, pp. 3–24.

— (2016). "Cone penetration test (CPT)-based soil behaviour type (SBT) classification system — An update". In: *Canadian Geotechnical Journal* 53.12, pp. 1–18.

Robertson, P. K. and RG Campanella (1988). "Excess pore pressures and the flat dilatometer test". In: *Proceedings International Symposium Penetration Testing, ISPOT–1*. Orlando: AA Balkema Publishers.

Rqebuck, J R, Osterberg, and H (1935). "The Joule-Thomson Effect in Nitrogen". In: *Physical Review* 48.450.

Sachs, E., M. Cima, and J. Cornie (1990). "Three-Dimensional Printing: Rapid Tooling and Prototypes Directly from a CAD Model". In: *CIRP Annals - Manufacturing Technology* 39.1, pp. 201–204.

Schanz, T and P A Vermeer (1998). "On the Stiffness of Sands". In: *Pre-failure deformation behaviour of geomaterials*. London: ICE, pp. 383–387.

Schanz, T, P Vermeer, and P Bonnier (1999). "The hardening soil model: Formulation and verification". In: *Beyond 2000 in computational geotechnics- 10 years of PLAXIS*. Rotterdam, pp. 1–16.

Schmertmann, J. H. (1982). "A method for determining the friction angle in sands from the Marchetti dilatometer test (DMT)". In: *Proceedings of the Second European Symposium on Penetration Testing*. Amsterdam, pp. 853–861.

— (1984). *DMT Manual – Guidelines for using the CPT, CPTU and Marchetti DMT for Geotechnical Design*. Tech. rep. Report Number FHWA-PA-87-024+84-24, Vol. III of IV – DMT Test Methods and Data Reduction.

— (1986). "Dilatometer to compute foundation settlement". In: *Proc. In Situ '86, ASCE Spec. Conf. on "Use of In Situ Tests in Geotechn. Engineering"*. Blacksburg, pp. 303–321.

Schmertmann, J. H. and D K Crapps (2016). "Ground Property Characterization from In-Situ Tests Opportunities offered by Measuring Thrust during Flat Plate Dilatometer Testing". In: *5th International Conference on Geotechnical and Geophysical Site Characterisation*. Gold Coast, pp. 797–802.

Schnaid, F. (2008). *In situ testing in geomechanics: the main tests*. London: Taylor & Francis.

Schnaid, F., E. Odebrecht, Jonatas Sosnoski, and Peter Robertson (2016). "The effects of test procedure on DMT results in intermediate soils". In: *Canadian Geotechnical Journal* 53.8, pp. 1270–1280.

Stetson, K P, J Benoit, and M J Carter (2003). "Design of an instrumented flat dilatometer". In: *Geotechnical Testing Journal* 26.3, pp. 302–309.

Terzaghi, Karl (1936). "The shearing resistance of saturated soil and the angle between the planes of shear". In: *Proceedings of 1st International SMFE Conference*. Harvard, pp. 54–56.

Wroth, C. P. (1982). "British experience with the self-boring pressuremeter". In: *Proc. of Int. Symp. Pressuremeter and its Marine Applications*. Paris, pp. 143–164.

Yu, H. S. (2004). "The First James K. Mitchell Lecture In situ soil testing: from mechanics to interpretation". In: *Geomechanics and Geoengineering* 1.3, pp. 165–195.

Yu, H. S., J. P. Carter, and J. R. Booker (1993). "Analysis of the dilatometer test in undrained clay". In: *Predictive Soil Mechanics*. London: Thomas Telford. Chap. 2, pp. 783–795.

Yuan, Q., Y. H. Wang, P. O. Tam, X. Li, and Y. Gao (2016). "Making a Biaxial Testing System With the Aid of 3D Printing Technique to Examine the Kinetic Behavior of Particulate Media". In: *Geotechnical Testing Journal* 39.2, pp. 264–281.

Zhou, Hang, Gangqiang Kong, Ping Li, and Hanlong Liu (2015). "Flat Cavity Expansion: Theoretical Model and Application to the Interpretation of the Flat Dilatometer Test". In: *Journal of Engineering Mechanics* 142.1.